Developing novel tools for the detection and modulation of ion channels

Robert Jordan Bedford

Submitted in accordance with the requirements for the degree of

Doctor of Philosophy

University of Leeds

Faculty of Biological Sciences

School of Molecular and Cellular Biology

September 2018

The candidate confirms that the work submitted is his own, except where work which has formed part of jointly authored publications has been included. The contribution of the candidate and the other authors to this work has been explicitly indicated below. The candidate confirms that appropriate credit has been given within this thesis where reference has been made to the work of others.

The work described in chapter 3 of this thesis is based on work from the following jointly authored publication: Tiede. C *et al* (2017). Affimer proteins are versatile and renewable affinity reagents. *eLife*. doi: 10.7554/eLife.24903.

Acknowledgements

First of all, I would like to thank my primary supervisor Dr Darren Tomlinson for providing me with the opportunity to conduct a PhD under his guidance and for helping to keep my project on track when it was drifting quite heavily off of it. His words of advice and enthusiasm for science have helped keep me motivated throughout. I would also like to thank my co-supervisor Dr Jon Lippiat for his excellent advice on ion channels and for putting up with numerous questions of how to study them.

All current and previous members of the Tomlinson and McPherson groups have provided motivation throughout my project. In particular, special thank you to Dr Christian Tiede for teaching me about phage display and continuing to provide advice on it, especially at Veritas. Thanks to Dr Christopher Watson for providing training in mammalian cell culture and thanks to Anna Tang for training me in molecular biology techniques. I would also like to thank Vishakha Tyagi and Freya Leif for assistance with phage display and site-directed mutagenesis experiments and Jaida Begum for assistance with small molecule screening. Finally, my project wouldn't have been the same without Lia De Faveri, Sophie Heseltine and Tom Taylor - you've helped keep me sane throughout!

Next, I would like to thank my friends for being there. In particular, Andrew Tsatsanis, Gareth Fearnley, Gina Smith and Izma Abdul Zani – Tenerife was awesome. Cream of sound was better. Jade - although you weren't here at the start of this PhD, thank you for keeping me motivated towards the end of it and for providing constant support throughout the writing of this thesis.

Finally, I would like to thank my family, not only for pretending to appear interested when I talked about my experiments, but for striving to provide me with the opportunity to make the most of life. Without you, this achievement wouldn't have been possible.

Abstract

Pain is a vital sensory function however when its associated pathways become damaged chronic pain occurs. Major contributors to this pathological process are ion channels, providing a rationale for targeting them therapeutically.

The development of detection and therapeutic reagents against ion channels has proved challenging. With the lack of selective chemical probes, most researchers are now studying biological reagents for their ability to target ion channels. These include antibodies and toxins. However, antibodies and toxins have disadvantages of their own, for example they can be difficult to produce. As a result, Affimers may present as an alternative for studying ion channel function.

Ion channels are difficult to produce in a format appropriate for isolating binding reagents against. As a result, a number of methods have been developed in an attempt to produce recombinant ion channel proteins suitable for such applications including expression of ion channel extracellular domains, peptide mimotopes and cell-based screening methods.

This study investigates a number of methods for presenting ion channels for isolation of Affimer reagents by phage display. Affimer reagents that were able to detect the ion channels TRPV1 and P2X3 in their native cellular context were isolated and characterised by biophysical and cellular assays demonstrating the ability to isolate Affimer reagents capable of binding to and modulating ion channel function. In addition, this study provides a proof-of-concept result demonstrating the use of Affimer reagents in aiding the discovery of small molecule mimetics. The identified molecules demonstrated the ability to modulate TRPV1 when tested *in vitro*.

In conclusion, this study describes a number of methods that have been used to isolate Affimer reagents that are able to detect and modulate ion channels involved in chronic pain.

Table of Contents

Acknowledgements i

Abstract ii

Table of Contents iii

List of Tables vi

List of Figures vii

Abbreviations xi

1 Introduction 2

1.1 Ion channels 2
1.2 Ion channel classification 2
1.2.1 Voltage-gated ion channels 2
1.2.2 Ligand-gated ion channels 23
1.2.3 Targeting TRP and P2X channels in the treatment of chronic pain 26
1.3 From bench to bedside 32
1.4 Targeting ion channels using alternatives to antibodies 33
1.4.1 Animal toxins as ion channel tools 33
1.4.2 Targeting ion channels using chemical compounds 42
1.4.3 Targeting ion channels using novel biologics 43
1.5 Aims of the project 51

2 Materials and Methods 53

2.1 General reagents 53
2.2 Bacterial cell culture 56
2.3 DNA methods 56
2.3.1 Expression plasmids 56
2.3.2 Polymerase Chain Reaction (PCR) 58
2.3.3 DNA agarose gel electrophoresis 58
2.3.4 Purification of DNA 58
2.3.5 Plasmid purification from *E. coli* 59
2.3.6 DNA sequencing 59
2.4 Molecular cloning 59
2.4.1 Cloning into expression vectors 59
2.4.2 Restriction digestion 61
2.4.3 DNA ligation 61
2.5 Expression and purification of proteins 62
2.5.1 Transformation of chemically competent *E. coli* 62
2.5.2 Production of recombinant protein 63
2.5.3 Purification of recombinant protein 63
2.5.4 Protein concentration 64
2.5.5 Biotinylation of recombinant proteins 65
2.5.6 ELISA to analyse biotinylation of proteins 65
2.6 Protein characterisation 66
2.6.1 Sodium Dodecyl Sulphate Polyacrylamide Gel Electrophoresis (SDS PAGE) 66

2.6.2 Western blot 66
2.6.3 Circular Dichroism (CD) 67
2.6.4 Fluorescence Anisotropy 67
2.6.5 X-ray crystallography 67
2.6.6 Small molecule screening 68
2.7 Mammalian cell culture 68
2.7.1 Cell passage 68
2.7.2 Mammalian cell transfection 68
2.7.3 Ion channel modulation assays 69
2.7.4 Immunocytochemistry 69
2.8 Affimer identification 70
2.8.1 Phage display of recombinant proteins 70
2.8.2 Phage ELISA 72
2.8.3 Phage display against mammalian cells 73
2.8.4 Cell-based phage ELISA 73
2.8.5 Affimer production and purification 73
2.8.6 Protein dialysis and refolding 74
2.8.7 Protein-ELISA to assess Affimer binding to target 74
2.8.8 Data analysis 74

3 Positive allosteric modulation of TRPV1 by Affimer reagents 77

3.1 Introduction 77
3.2 Results 81
3.2.1 Selection of TRPV1-specific Affimers against a peptide mimicking the TRPV1 outer pore domain 81
3.2.2 Production of anti-TRPV1 Affimers in *E. coli* 83
3.2.3 Affimers bind to TRPV1 expressed in mammalian cells 90
3.2.4 Affimers induce positive allosteric modulation of TRPV1 95
3.3 Discussion 102

4 Structural insights into the modulation of TRPV1 by Affimer 45 108

4.1 Introduction 108
4.2 Results 111
4.2.1 Site-directed mutagenesis of Affimer 45 111
4.2.2 Structural analysis of the Affimer 45-TRPV1 interaction by X-ray crystallography 122
4.2.3 Affinity maturation of Affimer 45 towards TRPV1 130
4.2.4 Identification of Affimer 45 small molecule mimetics 146
4.3 Discussion 152

5 Development of a cell-based phage display protocol for screening membrane proteins 157

5.1 Introduction 157
5.2 Results 157
5.2.1 Expression of membrane-bound Herpes Simplex Virus 1 (HSV1) glycoprotein D (gD) target. 157
5.2.2 Cell-based biopanning against HSV1 gD. 158
5.2.3 Further characterisation of HSV1 gD Affimer clones. 166
5.2.4 Using the optimised cell-based phage display protocol to screen ion channel targets. 169
5.3 Discussion 175

6 The identification of Affimer reagents against P2X3, a major drug target for chronic pain 179

6.1 Introduction 179
6.2 Results 182
6.2.1 Expression and characterisation of P2X3 extracellular domain (ECD) segments in *E. coli* 182
6.2.2 Expression and purification of P2X3 ECD chimera's in HEK293 cells 183
6.2.3 P2X3 ECD phage display 188
6.2.4 Human P2X3 immunocytochemistry 190
6.2.5 Rat P2X3 immunocytochemistry 199
6.3 Discussion 208

7 Discussion 213

7.1 Developing phage display methods for screening ion channel targets 214
7.2 Affimers for use in structural studies 222
7.3 Conclusion 224

8 References i

List of Tables

Table 1.1. Human diseases resulting from voltage-gated sodium channel mutations 7
Table 1.2. Human voltage-gated calcium channelopathies 12
Table 1.3. Human diseases resulting from K_{IR} channel mutations 17
Table 1.4. A number of toxins have been identified that bind to the receptors of the central nervous system involved in fast synaptic transmission 42
Table 2.1. *E. coli* cell strains used in this study alongside their genotypes and product information. 56
Table 2.2. Expression plasmids used in this study for the production of recombinant target proteins and Affimers 57
Table 2.3. Primers used in this study for the amplification of recombinant target protein and Affimer DNA for expression. Restriction sites underlined. 61
Table 3.1. Overview of small molecule inhibitors of TRPV1 tested in clinical trials. *Adapted from (Moran et al. 2011).* 79
Table 3.2. Amino acid sequences of the variable regions of Affimers isolated from phage display 83
Table 3.3. TRPV1 Affimer concentration measurements and normalisation to 100 µg/mL for use in binding assays 84
Table 3.4. K_d values of Affimer binding to TRPV1 peptide when immobilised at 160 ng/mL 90
Table 3.5. EC_{50} values for Affimers when tested for potentiation of capsaicin-evoked TRPV1 activation 99
Table 3.6. Tissue expression of TRPV channel family members 105
Table 4.1. Site-directed mutagenesis primers 113
Table 4.2. Sequencing results of Affimer 45 variable regions after site-directed mutagenesis 113
Table 4.3. TRPV1 Affimer mutant concentration measurements and normalisation to 1 mg/mL for use in binding assays 115
Table 4.4. K_d values for Affimer variants tested for binding against immobilised TRPV1 peptide 121
Table 4.5. Sequencing results of a selected number of clones from the initial library. 132
Table 4.6. K_d values for Affimer 45 (WG) variants when incubated against 40 ng/mL of TRPV1 peptide 145
Table 5.1. Colony counts to enable comparison of phage recovery using either a naïve library or libraries with various levels of enrichment against soluble protein. 162
Table 5.2. Affimer variable regions for HSV1 gD-binding Affimers from both enriched and naïve libraries 166
Table 5.3. HSV1 gD Affimer concentration measurements and normalisation to 10 µM for use in binding assays 168
Table 6.1. Affimer sequences identified from recombinant P2X3 ECD screen .. 188
Table 6.2. Tissue localisation of P2X family members. 212

List of Figures

Figure 1.1. Architecture of voltage-gated cation channels (VGCC's) 4
Figure 1.2. Structural modelling of the $Na_v1.7$ F1449V mutation resulting in inherited erythromalalgia (IEM) 8
Figure 1.3. The sub-types of potassium ion channels 13
Figure 1.4. K_{Ca} channel mutations resulting in human disease 19
Figure 1.5. Human disorders caused by defects within K_{2P} channels 20
Figure 1.6. Voltage-gated potassium channel mutations resulting in human disorders 23
Figure 1.7. Sequence alignment of the six TRPV channel subtypes 30
Figure 1.8. VGSC binding sites for toxins isolated from venomous species 34
Figure 1.9. Pore-blocking potassium channel toxins. 37
Figure 1.10. Immunoglobulin and non-immunoglobulin-based binding reagents 45
Figure 1.11. Structural analysis of the Monobody S12-FluC channel complex 47
Figure 3.1. TRPV channel phylogenetic tree showing varying levels of homology 78
Figure 3.2. Positive allosteric modulation of TRPV1 80
Figure 3.3. Phage ELISA demonstrating binding of monoclonal Affimer clones to a TRPV1 peptide. 82
Figure 3.4. SDS PAGE gel of anti-TRPV1 Affimers developed using Coomassie stain 84
Figure 3.5. TRPV1 peptide ELISA using purified Affimers 86
Figure 3.6. TRPV1 Affimer concentration-response ELISA 89
Figure 3.7. Immunocytochemistry against TRPV1-expressing cells in their fixed state. 92
Figure 3.8. Immunocytochemistry against TRPV1-expressing cells in their live state 93
Figure 3.9. Affimer 2 and anti-TRPV1 antibody provide putatively similar staining patterns by immunocytochemistry 94
Figure 3.10. Validation of rat TRPV1 activity when transiently expressed in a U-2 OS cell line 96
Figure 3.11. Potentiation of TRPV1 response by Affimers when activated by capsaicin at its EC_{20} concentration 97
Figure 3.12. Affimer potentiation of TRPV1 response when activated by a range of capsaicin concentrations 98
Figure 3.13. Schematic of a dimeric Affimer 45 to test for TRPV1 activating properties 100
Figure 3.14. Production of a dimeric Affimer 45 to test for its ability to directly activate TRPV1. 101
Figure 3.15. Schematic view of a TRPV1 subunit with the binding regions of activating peptide toxins (DkTx, RhTx), a small molecule potentiator, MRS1477 and the Affimers described in this chapter, highlighted 104
Figure 4.1. The outer pore domain epitope of TRPV1 targeted by the activating toxin, DkTx 109
Figure 4.2. Production of Affimer 45 SDM variants and analysis by SDS PAGE. 114

Figure 4.3. ELISA was used to test binding of Affimer 45 mutants to a TRPV1 peptide. 117
Figure 4.4. Concentration-response ELISA to test the extent to which each of the Affimer 45 mutations disturbed the interaction with TRPV1. 120
Figure 4.5. Size exclusion chromatography trace (A) and SDS PAGE analysis (B) of protein obtained from eluted fractions 123
Figure 4.6. An image demonstrating the growth of the crystal used for analysis of the Affimer 45-TRPV1 peptide complex. 124
Figure 4.7. Affimer 45 was crystallised in complex with the peptide mimicking a region of the TRPV1 outer pore domain. 125
Figure 4.8. Affimer 45 interacts with the TRPV1 peptide using both variable regions 127
Figure 4.9. Alignment of Affimer 45-TRPV1 peptide crystal structure with DkTx-TRPV1 cryo-EM structure (PDB: 5IRX) demonstrates identical epitope. 129
Figure 4.10. Affinity maturation of Affimer 45 to try and improve its affinity towards its cognate TRPV1 peptide was conducted using splicing by overlap extension PCR 131
Figure 4.11. Graph showing a concentration response phage ELISA using a constant amount of Affimer 45 phage against a range of TRPV1 peptide concentrations 133
Figure 4.12. Phage ELISA and sequencing results following one round of biopanning against the TRPV1 peptide with the Affimer 45 (WG) library. 134
Figure 4.13. Phage ELISA and sequencing results following a second round of biopanning with one day of washing under standard conditions against the TRPV1 peptide with the Affimer 45 (WG) library. 136
Figure 4.14. Phage ELISA and sequencing results following a second round of biopanning with one day of washing with competition with Affimer 45 wild-type 137
Figure 4.15. Phage ELISA and sequencing results following a second round of biopanning with five days of washing under standard conditions. 138
Figure 4.16. Phage ELISA and sequencing results following a second round of biopanning with five days of washing with competition with the Affimer 45 wild-type. 139
Figure 4.17. Analysis of Affimer 45 (WG) variant proteins by SDS PAGE and Coomassie staining. 141
Figure 4.18. Concentration-dependent ELISA's to test for improved binding of Affimer 45 (WG) variants compared to the wild-type Affimer 45. 144
Figure 4.19. Affimer 45 (WG) variants 3 and 9 may demonstrate improved binding to the TRPV1 peptide using enriched negatively and positively charged residues 146
Figure 4.20. Variable region one residues of Affimer 45 essential to the TRPV1 interaction are shown. 147
Figure 4.21. *In vitro* cell-based assays to test for TRPV1 inhibition using identified MCCB compounds 148
Figure 4.22. Chemical structures of the five MCCB compounds observed to have an inhibitory effect in cell-based studies. 149

Figure 4.23. Concentration-response studies of the five compounds identified from preliminary TRPV1 inhibition studies 152
Figure 4.24. Amino acids involved in the TRPV1 interaction are similar between DkTx and Affimer 45. 153
Figure 5.1. Phage ELISA showing binding of Affimer phage to HSV1 gD-expressing cells following isolation against recombinant protein 159
Figure 5.2. Methodology used for the biopanning of membrane-based targets using the Affimer phage display library 160
Figure 5.3. Phage ELISA showing binding of Affimer phage to HSV1 gD expressing cells following isolation after seven rounds of biopanning against cells. .. 163
Figure 5.4. Comparison of enrichment of bound Affimer phage when screened against cells in suspension or when adherent 164
Figure 5.5. Phage ELISA showing binding of Affimers to HSV1 gD-expressing cells following isolation after three rounds of biopanning. 165
Figure 5.6. Analysis of anti-HSV1 gD Affimers and anti-P2X3 Affimers by SDS PAGE and Coomassie staining 167
Figure 5.7. Validation of HSV1 gD-specific Affimer binding to their target by ELISA and ICC. 168
Figure 5.8. Phage ELISA showing binding by Affimers isolated from three rounds of biopanning against P2X3 expressing cells. 171
Figure 5.9. ELISA testing binding of Affimer clones B2 and H8 to P2X3 expressing cells. 172
Figure 5.10. Phage ELISA showing binding of Affimer phage isolated after three rounds of biopanning against TRPV1 expressing cells. 173
Figure 5.11. Phage ELISA to test for binding to TRPV1-expressing cells by TRPV1 Affimer 2 when expressed with or without the pIII coat protein 174
Figure 6.1. Trafficking and processing of the P2X family of ion channels 181
Figure 6.2. Aligned amino acid sequence of the open reading frames of the human P2X3 ion channel ECD segments cloned in to a pET11a expression vector 184
Figure 6.3. P2X3 ECD segments were expressed in *E. coli* (A) and HEK293 cells (B). 185
Figure 6.4. Characterisation of P2X3 ECD secondary structure by circular dichroism (CD) 186
Figure 6.5. Characterisation of P2X3 ECD tertiary structure by fluorescence polarisation 187
Figure 6.6. Phage ELISA showing binding of P2X3 Affimer clones to recombinant P2X3 ECD-Fc protein. 189
Figure 6.7. Analysis of anti-P2X3 Affimer proteins by SDS PAGE and Coomassie staining. 190
Figure 6.8. Human P2X3 immunocytochemistry against fixed cells 192
Figure 6.9. Human P2X3 immunocytochemistry against live cells 197
Figure 6.10. Co-staining of hP2X3 using Affimers 1 and 7 alongside anti-P2X3 antibody 198
Figure 6.11. Rat P2X3 immunocytochemistry against fixed cells. 200
Figure 6.12. Rat P2X3 immunocytochemistry against live cells. 205

Figure 6.13. Co-staining of rP2X3 using Affimers 1 and 7 alongside anti-P2X3 antibody. 206
Figure 6.14. Sequence alignment of human and rat P2X3 prepared using Clustal Omega. 207

Abbreviations

2YT	2 x yeast and tryptone
5-HT3	5-hydroxytryptamine
ANOVA	Analysis of Variance
ASIC	Acid sensing ion channel
ATP	Adenosine Triphosphate
BSA	Bovine serum albumin
BSTG	Bioscreening Technology Group
Ca_v channel	Voltage-gated calcium channel
CD	Circular dichroism
CHO	Chinese Hamster Ovary
CIP	Congenital Insensitivity to Pain
CNS	Central nervous system
DARPin	Designed Ankyrin Repeat proteins
DkTx	Double Knot Toxin
DMEM	Dulbecco's Modified Eagle Medium
DMSO	Dimethyl Sulfoxide
DNA	Deoxyribonucleic acid
dNTP	Deoxynucleotide triphosphate
DTT	Dithiothreitol
ELISA	Enzyme-linked immunosorbent assay
EM	Electron microscopy
FBS	Foetal bovine serum
FDA	Food and Drug Administration
FP	Fluorescence Polarisation
GABA	Gamma aminobutyric acid
GlyR	Glycine receptor
GPC3	Glypican 3
HEK	Human Embryonic Kidney
hERG	Human Ether-Go-Go Channel
HRP	Horseradish peroxidase
ICK	Inhibitory Cysteine Knot

IEM	Inherited Erytheromalalgia
IF	Immunofluorescence
IMAC	Ion Metal Affinity Chromatography
IPTG	Isopropyl β-D-1 thiogalactopyranoside
ITC	Isothermal Calorimetry
JCSG	Joint Centre for Structural Genomics
K_v channel	Voltage-gated potassium channel
LB	Luria broth
MANT-ATP	2'/3'-O-(N-methylanthraniloyl) Adenosine 5'-triphosphate
MWCO	Molecular Weight Cut Off
nACh	Nicotinic acetylcholine
Na_v channel	Voltage-gated sodium channel
NiNTA	Nickel Nitrilotriacetic Acid
ORF	Open reading frame
PAGE	Polyacrylamide Gel Electrophoresis
PCR	Polymerase Chain Reaction
PEG	Polyethylene Glycol
PEPD	Paroxysmal Extreme Pain Disorder
PFA	Paraformaldehyde
PNS	Peripheral nervous system
SDS	Sodium dodecyl sulphate
SEC	Size Exclusion Chromatography
SOB	Super Optimal Broth
SOC	Super Optimal broth with Catabolite repression
SPR	Surface Plasmon Resonance
TAE	Tris-acetate-EDTA
TBS	Tris buffered saline
TCEP	Tris (2-carboxyethyl) phosphine
TE	Tris-EDTA
TEMED	N, N, N', N'-tetramethylethane-1, 2 diamine
TMB	3, 3', 5, 5'-Tetramethylbenzidine
TRP	Transient Receptor Potential

TTX	Tetrodotoxin
UV	Ultraviolet
VGCC	Voltage-gated cation channel
VGSC	Voltage-gated sodium channel
VSD	Voltage-sensing domain

Chapter 1

Introduction

1 Introduction

1.1 Ion channels

Genes encoding membrane proteins form approximately 30% of the human genome. Despite this, only a fraction of their structures have been solved by biophysical techniques such as X-ray crystallography. The lack of structures of membrane proteins contributes to the difficulty of discovering or designing reagents able to bind and modulate their function. When compared to the large number of membrane proteins involved in human disease and identified as drug targets, the development of new techniques for such drug discovery is essential.

One class of membrane protein involved in a number of human pathologies are ion channels. Hodgkin and Huxley built the platform for ion channel research after revealing a propagation of impulses along a 'cable-like' fibre causing excitation (Hodgkin and Huxley 1952). Ion channel research has advanced greatly in the last century, from initial experiments involving electrode insertion into the squid giant axon, to the introduction of patch-clamp experiments providing the ability to measure currents of a single cell, or even ion channel (Neher and Sakmann 1976). These improvements in recording techniques revealed separate conducting structures for specific ions, eventually being termed ‘ion channels’ (Beneski and Catterall 1980, Papazian *et al.* 1987). These ion channels are responsible for many of the ion channelopathies observed in humans (1999, Lacroix-Fralish and Mogil 2009).

1.2 Ion channel classification

1.2.1 Voltage-gated ion channels

The voltage-gated cation channels (VGCC’s), namely sodium (Na_v), calcium (Ca_v) and potassium (K_v), can be described as the engines of the human nervous system. The Na_v channels initiate the action potential, prompting Ca_v channels to perform their function such as stimulating muscle contraction. Finally, K_v channels terminate the action potential, returning the membrane potential to its resting state (Hille 2001). Structurally, voltage-gated cation channels are composed of a large α-sub-unit surrounded by various combinations of auxiliary β, γ and δ-subunits, depending on cation selectivity (**Figure 1.1**). The main α-

subunit of Na_v and Ca_v channels is a single polypeptide chain consisting of four homologous repeat domains (I-IV), each arranged as six transmembrane segments (S1-S6) forming a pore structure (Catterall 1995). In addition to the pore-forming α-subunit, Ca_v channels contain α2, δ, β and γ-subunits whilst Na_v channels contain only auxiliary β-subunits (Catterall 2011). In contrast to Na_v and Ca_v channels, K_v channels are tetramers composed of four individual polypeptide chains that adjoin to form a pore-forming channel. Again, each domain consists of six transmembrane segments (S1-S6). Furthermore, various auxiliary subunits are present. The S4 segment of each ion channel family domain contains a large population of positively charged amino acid residues flanked by hydrophobic residues enabling it to act as a voltage-sensor (Noda *et al.* 1984), able to control pore opening and closing through its cooperation with the S1-S3 segments, a structure termed the voltage-sensing domain (VSD)(Guy and Seetharamulu 1986, Catterall 2011). Structural data was initially provided for the potassium and sodium channels by the labs of Roderick MacKinnon and William Catterall, respectively (Doyle *et al.* 1998, Payandeh *et al.* 2011). More recently, the crystal structure and mechanism of action of the potassium channel VSD has also been elucidated (Jensen *et al.* 2012). The ability of the VSD to control pore opening and closing have identified it as a unique target site for channel modulation (Li *et al.* 2013).

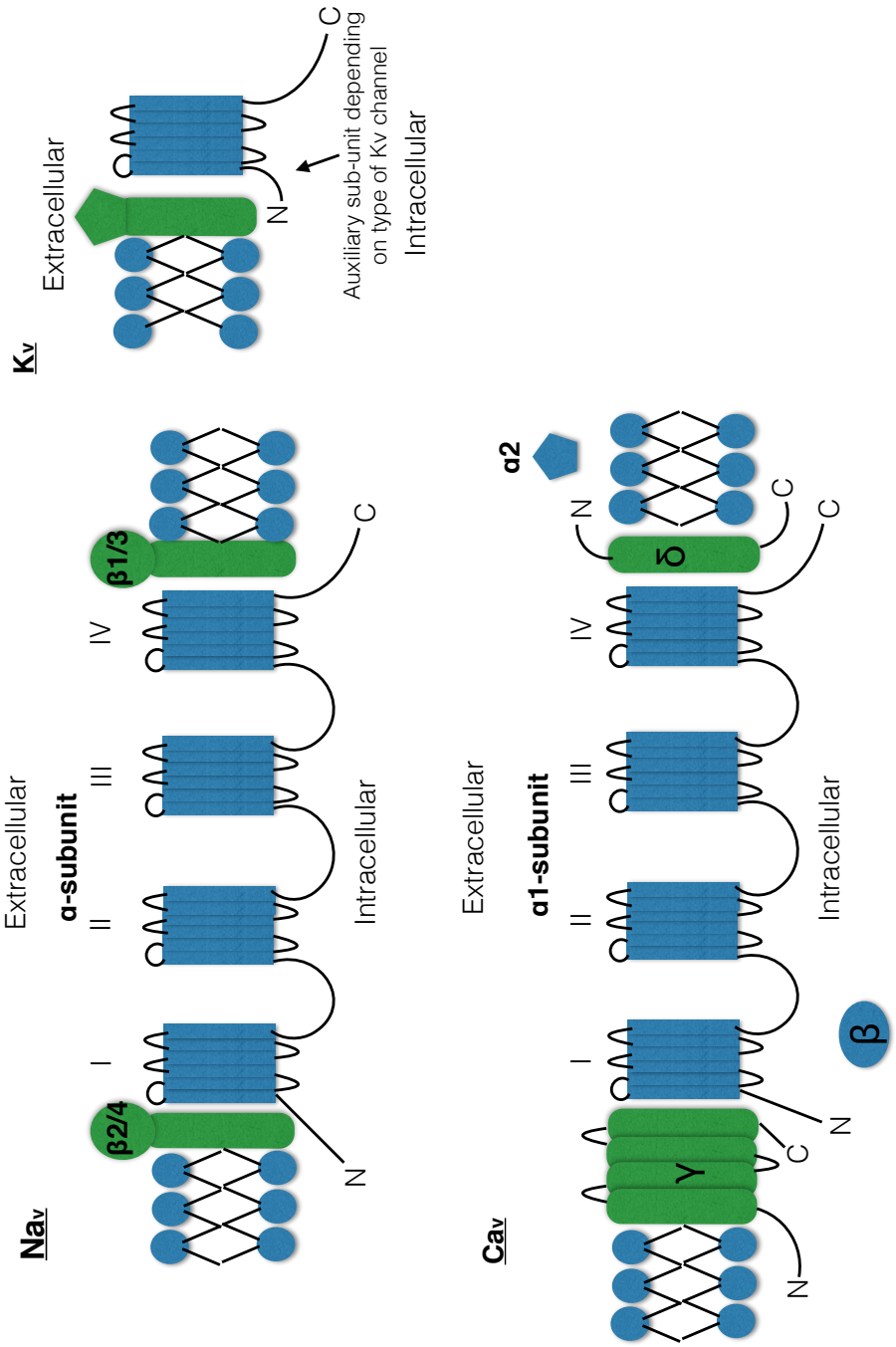

Figure 1.1. Architecture of voltage-gated cation channels (VGCC's). Na_v and Ca_v channels are both composed of a α-subunit of four domains each of six transmembrane segments. In contrast, K_v channels are tetramers composed of individual subunits each comprising six transmembrane segments. Each channel type differs in the auxiliary subunits attached to the α-subunit domains, for example Na_v channels contain auxiliary β-subunits whilst Ca_v channels contain auxiliary β, δ and γ subunits. K_v channels can contain a wide range of auxiliary subunits dependent on the family of K_v channel.

1.2.1.1 Voltage-gated sodium (Na_v) channels

Na_v channels were the primary ion channel family to be discovered and sequenced following their isolation from the eel electroplax (Recio-Pinto *et al.* 1987). Nine mammalian Na_v channel isoforms of close homology have been identified, all showing greater than 75% similarity, producing difficulties with targeting them in a sub-type specific manner (1999, Goldin *et al.* 2000). A number of these isoforms have been identified as the causative channel in a number of human diseases (**Table 1.1**)

Channel	Gene	Tissue	Disorder	Genetic cause	Reference
$Na_v1.1$, $Na_v1.2$	*SCN1A, SCN2A, SCN1B*	Brain	Generalised epilepsy with febrile seizures plus	A large number of mutations have been noted in the literature (>150)	(Escayg and Goldin 2010)
			Dravet Syndrome		
			Intractable childhood epilepsy		
$Na_v1.4$	*SCN4A*	Muscle	Hyperkalemic periodic paralysis (HKPP)	M1592V T704M	(Rojas *et al.* 1991)
			Paramyotonia congenita	R1448C, R1448H G1306V, T1313M	(Ptacek *et al.* 1992)
			Potassium-aggravated myotonia	G1306V, G1306A, G1306E V1589M	(Lerche *et al.* 1993)
			Myasthenic	V1442E	(Tsujino *et al.*

			syndrome		2003)
			Hypokalemic periodic paralysis type 2	R669H R672H, R672G P1158S	(Bulman *et al.* 1999)
$Na_v1.5$	*SCN5A*	Cardiac	Congenital long QT syndrome (Romano-Ward syndrome)	R1623Q N1325S ΔKPQ	(Yamagishi *et al.* 1998)
			Idiopathic ventricular fibrillation (Brugada syndrome)	S1710L	(Akai *et al.* 2000)
			Isolated cardiac conduction system disease	G514C T1620M	(Tan *et al.* 2001)
			Atrial standstill	D1275N L212P	(Groenewegen *et al.* 2003)
			Congenital sick sinus syndrome	P1298L	(Benson *et al.* 2003)
			Sudden infant death syndrome (SIDS)	S941N A997S S1103Y	
			Dilated cardiomyopathy (DCM)	A1180V D1275N T220I, D1595H, R814W	(Ge *et al.* 2008)
$Na_v1.7$	*SCN9A*	PNS	Familial primary erythermalgia	T2573A, T2543C	(Yang *et al.* 2004, Dib-Hajj

				S241T F1449V	*et al.* 2005)
			Paroxysmal Extreme Pain Disorder (PEPD)	R996C, V1298F, V1298D, V1299F, I1461T, F1462V, T1464I, M1627K	(Fertleman *et al.* 2006)
			Congenital Indifference to Pain (CIP)	ΔW897, ΔI767, ΔS459	(Cox *et al.* 2010)

Table 1.1. Human diseases resulting from voltage-gated sodium channel mutations. The majority of mutations resulting in Na_v channelopathies occur in similar regions of the sodium channel genes, representing similar regions of the sodium channel structure. These regions include amino acids (AA) 1300-1700, a region responsible for the inactivation gate voltage-sensor (Vassilev *et al.* 1988). AA200-300 (S4DI) and AA500-800 (S6DI-S1DII) are also areas of the genes responsible for many of the channelopathies. Mutations in these areas generally stabilise the fast inactivation state, as noted in hypokalemic periodic paralysis (Jurkat-Rott *et al.* 2000).

$Na_v1.7$ (encoded by the gene *SCN9A*) has been implicated in the sensation of painful stimuli, supported by its role in inherited pain disorders. Recently, gain-of-function mutations in *SCN9A* have been linked with the pain disorders, inherited erythromalalgia (IEM) and paroxysmal extreme pain disorder (PEPD), whilst loss-of-function mutations are linked with complete insensitivity to pain (CIP) (Yang *et al.* 2004). Structural modelling following crystallisation of the *Arcobacter butzleri* Na_v channel (Na_vAb) has improved our understanding of the structure-function relationship of human *SCN9A* mutations. The formation of aromatic residues within the pore-forming S6 segments of each domain (DI Y405, DII F960, DIII F1449 and DIV F1752) stabilises the channel in a pre-open state.

Following F1449V mutation in *SCN9A* (**Figure 1.2**), as found in IEM patients, this stability is reduced lowering the opening threshold. This causes increased channel activation and consequently, enhanced pain sensation (Dib-Hajj *et al.* 2005).

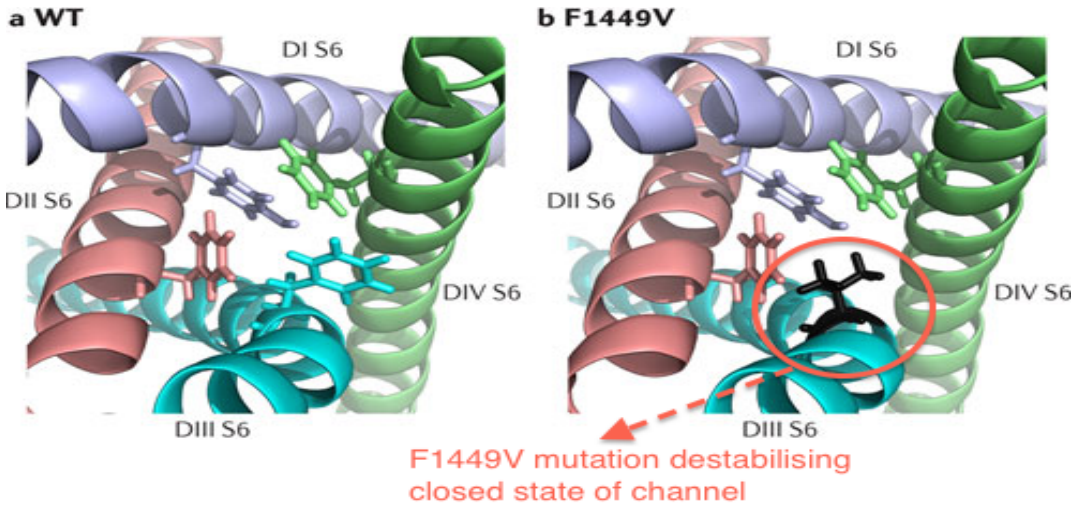

Figure 1.2. Structural modelling of the $Na_v1.7$ F1449V mutation resulting in inherited erythromalalgia (IEM). The mutation in the *SCN9A* gene resulting in the substitution of phenylalanine to valine at position 1449 results in a collapse of the aromatic bonds likely formed through stacking interactions, resulting in the channel pore favouring an open state. This open state subsequently enables the influx of sodium ions into nociceptors, resulting in enhanced neuronal excitability and pain sensation (Dib-Hajj *et al.* 2005).

Interestingly, despite their role in nociception, *SCN9A* mutations have little effect on other sensory functions, presenting $Na_v1.7$ as an ideal target for therapeutic intervention. Despite this, identifying reagents able to bind selectively to $Na_v1.7$ has proven difficult. Initially, toxins such as tetrodotoxin (TTX) were explored for this purpose. TTX has shown binding to the Na_v channel outer-pore selectivity filter without affecting other voltage-gated cation channels. However, its inability to differentiate between some Na_v channels has provided a classification system with channels being divided into TTX-sensitive (TTX-S) and TTX-resistant (TTX-R) channels. A compound able to target TTX-R channels (present in pain-associated DRG neurones) without binding TTX-S channels (such as those present in the cardiac tissue) may provide pain relief by blocking the passage of pain

information from the DRG to the brain. Currently however TTX has only been utilised as a therapy against stroke and seizures (Grosskreutz *et al.* 1996).

The high sequence similarity between Na_v channels is a major reason for the lack of therapeutically viable TTX and has also limited the development of Na_v sub-type specific modulators. By targeting less conserved structures, such as the VSD, monoclonal antibodies with sub-type specific effects are beginning to demonstrate success (Lee *et al.* 2014).

1.2.1.2 Voltage-gated calcium channels

The voltage-gated sodium channels control the initiation of the action potential however a second family of ion channels are required for the downstream processing of action potentials to occur. These ion channels are termed voltage-gated calcium (Ca_v) channels.

Sub-divided according to their pharmacological characteristics in to L-, T- and P/Q/N/R-type channels, widespread distribution of L and T-type channels is observed whilst P, Q, N and R-type channels are most prominent in neuronal tissue. Structurally, voltage-gated calcium channels consist of a principle, transmembrane α1 subunit linked by a disulphide bond to a α2δ dimer. An associated intracellular phosphorylated β-subunit and transmembrane γ-subunit are also present (**Figure 1.1**). As with the Na_v channels, four repeated domains (I-IV) each of six transmembrane segments (S1-S6) are present with a membrane-associated P-loop between S5 and S6 (Curtis and Catterall 1984, Curtis and Catterall 1986, Takahashi *et al.* 1987, Ellis *et al.* 1988, Jay *et al.* 1990, Gurnett *et al.* 1996, Wu *et al.* 2015).

As mentioned previously, different types of Ca^{2+} currents occur, each defined by different α1 subunits of which 10 different subunits have been characterised. These subunits are divided into three families; Ca_v1, Ca_v2 and Ca_v3. L-type currents are mediated by Ca_v1 α1 subunits which are ~75% homologous. Ca_v2 α1 subunits mediate P/Q-type ($Ca_v2.1$), N-type ($Ca_v2.2$) and R-type ($Ca_v2.3$) currents. Although showing >70% homology between each other, the Ca_v2 α1 subunit demonstrates <40% homology to the Ca_v1 subunit. Finally, the distantly related Ca_v3 α1 subunit (<25% homology to the related sub-

families) mediates T-type currents. Each of the channel sub-types is responsible for various human disorders with many of the mutations responsible present within the S5-S6 regions responsible for calcium selectivity and permeability. Much of our knowledge surrounding the voltage-gated calcium channel selectivity filter comes from work carried out by the lab of William Catterall in 2014 (Tang *et al.* 2014). Despite Na^+ and Ca^{2+} being of almost identical size, 116 and 114pm respectively, the difference in charge enables voltage-gated calcium channels to conduct Ca^{2+} ions at a rate 500-fold higher than that of Na^+, a feature of Ca^{2+} channels essential for eukaryotic life. During work conducted by Catterall's lab, aspartate residues were introduced into well-known Na^+ binding sites of the previously elucidated Na_vAb selectivity filter, resulting in the 'CavAb' channel showing preferential conductance for Ca^{2+} over Na^+ (Tang *et al.* 2014). Later structural studies proposed the presence of three Ca^{2+} binding sites in the selectivity filter able to bind Ca^{2+} in its fully hydrated state. This feature alongside the enhanced electronegative properties of the channel provide preferential conductance towards Ca^{2+} over Na^+ and K^+ (Tang *et al.* 2014, Wu *et al.* 2015, Wu *et al.* 2016). During circumstances that prevent voltage-gated calcium channels from functioning in this manner, a number of disorders can occur (**Table 1.2**).

Channel	**Gene**	**Tissue**	**Disorder**	**Genetic cause**	**Reference**
$Ca_v1.1$	*CACNA1S*	Skeletal muscle	Hypokalemic Periodic Paralysis Type 1	R1239H, R1239G, R528H	(Ptacek *et al.* 1994)
			Malignant Hyperthermia	R1086H	(Monnier *et al.* 1997)
$Ca_v1.2$	CACNA1C	Cardiac	Timothy Syndrome. Brugada Syndrome	G406R G490R, A39V	(Splawski *et al.* 2004, Antzelevitch *et al.* 2007)
$Ca_v1.3$	*CACNA1D*	Neuronal, pancreatic,	Sinoatrial node dysfunction and	G403D, I770M	(Antzelevitch *et al.* 2007,

		cardiac.	deafness. Primary aldosteronism, seizures and neurological abnormalities.		Scholl *et al.* 2013)
$Ca_v1.4$	*CACNA1F*	Retinal	Incomplete congenital stationary night blindness type 2A. Cone rod dystrophy 3. Aland Island Eye disease	I745T G369D, R958X R830X G848S	(Bech-Hansen *et al.* 1998, Strom *et al.* 1998, Hemara-Wahanui *et al.* 2005, Huang *et al.* 2013)
$Ca_v2.1$	*CACNA1A*	CNS	Episodic ataxia type 2, familial hemiplegic migraine and spinocerebell-ar ataxia 6.	E1757K R1666H F1491S R1281X R1549X F1406C R1820X C287Y T666M, D715E, R192Q, V714A, I1811L R583Q V1457L	(Ophoff *et al.* 1996, Yue *et al.* 1997, Yue *et al.* 1998, Battistini *et al.* 1999, Carrera *et al.* 1999, Friend *et al.* 1999, Jen *et al.* 1999, Denier *et al.* 2001, Guida *et al.* 2001, Jen *et al.* 2001,

				I1710T R1347Q G293R	Jouvenceau *et al.* 2001, Kors *et al.* 2004, Wan *et al.* 2005, Stam *et al.* 2008)
$Ca_v2.2$	*CACNA1B*	CNS	Dystonia 23	R1389H	(Groen *et al.* 2011)
$Ca_v3.1$	*CACNA1G*	Purkinje, cerebellum, testis.	Spinocerebell-ar ataxia 42	R1715H	(Coutelier *et al.* 2015)
$Ca_v3.2$	*CACNA1H*	Cardiac, kidney, liver	Childhood absence epilepsy	F161L, E282K, V831M, G773D, R788C	(Chen *et al.* 2003)
			Generalised idiopathic epilepsy	P618L A876T	(Heron *et al.* 2007)

Table 1.2. Human voltage-gated calcium channelopathies. A number of disorders result from mutations within the voltage-gated calcium channel genome with a wide variety of tissue-specific phenotypes depending on the localisation of the various channels.

1.2.1.3 Potassium (K^+) channels

Composed of approximately 78 different genes - over half of the ion channel genome, high interest has been placed on K^+ channels as drug targets. K^+ channels can be divided into four structural sub-types including; inwardly-rectifying (2TM) channels (K_{IR}), Ca^{2+} activated (6TM or 7TM) channels (K_{Ca}), 2-pore (4TM) channels (K_{2P}) and voltage-gated (6TM) channels (K_v) (**Figure 1.3**). This vast array of sub-types, as with other channels, complicates their targeting. By targeting one disease-related channel, an alternatively localised channel of high

homology may also be targeted, resulting in unwanted and even fatal side effects. For example, hERG testing has now become a mandatory checkpoint for any drug to be approved for use by the FDA as a result of fatal side effects caused by targeting of this channel due to its localisation in cardiac tissue (Braga *et al.* 2014). Despite this, a number of K^+ channel family members have shown promise as therapeutic targets (Xu *et al.* 2010).

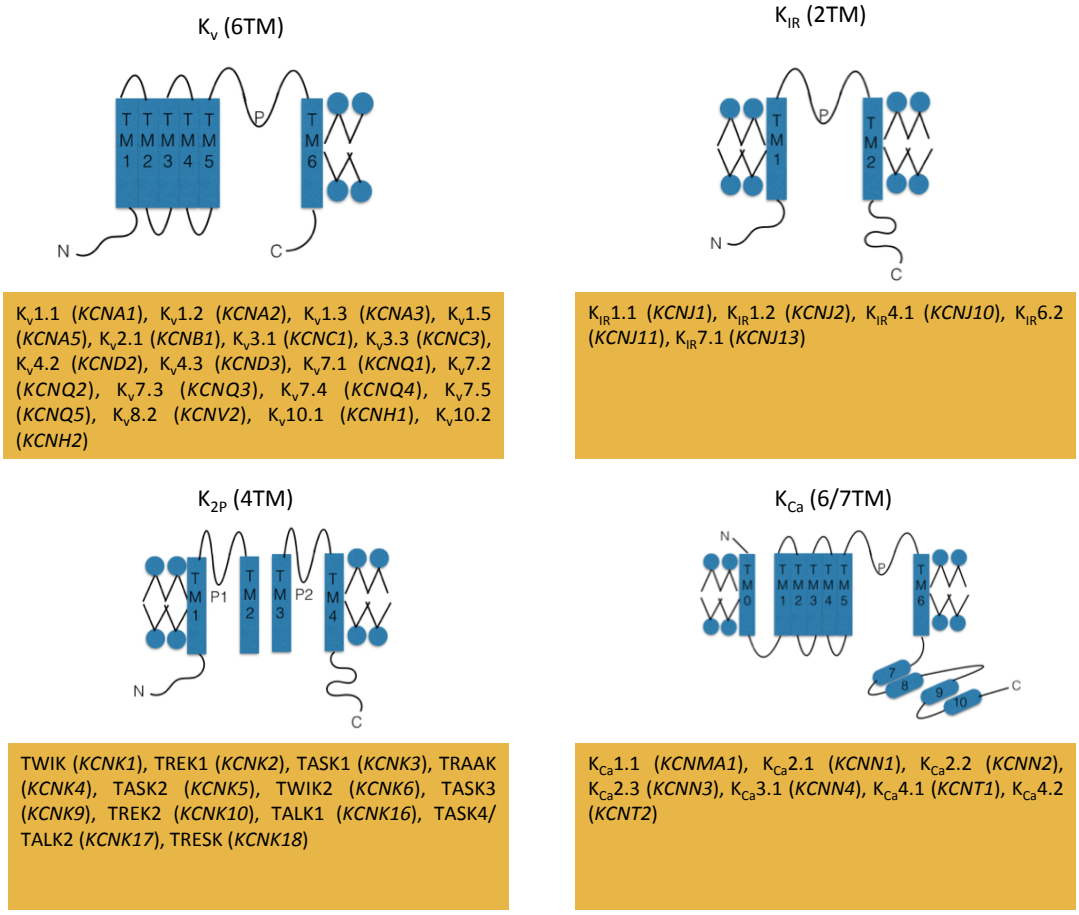

Figure 1.3. The sub-types of potassium ion channels. A large number of potassium channel families are described with further sub-types present within each family. A number of features can help to distinguish the channel families from each other such as the number of transmembrane segments present and the functional properties of the N- and C-terminal domains. A feature of potassium ion channels that has been conserved between families is the P-region containing the potassium channel signature sequence motif, TVGYG.

Despite the large number of genes encoding potassium ion channels, one particular feature that has been conserved throughout the potassium channel family is that of the signature sequence, represented by the amino acids TVGYG. This sequence provides a unique mechanism by which potassium channels are able to allow the passage of potassium ions at a rate close to that of diffusion, whilst at the same time selecting for potassium ions over sodium ions despite an identical charge and a size difference of only 36 pm. The mechanism by which the selectivity filter, and particularly the signature sequence, enables this phenomenon was elucidated in a Nobel prize winning study conducted by the lab of Roderick MacKinnon in 1998 (Doyle *et al.* 1998).

Despite similarities between different channel families such as the signature sequence, a number of differences providing unique functions and localisations are also present.

K_{IR} channels were originally termed 'anomalous' rectifier K^+ channels as a result of their unusual inward rectification, an attribute which ignored the expected behaviour of an ion channel set by the Nernst equation (Hodgkin *et al.* 1952). The basic building block of K_{IR} channels is that of cytoplasmic amino (NH_2) and carboxyl (COOH) termini joined together by two transmembrane domains (TM1 and TM2) and an extracellular pore-forming region (Heginbotham *et al.* 1994). The primary structure described above combines with homologous structures to form a functional tetrameric complex able to transport K^+ across the membrane (Glowatzki *et al.* 1995). Currently, the identity of 15 K_{IR} subunit genes has been ascertained, enabling the formation of 7 subfamilies (K_{IR}1.x to K_{IR}7.x), categorised further into classical, G-protein gated, ATP-sensitive and K^+-transport functional groups. A major problem for K_{IR}-specific drug discovery is the high level of homology set by different sub-families, a result of different patterns of heteromerization between members of the same sub-family, contributing to different functions and tissue localisation (Preisig-Muller *et al.* 2002, Schram *et al.* 2002). For a more comprehensive review of K_{IR} channel structure and localisation, readers are directed to (Hibino *et al.* 2010). As expected with such a large family of proteins, K_{IR} channel dysfunction results in a

variety of human channelopathies (**Table 1.3**).

A large number of K_{IR}-related channelopathies have been attributed to defects in the channels ability to interact with their activator ligand $PI(_{4,5})P_2$ (Huang *et al.* 1998, Lopes *et al.* 2002, Pegan *et al.* 2006, Haider *et al.* 2007, D'Avanzo *et al.* 2013).

Channel	**Gene**	**Tissue**	**Disorder**	**Genetic cause**	**Reference**
K_{IR}1.1	*KCNJ1*	Kidney	Bartter's Syndrome (Type II)	ΔW58, ΔY60, A195V, S200R, M338T A198T, G167E, D108H, P110L, V72E, V315G, W99C, A198T, ΔR338, V122E, D74Y	(Simon *et al.* 1996)
K_{IR}2.1	*KCNJ2*	Cardiac	Andersen Syndrome (LQT7)	D71V, S136F, G144S, R218W, R218Q, G300V, E303K,	(Plaster *et al.* 2001, Ai *et al.* 2002, Andelfinger *et al.* 2002, Kobori *et al.* 2004,

				ΔSWLF, ΔSY R67W R67Q G146S, T192A G215D T309I	Bendahhou *et al.* 2005)
			Short Q-T syndrome	D172N	(Priori *et al.* 2005)
$K_{IR}4.1$	*KCNJ10*	Renal, auditory and CNS	SeSAME	R65P, R199X R65C, F75L, ΔG775 R175Q	(Scholl *et al.* 2009, Reichold *et al.* 2010, Freudenthal *et al.* 2011)
			Autosomal recessive deafness 4 with enlarged vestibular aqueduct	P194H, R348C	(Yang *et al.* 2009)
$K_{IR}6.2$	*KCNJ11*	Pancreas, Neuronal, Muscle	Persistent hyperinsulinemic hypoglycaemia of infancy	L147P ΔY12 P254L H259R G156R	(Thomas *et al.* 1996, Nestorowicz *et al.* 1997, Tornovsky *et al.* 2004, Marthinet *et al.* 2005, Pinney *et al.*

					2008)
			Permanent neonatal diabetes	R201H, V59M, R201C, V59G F60Y, V64L C42R R201H	(Colombo *et al.* 2005, Yorifuji *et al.* 2005, Gloyn *et al.* 2006, Gloyn *et al.* 2006, Mannikko *et al.* 2010)
$K_{IR}7.1$	*KCNJ13*	GI tract, kidney, CNS	Snowflake vitreoretinal degeneration	R162W	(Hejtmancik *et al.* 2008)
			Leber congenital amaurosis 16	R66X, L241P	(Sergouniotis *et al.* 2011)

Table 1.3. Human diseases resulting from K_{IR} channel mutations. Mutations resulting in K_{IR} channelopathies occur in a variety of regions of the channel, responsible for different functions. These regions include amino acids (AA) 58-99, the N-terminal cytoplasmic domain, and AA 100-200 that includes the pore-forming regions alongside the selectivity filter. The majority of mutations however are located in the cytoplasmic C-terminus (AA 200-300). Many of the aforementioned mutations have been linked with defects in $PI(_{4,5})P_2$ binding and thus aberrant downstream signalling (Huang *et al.* 1998, Lopes *et al.* 2002, Donaldson *et al.* 2003, Pegan *et al.* 2006, Haider *et al.* 2007)

K_{Ca}//K_{Na} channels differ from K_{IR} channels structurally in that they contain a greater number of transmembrane segments and a much larger C-terminus that plays an important role in channel gating. K_{Ca}/K_{Na} channels can be sub-divided into two distantly related groups; small (SK) and intermediate-conductance (IK) channels referred to as $K_{Ca2.x}$ and $K_{Ca3.1}$ (Kohler *et al.* 1996, Ishii *et al.* 1997, Joiner *et al.* 1997), respectively. Both small and intermediate conductance channels play a role in Ca^{2+}-signalling through binding of Ca^{2+} to calmodulin constitutively

bound to the C-terminus of the channel. This interaction activates the channel making it conductive to K^+, independent of voltage. A second group of K_{Ca} channels are the Slo channels; $K_{Ca1.1}$/Slo1 (big conductance or BK), $K_{Ca4.1}$/Slo2.2 (now referred to as $K_{Na1.1}$), $K_{Ca4.2}$/Slo2.1 (now referred to as $K_{Na1.2}$) and $K_{Ca5.1}$/Slo3. Unlike binding of calcium to channel-bound calmodulin, binding of Ca^{2+} to $K_{Ca1.1}$ takes place via three divalent cation-binding sites within the C-terminus (Schreiber and Salkoff 1997, Bao *et al.* 2002, Shi *et al.* 2002, Xia *et al.* 2002). This binding leads to channel opening in a voltage-dependent manner. It has been hypothesised that a calcium-binding domain resides adjacent to the S6 segment of the channel, resulting in gating changes of the channel up on calcium binding. This binding by calcium results in exposure of a hydrophobic patch of the calcium-binding domain, enabling interaction with a neighbouring domain, subsequently causing a conformational change that promotes opening of the channel (Schumacher *et al.* 2001). Functionally, the other three members of this group are perhaps inaccurately named, as they are activated by other ions, rather than by Ca^{2+}. As a result, they have more recently received up-to-date nomenclature with $K_{Ca4.1}$ being referred to as $K_{Na1.1}$ and $K_{Ca4.2}$ being referred to as $K_{Na1.2}$, a result of their activation by Na^+. Despite their functional differences, their association with this group is based solely on structural characteristics (Schreiber *et al.* 1998, Yuan *et al.* 2003). As described, BK channels differ structurally to SK channels in that they contain seven transmembrane segments (SK contain six) and also contain four intracellular, hydrophobic segments that form the three cation binding sites. The SK channels contain a calmodulin-binding domain.

A number of disorders have been identified resulting from K_{Ca} channel defects. The defects have been found to be present mainly in the C-terminal calcium-binding region, or 'calcium bowl' (**Figure 1.4**). A BK/ $K_{Ca1.1}$ mutation found within the 'calcium bowl', D434G, results in generalised epilepsy and paroxysmal dyskinesia whilst two separate mutations, R352H and V282M, identified in the $K_{Ca3.1}$, or Gardos channel, result in chronic congenital haemolytic anaemia (Du *et al.* 2005, Andolfo *et al.* 2015, Glogowska *et al.* 2015, Rapetti-Mauss *et al.* 2015).

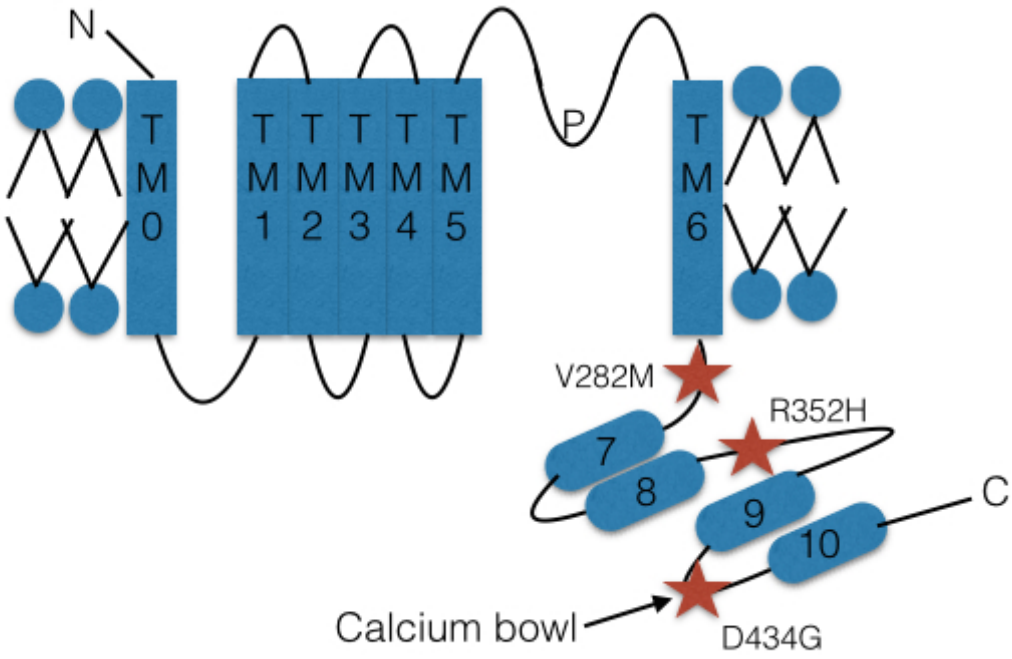

Figure 1.4. K_{Ca} channel mutations resulting in human disease. A number of novel mutations have been identified in K_{Ca} channels, specifically, the BK/$K_{Ca1.1}$ and $K_{Ca3.1}$/ Gardos channels, resulting in the human disorders, generalised epilepsy with paroxysmal dyskinesia and chronic congenital haemolytic anaemia, respectively. All mutations are located in the C-terminal calcium-binding domain of the channels and thus are likely to influence calcium binding and as a result, channel activation.

The class of channel responsible for background 'leak' potassium current was not discovered until 1996, a date by which the cDNA's of all other potassium channel families had been cloned. The name given to this family of channel, two-pore domain potassium channel, or K_{2P}, is based on the unique (among potassium channels) topology. Each sub-unit contains two P-loops (contrasting with other potassium channels which contain one P-loop) that then dimerize to form four P-loops, forming the functional K^+ selectivity filter (Enyedi and Czirjak 2010). The high number of K_{2P} subunits with wide expression levels results in contribution by the K_{2P} channel family to a number of human disorders. These disorders have been outlined in a recent review by Es-Salah-Lamoureux (Es-Salah-Lamoureux *et al.* 2010). Each subfamily plays a role in various disorders including cancer

progression, pain disorders and kidney disorders (**Figure 1.5**) (Heurteaux *et al.* 2004, Heurteaux *et al.* 2006, Barel *et al.* 2008, Kucheryavykh *et al.* 2009, Dillon *et al.* 2010, Santarius *et al.* 2010, Bittner *et al.* 2011, Andres-Enguix *et al.* 2012, Chatelain *et al.* 2012, Cho *et al.* 2012, Fischer *et al.* 2012, Ma *et al.* 2013, Williams *et al.* 2013, Friedrich *et al.* 2014, Lenzini *et al.* 2014, Pandit *et al.* 2014, Perry *et al.* 2014, Toncheva *et al.* 2014, Rivera-Pagan *et al.* 2015). Their recent discovery and widespread localisation however presents a high likelihood of further human disorders caused by K_{2P} defects yet to be revealed.

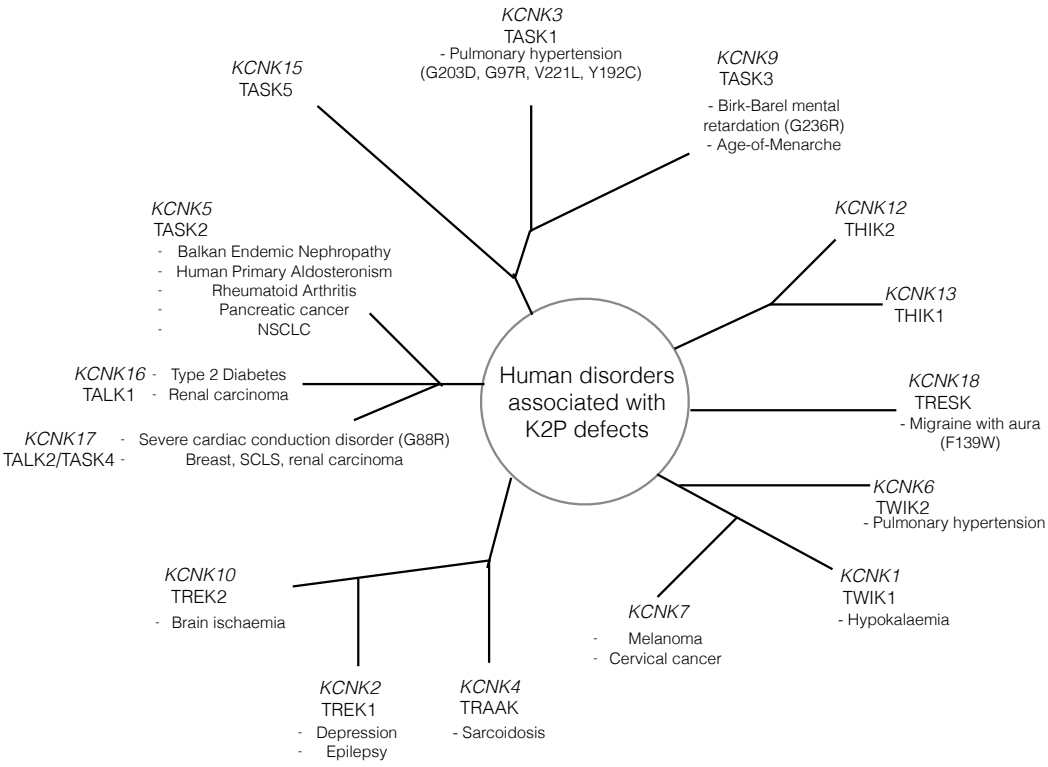

Figure 1.5. Human disorders caused by defects within K_{2P} channels. A myriad of disorders result from defects in the K_{2P} genome, either a result of missense mutation, over- or under-expression. The widespread tissue localisation of these channels results in a range of human disorders associated with different systems of the human body.

Whilst the channels responsible for the depolarisation stage of an action potential, Na_v channels, have already been discussed, this highly organised process enabling the conduction of millions of pieces of information every second would be impossible without the proteins that enable the action

potential to repolarise, namely voltage-gated potassium (K_v) channels. These channels are highly selective for K^+ ions and upon opening, K^+ flows down its concentration gradient into the extracellular space and in doing so, returns the membrane potential back to a negative value. This enables, after a brief period of hyperpolarisation, the action potential to re-occur.

K_v channels are homotetrameric channels with each subunit containing a voltage-sensor and contributing to the central pore and composed of six transmembrane regions. The already noted K^+ channel signature sequence, TVGYG, enables the potassium channel to be highly selective for potassium ions and also enables passage through the channel at a limit close to that of diffusion. This selectivity and speed is essential for allowing the action potential to occur at such high velocity – approximately 1 millisecond in duration. During the depolarisation stage of the action potential, as positively charged Na^+ flows into the cell, the enhanced positive charge activates other channels, including those of voltage-gated potassium channels (as well as Cl^- channels). Activation of these channels results in action potential termination by returning the cytoplasmic charge to a negative, or resting value. For this to happen efficiently, high throughput and selectivity are essential. K_v channels have a number of features that enable high throughput alongside high selectivity; a water-filled cavity that provides an 'attractive' environment for the K^+ ions, stabilisation of cations at the channel intracellular vestibule by *p*-helix negative dipoles, mimicking of surrounding oxygen atoms of water by backbone carbonyl oxygens of the selectivity filter, and finally electrostatic repulsion between queuing K^+ ions produces rapid permeation through the channel essentially preventing a 'traffic jam' from building in the filter (Doyle *et al.* 1998, Morais-Cabral *et al.* 2001, Zhou *et al.* 2001, Jiang *et al.* 2002).

As important as high throughput and selectivity, the ability to stop the flow of K^+ through the channel is also a requirement, a phenomenon termed 'gating'. Three mechanisms are known to enable this process; shutting at the intracellular opening via the intracellular region of the S6 transmembrane segment, a primary target for channel blockers such as anti-convulsion therapies

(Liu *et al.* 1997, Holmgren *et al.* 1998, del Camino and Yellen 2001). Secondly, a mechanism termed 'ball and chain gating' or N-type inactivation (due to the pore blocking by an N-terminal 'ball') controls gating. This N-terminal peptide can be associated with either the α-subunit or an associated β-subunit of which sequence conservation between voltage-gated potassium channels as well as mutation studies demonstrates its importance in control of channel activation (Hoshi *et al.* 1990, Murrell-Lagnado and Aldrich 1993, Rettig *et al.* 1994). Finally, constriction of the selectivity filter region itself can result in channel inactivation, a process termed C-type inactivation. This process is hypothesised to take place via 'collapse' of the carbonyl oxygen groups of the signature sequence into the pore, a hypothesis explained by the increased conduction of the normally excluded and smaller Na^+ ion (Kiss *et al.* 1999). These channel structural features enabling high throughput, selectivity and gating to take place provides channel regions to exploit for modulation. Indeed, a variety of human disorders have occurred as a result of mutations to these channel regions, resulting in defective channel function. Due to the widespread distribution of K_v channels, even those within the same sub-family, throughout the body, different types of disorders are linked with each channel. As an example, whilst K_v1.1 (*KCNA1*) is found in kidney and muscle, myokymia with episodic ataxia results from *KCNA1* defect. However, the close relative of K_v1.1, K_v1.2 (*KCNA2*) is found localised within the central nervous system, of which mutation results in epileptic encephalopathy. In addition to widespread localisation throughout the body, widespread occurrence of mutations within the channel itself are observed (**Figure 1.6**).

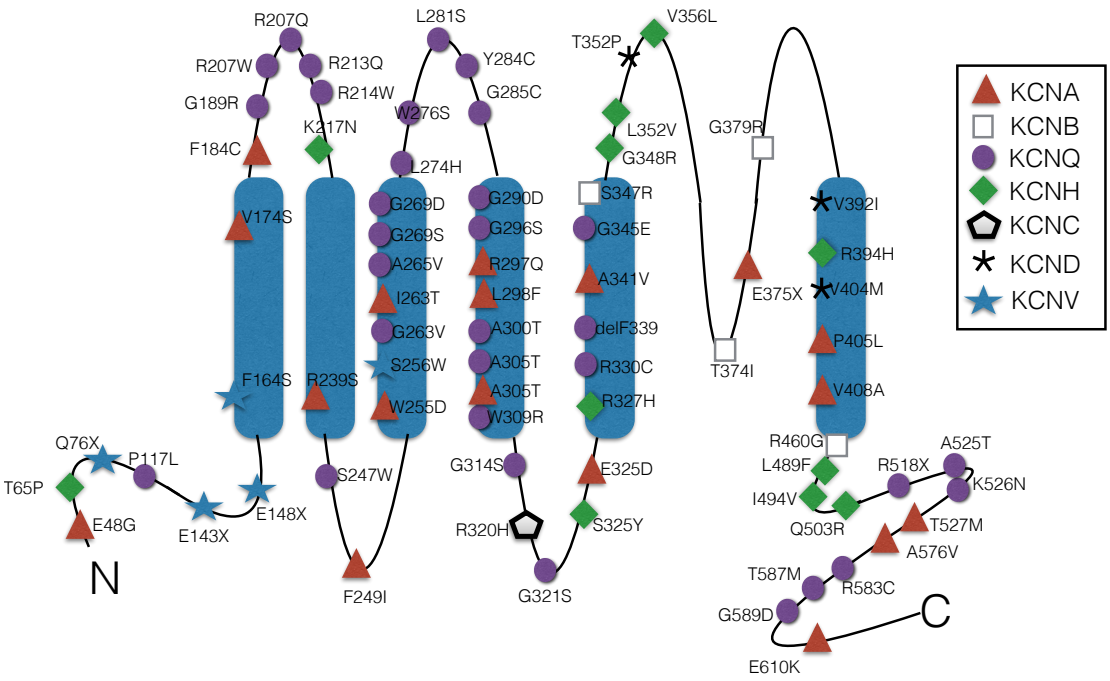

Figure 1.6. Voltage-gated potassium channel mutations resulting in human disorders. A large array of channel mutations of a variety of voltage-gated potassium channel sub-families are depicted. These sub-families include *KCNA*, *KCNB*, *KCNQ*, *KCNH*, *KCNC*, *KCND* and *KCNV*. The majority of disorders caused by channel mutations are observed in the *KCNQ* gene encoding the $K_v7.x$ sub-family of potassium channels (Browne *et al.* 1994, Russell *et al.* 1996, Wang *et al.* 1996, Donger *et al.* 1997, Neyroud *et al.* 1997, Ackerman *et al.* 1998, Priori *et al.* 1998, Singh *et al.* 1998, Jongbloed *et al.* 1999, Larsen *et al.* 1999, Dedek *et al.* 2001, Piippo *et al.* 2001, Schwartz *et al.* 2001, Chen *et al.* 2003, Olson *et al.* 2006, Glaudemans *et al.* 2009, Yang *et al.* 2009, Christophersen *et al.* 2013, Juang *et al.* 2014, Torkamani *et al.* 2014, Muona *et al.* 2015, Pena and Coimbra 2015, Syrbe *et al.* 2015).

1.2.2 Ligand-gated ion channels

A problem associated with targeting the described voltage gated channels is the lack of exposed binding surfaces available. In contrast, the ligand-gated ion channels contain a large extracellular domain required for binding their native ligand. This large domain provides an ideal binding interface for potential modulators.

The Cys-loop family of receptors are ligand-gated ion channels comprising the $GABA_A$, nicotinic acetylcholine (nAChR), 5-hydroxytryptamine serotonin type 3 ($5\text{-}HT_3R$) and glycine (GlyR) receptors. $GABA_A$ receptor subunits are encoded by 19 different subunits; 6 α subunits, three β subunits, three γ subunits, three ρ subunits, and one each of the ε, δ, θ and μ subunits. The major adult isoform of $GABA_A$ is accepted to be composed of α2, β2 and γ1 subunits to form a functional pentameric protein. As a chloride-selective ion channel localised in the central nervous system, activation of $GABA_A$ by its ligand, GABA, results in the depression of neuronal excitability. Each subunit contains an extracellular domain of approximately 250 amino acids, highlighting the potential for using this region of the receptor for drug development purposes. Historically, structural information for the $GABA_A$ receptor was limited with the most closely related structure available being that of the nAChR (Miyazawa *et al.* 2003) however more recently, the structural elucidation of the human $GABA_A$ receptor at high resolution is likely to enable improvements in our knowledge of how the $GABA_A$ receptor interacts with its ligands and as a result, improvements in developing reagents that are able to disrupt these interactions (Miller and Aricescu 2014). The structure resolved in this study also provides a high level of detail of the determinants of assembly between the five subunits of $GABA_A$, selected from a possible 19 subunits. For example, within the upper portion of the extracellular domain, interactions between Arg26 and Asp17 alongside interactions between Asp24 and Lys13, results specifically in α-β and β-β subunit combinations. The neurotransmitter-binding pocket has also been revealed by this study with equivalent motifs of adjacent α-subunits being largely responsible. One particularly important observation in terms of producing reagents by screening methods that utilise recombinant protein is the importance of N-linked glycosylation to $GABA_A$ function. Asn149, a residue that undergoes glycosylation, is conserved in almost all $GABA_A$, nACh and $5\text{-}HT_3$ receptor subunits. Furthermore, substitution of this residue in $GABA_A$ receptors reduces sensitivity to GABA, suggesting a change in conformation. As a result, in attempts at identifying reagents that are able to perturb the native $GABA_A$ receptor interaction with GABA, it is likely to be critical that any recombinant

protein used for screening is produced in a manner amenable to glycosylation. The expression of the $GABA_A$ receptor in the central nervous system alongside the observation of reduced pain sensation following $GABA_A$ receptor activation, has implicated this receptor as a target for treating chronic pain. A major problem in the treatment of pain via GABAergic activation is the simultaneous activation of GABA-expressing neurones that are not involved in pain perception, resulting in CNS side effects such as sedation. Ultimately, treatment of chronic pain through GABAergic mechanisms is likely to only be possible when the molecular mechanisms are further investigated, for example, differences in GABA receptors involved in the pain pathway compared to those present in non-nociceptive neurones (Enna and McCarson 2006).

Like $GABA_A$ receptors, nAChR's are also pentamers that can be made up of a combination of subunits encoded by 17 genes. Unlike $GABA_A$ receptors however, the predominant subunit combination is dependent on the tissue localisation. For example, the neuromuscular junction consists of $(\alpha1)_2\beta1\delta\varepsilon$ subunits while $(\alpha1)_2\beta1\gamma\delta$ subunits predominate in denervated skeletal muscle (Gotti *et al.* 2009). This presence of different populations of subunits in different tissues opens the possibility of targeting this receptor for the treatment of chronic pain, as off-target effects are less likely. Recently, α9-containing receptors have been postulated as a potential target for chronic pain treatment due to their localisation in immune cells, thus combating symptoms associated with inflammatory pain (Hone *et al.* 2018).

The $5\text{-}HT_3$ receptor is a pentamer consisting of four transmembrane subunits that forms a cation-selective channel. Five human $5\text{-}HT_3$ receptor subunits have been identified with $5\text{-}HT_3A$ subunits forming homomeric channels. The other four subunits (B, C, D and E) do not form homomeric channels however are able to influence expression characteristics by forming heteromeric channels with $5\text{-}HT_3A$ subunit. Recently, the reagent tropisetron has been identified as a potential anti-nociceptive reagent through its inhibitory action of $5\text{-}HT_3$ receptors in the central nervous system (Nasirinezhad *et al.* 2016).

Extracellular acidosis caused by a reduction in pH is often detected during

the release of chemical mediators of pain. This detection takes place by a sub-set of ion channels termed acid-sensing ion channels (ASICs).

Interestingly, the black mamba venom, mambalgin-1, has highlighted the ability of different ASIC sub-units to mediate pain peripherally and centrally, as central pain inhibition caused by mambalgin-1 were dependent on ASIC1A and ASIC2A, whilst peripheral effects were dependent on ASIC1B. This observation offers the possibility of treating pain with limited centrally occurring side effects such as sedation and nausea (Diochot *et al.* 2012).

1.2.3 Targeting TRP and P2X channels in the treatment of chronic pain

The high level of homology between ion channel subtypes can complicate their targeting. One family of ion channels that demonstrate reduced homology are the Transient Receptor Potential (TRP) channels. TRP channel members contain six transmembrane segments that vary in sequence similarity. Unlike the previously described cation-specific channels, TRP channels have a wider range of ion selectivity, a result of their increased sequence and structural diversity (Voets *et al.* 2004, Wu *et al.* 2010), as demonstrated by the TRPV channel subtypes (**Figure 1.7**).

```
TRPV1      MKKWSSTDLGAAADPLQKDT------------------------------CPDPLDGDPN    30
TRPV2      MT-------SPSSSPVF--------------------------------RLETLDGGQE    20
TRPV3      ----------MKAHPKEMVPLMGKRVAAPSGNPAI-------------------LPE---    28
TRPV4      ---MADSSEGPRAGPGEVAELPGDESGTPGGEAFPLSSLANLFEGEDGSLSPSPADASRP    57
TRPV5      ------------------------------------------------------------    0
TRPV6      ------------------------------------------------MGPLQGDGGPA    11


TRPV1      SRPPPAKPQLSTAKSR----------TRLFGKGDSEEA------------------FPVD    62
TRPV2      DGSE--------ADRG----------KLDFGSGLP----------------------PME    40
TRPV3      KRPAEITPTKKSAHF-----------FLEIEGFEPNPT--------VAKTSPPVFSKPMD    69
TRPV4      AGPGDGRPNLRMKFQ------------GAFRKGVPNPIDLLESTLYESSVVPGPKKAPMD    105
TRPV5      ----------------------------MGGFLPKAE------------------GPGS    13
TRPV6      LGGADVAPRLSPVRVWPRPQAPKEPALHPMGLSLPKEK------------------GLIL    53
                                        :


TRPV1      CPHEEGELDSCPTITVSPVITIQRPGDGPTGARLLSQDSVAAS----TEKTLRLYDRRSI    118
TRPV2      SQFQGEDRKFAPQIRVNL---NYRKG--------------TGA----SQPDPNRFDRDRL    79
TRPV3      SNIRQCISGNCDDM-----DSPQSPQDDVT-ETPSNPNSPSAQLAKEEQRRKKRRLKKRI    123
TRPV4      SLFDYGTYRHHSSD-------NKRWRKKIIEKQPQSPKAPAPQ----PPPILKVFNRPIL    154
TRPV5      QLQ----KLLPSF-----LVREQDWDQHLDKLHML---------------QQKRILESPL    49
TRPV6      CLW----SKFCRW-----FQRRESWAQSRDEQNLL---------------QQKRIWESPL    89
                                                              .   .  :


TRPV1      FEAVAQNNCQDLESLLLFLQKSKKHLTDN--------EFKDPETGKTCLLKAMLNLHDGQ    170
TRPV2      FNAVSRGVPEDLAGLPEYLSKTSKYLTDS--------EYTEGSTGKTCLMKAVLNLKDGV    131
TRPV3      FAAVSEGCVEELVELLVELQELCRRRHDEDVPDFLMHKLTASDTGKTCLMKALLNINPNT    183
TRPV4      FDIVSRGSTADLDGLLPFLLTHKKRLTDE--------EFREPSTGKTCLPKALLNLSNGR    206
TRPV5      LRASKENDLSVLRQLLLDC--TCD-------------VRQRGALGETALHIAALY--DNL    92
TRPV6      LLAAKDNDVQALNKLLKYE--DCK-------------VHQRGAMGETALHIAALY--DNL    132
           :     .    *  *                           *:*.*  * *    .


TRPV1      NTTIPLLLEIARQTDSLKELVNASYTDSYYKGQTALHIAIERRNMALVTLLVENGADVQA    230
TRPV2      NACILPLLQIDRDSGNPQPLVNAQCTDDYYRGHSALHIAIEKRSLQCVKLLVENGANVHA    191
TRPV3      KEIVRILLAFAEENDILGRFINAEYTEEAYEGQTALNIAIERRQGDIAALLIAAGADVNA    243
TRPV4      NDTIPVLLDIAERTGNMREFINSPFRDIYYRGQTALHIAIERRCKHYVELLVAQGADVHA    266
TRPV5      EAA-LVLM------EAAPELVFEPTTCEAFAGQTALHIAVVNQNVNLVRALLTRRASVSA    145
```

```
TRPV6      EAA-MVLM------EAAPELVFEPMTSELYEGQTALHIAVVNQNMNLVRALLARRASVSA    185
           :     *:           ::        : *::**:**: .:    .  *:   *.* *

TRPV1      AAHGDFFKKTKGRPGFYFGELPLSLAACTNQLGIVKFLLQNSWQTADISARDSVGNTVLH    290
TRPV2      RACGRFFQKGQG-TCFYFGELPLSLAACTKQWDVVSYLLENPHQPASLQATDSQGNTVLH    250
TRPV3      HAKGAFFNPKYQHEGFYFGETPLALAACTNQPEIVQLLME--HEQTDITSRDSRGNNILH    301
TRPV4      QARGRFFQPKDEGGYFYFGELPLSLAACTNQPHIVNYLTENPHKKADMRRQDSRGNTVLH    326
TRPV5      RATGTAFRRSPR-NLIYFGEHPLSFAACVNSEEIVRLLIE---HGADIRAQDSLGNTVLH    201
TRPV6      RATGTAFRRSPC-NLIYFGEHPLSFAACVNSEEIVRLLIE---HGADIRAQDSLGNTVLH    241
            * *  *.       :**** **::***.:.  :*  * :   . :.:   ** **.:**

TRPV1      ALVEVADNTADNTKFVTSMYNEILMLGAKLHPTLKLEELTNKKGMTPLALAAGTGKIGVL    350
TRPV2      ALVMISDNSAENIALVTSMYDGLLQAGARLCPTVQLEDIRNLQDLTPLKLAAKEGKIEIF    310
TRPV3      ALVTVAEDFKTQNDFVKRMYDMILLRSGN----WELETTRNNDGLTPLQLAAKMGKAEIL    357
TRPV4      ALVAIADNTRENTKFVTKMYDLLLLKCARLFPDSNLEAVLNNDGLSPLMMAAKTGKIGIF    386
TRPV5      ILILQ-----PNKTFACQMYNLLLSYDGHGDHLQPLDLVPNHQGLTPFKLAGVEGNTVMF    256
TRPV6      ILILQ-----PNKTFACQMYNLLLSYDRHGDHLQPLDLVPNHQGLTPFKLAGVEGNTVMF    296
            *:        :  :.  **: :*    .      *:   * ..::*: :*.  *:  ::

TRPV1      AYILQREIQEPECRHLSRKFTEWAYGPVHSSLYDLSCIDTCEKN-SVLEVIAYSSSETPN    409
TRPV2      RHILQREFS--GLSHLSRKFTEWCYGPVRVSLYDLASVDSCEEN-SVLEIIAFHC-KSPH    366
TRPV3      KYILSREIKEKRLRSLSRKFTDWAYGPVSSSLYDLTNVDTTTDN-SVLEITVYNT-NIDN    415
TRPV4      QHIIRREVTDEDTRHLSRKFKDWAYGPVYSSLYDLSSLDTCGEEASVLEILVYNS-KIEN    445
TRPV5      QHLMQK-----------RRHIQWTYGPLTSILYDLTEIDSWGEELSFLELVVSSD--KRE    303
TRPV6      QHLMQK-----------RKHTQWTYGPLTSTLYDLTEIDSSGDEQSLLELIITTK--KRE    343
            ::: :           *:. :* ***:   ****: :*:  .: *.**:         .

TRPV1      RHDMLLVEPLNRLLQDKWDRFVKRIFYFNFLVYCLYMIIFTMAAYYRPVDG--LP-----    462
TRPV2      RHRMVVLEPLNKLLQAKWDLLIPK-FFLNFLCNLIYMFIFTAVAYHQPTLKKQAA-----    420
TRPV3      RHEMLTLEPLHTLLHMKWKKFAKHMFFLSFCFYFFYNITLTLVSYYRPREEEAIPH----    471
TRPV4      RHEMLAVEPINELLRDKWRKFGAVSFYINVVSYLCAMVIFTLTAYYQPLEG--TP-----    498
TRPV5      ARQILEQTPVKELVSFKWNKYGRPYFCILAALYLLYMICFTTCCVYRPLKFRGGNRTHSR    363
TRPV6      ARQILDQTPVKELVSLKWKRYGRPYFCMLGAIYLLYIICFTMCCIYRPLKPRTNNRTSPR    403
            : ::   *:: *:  **       * :         . :*  . ::*

TRPV1      ----------PFKMEKTGDYFRVTGEILSVLGGVYFFFRGIQ-YFLQRRP-SMKTLFVDS    510
TRPV2      ----------PHLKAEVGNSMLLTGHILILLGGIYLLVGQLW-YFWRRHV-FIWISFIDS    468
```

```
TRPV3      ----------PLALTHKMGWLQLLGRMFVLIWAMCISVKEGIAIFLLRPS-DLQSILSDA    520
TRPV4      ----------PYPYRTTVDYLRLAGEVITLFTGVLFFFTNIKDLFMKKCP-GVNSLFIDG    547
TRPV5      DITILQQKLLQEAYETREDIIRLVGELVSIVGAVIILLLEIPDIFRVGASRYFGKTILGG    423
TRPV6      DNTLLQQKLLQEAYMTPKDDIRLVGELVTVIGAIIILLVEVPDIFRMGVTRFFGQTILGG    463
                          . : : *.:. :. .: : .      *       .   : ..

TRPV1      YSEMLFFLQSLFMLATVVLYFSHLKEYVASMVFSLALGWTNMLYYTRGFQQMGIYAVMIE    570
TRPV2      YFEILFLFQALLTVVSQVLCFLAIEWYLPLLVSALVLGWLNLLYYTRGFQHTGIYSVMIQ    528
TRPV3      WFHFVFFIQAVLVILSVFLYLFAYKEYLACLVLAMALGWANMLYYTRGFQSMGMYSVMIQ    580
TRPV4      SFQLLYFIYSVLVIVSAALYLAGIEAYLAVMVFALVLGWMNALYFTRGLKLTGTYSIMIQ    607
TRPV5      PFHVIIITYASLVLVTMVMRLTNTNGEVVPMSFALVLGWCSVMYFTRGFQMLGPFTIMIQ    483
TRPV6      PFHVLIITYAFMVLVTMVMRLISASGEVVPMSFALVLGWCNVMYFARGFQMLGPFTIMIQ    523
             ..: :  : : : :  : :   .  :  :  ::.*** . :*::**::  * :::**:

TRPV1      KMILRDLCRFMFVYIVFLFGFSTAVVTLIEDGKNDSLPSESTSH----RWRGPACRPPDS    626
TRPV2      KVILRDLLRFLLIYLVFLFGFAVALVSLSQEAWRPEAPTGPNATESVQPMEGQEDEGNGA    588
TRPV3      KVILHDVLKFLFVYIVFLLGFGVALASLIEKCPKD--------------------NKDCS    620
TRPV4      KILFKDLFRFLLVYLLFMIGYASALVSLLNPCANMKVCNEDQTNCTVPT--YPSCRDS--    663
TRPV5      KMIFGDLMRFCWLMAVVILGFASAFYIIFQTEDPT-------------------------    518
TRPV6      KMIFGDLMRFCWLMAVVILGFASAFYIIFQTEDPE-------------------------    558
           *::: *: :*  :  :.::*:. *.  : :

TRPV1      SYNSLYSTC---LELFKFTIGMGDLEFTENYDFKAVFIILLLAYVILTYILLLNMLIALM    683
TRPV2      QYRGILEAS---LELFKFTIGMGELAFQEQLHFRGMVLLLLLAYVLLTYILLLNMLIALM    645
TRPV3      SYGSFSDAV---LELFKLTIGLGDLNIQQNSKYPILFLFLLITYVILTFVLLLNMLIALM    677
TRPV4      --ETFSTFL---LDLFKLTIGMGDLEMLSSTKYPVVFIILLVTYIILTFVLLLNMLIALM    718
TRPV5      SLGQFYDYPMALFTTFELFLTVIDAPANYDVDLPFMFSIVNFAFAIIATLLMLNLFIAMM    578
TRPV6      ELGHFYDYPMALFSTFELFLTIIDGPANYNVDLPFMYSITYAAFAIIATLLMLNLLIAMM    618
               :       :  *:: : : :     . .   :  :   :: ::: :*:**::**:*

TRPV1      GETVNKIAQESKNIWKLQRAITILDTEKSFLKCMRKAFRSGKLLQVGYTPDGKDDYRWCF    743
TRPV2      SETVNSVATDSWSIWKLQKAISVLEMENGYWWCRK-KQRAGVMLTVGTKPDGSPDERWCF    704
TRPV3      GETVENVSKESERIWRLQRARTILEFEKMLPEWLRSRFRMGELCKVA-----EDDFRLCL    732
TRPV4      GETVGQVSKESKHIWKLQWATTILDIERSFPVFLRKAFRSGEMVTVGKSSDGTPDRRWCF    778
TRPV5      GDTHWRVAQERDELWRAQVVATTVMLERKLPRCLWPR--SGI-CGCE----FGLGDRWFL    631
TRPV6      GDTHWRVAHERDELWRAQIVATTVMLERKLPRCLWPR--SGI-CGRE----YGLGDRWFL    671
           .:*   :: :   :*: * . : :  *.           *            . *  :
```

```
TRPV1      RVDEVNWTTWNTNVGIINEDPGNCEGVKRTLSFSLRSS----RVSGRHWKNFALVPLL-R    798
TRPV2      RVEEVNWASWEQTLPTLCEDPSGA-GVPRTLENPVLASPPKEDEDGASEENYVPVQLL-Q    762
TRPV3      RINEVKWTEWKTHVSFLNEDPGPVRRTDFN----KIQDSSRN-NSKTTLNAFEEV-EE--    784
TRPV4      RVDEVNWSHWNQNLGIINEDPGKNETYQYY-GFSHT----VGRLRRDRWSSVVPRVVELN    833
TRPV5      RVENHNDQNPL--------------RVLRYVEVFKNSD--KEDDQEHPSEKQP-SGAE-S    673
TRPV6      RVEDRQDLNRQ--------------RIQRYAQAFHTRG--SEDLDKDSVEKLE-LG----    710
           *::: :                                              .

TRPV1      EASARDR-----------QSA-QPEEVYLRQFSGSLKPEDAEVFKSPAASGEK-----      839
TRPV2      SN-----------------------------------------------------      764
TRPV3      ---FPETSV-----------------------------------------------      790
TRPV4      KNSNPDEVVVPLDSMGNPRCD-GHQQGYPRKWRT----DDAPL---------------      871
TRPV5      GTLARASLALPTSSLSRTASQSSSHRGWEILRQNTLGHLNLGLNLSEGDGEEVYHF--      729
TRPV6      -CPFSPHLSLPMPSVSRST--SRSSANWERLRQGTLRRDLRGIINRGLEDGESWEYQI      765
```

Figure 1.7. Sequence alignment of the six TRPV channel subtypes. Six TRPV channel subtypes have been identified, all sharing different levels of amino acid similarity. These differences in amino acid sequence provides sites that may enable channel selective therapeutic targeting. * = present in all subtypes, : and . = similar properties shared between amino acids present in all subtypes.

TRP channels are located in a wide variety of physiological tissues including the CNS, playing a fundamental role in temperature sensation (Nilius and Owsianik 2011). Despite our knowledge of TRP channels still being at an early stage, a role in the pain pathway has been identified, particularly for TRPV1, TRPM8 and TRPA1. For example, TRPV1 gene silencing in mice diminishes thermal hyperalgesia following tissue injury (Szallasi *et al.* 2007). This analgesic potential of TRPV1 knockdown would suggest agonists as pain causing. However, agonists of TRPV1, such as capsaicin and resiniferatoxin (RTX) were initially tested as analgesics due to their ability to desensitise the channel, albeit, following an initially painful stimulus. Desensitisation occurs as a result of calcium overload in nociceptors resulting in cell death and thus an inability to detect painful stimuli. Furthermore, increased secretion of analgesic substances occurs (Szolcsanyi 2004). Capsaicin-containing creams such as Zostrix have been developed based

on this desensitisation phenomenon. RTX is a capsaicin-analogue with increased potency and its ability to induce permanent analgesia caters for unique clinical needs, such as patients with terminal illness. Human trials are currently in progress (Brown *et al.* 2005, Menendez *et al.* 2006, ClinicalTrials.gov 2014). However, prolonged use of TRP channel activators can cause ablation of the targeted nerve endings, making their pain-relieving use undesired (Jancso *et al.* 1977, Anand and Bley 2011). These problems with long-term use of TRPV1 agonists have prompted antagonist development. Examples include GRC-15133 (Glenmark), SB-705598 (GlaxoSmithKline) and MK-2295 (Merck/Neurogen). Despite initial success, side effects including hyperthermia and impaired heat sensation were noted – cases serious enough to halt clinical development. As an example, potential for scalding was reported with the use of MK-2295 (Eid 2009). In response, second-generation TRPV1 antagonists with limited effect on thermoception are in development, including AS1928370 and A-1165442 by Astellas and Abbott, respectively (Watabiki *et al.* 2011).

The literature demonstrates a four-fold greater interest in the causal link between TRPV1 and pain in comparison to the role of TRPA1 in pain conditions. Despite this, TRPA1 channels have shown promise in their ability to desensitise against pain. The major TRPA1 activator, curcumin has a similar desensitisation mechanism to that of capsaicin on TRPV1 channels. This mechanism is exploited by the pain-relief medication, Curamin (Nurullahoglu *et al.* 2014). TRPA1 inhibitors such as HC-030031 and Resolvins (RvD1, RvD2 and RvE1) have also shown success in pain models (Eid *et al.* 2008, Kwan *et al.* 2009, Park *et al.* 2011, Radresa O 2013).

The ability of ATP to induce pain makes the ATP-activated P2X channels a primary candidate in the search for pain therapies. Classified as $P2X_1$-$P2X_7$, $P2X_3$ and $P2X_2/P2X_3$ heteromers are the major pain candidates due to their localisation in nociceptive neurons, however, $P2X_4$ and $P2X_7$ also play a role in modulating the pain response (Jarvis *et al.* 2002). The alleviation of the pain pathway by various P2X channel antagonists alongside the role of P2X channels in traditional Chinese medicine has sparked an interest of pharmaceutical

companies in developing novel P2X channel modulators (Liang *et al.* 2010). Furthermore, the up-regulation and contribution of $P2X_3$ channels to bone pain in cancer models has implicated P2X with a role in cancer pain. Expression of $P2X_4$ and $P2X_7$ sub-types by immune cancer cells alongside reduced neuropathic pain in P2X knockout mice provides the P2X family of ion channels with further implication in pain sensation. Interestingly, $P2X_7$ inhibition has also demonstrated blockade of tumour growth and neovascularization in addition to its anti-nociceptive properties (Qiu *et al.* 2014). Problems with inter-species differences do remain, even between closely-related rat and mice models, outlining the heterologous nature of P2X channels between species and hence the difficulties in developing, and testing potential compounds, particularly for use in humans (Hibell *et al.* 2000).

1.3 From bench to bedside

Despite improvements in the underlying molecular biology of chronic pain, there is still an unmet clinical need for pain disorders, with 1 in 5 adults estimated to struggle with pain (Harstall 2003). Historically, drug development has rarely resulted from rational design, demonstrated by the discoveries of antibiotics in the treatment of bacterial infections and calcium channel blockers to treat cardiovascular disease. In these cases, drugs were often marketed without fully understanding their underlying mechanism of action. In the current era however, focus lies on identifying target candidates using appropriate and rationally designed assays. Ion channels pose certain problems for compound identification, such as the existence of numerous channel isoforms and widespread tissue expression. This has posed difficulties with developing reagents towards ion channels, however some examples are available, such as antibodies that target $Na_v1.7$ (Lee *et al.* 2014). This antibody was raised against a peptide mimicking the voltage-sensor paddle of $Na_v1.7$, a region that differs by only a few amino acids when compared to other Na_v subtypes. Despite this, the amino acids that are different provide the antibody with its ability to selectively target the $Na_v1.7$ subtype. For example, the presence of an aromatic phenylalanine residue in $Na_v1.7$ compared to a glycine or serine residue in the

other subtypes, and the presence of a negatively charged aspartate residue compared to neutral residues in the other subtypes (except $Na_v1.6$) provides as much as a thousand-fold selectivity and potency.

In addition to the voltage-sensor domain, reagents have been used to target ion channels in other regions, ranging from the highly conserved pore-forming domain (Wyatt *et al.* 1997) to less conserved regions (Sammar *et al.* 1992, Zhou *et al.* 1998). The homologous nature of the pore-forming regions between ion channel subtypes can be a major hurdle however, as off-target ion channel effects may occur. Alternatively, targeting of less conserved regions is possible. One example includes the third extracellular loop, a process called E3 targeting (Zhou *et al.* 1998). Various accessory sub-units have also been targeted, a method utilised well by Lectus Therapeutics (USA 2009). In this method, accessory ion channel proteins are immobilised and interrogated with the pore-forming domain in the presence of test compounds. Similar technologies testing the effect of compounds on accessory protein linkers and the pore-forming domain have also demonstrated channel selectivity (Kanumilli S 2005).

In addition to their use against ion channels, an increasing use of antibodies in a therapeutic setting in general has been observed, with FDA approval being gained for numerous antibody therapies (Link 2013). Despite these successes, certain limitations hinder the applications of antibodies, such as their large size (>100kDa) and labour-intensive manufacturing, among others, making them a less desirable and expensive tool for therapeutic and assay purposes.

1.4 Targeting ion channels using alternatives to antibodies

1.4.1 Animal toxins as ion channel tools

One of the first identified biological reagents targeting ion channels evolved through natural selection, with venomous animals using toxin peptides to incapacitate their prey. These toxins have provided insights into the structural and functional features of a variety of ion channels. A number of sites on Na_v channels interact with toxins (**Figure 1.8**) either becoming blocked by pore occlusion or modulated by altering channel gating. For example, tetrodotoxin

(TTX) binds at the inner vestibule of VGSC's resulting in their inhibition, an effect that has prompted its progression into clinical trials (Nieto *et al.* 2012). In addition to non-selective toxins such as TTX, a family of toxins that are highly selective are the μ-conotoxins. Despite sharing part of their binding site with TTX at the inner pore, further interactions at the outer vestibule produces subtype selectivity due to divergence at this region. For example, the μ-conotoxin PIIIA and GIIIA interact with unique acidic residues (D1248, D1241, E403, D762, E758, D1532) in the outer vestibule of $Na_v1.4$ enabling selective targeting of this sub-type (Li *et al.* 2003, Mahdavi and Kuyucak 2014). The $Na_v1.7$ selectivity of ProTx-II, conferred by its interaction with a unique residue (F813) in the voltage sensor region has prompted the use of a ProTx-II scaffold to identify reagents with even greater selectivity (Schmalhofer *et al.* 2008). By screening a library based on this scaffold, an identified peptide, JNJ63955918, contained substitutions at residues 7 and 30, W7N and W30L respectively, that provided improved selectivity (Flinspach *et al.* 2017). A class of toxins acting away from the pore region, the β-scorpion toxins, interact at domain III to enable subtype-specificity and at the voltage-sensor of domain II (G845, E1438 and D1445) to evoke its effect (Leipold *et al.* 2006, Zhang *et al.* 2012).

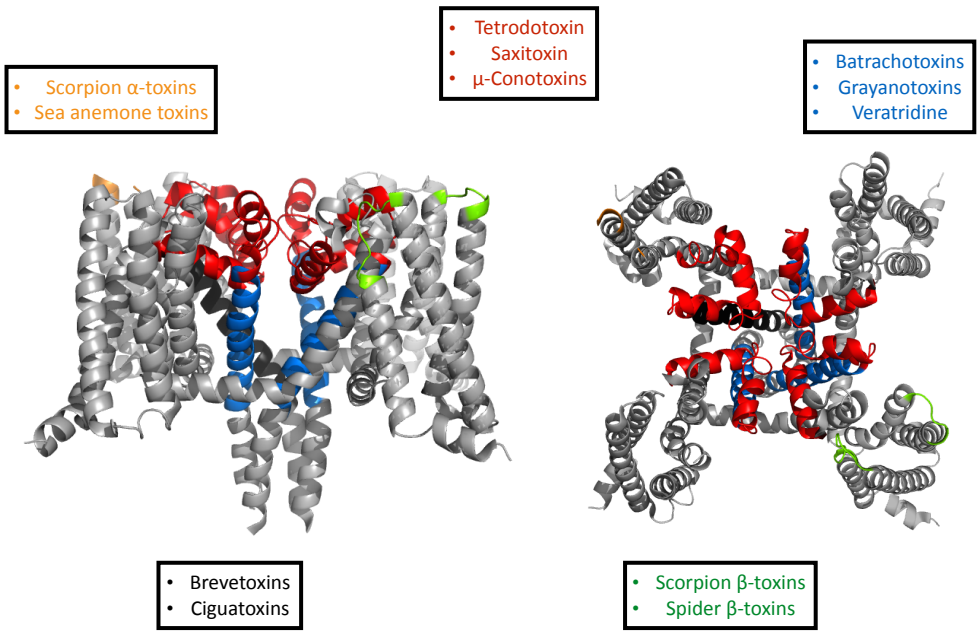

Figure 1.8. VGSC binding sites for toxins isolated from venomous species. A number of binding sites within the VGSC architecture have been identified, with different sites

resulting in various functional effects. For example, the binding of TTX, an inner vestibule-binding toxin, results in pore occlusion and thus inability to activate. In contrast, binding of the VGSC by batrachotoxin, a selectivity filter toxin, results in persistent activation of the channel. Image was adapted from (Stevens *et al.* 2011) on MacPyMol using PDB file 5EK0. The colour presented on the ion channel denotes the area targeted by different toxins, described and matched by the colour in the outside boxes.

In addition to the VGSC's, a number of toxins targeting the Na^+ permeable acid sensing ion channels (ASIC's) have been identified. MitTx forms interactions between its F14 residue and the ASIC1 channel A82-T84 residues, a region of the channel central to gating. Furthermore, K16 interacts with the channel, a residue that is highly conserved between all MitTx relatives, driving their interactions in a similar manner (Baconguis *et al.* 2014). In addition to classical 'pore-blocking' toxins, inhibitory toxins acting via different mechanisms have been identified. These include Mambalgins 1 and 2 (Diochot *et al.* 2012, Salinas *et al.* 2014) and PcTx-1 (Dawson *et al.* 2012) all of which interact with ASIC1 at residues critical for proton sensing, thus preventing activation. In addition to ASIC1 inhibitors, ASIC3 is selectively inhibited by APETx2 (Diochot *et al.* 2004).

As with channels permeable to Na^+ ions, a wide range of toxins have enabled the structural and functional determination of K^+-selective channels. The applications for these toxins range from localisation studies to identifying novel ligands through competition assays (Bergeron and Bingham 2012). Furthermore, the role of K^+ channels in a number of human pathologies, as outlined in Section 1 of this review, has also driven the investigation in to the therapeutic relevance of these toxins.

One of the first potassium channel toxins to be characterised was charybdotoxin, a scorpion toxin that targets the pore region of K_v channels with subsequent crystallisation data revealing the close proximity of the toxin to the potassium ion selectivity filter. Recently, the crystal structure of this toxin in complex with a mutant version of the $K_v1.2$ channel has been solved (Banerjee *et*

al. 2013). This study highlights the mechanism of pore occlusion through insertion of a highly conserved K27 residue into the channel selectivity filter, acting as a 'surrogate' cation and blocking the ion conduction pathway. The conserved nature of this lysine residue between scorpion toxin molecules (**Figure 1.9**) and the conservation of the selectivity filter in all K^+ channels suggests a similar mechanism of action (Galvez *et al.* 1990, Garcia-Valdes *et al.* 2001, Banerjee *et al.* 2013).

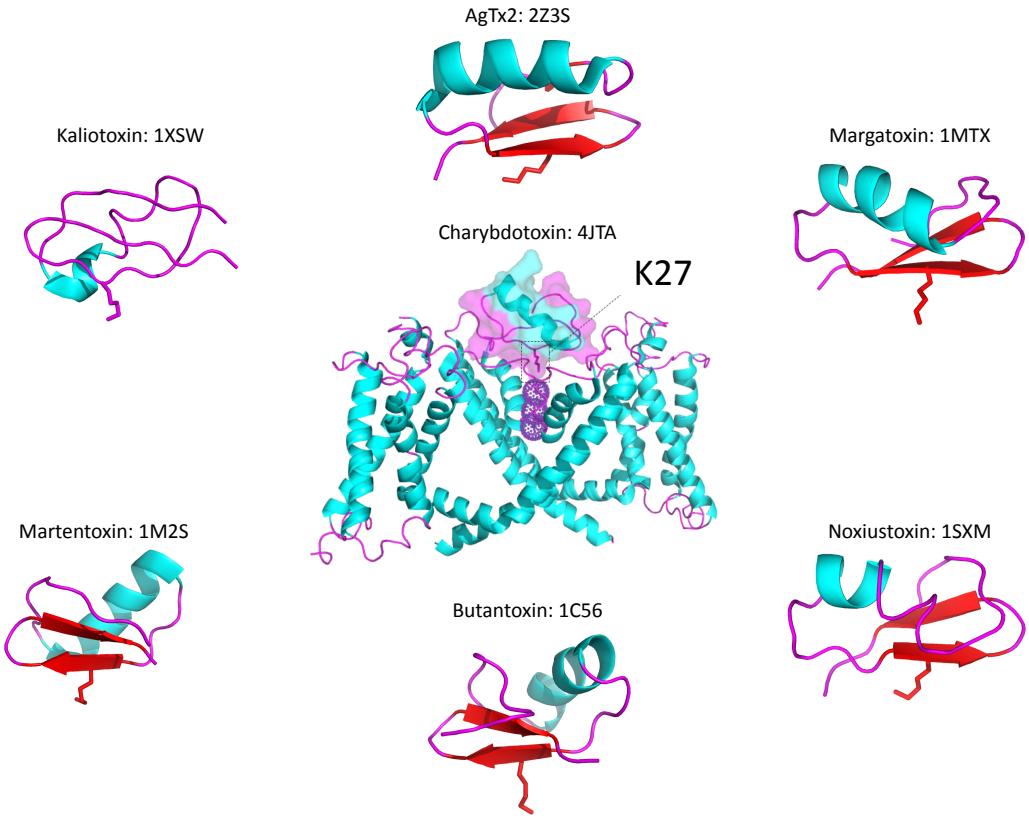

Figure 1.9. Pore-blocking potassium channel toxins. Since the discovery and characterisation of Charybdotoxin in the 1980's, a number of other toxins acting in a similar fashion have been discovered. The recent crystal structure of $K_v1.2$ in complex with Charybdotoxin (central image) has helped to determine the mechanism of action of these toxins. A conserved lysine residue (shown in each image as a stick) orientates the toxin in the pore of the potassium channel and competes with the outermost potassium ion, resulting in pore occlusion.

Molecular docking studies have provided insights into the different levels of selectivity of these toxins (Chen *et al.* 2011) with variations in interactions with the channels peripheral acidic residues (E420, D423 and D433) crucial. An interesting study conducted by Li *et al* (2012) investigated the design of a novel peptide (ADWX-1) based on the pore-targeting scorpion toxin BmKTX. The mutation of three residues present in BmKTX to produce a novel peptide resulted in improved selectivity for $K_v1.3$. This novel peptide was also shown to block $K_v1.3$ currents with 100-fold greater affinity than the native BmKTX toxin. Subsequent *in vivo* studies demonstrated an ability of the ADWX-1 peptide to

inhibit the proliferation of $CD4^+CCR7^-$ effector T cells, an underlying abnormality resulting in multiple sclerosis (Li *et al.* 2012). The structural basis of the interaction between ADWX-1 and $K_v1.3$ has identified the presence of the previously described 'pore-plugging' lysine side chain (K26) of the peptide, present in both the native BmKTX and the 'improved' ADWX-1, however the introduction of an arginine residue at position 11, instead of a glycine residue, enables another contact point between ADWX-1 and $K_v1.3$ due to it's proximity to D386 of $K_v1.3$ in the outer pore turret (Han *et al.* 2008). This study emphasises the potential of using animal toxins to design potential drug leads that target ion channels.

Whilst the pore forming region of potassium channels makes a sensible target for toxins to prevent the propagation of action potentials through inhibiting repolarisation, another region of the potassium channel frequently targeted by animal toxins is the VSD, thus altering the conformational stability of the potassium channel in its open and closed states. Recently, the structures of a number of these VSD toxins have been revealed with common features observed, such as a hydrophobic patch of residues enabling the toxins to partition into the membrane (Lee and MacKinnon 2004). Possibly the most studied of these toxins is hanatoxin. Molecular simulation studies have suggested a number of interaction sites of the K_v channel with hanatoxin; a hydrophobic patch at the membrane boundary and residues of the S3 segment directed towards the external crevice (Lou *et al.* 2002). Furthermore, hanatoxin binds to and stabilises the $K_v1.2$ voltage sensor in its resting state (Lee *et al.* 2003). Despite providing mechanistic insights into inhibition by hanatoxin, other toxins are likely to function via different mechanisms based on their interacting residues (Swartz 2007, Milescu *et al.* 2013, Gupta *et al.* 2015).

Voltage-gated calcium channels are structurally similar to voltage-gated sodium channels with the major exception being the selectivity filter within the pore-forming region of the channel. This difference enables targeting by different types of toxins. As with the previously discussed toxins, two classes have been identified; pore-blocking toxins and gating modifier toxins. A major

group of pore-blocking toxins are the ω-conotoxins from the marine snails. The selectivity of ω-conotoxin binding to Ca_v channels has been explored in detail. A single residue of $Ca_v2.2$, G1326, is essential for channel block by the ω-conotoxins GVIA and MVIIA (Feng *et al.* 2001). The essential residues of GVIA and MVIIA for this interaction are K2 and Y13 (Kim *et al.* 1994). Interestingly, the ω-conotoxin, TxVII has a similar framework to the other ω-conotoxins, and also contains the conserved K2 residue, however, the presence of several negatively charged residues in close proximity to K2, alongside the absence of Y13, results in ω-conotoxin TxVII binding to L-type Ca_v channels instead (Fainzilber *et al.* 1996). The ability of ω-conotoxin MVIIA to selectively block $Ca_v2.2$ has resulted in its approval by the FDA as an intrathecal analgesic marketed as Ziconotide, Prialt. Another ω-conotoxin, CVID (AM336) has demonstrated reduced side effects to those observed by Ziconotide (Smith *et al.* 2002). The remarkable channel specificity of these conotoxins is currently being exploited in an attempt to develop small molecules that are able to mimic their mechanism of action but with improved pharmacodynamics properties (Vink and Alewood 2012).

Another region of the voltage-gated calcium channel targeted by toxins is the paddle motif, a section of the channel that is present at the protein-lipid interface and plays a central role in channel gating. The structural mechanism by which a well-known $Ca_v3.1$ gating modifier, ProTx-II, interacts with the paddle motif has recently been established. The toxin has been shown to bind most strongly to the DIII paddle motif with residue D1372 shown to be important for the interaction. Other toxins including PaTx-1 and GsAF-I appear to act on $Ca_v3.1$ by a similar mechanism. Another family of toxins identified as non-pore blocking toxins are the ω-agatoxins, toxins that inhibit the calcium channel by preventing movement of the voltage sensor (Mintz *et al.* 1992). This family of toxins has a wide variation in subtype selectivity, for example ω-agatoxin IVA acts as a Ca_v2 inhibitor (Sidach and Mintz 2000) whilst ω-agatoxin IIIA demonstrates poor selectivity and interacts with L-type, P/Q-type and N-type channels (Mintz *et al.* 1991). Interestingly, these two toxins, despite being a part of the same family and sharing sequence homology, have different binding sites, with ω-agatoxin

IIIA acting via pore occlusion whilst ω-agatoxin IVA acts via the voltage-sensor (Yan and Adams 2000). Future structural studies are likely to unveil these differences in binding.

The toxins described in this section alongside their various mechanisms of action, many of which have been reviewed in depth elsewhere (Stevens *et al.* 2011, Zhang *et al.* 2012), demonstrates the potential for utilising these toxins for developing novel ion channel tools. Additionally, much focus has been placed on trying to develop these toxins as therapeutic drugs. Ziconotide is one example that has already been mentioned that has reached the clinic, however, problems such as the requirement for intrathecal delivery motivate further improvements. Furthermore, the lack of high-resolution structural data to demonstrate the interaction between these toxins and their cognate channel has limited their use for developing small molecule mimetics. Recent advancements in cryo-EM may improve our understanding of these interactions with the structure of the mammalian $Ca_v1.1$ channel recently being solved at 3.6 Å resolution (Wu *et al.* 2015).

Progress in understanding the interactions between toxins and other Ca^{2+}-permeable ion channels has seen greater success. The Ca^{2+}-permeable TRPV1 ion channel structure in complex with its activating toxin Double-Knot Toxin (DkTx) has been solved at 3.8 Å and more recently 2.9 Å (Liao *et al.* 2013, Gao *et al.* 2016). DkTx acts as an irreversible channel activator by positioning itself in a bivalent manner at the extracellular opening of TRPV1, pushing two monomers of the heteromer apart and thus enabling the constant flow of ions through the channel pore. A number of residues in the pore domain are essential for this interaction including I599, F649, A657 and F659 (Bohlen *et al.* 2010). The crystal structure of TRPV1 in complex with DkTx further reveals the importance of interactions with the aliphatic tail groups of the lipid bilayer, for example between W11 of Inhibitory Cysteine Knot (ICK) one and R534 of TRPV1 as well as F27 of ICK one with the aliphatic tail coordinated by the side chain of S629 of TRPV1 (Gao *et al.* 2016). In fact, a number of animal toxins have demonstrated the ability to activate the TRPV1 channel by binding this outer pore domain

region, with many of them providing insights into the channels mechanism of activation (Geron *et al.* 2017). One of these toxins is RhTx, a centipede toxin targeting residues D602, Y632 and T634, all clustered among those targeted by DkTx, demonstrating a similar epitope, albeit, without the hydrophobic interaction observed with DkTx (Yang *et al.* 2015). The toxins BmPO1 and HCRG21 are also hypothesised to interact with the outer pore region (Hakim *et al.* 2015, Monastyrnaya *et al.* 2016). Whilst the remaining TRP channels have had fewer toxins identified that modulate them, various toxins have been identified, for example GsMTx-4, an inhibitor of the TRPV4 subtype (Jung *et al.* 2006, Bowman *et al.* 2007) and ProTx-I, a non-selective inhibitor of TRPA1 (Gui *et al.* 2014).

A number of toxins have been identified that bind to a large family of Cys-loop channels that mediate fast chemical transmission of electrical signals in the nervous system. These channels include the gamma-amino butyric acid receptors ($GABA_A$ and $GABA_C$), nicotinic acetylcholine receptors (nAChR), serotonin (5-HT3) receptors, glycine receptors (GlyR) and glutamate receptors (GluR) (**Table 1.4**).

These channels are important targets for the treatment of a number of disorders including myasthenia gravis, epilepsy and substance addiction, however, a number of them have also been implicated in chronic pain disorders (Treiman 2001, Meriggioli 2009, Umana *et al.* 2013).

Channel	Toxin	Epitope	Reference
$GABA_A$	Picrotoxin (PTX)	Channel pore and ligand binding domain/TM interface	(Takeuchi and Takeuchi 1969)
	Microurotoxin 1 (MmTx1)	α+β- interface	(Rosso *et al.* 2015)
	Microurotoxin 2 (MmTx2)	α+β- interface	(Rosso *et al.* 2015)
nAChR	α-conotoxin	ACh binding pocket	(Abraham *et al.* 2017)
	α-bungarotoxin	α-subunit	(Dellisanti *et al.* 2007)
	α-cobratoxin	Ach binding pocket	(Bourne *et al.* 2005)
5-HT3	Bunodosine 391 (BDS 391)	Unknown	(Ferreira Junior *et al.* 2017)
GlyR	Tutin	Unknown	(Fuentealba *et al.* 2011)

Table 1.4. A number of toxins have been identified that bind to the receptors of the central nervous system involved in fast synaptic transmission. These receptors include the $GABA_A$, nAchR, 5-HT_3, GlyR and glutamate receptors. Each of the toxins that bind these receptors have a wide range of epitopes including the channel pore, agonist-binding pockets and subunit interfaces.

1.4.2 Targeting ion channels using chemical compounds

After a rush of blockbuster drugs in the 20th century, the FDA has since approved only a handful of novel small molecule modulators of ion channels for clinical use. Whilst previous efforts on small molecule drug discovery focussed on mass screening attempts in the hope of identifying a compound, more recent attempts are focusing on understanding the structural basis of ion channel – small molecule interactions and then designing compounds that are likely to improve efficacy and selectivity of current or novel compounds.

The majority of Na_v channel modulators used clinically bind to the pore region to prevent conductance of Na^+ ions however this region is conserved throughout all Na_v channels causing problems with selectivity. Despite the discovery of a number of toxins that are able to bind to the outer vestibule of the pore domain, a region that is channel specific, as discussed in the previous section, these reagents demonstrate poor drug-like properties. An alternative site that can be targeted for channel-specific modulation is the VSD. Aryl sulfonamide antagonists have recently been described that are able to bind to the $Na_v1.7$ VSD resulting in selectivity (Ahuja *et al.* 2015). The aryl sulfonamide GX-936 becomes enclosed in the VSD regions composed by S1-S2 and S3-S4 segments of $Na_v1.7$. GX-936 and related aryl sulfonamides are able to interact with the $Na_v1.7$ VSD via three sites. These include an anion binding site composed of a number of arginine residues, a selectivity pocket, with a number of aromatic and hydrophobic residues resulting in a strong interaction, and finally, a lipid-exposed region, in which interactions take place between the aryl sulfonamides and the lipid bilayer.

A number of calcium channel blockers have reached the clinic for the treatment of high blood pressure with three groups described; benzothiazepines, dihydropyridines and phenylakylamines. Dihydropyridines include amlodipine, felodipine, lacidipine and nicardipine. One of the major breakthrough compounds of the 1980's however was amlodipine besylate, marketed by Pfizer as Norvasc and recording a 2017 revenue of $926 million (Toal *et al.* 2012).

One of the most marketed drugs acting at potassium channels are the sulphonylureas for use in the treatment of diabetes. Sulphonylureas stimulate insulin secretion by binding to and blocking K_{ATP} channels, resulting in the opening of calcium channels and subsequent stimulation of the Ca^{2+}-dependent insulin exocytosis from the pancreatic β-cells (de Wet and Proks 2015) .

1.4.3 Targeting ion channels using novel biologics

The next section of this chapter will discuss the more recent use of some of the novel biologics for targeting ion channels. A number of reagents have been developed as alternatives to antibodies, generally derived from synthetic

libraries that do not require the use of animals. Although these reagents are much smaller (**Figure 1.10**) and more stable than antibodies, they do have the disadvantage that the ability to identify useful reagents from designed libraries is based on the quality and display format of the library, rather than the immune response provided by an animal. Whilst a structural overview of such non-antibody proteins can be observed in **Figure 1.10** and have been reviewed in depth elsewhere (Hey *et al.* 2005, Skerra 2007, Simeon and Chen 2018) some of the reagents that have demonstrated success in targeting ion channels or other membrane proteins will be briefly discussed in this chapter. These include Nanobodies, Monobodies, DARPins and the more recently described Affimers.

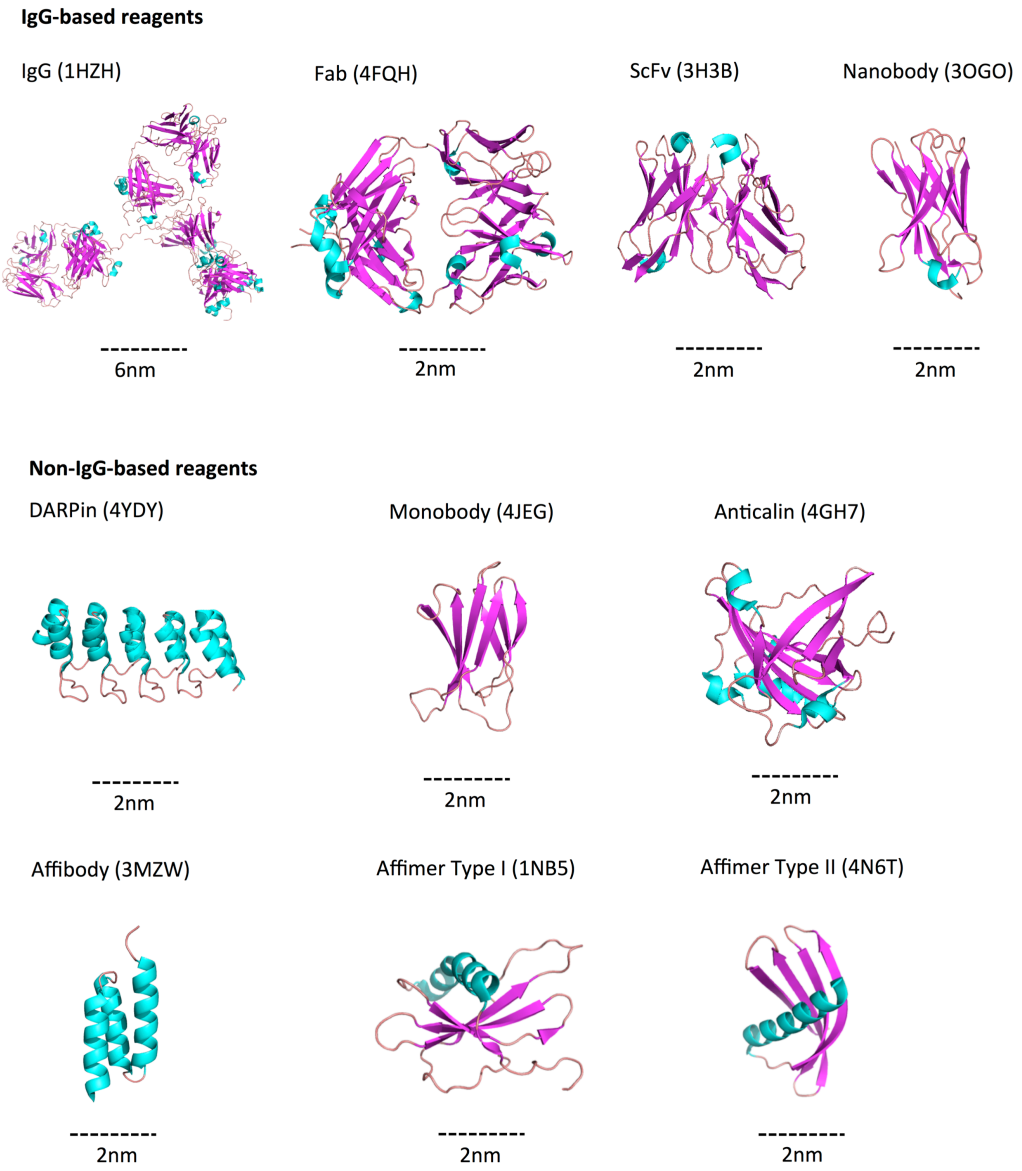

Figure 1.10. Immunoglobulin and non-immunoglobulin-based binding reagents. A number of IgG-based variants have been developed to utilise the advantages of antibodies alongside enhanced properties such as smaller size and easier production. These include Fab's, ScFv's and nanobodies. In addition, a variety of non-IgG-based scaffolds have also been developed including DARPins, Monobodies, Anticalins, Affibodies and Affimers (Bedford *et al.* 2017).

1.4.3.1 Nanobodies

Nanobodies are based on the smallest antigen binding domains of heavy chain only antibodies from *Camelidae* (Hamers-Casterman *et al.* 1993). The P2X7 ion channel has been targeted by nanobodies with the group of Koch-Nolte identifying both nanobody blockers and potentiators of P2X7 (Danquah *et al.* 2016). These nanobodies also had *in vivo* effects in mice and were more potent at inhibiting the release of interleukin-β than a small molecule blocker currently undergoing clinical assessment (Danquah *et al.* 2016). This demonstrates the clinical potential of these reagents. In addition to the development of nanobodies against ligand-gated channels with large extracellular domains, nanobodies have also been identified that are able to modulate the voltage-gated channel, $K_v1.3$. In this study, a novel ion channel expression platform on the free-living ciliate, *Tetrahymena thermophila* was used to enable the screening of recombinant libraries against the over-expressed ion channel. The identified nanobodies were able to inhibit $K_v1.3$ with considerable potency and selectivity (Bednenko *et al.* 2018).

1.4.3.2 Monobodies

Monobodies are based on the fibronectin type III domain (Koide *et al.* 1998). This domain adopts a β-sandwich structure composed of seven β-sheets and contains three exposed loops available for target recognition. Two Monobody scaffolds have been designed; amino acids are diversified in the loop regions of the original scaffold whilst in a second-generation scaffold, a segment of the β-sheet is also diversified (Koide *et al.* 1998, Koide *et al.* 2012). These different scaffolds enable different binding conformations and thus increase the range of targets available for selection with those involved in protein–protein interactions favored by the second-generation 'side and loop' scaffold. Monobodies have been used to enable the crystallisation of the fluoride ion channel Fluc (Stockbridge *et al.* 2015). In this study, crystals of the fluoride ion channel Fluc could not be grown unless the binding Monobody was present. Under conditions in which a Monobody named 'L2' was present, crystals that diffracted to a resolution of 2.1 Å were grown enabling the identification of features such as the

notable presence of a cation at the center of the anion diffusion pathway. Another monobody, S12, that demonstrated pore occlusion, appeared to bind via a number of tyrosine residues within its FG loop (**Figure 1.11**). Interestingly, a number of tyrosine residues pivotal to this interaction were essential to binding with mutation to other residues including a phenylalanine highly disruptive to binding. This disruption to binding observed following mutagenesis of the key residues demonstrates the efficacy of selecting for high affinity Monobodies from the highly diverse library. Indeed, attempts at designing higher affinity monobody mutants failed (Turman *et al.* 2018).

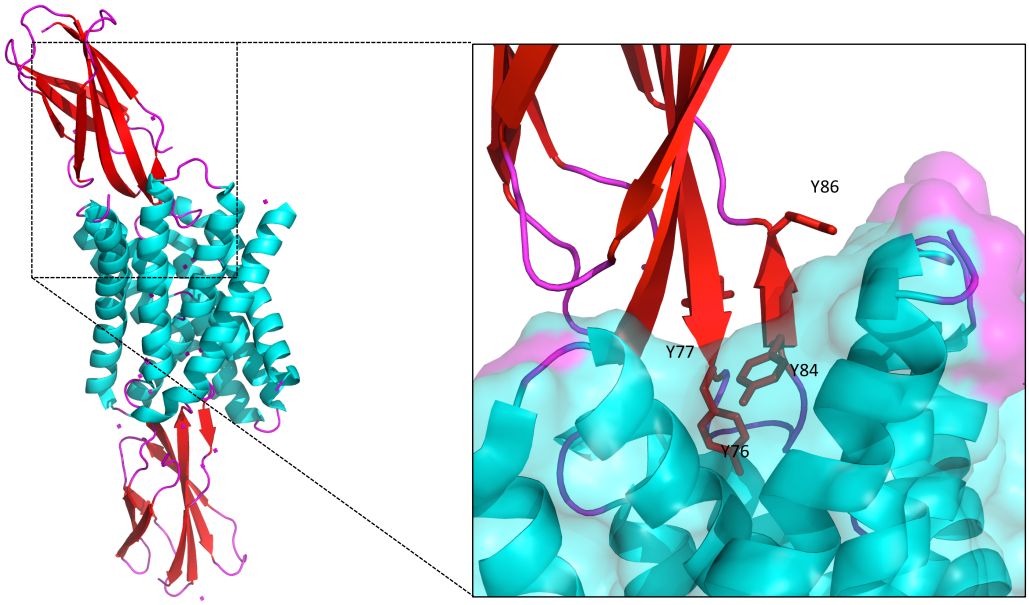

Figure 1.11. Structural analysis of the Monobody S12-FluC channel complex. A number of tyrosine residues are at the centre of the interactions between monobody S12 and the FluC channel with Y76, Y77, Y84 and Y86 taking part in hydrogen bonding with the channel. Subsequent mutation of these tyrosine residues resulted in weaker and in some cases abolished binding. The figure was adapted using MacPyMol (Turman *et al.* 2018).

1.4.3.3 Designed Ankyrin Repeat Proteins (DARPins)

DARPins are designed from the ankyrin repeat motif that can be found in a number of proteins involved in various biological functions (Binz *et al.* 2003). The ankyrin repeat motif is a 33 amino acid sequence composed of two α-helices and

a β-turn with each repeat connected by a loop. A consensus strategy was used to enable the incorporation or shuffling of these repeats whilst maintaining high stability and expression rates in *E. coli*. During this strategy, an alignment was built and residues identified to be involved in target binding randomised by the use of trinucleotide primers during library generation (Forrer *et al.* 2004). Following its generation, the DARPin library comprised fixed and variable positions, with fixed regions stabilizing the structure and variable regions enabling target binding. The actual size of the DARPin libraries, including the two- and three-module libraries, was estimated as 10^{10} (Steiner *et al.* 2008).

DARPins have been used in a number of applications including studying protein interactions, for example those involved in the mitogen-activated protein kinase (MAPK) pathway. This work was used to develop an assay that could study MAPK phosphorylation in real-time, an application that could be used to study a plethora of protein interactions in real-time (Kummer *et al.* 2013).

Many studies have confirmed the use of DARPins as crystallisation chaperones, another tool that can be extremely useful for studying protein interactions, however at the atomic level (Huber *et al.* 2007).

As diagnostic tools, DARPins have demonstrated improved specificity over an FDA-approved antibody for staining of HER2 (Theurillat *et al.* 2010). Using bispecific DARPins for targeting cells overexpressing HER2 enabling selective targeting of tumor cells expanded this work. The subsequent crystal structure of this interaction demonstrated locking of the HER2 extracellular domain by the bispecific DARPin molecules in a manner that prevented the intracellular dimerization arms of HER2 from interacting, resulting in perturbation of the intracellular signaling cascade (Jost *et al.* 2013).

Despite the variety of applications DARPins have been used in, the number of DARPins identified that are able to bind ion channels is limited. The integral membrane protein AcrB, a multidrug exporter found in *E. coli*, has been screened using the DARPin library from which the DARPin labelled 110819 was identified. This DARPin facilitated the crystallisation of the AcrB membrane protein (Sennhauser *et al.* 2007) with resulting crystals defracting to 2.54 Å resolution, a substantial improvement on those yielded from AcrB alone

(Murakami *et al.* 2002). This study suggests the potential applications of DARPins in aiding the crystallisation of other membrane proteins, including ion channels, a notoriously difficult target for structural studies.

1.4.3.4 Affimer reagents

Affimer reagents are classified as type I and type II based on their scaffold of either the human stefin A protein (Hoffmann *et al.* 2010) or consensus plant phytocystatin protein, respectively (Tiede *et al.* 2014). Both scaffolds contain a α-helix and four β-sheets with the binding region present in two variable loops presented between pairs of β-sheets. The type II Affimer scaffold will be the focus of this study. Following its initial publication in 2014, a diverse set of targets have been screened using the type II Affimer library and identified Affimer reagents have demonstrated their use in many different molecular biology applications, including ion channel detection and modulation, results that will be presented in this thesis (Kyle *et al.* 2015, Sharma *et al.* 2016, Tiede *et al.* 2017, Robinson *et al.* 2018).

Affimer reagents contain a number of properties that make them an ideal binding reagent including; small size (~100 amino acids), high thermostability (>100^{o}C), and the absence of cysteine residues unless inserted in to the C-terminus for site-specific conjugation. Finally, the ability to express Affimers in the *E. coli* cytosol provides a cheap method for the production of large quantities, a process that normally requires expensive rounds of optimization and fermentation for antibodies and their single chain variants (Frenzel *et al.* 2013). Furthermore, the complete removal of animals from the production of Affimers has recently seen the BioScreening Technology Group (BSTG) awarded by the National Centre for the Replacement, Refinement and Reduction of Animals in Research for its work in helping to reduce the number of animals involved in scientific research. This award further highlights the advantages of Affimers over binding reagents that require animal use.

The favorable properties of Affimer reagents have resulted in a large number of examples of their applications, many of which were recently

published in eLife (Tiede *et al.* 2017). In addition to these examples of their applications, Affimer reagents have provided insights in to various disease areas.

Affimer reagents have been isolated against FcγRIIIa that are able to block TNF release and phagocytosis via a number of modes of action (Robinson *et al.* 2018). One Affimer reagent demonstrated direct competition for the Fc binding site whilst another acted through allosteric modulation. The Affimer reagent that acted by steric hindrance of the Fc binding site, AfF4, was able to discriminate between FcγRIIIa and FcγRIIIb due to subtle differences in amino acid composition at positions 129 and 140. The Affimer reagent that functions by an allosteric mode of inhibition, AfG3, interacts directly with Arg18 resulting in narrowing of the D1-D2 inter-domain angle of FcγRIIIa. This brings variable region two of AfG3 into close contact with a Trp99 residue enhancing the interaction further. Both of these Affimer-FcγRIIIa interactions resulted in inhibition of downstream effector functions in monocytes (Robinson *et al.* 2018).

Another protein that Affimer reagents have been isolated against to enable the inhibition of key signalling cascades is SUMO (Hughes *et al.* 2017). SUMOylation regulates a number of cellular pathways and occurs by the covalent linkage of SUMO proteins. This 'SUMOylation' results in detection by proteins that carry SIM's, or SUMO interaction motifs that influences cellular function, for example transcriptional regulation. Affimers were detected that were able to inhibit the SUMO-driven protein-protein interactions both *in vitro* and in cells. Furthermore, these interactions were explored in atomic resolution, results that may yet help identify therapeutic reagents that can target protein-protein interactions (Hughes *et al.* 2017).

In addition to the ability of Affimer reagents to inhibit protein interactions, they have also provided a more detailed understanding of the interactions between other proteins involved in cell signalling. The HIF1α and p300 proteins are key molecules in tumour metabolism. Affimer reagents have been isolated that were able to disturb the interaction between HIF1α and p300 with micromolar affinity however the potential use of these Affimers for the development of pharmacophores through the elucidation of their molecular interaction is the major highlight of this study (Kyle *et al.* 2015).

The study of ubiquitin linkages has been limited in the past due to a lack of detection tools. K6 and K11/K33-Ubiquitin specific Affimer reagents have been isolated with their mode of interaction revealed in high resolution. These Affimers had comparable performance to currently available antibodies in a range of applications including western blotting and affinity fluorescence techniques (Michel *et al.* 2017).

In addition to the potential of Affimers in highlighting the underlying mechanisms of disease states and their potential as therapeutics, they have been developed as detection reagents. Affimers have been identified against glypican-3 (GPC3), a biomarker for hepatocellular carcinoma, and combined with a monoclonal antibody for use in a chemiluminescence-based assay (Xie *et al.* 2017). This assay was able to detect GPC3 when present at low levels (0.03 ng/mL) with high specificity, correlating with the gold standard histochemistry test currently used (Xie *et al.* 2017). Furthermore, Affimer reagents have also been isolated for the detection of IL-8 (Sharma *et al.* 2016) and HER4 (Zhurauski *et al.* 2018). More recently, the bioimaging of F-actin has been demonstrated by Affimer reagents (Lopata *et al.* 2018). Although currently available reagents such as phalloidin are commonly used in the fluorescent imaging of F-actin in non-methanol fixed cells, the identified Affimer reagents in this study were able to image F-actin in cells fixed with methanol or in live cells. Although nanobodies have been described that are able to detect F-actin in live cells, its behaviour in cells is yet to be more clearly studied. Results from this study suggests that Affimer reagents that bind to F-actin are able to discriminate between structures of F-actin with slight differences (Lopata *et al.* 2018), a property that makes them ideal for targeting ion channels, proteins that can be very similar.

1.5 Aims of the project

Reagents that are able to detect and modulate ion channel function are highly sought. However, methods for producing such reagents are lacking. The aim of this study was to investigate and develop approaches for isolating Affimer reagents able to detect and modulate the ion channels, TRPV1 and P2X3.

Chapter 2

Materials and Methods

2 Materials and Methods

2.1 General reagents

- ER2738 DUOs (Lucigen, Cat. No. 60522-3).
- One Shot BL21 Star (DE3) Chemically Competent *E. coli* (Life Technologies, Cat. No. C6010-03).
- XL-1 Blue Supercompetent *E. coli* (Agilent Technologies, Cat. No. 200236).
- JM83 cells (ATTC)
- Carbenicillin (500X stock: 50 mg/ml in ddH20).
- Tetracycline hydrochloride (1000X stock: 12 mg/ml in 70% ethanol).
- Kanamycin (500X stock: 25 mg/ml in ddH20).
- 2TY media (per litre: 10 g yeast extract; 16 g tryptone; 5 g NaCl).
- LB Agar: 10 g/L SELECT peptone 140, 5 g/L SELECT yeast extract, 5 g/L sodium chloride, 12 g/L SELECT agar (Invitrogen, Cat. No. 22700-025).
- LB Broth Base: 5 g/L SELECT yeast extract, 5 g/L sodium chloride, 10 g/L SELECT peptone 140 (Invitrogen, Cat. No. 12780-052).
- Phusion High-Fidelity DNA Polymerase (Thermo Scientific, Cat. No. F-530).
- dNTP Mix, 25 mM (MP Biomedicals, Cat. No. NTPMX255).
- *NheI*-HF (NEB, Cat. No. R3131S). Restriction site; G^CTAG_C.
- *NotI*-HF (NEB, Cat. No. R3189S). Restriction site; GC^GGCC_GC.
- *DpnI* (NEB, Cat. No. R0176).
- Alkaline Phosphatase, Calf Intestine (NEB, Cat. No. M0290S)
- T4 DNA ligase (NEB, Cat. No. M0202).
- QIAprep Spin Miniprep Kit (QIAGEN, Cat. No. 27106).
- QIAquick Gel Extraction Kit (QIAGEN, Cat. No. 28704)
- QIAquick PCR purification Kit (QIAGEN, Cat. No. 28104)
- 15% SDS-PAGE resolving gel; to polymerise gel add 0.2% APS and 0.06% TEMED.
- 5% SDS-PAGE stacking gel; to polymerise gel add 0.2% APS and 0.06% TEMED.
- 1X SDS-PAGE running buffer; 0.25 M Tris, 1.91 M Glycine, 1% SDS. Diluted 1:10.

- 1X SDS-PAGE sample buffer; 50 mM Tris-HCl, pH7, 2% SDS, 5% Glycerol, 5% Mercaptoethanol, 1 mg Bromophenol blue.
- 1X Lysis Buffer; 50 mM NaH_2PO_4, 300 mM NaCl, 20 mM Imidazole, pH 7.4. Before use, lysozyme (Life Technologies, Cat. No. 90082), Triton X-100 (Sigma-Aldrich, Cat. No. X100-5ML), Halt protease cocktail inhibitor (Fisher Scientific, Cat. No. 10320015) and Benzonase Nuclease (Merck Millipore, Cat. No. 70746) were added to a final 1X concentration from pre-made stock solutions.
- 1X Wash Buffer; 50 mM NaH_2PO_4, 500 mM NaCl, 20 mM Imidazole, pH 7.4.
- 1X Elution Buffer; 50 mM NaH_2PO_4, 500 mM NaCl, 300 mM Imidazole, pH 7.4.
- HisPur Ni-NTA Resin (Life Technologies, Cat. No. 88221)
- 1X Dialysis Buffer; 5L 1 X PBS, pH 7.4.
- TAE buffer; 40 mM Tris, 20 mM acetate and 1 mM EDTA
- Anti-6X His tag antibody (HRP) (Abcam, Cat. No. ab1187). Used at 1:3000 dilution.
- Anti-TRPV1 antibody (Guinea pig) (Abcam: Cat. No. Ab10295). Used at 1:1000 dilution.
- Anti-6X His tag antibody (Mouse) (Abcam, Cat. No. ab18184). Used at 1:3000 dilution.
- Anti-Mouse 488 antibody (Thermo, Cat. No. A11001). Used at 1:1000 dilution.
- Goat anti-guinea pig antibody (Alexa Fluor 647 conjugated) (Abcam, Cat. No. ab150187). Used at 1:500 dilution.
- Anti-P2X3 antibody (Rabbit) (Millipore, Cat. No. Ab5895).
- Goat anti-rabbit antibody (Alexa Fluor 594 conjugated) (Thermo, Cat. No. A11012)
- Human Embryonic Kidney (HEK) 293-T cells.
- Chinese Hamster Ovary (CHO) cells.
- U-2 OS cells.

- Dulbecco's Modified Eagle Medium (DMEM) (Gibco, Cat. No. 31966-021) supplemented with 10% fetal bovine serum (FBS) (v/v) and 5% penicillin and streptomycin (v/v); pre-warmed at 37^{o}C.
- OptiMEM 1X (Gibco, Cat. No. 31985-047)
- FuGENE HD transfection reagent (Promega Cat. No. E2311).
- 0.05% Trypsin-EDTA (Gibco, Cat. No. 25300-054).
- Cell wash buffer: 137 mM NaCl, 5.4 mM KCl, 0.25 mM Na_2HPO_4, 0.44 mM KH_2PO_4, 1.3 mM $CaCl_2$, 1.0 mM $MgSO_4$, 1.0 mM $MgCl_2$, 10 mM glucose, 10 mM HEPES, with pH adjusted to 7.4 using 1 M NaOH.
- Fluo-4 AM, cell-permeant (Thermo Fisher, Cat. No. F14201)
- Pluronic F127 (Sigma Aldrich, Cat. No. P2443)
- 10X blocking buffer (Sigma-Aldrich, Cat. No. B6429).
- 0.2 M glycine, pH 2.2.
- 1 M Tris-HCl, pH 9.1.
- Triethylamine (Sigma-Aldrich, Cat. No. T0886).
- 1 M Tris-HCl, pH 7.0.
- M13K07 helper phage (titre ca. 10^{14}/ml).
- PEG-NaCl precipitation solution (20% (w/v) PEG 8000, 2.5 M NaCl).
- TE (10 mM Tris, 1 mM EDTA, pH 8.0).
- Anti-Fd bacteriophage-HRP (Seramun Diagnostica GmbH, Cat. No. A-020-I-HRP).
- High Sensitivity Streptavidin-HRP (Thermo Scientific, Cat. No. 21130).
- TMB (Seramun Blau fast TMB/ substrate solution) (Seramun Cat. No. S-001-TMB).
- Slide-A-Lyzer^{TM} Dialysis Cassette (Thermo Fisher Scientific, Cat. No. 66370)

2.2 Bacterial cell culture

Various bacterial cell strains were used in this study for different purposes including DNA replication, general cloning, phage growth and protein expression. The strains used in this study are highlighted in **Table 2.1**. Cells were generally grown in 2YT media (10 g yeast extract; 16 g tryptone; 5 g NaCl per litre) with shaking at 37^{o}C. Colonies were grown on Lennox L agar (10 g/L SELECT peptone 140, 5 g/L SELECT yeast extract, 5 g/L sodium chloride, 12 g/L SELECT agar).

***E. coli* strain**	**Genotype**	**Manufacturer**	**Product code**
XL1 Blue Supercompetent	*recA1 endA1 gyrA96 thi-1 hsdR17 supE44 relA1 lac [F' proAB lacI^{q}ZΔM15 Tn10* (Tet')]	Agilent Technologies	200236
One Shot^{TM} BL21 Star^{TM} (DE3)	F-*omp*T *hsd*SB (rB-, mB-) *galdcmrne*131 (DE3)	Invitrogen^{TM}	C601003
JM83	F– *ara Δ(lac-proAB) rpsL* (StrR)*[φ80 dlacΔ(lacZ)M15] thi*	ATCC	50348
ER2738 electrocompetent	[F'*proA+B+ lacIq Δ(lacZ)M15 zzf::Tn10* (tetr)*] fhuA2 glnVΔ(lac-proAB) thi-1Δ(hsdS-mcrB)5*	Lucigen	60522

Table 2.1. *E. coli* cell strains used in this study alongside their genotypes and product information.

2.3 DNA methods

2.3.1 Expression plasmids

Various expression plasmids were used in this study for the expression of recombinant target proteins and Affimers. Target protein was expressed in both bacterial and mammalian expression systems whilst Affimer-encoding DNA was

expressed in a bacterial expression system. These plasmids are outlined in **Table 2.2** with a brief description and product details.

Plasmid	Description	Source
pET11a	A bacterial expression vector with a T7 promoter and lac operon	Novagen®
pBSTG1	A phagemid cloning vector derived from pHEN1. This vector contains a DsbA signal sequence and an amber stop codon between an Adhiron coding region and a truncated gpIII coding region.	(Hoogenboom *et al.* 1991, Tiede *et al.* 2014)
pD649-D	A mammalian expression vector with a CMV promoter. An IRES is also available between your gene of interest and DNA encoding GFP.	ATUM
pOPINTTGneo	A versatile suite of expression vectors designed by the Oxford Protein Production Facility (OPPF), Oxford to enable expression of protein in bacterial, mammalian and insect cells.	(Berrow *et al.* 2007)
pOPINTTGneo-3c-Fc	A derivative of pOPINTTGneo with a c-terminal Fc tag for improved solubility.	(Berrow *et al.* 2007)
pOPINTTGneo-3c-HALO7	A derivative of pOPINTTGneo with a C-terminal HALO7 tag for improved solubility.	(Berrow *et al.* 2007)
pOPINTTGneo-3c-CD4	A derivative of pOPINTTGneo with a C-terminal CD4 tag for improved solubility.	(Berrow *et al.* 2007)

Table 2.2. Expression plasmids used in this study for the production of recombinant target proteins and Affimers

2.3.2 Polymerase Chain Reaction (PCR)

PCR was conducted in 0.2 ml PCR tubes (Thermo Fisher) using a G-Storm GS2 Thermal Cycler (Gene Technologies). Reactions were set up using Phusion® High-Fidelity DNA Polymerase (New England Biolabs, Inc). Primers used in PCR reactions are detailed in **Table 2.3**. PCR mixtures included 0.2 mM dNTPs, 0.5 µM forward primer, 0.5 µM reverse primer, 10 ng template DNA 1X Phusion HF Buffer and 1 unit of Phusion® High-Fidelity DNA Polymerase per 50µl reaction. The cycling conditions of PCR reactions were as follows: initial denaturation at 98 ^{o}C for 30 seconds. 30 cycles of 98 ^{o}C for 10 seconds, 45-72 ^{o}C for 30 seconds and 72 ^{o}C for 30 seconds (per kb of DNA to be amplified). A final extension at 72 ^{o}C for 10 minutes was then conducted.

2.3.3 DNA agarose gel electrophoresis

DNA samples were mixed with an appropriate volume of 6X purple gel loading dye (New England Biolabs, Inc) and 5 µl of each sample was loaded on to an appropriate percentage agarose gel in TAE (40 mM Tris, 20 mM acetate and 1 mM EDTA) containing 1X SYBR Safe (Thermo Scientific). A 1 kb plus DNA ladder, previously 2-log DNA ladder (New England Biolabs, Inc) was also added to the gel to determine the molecular weight of the analysed DNA. Electrophoresis was conducted in a wide mini-sub cell GT cell system (Bio-Rad) in TAE buffer at 100 V and bands were visualised under UV using Amersham™ Imager 680 (GE Healthcare).

2.3.4 Purification of DNA

Purification of DNA was conducted by PCR clean-up using a QIAquick PCR purification kit (Qiagen) or extracted from agarose gel using a QIAquick Gel Extraction kit (Qiagen), both according to manufacturers instructions however DNA was eluted using ddH_2O as an alternative to the recommended TE elution buffer. DNA was stored at 4 ^{o}C for short-term storage or -20 ^{o}C for long-term storage.

2.3.5 Plasmid purification from *E. coli*

A single colony from an LB agar plate was inoculated in to either 3 mL or 250 mL of LB broth supplemented with the appropriate antibiotic to be processed by mini-preparation or maxi-preparation of DNA respectively. Cells were incubated overnight at 37 ^{o}C, 230 rpm. The following day, cells were processed using a QIAprep spin miniprep kit (Qiagen) or a Qiagen Plasmid Maxiprep Kit (Qiagen) according to manufacturer's instructions. DNA was eluted in an appropriate volume of ddH_2O.

2.3.6 DNA sequencing

Following purification of plasmid DNA, a 15 µl aliquot at a concentration of 50-100 ng/µl was sent for sequencing using Genewiz (previously Beckman Genomics) using a vector specific primer. For example, pET vectors were sequenced with a T7 forward primer and a T7 reverse primer whilst pD649-D was sequenced using a CMV forward primer and a BGH reverse primer. pDHis was sequenced using an M13 reverse primer. Analysis of DNA sequences was performed using MacVector.

2.4 Molecular cloning

2.4.1 Cloning into expression vectors

The expression vector pET11a was used for bacterial production of recombinant target proteins and Affimers and the genes of interest were cloned into them from parental vectors using the primers detailed in **Table 2.3**. Primers for the pOPIN vectors used for mammalian expression were designed using the online tool https://www.oppf.rc-harwell.ac.uk/Opiner/. All other primers were available from BioScreening Technology group, Leeds, or designed manually.

Expression vector	**Expression system**	**Parental vector**	**Forward primer (5' – 3')**	**Reverse primer (5' – 3')**	**Restriction enzyme**
pET11a – Affimer (no cysteine)	Bacterial	pDHis	ATGGCTAG CAACTCCCT GGAAATCG AAG	TACCCTAGTGG TGATGATGGT GATGC	*NheI/NotI*
pET11a-Affimer (cysteine)	Bacterial	pDHis	ATGGCTAG CAACTCCCT GGAAATCG AAG	TTACTAATGCG GCCGCACAAG CGTCACCAACC GGTTTG	*NheI/NotI*
pET11a-P2X3 L44-T155	Bacterial	P2X3-pD649-D	AGAGTGCT AGCATGCTC CACGAAAA AGCC	TATATATATCG CGGCCGCGGT CGGGCACCAG CCCTGAATTT	*NheI/NotI*
pET11a-P2X3 T155-N317	Bacterial	P2X3-pD649-D	AGAGTGCT AGCATGAC CGAGGTGG ACA	TATATATATCG CGGCCGCGTT GAACTTCC	*NheI/NotI*
pET11a-P2X3 L44-N317	Bacterial	P2X3-pD649-D	AGAGTGCT AGCATGCTC CACGAAAA AGCC	TATATATATCG CGGCCGCGTT GAACTTCC	*NheI/NotI*
pOPINTTGneo	Mammalian	P2X3-pD649-D	GCGTAGCT GAAACCGG CCTCCACGA AAAAGCCT ACCAA	GTGATGGTGA TGTTTGTTGAA CTTCCCGGCGT TGCC	InFusion Cloning
pOPINTGneo-3C-Fc	Mammalian	P2X3-pD649-D	GCGTAGCT GAAACCGG CCTCCACGA	CAGAACTTCCA GTTTGTTGAAC TTCCCGGCGTT	InFusion Cloning

			AAAAGCCT ACCAA	GCC	
pOPINTTGneo-3C-CD4	Mammalian	P2X3-pD649-D	GCGTAGCT GAAACCGG CCTCCACGA AAAAGCCT ACCAA	CAGAACTTCCA GTTTGTTGAAC TTCCCGGCGTT GCC	InFusion Cloning
pOPINTTGneo-3C-HALO7	Mammalian	P2X3-pD649-D	GCGTAGCT GAAACCGG CCTCCACGA AAAAGCCT ACCAA	CAGAACTTCCA GTTTGTTGAAC TTCCCGGCGTT GCC	InFusion Cloning

Table 2.3. Primers used in this study for the amplification of recombinant target protein and Affimer DNA for expression. Restriction sites underlined.

2.4.2 Restriction digestion

Restriction digestion of amplified DNA was performed according to manufacturer's instructions using the appropriate restriction enzymes as outlined in **Table 2.3**. Digestion of DNA took place for one hour at the appropriate temperature and where possible, enzymes with compatible buffers were used. In cases where this was not possible, a DNA clean up procedure took place between incubation with different enzymes so that the appropriate buffer could be used. The restriction digest took place by incubating 1 µg of template DNA with 1 unit of enzyme, 1x CutSmart Buffer made up to a total volume of 50 µl with ddH_2O. The resulting DNA was analysed by agarose gel electrophoresis on an appropriate percentage gel. Generally, amplified DNA product was analysed using a 2% (w/v) agarose gel and digested vector analysed using a 1% (w/v) agarose gel. DNA was purified according to section 2.3.4.

2.4.3 DNA ligation

Following purification of digested DNA products, insert DNA was ligated into appropriately restriction digested vector DNA using T4 DNA ligase (NEB)

according to manufacturer's instructions. Vector and insert DNA were mixed with 1x T4 DNA ligase buffer and 1 unit of T4 DNA ligase in a total volume of 20 µl. Generally, a 3:1 molar ratio of insert to vector DNA was used in a total DNA amount of ~100 ng. As an example, the following equation was used to set up the ligation reaction for Affimer insert in to pET11a vector:

Size of pET11-a plasmid = 5639bp

Molecular mass of dsDNA fragment = number of bps X 660 Da.

Molecular mass of ds plasmid = 5639 x 660 = 3.7 x 10^6 Da.

1 mole = 3.7 x 10^6 g

1 fmol = 3.7 ng

15 fmol = 55.5 ng

Size of Affimer insert = 309 bp

Molecular mass of ds insert = 309 x 660 Da.

1 mole = 309 x 660 = 2 x 10^5 Da

1 fmol = 0.2 ng.

45 fmol = 9 ng.

Total DNA = 64.5 ng.

Ligated DNA was transformed in to XL-1 Blue super-competent cells (see section 2.5.1) for culturing and DNA extracted by mini-preparation according to section 2.3.5. Resulting DNA was sent for sequencing to check for successful ligation according to section 2.3.6. On return of sequencing data, successfully cloned DNA was transformed into an appropriate bacterial cell strain (**Table 2.1**) for protein expression.

2.5 Expression and purification of proteins

2.5.1 Transformation of chemically competent *E. coli*

20 µl of the appropriate chemically competent *E. coli* cells (**Table 2.1**) were incubated with 2 µl of DNA encoding the protein of interest for thirty minutes on ice. Cells were then incubated at 42 ^{o}C for 45 seconds and then returned back to ice for a further two minutes. 180 µl of SOC medium was then added to cells and incubated for one hour at 37 ^{o}C, 230 rpm. 20 µl of recovered cells were then

plated on to LB agar containing the appropriate antibiotic (carbenicillin at 100 µg/mL or kanamycin at 50 µg/mL) and incubated for 16 hours at 37 ^{o}C.

2.5.2 Production of recombinant protein

Following transformation of the appropriate cell strain with the protein-encoding DNA, a colony from a fresh transformation plate was inoculated in to 10 mL of 2YT broth with the appropriate antibiotic and incubated at 37 ^{o}C, 230 rpm for 16 hours. The following day, the OD_{600} of the starter volume was measured by spectrophotometry and the required volume of starter culture was inoculated in to the expression culture media to reach a starting OD_{600} of 0.1. The volume of expression culture media was dependent on how well the protein of interest expressed, for example, Affimer proteins were generally expressed in 50 mL cultures while recombinant ion channel fragments were expressed in 500 mL cultures as a starting point. Cells were grown at 37 ^{o}C, 230 rpm until an OD_{600} of 1.0 was reached. Protein expression was induced with 0.25 mM IPTG (Sigma Aldrich). Protein expression then took place by incubating cells at 25 ^{o}C, 150 rpm for 16 hours. Cells were then harvested by centrifugation using a Sorvall^{TM} Legend^{TM} XTR centrifuge (Thermo Scientific) at 4,000 x g for 20 minutes. Cell pellets were either stored at -20 ^{o}C or processed immediately.

2.5.3 Purification of recombinant protein

Following expression of recombinant protein, cell pellets were lysed by resuspension in lysis buffer supplemented with 0.1% Triton X-100 (v/v), 250 µg/ml lysozyme (Sigma Aldrich), 1 x Halt protease inhibitor cocktail (Thermo Fisher) and 1 unit of benzonase nuclease (Merck Millipore) for one hour with agitation at room temperature. Cells were then incubated for 20 minutes at 37 ^{o}C and cell debris pelleted by centrifugation at 4,000 x g for 30 minutes using a Sorvall^{TM} Legend^{TM} XTR centrifuge (Thermo Fisher). A sample of pellet and supernatant was retrieved for analysis by SDS PAGE (see section 2.6.1). Cell supernatant was then processed for purification of recombinant protein.

2.5.3.1 Ion Metal Affinity Chromatography (Batch method)

Prior to use, 500 µL HisPur Ni-NTA agarose resin (Life Technologies) was prepared by removal of storage ethanol and resuspension in wash buffer. Prepared resin was then incubated in protein-containing supernatant for one hour at room temperature with agitation. After incubation with supernatant for one hour, resin was retrieved by centrifugation at 1,000 x g for one minute. Unbound fraction was removed and stored at -20 ^{o}C and resin was washed in an initial volume of 50 mL wash buffer followed by five sequential wash steps with 1 mL of wash buffer until an OD_{280} reading of <0.05 was achieved by Nanodrop spectrophotometry (Nanodrop Lite, Thermo Scientific). Bound protein was eluted by incubation of resin with 1 mL of elution buffer for 5 minutes followed by collection. Eluted protein was stored at 4 ^{o}C for future use. SDS PAGE was used to analyse samples from unbound, wash and bound fractions (see section 2.6.1).

2.5.3.2 Size exclusion chromatography (SEC)

A superdex G-75 pre-packed column (GE Healthcare) was prepared by washing in ddH_2O and equilibrated with Tris buffered phosphate, pH 7.4, using a ÄKTA system (GE Healthcare). After an initial IMAC purification, eluted protein was concentrated to a volume of 2 mL using an Amicon® Ultra 15 mL 3K MWCO centrifugal filter (Merck) and filtered using a 0.25 µm filter (Sartorius) and loaded on to the SEC column using a 5 mL injection loop. Purified samples were collected in 1 mL fractions and fractions corresponding to observed peaks based on the monitored optical density at 280 nm were analysed by SDS PAGE. Following completion of the SEC method, the column was washed with ddH_2O and stored in 20% ethanol.

2.5.4 Protein concentration

Protein concentration of expressed and purified proteins was determined using A280 nm measurement on Nanodrop Lite Spectrophotometer (Thermo Scientific) and BCA assay according to manufacturers instructions (Bio-Rad: Cat. No. 23225).

2.5.5 Biotinylation of recombinant proteins

Following purification of recombinant target proteins, biotinylation was performed using EZ Link® NHS-SS-Biotin (Thermo Scientific: Cat. No. 21441) to label proteins via primary amines. A 5 mg/mL solution of EZ Link® NHS-SS-Biotin was prepared in DMSO and an appropriate volume (according to manufacturers instructions) incubated with a recombinant protein for one hour at room temperature. Excess biotin was then removed by desalting using a Zeba™ Spin Desalting Column, 7K MWCO (Thermo Fisher: Cat. No. 89882) according to the manufacturers instructions. The labelled protein was placed at 4 ^{o}C for short-term storage or mixed with an equal volume of 40% glycerol, frozen in liquid nitrogen and placed at -80 ^{o}C for long-term storage.

Alternatively to labelling via primary amine groups, available sulfhydryl groups were labelled using maleimide biotin (Sigma Aldrich: Cat. No. B1267). Initially, sulfhydryl groups were made available for labelling by reducing in TCEP reducing resin (Thermo Fisher: Cat. No. 77712) according to manufacturers instructions. Following reduction of sulfhydryl groups, a 5 mg/mL maleimide-biotin solution was prepared in DMSO. Maleimide-biotin was incubated with reduced protein for one hour at room temperature according to manufacturers instructions and excess biotin removed by desalting, as previously described.

2.5.6 ELISA to analyse biotinylation of proteins

Biotinylation of recombinant proteins was confirmed by ELISA. Biotinylated protein was adsorbed on to Nunc-Immuno™ maxisorp™ strips (VWR: Cat. No. 735-0054) in PBS overnight at 4 ^{o}C. Strips were then blocked in 2x blocking buffer (Sigma Aldrich: Cat. No. B6429) for one hour and washed and incubated with high-sensitivity streptavidin-HRP (Thermo: Cat. No. 21130) for one hour. Strips were then washed and the presence of streptavidin-HRP was assessed by addition of TMB (Seramun: Cat. No. S-001-1-TMB). The absorbance was measured at 620 nm using a Multiskan Ascent plate reader (MTX Lab System Inc: Cat. No. P97266). Non-biotinylated protein was included as a negative control.

2.6 Protein characterisation

2.6.1 Sodium Dodecyl Sulphate Polyacrylamide Gel Electrophoresis (SDS PAGE)

SDS PAGE was performed according to the method described by Laemmli (Laemmli 1970). Briefly, protein samples were mixed with 2x Laemmli loading buffer supplemented with β-mercaptoethanol (Sigma: Cat. No. 516732) at a 1:1 ratio and boiled at 95 ^{o}C for five minutes. Proteins were separated on a 12% SDS PAGE gel using a MINI-PROTEAN Tetra Cell system (Bio-Rad: Cat. No. 1658005EDU) in SDS PAGE running buffer at 180V for 30 minutes. A protein marker (Precision Plus Dual Colour Standard, Bio-Rad: Cat. No. 1610374) was also run alongside samples for molecular weight determination. Electrophoresed gels were stained using Coomassie blue stain (45% v/v methanol, 10% v/v acetic acid, 0.25% w/v Coomassie brilliant blue R-250) for thirty minutes followed by incubation in destain buffer (30% v/v methanol, 10% v/v acetic acid) until clear. Gels were visualised under a white light using Amersham^{TM} Imager 680 (GE Healthcare).

2.6.2 Western blot

For analysis by western blotting, proteins were separated as described in section 2.6.1 and the resulting proteins transferred to nitrocellulose using a Trans Blot Turbo Transfer system (Bio-Rad) according to manufacturers instructions. Nitrocellulose was subsequently blocked with 5% BSA supplemented with 0.05% Tween 20 for one hour at room temperature and then incubated for one hour with the detection antibody, for example, anti-His (HRP) conjugated antibody (Abcam), for one hour at room temperature in 5% BSA. Unbound antibody was subsequently removed by washing with Tris Buffered Saline supplemented with 0.1% Tween 20 (TBS-T) for three washes of five minutes each with gentle agitation. Visualisation of protein then took place by incubation with TMB substrate. Blots were imaged under white light using Amersham^{TM} Imager 680 (GE Healthcare: Cat. No. 29270772).

2.6.3 Circular Dichroism (CD)

CD was conducted using Applied Photophysics Chirascan apparatus and software. The following parameters were used for each CD scan: 190-260 nm range, time interval 0.5 sec, step = 1 nm, path length = 10 mm. Scans were averaged from triplicate samples and control buffer only samples subtracted from experimental samples. Secondary structure was determined using standard scans in the UV range.

2.6.4 Fluorescence Anisotropy

Fluorescence anisotropy was performed in 384 well, dark well plates (Thermo Scientific: Cat. No. 10713767) in triplicate. Control wells of buffer only were set up and deducted from experimental wells. 10 µl of 1 µM of expressed P2X3 extracellular domain recombinant protein was added to 10 µl of 1 µM MANT-ATP (Thermo Fisher: Cat. No. M12417) at a range of concentrations or buffer only (as a control). The plate was incubated in the dark for thirty minutes and then anisotropy of the MANT-ATP measured on a Tecan Spark 10M plate reader at 25 ^{o}C with excitation at 356 nm and emission at 448 nm. The intensity was calculated for each measurement using the equation I = (2PG) + S. Anisotropy was calculated using the equation R = (S-PG)/I.

2.6.5 X-ray crystallography

Crystallisation screens were set up in 96 well plates using 384 unique JCSG buffer conditions (Molecular Dimensions, JCSG). Trials were set up using a Douglas Oryx 6 plate loader using NT8 software with drops added at 0.2 µl volume at a 1:1 and 2:1 ratio with buffer (Molecular Dimensions, JCSG). Wells were sealed with adhesive plate sealant and stored at room temperature. Crystals were picked and coated in cryoprotectant and then stored in liquid nitrogen. All data were collected at Diamond Light Source. Assistance was provided throughout crystallisation screens and analysis of retrieved data by Dr. Chi Trinh.

2.6.6 Small molecule screening

Identification of small molecule Affimer mimetics was conducted using Rapid Overlay of Chemical Structures (ROCS) software (OpenEye Scientific). Affimer binding residues were selected from a crystal structure solved in this study with important residues used for creating a pharmacophore for the identification of small molecules of similar shape and structure using ROCS software. A large 150,000 compound library developed by the Medicinal Chemistry and Chemical Biology (MCCB) Technology Group at the University of Leeds was screened from which the top 1000 most similar compounds based on shape and structure were advanced into a secondary screen against the TRPV1 peptide crystallised in this study. In this secondary screen, AutoDock Vina was used to prepare the target peptide for screening with the 1000 identified compounds using PyRx virtual screening tool (Source Forge). The top 50 compounds based on estimated binding affinities were then taken forward for further studies.

2.7 Mammalian cell culture

2.7.1 Cell passage

Cell lines used in this study included HEK293, CHO and U2OS cell lines. Cells were generally maintained in a T75 vented tissue culture flask and incubated at 37 ^{o}C in a hydrated 5% CO_2 atmosphere until ~70-80% confluent. Cells were cultured in DMEM (+10% foetal calf serum and 1% v/v penicillin and streptomycin). For passaging cells, DMEM was aspirated and cells washed in PBS prior to incubation in 2 mL trypsin at 37 ^{o}C for 5 min. Trypsinisation was quenched with 8 mL DMEM (+10% FBS and 1% v/v penicillin and streptomycin) and cells centrifuged at 800 x g for 5 min and the pellet re-suspended in 4 mL DMEM. Cells were split 1:4 and cultured up to passage 30.

2.7.2 Mammalian cell transfection

Cell transfection took place using FuGENE HD Transfection Reagent according to manufacturers instructions. Briefly, FuGENE HD Transfection Reagent was mixed with DNA at a 3:1 ratio (µl:µg) and incubated for 10 minutes at room temperature in OptiMEM media (Note: volumes were dependent on the number

of cells being transfected). Cells were transfected at a confluence of approximately 60-80% and then incubated for 48 hours to enable expression of the protein of interest.

2.7.3 Ion channel modulation assays

Cell lines stably expressing the ion channel of interest were seeded in to black-walled 96 well plates (Greiner Bio-One) at 100,000 cells/well for use the following day. If cells were to be transfected with DNA encoding the ion channel of interest, cells were seeded to a T25 vented tissue culture flask and transfected at a confluence of 60%. DNA was transfected to cells according to section 2.7.2 and cells incubated for 24 hours prior to trypsinisation and seeding in to black-walled 96 well plates as above.

When at a confluence of ~95-100%, cells were incubated with 50 µL of 1 µM Fluo-4 AM (Thermo Fisher) and 0.1% pluronic F127 for one hour at 37 ^{o}C in the dark in the presence of 5% CO2. Cells were washed with 200 µL of assay buffer and incubated for a further 30 min (to enable de-esterification of the Fluo4-AM to allow for Ca^{2+} binding). Calcium imaging was then conducted using a FlexStation III system (Molecular Devices) with excitation and emission wavelengths set at 485 nm and 525 nm respectively. Triplicate wells were set up with a buffer only control used to normalise experimental conditions. Measurements were taken at 5 sec intervals and data analysed using GraphPad Prism software. The relative Fluo-4 AM fluorescence changes for each well were expressed as $\Delta F = (F - F_0)$, where F and F_0 are fluorescence values at the time of interest and beginning of the reading, respectively.

When testing for modulation of ion channel by Affimer, during the 30 min de-esterification incubation, 1 µM of Affimer was incubated on cells for testing inhibition or potentiation. For testing direct activation, 1 µM of Affimer was loaded on to cells using the Flexstation III plate reader.

2.7.4 Immunocytochemistry

Cells expressing the protein of interest were seeded on to sterile glass coverslips (Fisher Scientific) at a confluence of approximately 30% and incubated overnight at 37 ^{o}C, 5% CO_2. Next, for live cell staining, Affimers were incubated on live cells

at a concentration of 5 µg/mL for 20 min in assay buffer. Cells were washed three times for five min each in assay buffer and fixed in 4% PFA in PBS. Cells were then permeabilised with 0.1% Triton X-100 in PBS and then blocked with 1% BSA in PBS at room temperature for 30 min. Next, cells were incubated in anti-His antibody (mouse) (Abcam: Ab18184) for one hour and washed three times with PBS. Cells were then incubated in anti-mouse-488 antibody (Life Technologies: A11001) for one hour in the dark. Cells were washed twice with PBS-T for 5 min each followed by two 5 min washes with PBS and finally one 5 min wash with ddH_2O. Coverslips were then mounted on glass slides with ProLong Diamond Antifade Mountant with DAPI (Thermo Fisher Scientific). For fixed cell staining, cells were washed with sterile PBS and fixed using 4% PFA in PBS for 10 min. PFA was removed from cells and cells were washed with PBS. Cells were then permeabilised using 0.1% Triton X-100 in PBS for 20 min. Cells were washed with PBS and blocked using 1% BSA in PBS for one hour at room temperature. Cells were then incubated with 5 µg/mL Affimer in PBS for one hour with gentle agitation. Cells were then washed three times with PBS-T and anti-His antibody (mouse) (Abcam: Ab18184) incubated on cells for one hour and washed three times with PBS. Cells were then incubated with anti-mouse-488 antibody (Life Technologies: A11001) for one hour in the dark. Cells were washed twice with PBS-T, twice with PBS and once with ddH_20, each for 5 min. Coverslips were mounted on to glass slides (Fisher Scientific) using ProLong Diamond Antifade Mountant with DAPI (Thermo Fisher Scientific). The next day, samples were imaged using an EVOS FL imaging system (Thermo Fisher Scientific).

2.8 Affimer identification

2.8.1 Phage display of recombinant proteins

Recombinant protein was prepared for phage display by biotinylation according to section 2.5.5. For biopanning round one, biotinylated target protein was incubated on pre-blocked high-binding capacity (HBC) streptavidin-coated wells (Pierce: Cat. No. 15501) for one hour at room temperature with agitation. Wells were washed with TBS-T using a HydroFlex™ plate washer (Tecan) and 5 µl of Affimer phage library (Tiede *et al.* 2014) incubated with streptavidin only wells

for three incubation periods of 40 minutes each to remove non-specific binding Affimer phage. The remaining pool of Affimer phage that had not bound to the streptavidin-coated wells were then incubated with target protein for one hour and then the well was washed with TBS-T. Bound Affimer phage were eluted initially using 50 mM glycine-HCl (pH 2.2) and neutralised with 1 M Tris-HCl, pH 9.1 and subsequently with 100 mM triethylamine neutralised with 1 M Tris-HCl, pH 7.0. Eluted Affimer phage were infected into log-phase ER2738 *E. coli* cells (OD_{600} ~0.8) followed by incubation at 37 ^{o}C for one hour. Cells were plated on to LB agar plates supplemented with 100 µg/mL carbenicillin. The following day, cells were scraped and diluted in to 8 mL of 2TY broth supplemented with 100 µg/mL carbenicillin to achieve an OD_{600} of 0.1. Cells were grown to an OD_{600} of 1.0 following which incubation with 0.32 µl of M13K07 helper phage (titre ca 10^{14}/mL) for thirty minutes at 37 ^{o}C, 90 rpm took place. Kanamycin was then added to a concentration of 50 µg/mL and cells incubated overnight at 25 ^{o}C, 150 rpm. The following day, ER2738 *E. coli* cells were pelleted and phage-containing supernatant advanced in to a second round of biopanning.

The second round of biopanning was conducted on magnetic streptavidin-coated beads (Thermo: Cat. No. 88816). Two rounds of negative selection took place by incubating the Affimer phage enriched from panning round one with streptavidin-coated beads for three negative selection steps of thirty minutes each. Affimer phage that had not bound to the streptavidin beads only were then incubated with streptavidin-beads coated with target protein for one hour. Beads were then washed and bound Affimer phage eluted using a KingFisher™ Flex Purification System (Thermo Scientific). Elution and neutralisation buffers remained the same as those used in panning round one. Procedures conducted for infection of ER2738 *E. coli* cells and recovery of enriched phage also remained the same. Recovered Affimer phage were then advanced in to a final round of biopanning.

The third round of biopanning was conducted on NeutrAvidin™-coated strips (Thermo: Cat. No. 15127) with all steps remaining the same as those used in biopanning round one. However, in the positive selection stage, pre-panned phage were split between the target-containing well and a negative control,

NeutrAvidin™-coated strip well only. Following washing and elution steps, separate aliquots of ER2738 *E. coli* cells were infected with eluted phage from experimental and negative control wells and a range of volumes plated on to LB agar supplemented with 100 µg/mL carbenicillin. The next day, colony counts were conducted for comparison between experimental and negative control conditions. A substantial increase in colonies on the experimental plates compared to the control plates suggested target-specific phage had been isolated with subsequent confirmation by phage ELISA taking place (see section 2.8.2).

2.8.2 Phage ELISA

Individual colonies from the final round of biopanning were grown in 200 µl of 2TY broth supplemented with 100 µg/mL carbenicillin in deep well 96 well plates (Thermo Fisher: Cat. No. 13545450) at 37 ^{o}C, overnight with gentle agitation. The following day, 25 µl of overnight inoculum was added to 200 µl of 2TY supplemented with 100 µg/mL carbenicillin and grown at 37 ^{o}C with agitation for one hour. M13K07 helper phage (titre ca. 10^{14}/mL) was diluted 1/1000 in 2TY and 10 µl added to cells for thirty minutes at room temperature with agitation. Kanamycin was then added to cells at 50 µg/mL and cells incubated overnight at 37 ^{o}C with agitation. The following day, 96 well plates were centrifuged and phage-containing supernatant used for the phage ELISA procedure. During phage preparation, target preparation also took place. Nunc-Immuno™ maxi-sorp™ plates (Thermo: Cat. No. 44-2401-21) were coated with 50 µL of 5 µg/mL target protein (or buffer only as a negative control) overnight at 4 ^{o}C. The following day, plates were blocked using 2x blocking buffer at 37 ^{o}C overnight. The following day, plates were washed with TBS-T and available for incubation of Affimer clones during phage ELISA.

Following addition of prepared phage to target protein, phage were incubated against target protein for one hour at room temperature with agitation. Wells were then washed with TBS-T and incubated with anti-Fd (HRP conjugated) antibody according to manufacturer instructions for one hour at room temperature with gentle agitation. Wells were then washed with TBS-T and

TMB substrate added. Absorbance was measured at 620 nm using a Multiskan Ascent plate reader (MTX Lab Systems Inc).

2.8.3 Phage display against mammalian cells

Cell-based phage display will be described in chapter six of this thesis however briefly, for biopanning in suspension, two pre-panning rounds, each of one hour, against non-transfected cells (8.4×10^6) preceded a one-hour panning round against cells (2.8×10^6) transfected with target protein-encoding DNA. For the panning round, non-bound phage from the negative selection stage were divided between transfected and non-transfected cells. Cells were washed manually and bound phage eluted as described in section 2.8.1. Infection of ER2738 cells with eluted phage took place as described in section 2.8.1.

2.8.4 Cell-based phage ELISA

Cells were prepared as in section 2.7.3. Once fully confluent, cells were harvested and transferred to three tissue-culture 96-well plates (5×10^4 cells per well) (Sigma Aldrich: Cat. No. CLS3595) with transfected cells occupying columns 1-4, non-transfected cells occupying columns 5-8 and columns 9-12 remaining blank. Three 96-well plates enabled validation of binding of 96 Affimer clones from the final phage display round.

Adherent cells were fixed for 30 minutes with 2% PFA and blocked overnight with 2X blocking buffer at 4 ^{o}C. Phage clones were prepared as described in section 2.8.2. Phage clones were tested against each target well condition (transfected, non-transfected and blank well) and phage ELISA performed as described in section 2.8.2.

2.8.5 Affimer production and purification

Following identification of Affimer clones able to bind specifically to the screened target protein, the Affimer encoding region was sub-cloned from pBSTG1 to pET11a by amplifying the coding region using primers outlined in **Table 2.3**. Amplified DNA was then digested with *NheI* and *NotI* enzymes and ligated in to a similarly digested pET11a expression vector. Cloning was conducted as outlined in section 2.4.

2.8.6 Protein dialysis and refolding

Dialysis of purified proteins took place using Slide-A-Lyzer™ Dialysis Cassettes with a molecular weight cut-off appropriate for the protein being dialysed. The Slide-A-Lyzer™ Dialysis Cassette was prepared according to manufacturers instructions. Briefly, wetting of the membrane took place by incubation with PBS for 5 minutes. Next, a syringe and needle were used to insert a small amount of air in to the cassette to prevent puncture of the membrane. The protein to be dialysed was subsequently inserted in to the cassette using the syringe and needle. Excess air was removed from the cassette. The dialysis cassette was subsequently incubated in 5 L of PBS with occasional replacement of buffer.

For refolding of denatured proteins, for example the recombinant P2X3 extracellular domains, the previously described protocol was used however sequential reduction of urea took place in the dialysis buffer until buffer no longer contained urea. Protein was then removed from the dialysis cassette and aggregated protein removed by centrifugation.

2.8.7 Protein-ELISA to assess Affimer binding to target

Binding of expressed Affimer was validated by protein ELISA. 0.5 µg/ml Affimer was incubated on fixed cells or recombinant protein target for one hour. Unbound Affimer was washed away. Next, 1:1000 dilution of anti-6X His-HRP antibody (Abcam: Cat. No. ab1187) in a total volume of 200 µL 2X blocking buffer was added to cells for 1 hour. After incubation at room temperature with gentle agitation for one hour, unbound antibody was washed away with TBS-T and addition of TMB enabled identification of bound antibody. Absorbance was measured at 620 nm using Multiskan Ascent plate reader (MTX Lab Systems Inc).

2.8.8 Data analysis

Bioinformatic analysis was conducted using Clustal Omega Multiple Sequence Alignment (EMBL-EBI). Sequence data was obtained from National Centre for Biotechnology Information (NCBI) (www.ncbi.nlm.nih.gov) and then input in to Clustal Omega Multiple Sequence Alignment tool.

Data analysis was conducted using GraphPad Prism 7 software (GraphPad Software Inc). The following equations were used to fit data:

Receptor-ligand binding:

$$R + L \leftrightarrow C$$

In this equation, R denotes the receptor, L denotes the ligand and C denotes the complex. The dissociation constant (K_d) can be used to describe the equilibration constant of the receptor-ligand binding using the following equation:

$$K_d = K_{-1} / K_1 = [R]_{eq} [L]_{eq} / [C]_{eq}$$

In this equation, K_d is the dissociation constant, K_1 and K_{-1} are the forward and backward rate constants respectively.

Dose-response:

$$Y = Bottom + (Top – Bottom) / (1 + 10^{\wedge} ((LogEC_{50} – X)))$$

In this equation, EC_{50} is the concentration of agonist that gives a 50% response. Top and Bottom are plateaus in the units of the Y axis.

Conversion between units:

To convert units of concentration from mg/mL to M, the following equation was used:

Concentration (mg/mL) / Molecular weight (Daltons) = Concentration (Molar)

To convert from Angstrom (Å) to nanometer, the following equation was used:

$$1 Å = 0.1 nm$$

Chapter 3

Positive allosteric modulation of TRPV1 by Affimer reagents

3 Positive allosteric modulation of TRPV1 by Affimer reagents

3.1 Introduction

The limited development of novel analgesics in the past decade has resulted in increased use of opiates for the treatment of chronic pain (Johannes *et al.* 2010). The off-target side effects caused by targeting opioid receptors in the central nervous system has prompted the search for reagents able to treat chronic pain at its site of initiation within the peripheral nervous system (Wolfe *et al.* 2012). The Transient Receptor Potential family of ion channels, primarily located in the sensory nerve endings, have been implicated in pain signalling through their coupling to inflammatory signalling cascades and their overexpression in mice models of chronic pain (Pingle *et al.* 2007, Rosenbaum and Simon 2007, Luo *et al.* 2013).

The mammalian TRP channel family consists of >30 family members that can be divided in to TRPA (Ankyrin), TRPC (Classical), TRPM (Melastatin) and TRPV (Vanilloid) (Nilius and Owsianik 2011). Although some members outside the TRPV channel family have been shown to be up regulated in chronic pain, such as TRPA1 and TRPM8 (Julius 2013, Liu *et al.* 2013, Nassini *et al.* 2014), all of the TRPV channel members have been implicated in pain sensation to some extent (Levine and Alessandri-Haber 2007, De Schepper *et al.* 2008, Mitchell *et al.* 2010). The high expression of TRPV1 in non-myelinated C-fibres and lightly myelinated Aδ- fibres, along with its up-regulation in animal models of chronic pain, highlights this member of the TRPV family as a key target for drug development. Its sensitisation by inflammatory mediators (Brain 2011) and its increased expression in nerve damage (Zakir *et al.* 2012) implicate TRPV1 in both inflammatory and neuropathic pain. The variation in homology between TRPV channels (**Figure 3.1**A) makes selective targeting feasible, an essential attribute of any TRPV1-targeting drug due to the widespread expression of TRPV channels in a variety of tissues (Julius 2013).

The TRPV1 receptor responds to an array of stimuli including temperature (>43 ^{o}C), protons and vanilloid ligands such as capsaicin (Caterina *et al.* 1997, Dhaka *et al.* 2009). Additionally, a number of small molecules and peptide toxins

have demonstrated efficacy at TRPV1 receptors. The toxin, DkTx, from the Chinese bird spider has recently been identified as a potent activator of TRPV1 through targeting the outer pore domain (Bohlen *et al.* 2010, Gonzalez-Reyes *et al.* 2013). The low level of similarity of the DkTx epitope of TRPV1 between other family members (**Figure 3.1**B, *bold*) highlights a potential epitope that could be used for the development of highly selective reagents against TRPV1.

Figure 3.1. TRPV channel phylogenetic tree showing varying levels of homology. A. The phylogenetic relationship between the full-length TRPV channels is shown schematically. B. Alignment of the outer pore domain sequence between different TRPV channels is highlighted in bold.

In addition to peptide toxins such as DkTx, a large number of small molecule compounds have been explored as TRPV1 modulators (**Table 3.1**). Despite advancement of inhibitors into clinical trials, their success has been limited by devastating side effects, including hyperthermia and reduced sensation to thermal stimuli, with a number of compounds being withdrawn from clinical trials for this reason (Moran *et al.* 2011). More recently, the effect of ABT-102 on body temperature of healthy volunteers when administered at levels predicted to exert analgesia has been studied. Results demonstrated that an increased core body temperature of 0.6 to 0.8 ^{o}C was observed (Othman A, 2013. Effects of the TRPV1 antagonist ABT-102). The small molecule JTS-653 has recently been studied for its potential in attenuating bladder over activity (Kitagawa Y, 2013. JTS-653 blocks afferent nerve firing). More recently, the small molecule, NEO6860, a TRPV1 antagonist with novel modality has commenced phase I clinical trials (Chiche D, 2016. NEO6860, a novel modality selective TRPV1 antagonist).

Compound name	Company	Indication	Stage	Current status
ABT-102	Abbott	Unknown	Phase I	Initiated
AMG 517	Amgen	Dental pain	Phase Ib	Terminated
AZD1386	AstraZeneca	Dental pain	Phase II	Completed
GRC6211	Lilly/Glenmark	Dental pain	Phase II	Suspended
JTS-653	Japan Tobacco	Overactive bladder pain	Phase I	On going
MK2295	Merck/Neurogen	Dental pain	Phase II	Completed
SB-705498	GSK	Migraine, Rectal pain, Dental pain	Phase II	Terminated, Terminated, Completed
PF-4065463	Evotec/Pfizer	Unknown	Unknown	Unknown

Table 3.1. Overview of small molecule inhibitors of TRPV1 tested in clinical trials. ***Adapted from (Moran et al. 2011).***

As a result of the side effects associated with TRPV1 inhibition, activation of TRPV1 has been explored as an alternative method of producing analgesia through its ability to desensitise TRPV1 by calcium-induced cytotoxicity at the sensory neurons (Palazzo *et al.* 2010). A potential downfall of this method is the off-target effects that may be associated with activating all TRPV1 channels rather than those specifically involved in the pathology itself. For example, TRPV1 is also localised at the corneal epithelium (Zhang *et al.* 2007). Recently, a novel mechanism termed positive allosteric modulation has been described that proposes to overcome this problem. Reagents acting by this mechanism have no effect on TRPV1 channels without concurrent activation by a physiological, or pathological stimulus, for example inflammatory mediators produced in tissues inflicted by chronic pain (**Figure 3.2**). Positive allosteric modulators of TRPV1 would only act at channels predisposed to activation, such as those at a site of pain, resulting in a heightened activation and influx of Ca^{2+} leading to cytotoxicity and desensitisation of the sensory neuron, ultimately leading to analgesia.

Positive allosteric modulators of TRPV1 have already been identified, for example MRS1477 (Kaszas *et al.* 2012).

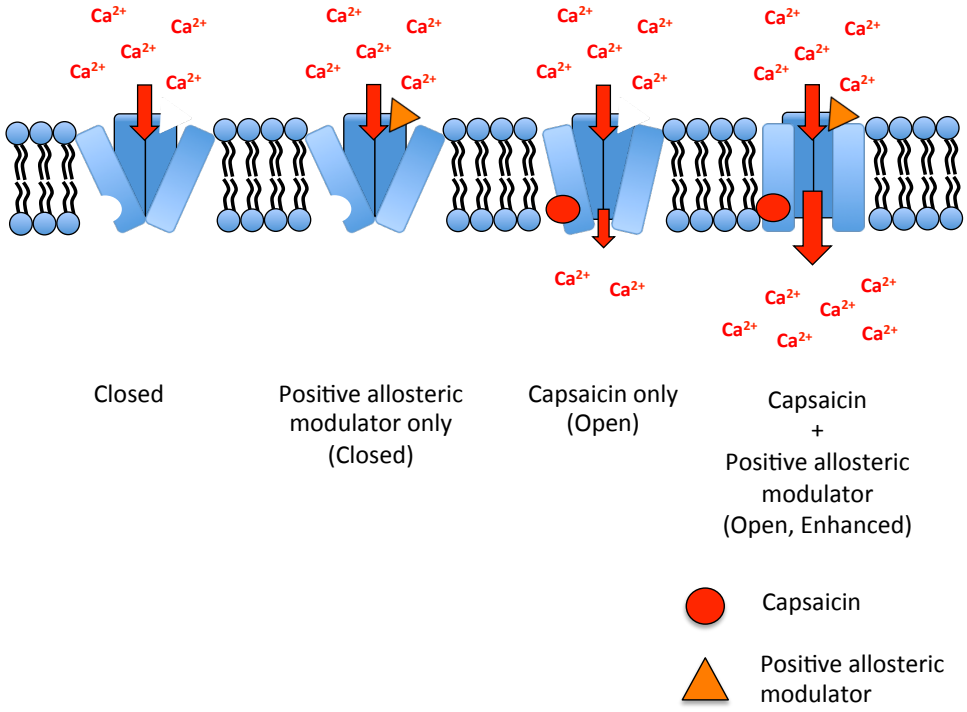

Figure 3.2. Positive allosteric modulation of TRPV1. In the absence of orthosteric agonist, in this case, capsaicin, the administration of a positive allosteric modulator alone would result in no activation of TRPV1 due to its inability to act as a direct agonist. When positive allosteric modulator is excluded and capsaicin is administered alone, such as in the case of chronic pain, the TRPV1 receptor would be activated to a low level, resulting in painful stimuli being processed. When positive allosteric modulator is administered alongside capsaicin however, TRPV1 activation is heightened resulting in calcium toxicity and subsequent desensitisation of TRPV1 to painful stimuli. *Adapted from* (Lebovitz *et al.* 2012).

In this chapter, the selection of Affimer reagents that are able to detect and modulate TRPV1 is described. Traditionally, using membrane proteins as targets for phage display selection can be problematic, with a number of methods described to try and overcome these problems. One such method is to screen against peptides mimicking the conformation of regions of full-length proteins. Despite having the disadvantage of excluding potentially important regions of

the full-length protein, this method provides the advantage of being able to selectively target regions of the protein known to be functionally important, for example regions of an ion channel pore.

To isolate Affimers against TRPV1, the peptide region mimicking DkTx epitope of TRPV1 (**Figure 3.1**B, *Bold*) was screened using the Affimer phage display library. A number of Affimer clones were isolated with the majority demonstrating similarity to the DkTx peptide described by (Bohlen *et al.* 2010). Further testing of these Affimers using *in vitro* assays revealed their ability to modulate the response of TRPV1 to capsaicin.

3.2 Results

3.2.1 Selection of TRPV1-specific Affimers against a peptide mimicking the TRPV1 outer pore domain

Affimers were isolated by phage display by screening a 15-mer peptide mimicking a region of the TRPV1 outer pore domain (residues 645-660 of human and rat TRPV1) (Tiede *et al.* 2017). This region was selected as a result of its accessibility and also as a result of its role in TRPV1 activation when bound by DkTx (Bohlen *et al.* 2010). Briefly, three rounds of positive selection were performed against the TRPV1 peptide followed by identification of monoclonal Affimers by phage ELISA. During the phage ELISA, a biotinylated peptide mimicking a region of the $Na_v1.7$ pore domain was used as a negative control due to its similar level of hydrophobicity. Results revealed a number of TRPV1-peptide specific Affimers (**Figure 3.3**). Sequencing of the isolated Affimers revealed common amino acids within the variable regions, particularly tryptophan and glycine residues within variable region one (**Table 3.2**). Furthermore, a lysine residue in the second variable region was common between Affimer clones. Interestingly, some of the clones, for example 3-5, that did not contain the tryptophan and glycine residues demonstrated a lower response by ELISA. Furthermore, these clones did not contain the truncated second variable region observed in the other clones. Despite this observation, some clones that did not contain the tryptophan and glycine residues were still able to produce a strong response by ELISA when incubated with the peptide,

possibly a result of binding to a different region of the peptide. The importance of the tryptophan-glycine motif in the DkTx inhibitor cysteine knot (ICK) one, along with a lysine residue in ICK two suggests a similar mechanism of binding (Bohlen *et al.* 2010).

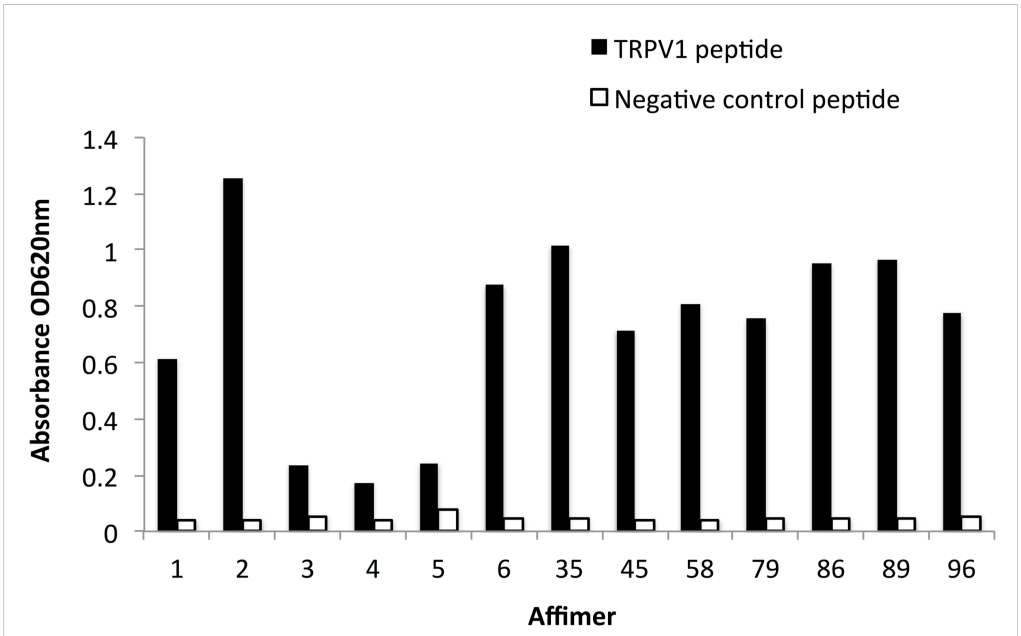

Figure 3.3. Phage ELISA demonstrating binding of monoclonal Affimer clones to a TRPV1 peptide. 50 µg/mL of TRPV1 peptide and a negative control peptide (each containing an N-terminal biotin) were immobilised on streptavidin-coated plates and then blocked overnight using 2X Casein blocking solution. All isolated Affimer phage clones were subsequently incubated against the peptides and then detected using an anti-Fd antibody conjugated to HRP. Addition of TMB then resulted in a colour change that could be detected at 620 nm.

Affimer^{TRPV1} clone	Variable region 1	Variable region 2
1	DIRPPLHEA	VRWFGR
2	H**E**EHT**WG**VF	F**K**
3	AYETTKWKV	KRYKAMGHL
4	HTEYVNMWY	KKPQMYLK
5	HFETTWWMK	ARRHQRMHE
6	**GE**LMQ**WGS**L	N**R**
35	QV**WG**FDDVV	FNKHAYLR
45	AQQTW**WG**GI	F**K**
58	QTRQDLAVP	KMWHGK
79	LFENN**FG**ML	A**K**
86	HWHKD**WG**FL	N**K**
89	PKMHQASKR	TYFIN
DkTx	DC**AKEGEV**CS**WG**K**K**CCDLDNFYC**P**ME**FIP**HCK**KY**KPYVPVTT-NC**AKEGEV**CG**WG**S**K**CCHGLDC**P**LA**FIP**YCE**KY**R	

Table 3.2. Amino acid sequences of the variable regions of Affimers isolated from phage display. TRPV1-specific Affimer clones are shown alongside DkTx, a toxin that binds to the same region of TRPV1 mimicked by the peptide screened. Regions of DkTx essential for TRPV1 specificity are highlighted in bold with similar Affimer amino acids also highlighted in bold.

3.2.2 Production of anti-TRPV1 Affimers in *E. coli*

The Affimers isolated from our phage display library were sub-cloned in to a pET11a expression vector. After 24 hours of induction with IPTG, the cells were lysed and Affimer protein purified using Ni-NTA resin. Protein was analysed by SDS-PAGE and Coomassie staining (**Figure 3.4**). Results demonstrated that proteins of approximately 12 kDa were present, with slight shifts in size corresponding to variations in the number of amino acids missing in the Affimer second variable region. One Affimer (lane 8) was discarded from future experiments due to difficulty of producing. Protein concentrations were

measured by Nanodrop spectrophotometry and concentrations normalised to 100 µg/mL for use in assays (**Table 3.3**).

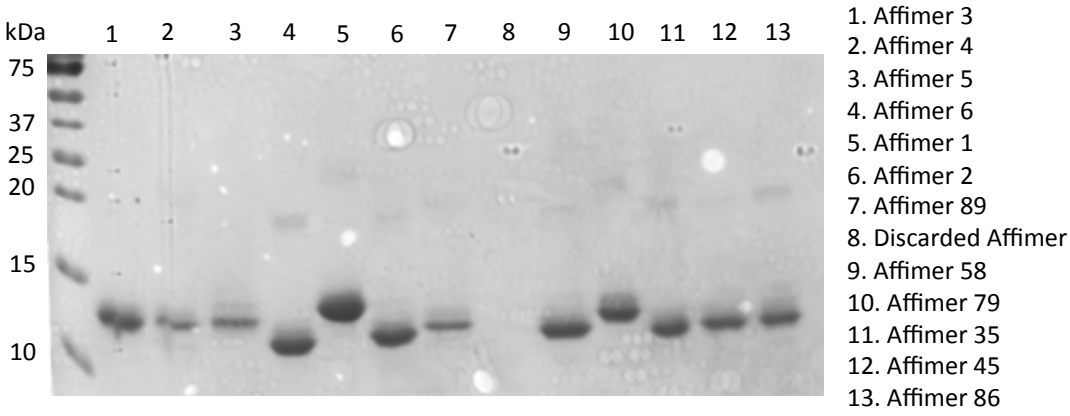

Figure 3.4. SDS PAGE gel of anti-TRPV1 Affimers developed using Coomassie stain. Affimer proteins were purified using Ni-NTA resin and then 5 µL of protein was analysed by SDS PAGE. The gel was subsequently developed using Coomassie stain.

Affimer	A280	Abs 0.1% (= 1 g/L)	Concentration (mg/mL)	Volume for 100 µg/mL (in 1 mL volume) (µL)
3	3.428	1.471	2.330	42.9
4	2.876	1.570	1.832	54.6
5	2.926	1.638	1.786	55.9
6	4.982	1.393	3.576	27.9
1	5.214	1.094	4.766	20.9
2	4.674	1.378	3.392	29.5
89	2.784	0.994	2.801	35.7
Discarded	-0.012	1.342	-0.009	-
58	5.001	1.333	3.752	26.7
79	5.102	0.898	5.682	17.6
35	4.896	1.352	3.621	27.6
45	4.777	1.901	2.513	39.8
86	4.345	1.859	2.337	42.8

Table 3.3. TRPV1 Affimer concentration measurements by Nanodrop spectrophotometry and normalisation to 100 µg/mL for use in binding assays. Absorption coefficients were calculated using the Expasy Protein Parameters online tool.

ELISA results demonstrated similar binding as previously observed by phage ELISA, suggesting Affimers could still recognise the TRPV1 peptide on removal of the pIII coat protein, with the exception of clone 89 (**Figure 3.5**). In this ELISA however, Affimer clones are detected by their His-tag using an anti-His antibody rather than being detected by their pIII protein. Therefore, this result may be contributed to by the anti-His antibody being unable to access the Affimer clones' His-tag. Despite attempts at establishing affinities of Affimers towards their cognate peptide using surface plasmon resonance (SPR), loss of peptide secondary structure on removal of bound Affimer with SDS made this technique difficult. Furthermore, the requirement of large amounts of DMSO to solubilise the peptide also made isothermal calorimetry (ITC) difficult. Therefore, to further scrutinise binding of TRPV1 Affimers against their target peptide, a concentration-response ELISA was conducted with each of the Affimers (**Figure 3.6**). The results from this ELISA demonstrated that various Affimers were able to still bind to and provide a response against the peptide when it was present at only 20 ng/mL. Furthermore, some Affimer clones were still able to provide a response against 160 ng/mL of peptide when incubated at very low concentrations. For example, Affimer 86 had a calculated K_d value against 160 ng/mL of peptide of 0.069 nM (**Table 3.4**).

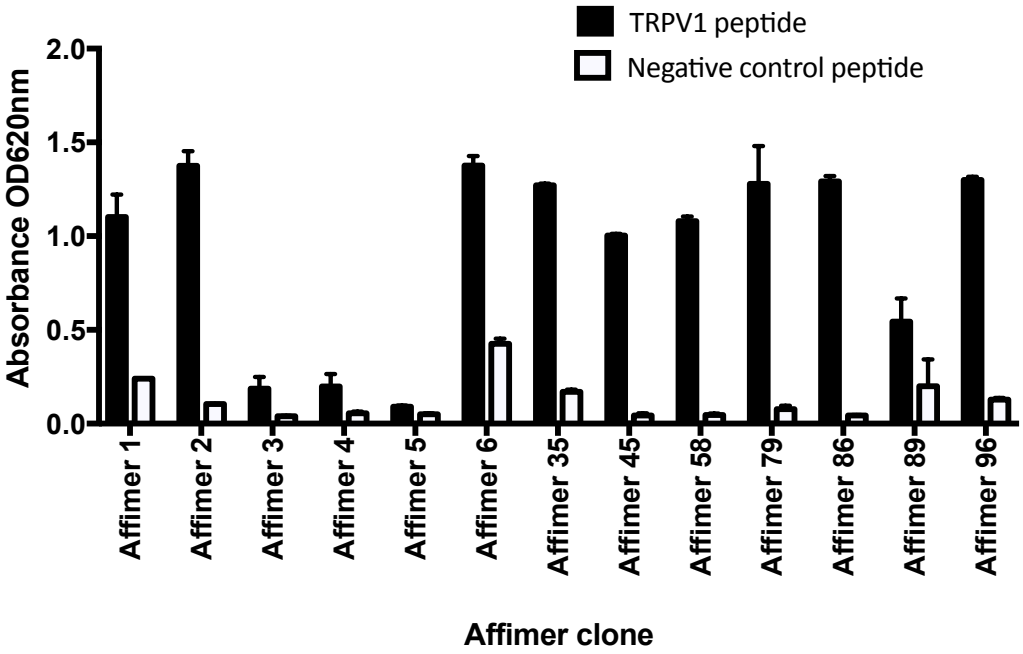

Figure 3.5. TRPV1 peptide ELISA using purified Affimers. To ensure Affimers identified against the TRPV1 peptide by phage display were still able to bind their target when expressed without the pIII coat protein, an ELISA was conducted. Biotinylated target TRPV1 peptide was immobilised on streptavidin-coated 96 well plates following which Affimers were incubated against peptide. Plates were washed and Affimers detected using anti-8X His antibody conjugated to HRP. Next, addition of the HRP substrate TMB resulted in a change in absorbance at 620 nm *(N = 2, error bars represent standard deviation).*

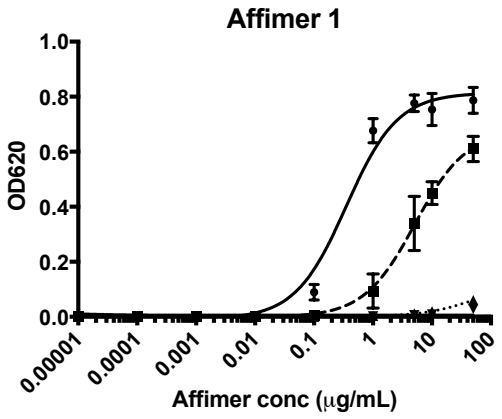
Affimer 1
OD620
1.0
0.8
0.6
0.4
0.2
0.0
0.00001
0.0001
0.001
0.01
0.1
1
10
100
Affimer conc (μg/mL)

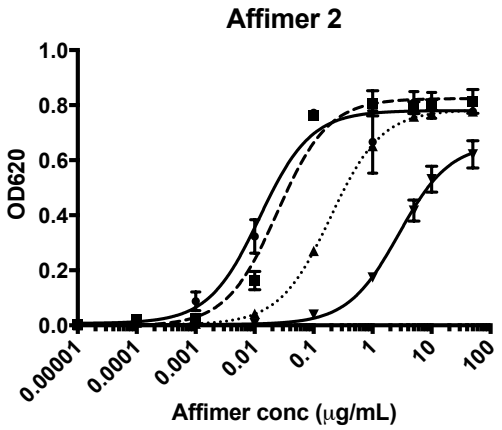
Affimer 2
OD620
1.0
0.8
0.6
0.4
0.2
0.0
0.00001
0.0001
0.001
0.01
0.1
1
10
100
Affimer conc (μg/mL)

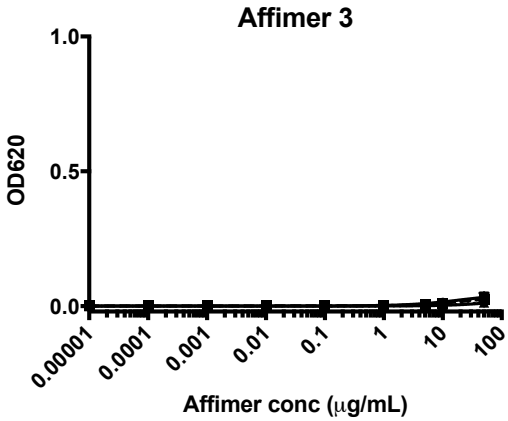
Affimer 3
OD620
1.0
0.5
0.0
0.00001
0.0001
0.001
0.01
0.1
1
10
100
Affimer conc (μg/mL)

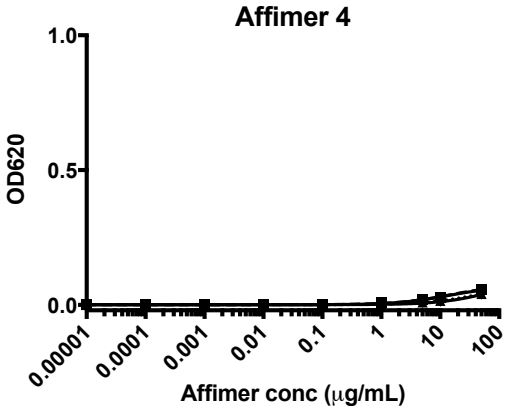
Affimer 4
OD620
1.0
0.5
0.0
0.00001
0.0001
0.001
0.01
0.1
1
10
100
Affimer conc (μg/mL)

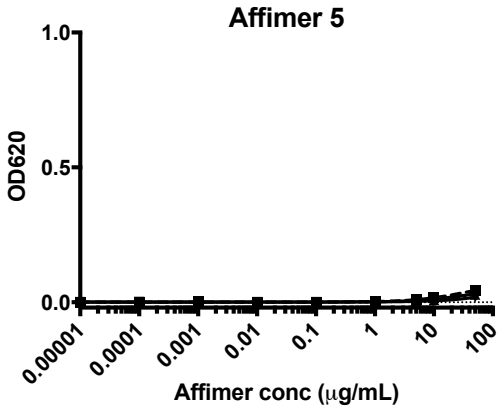
Affimer 5
OD620
1.0
0.5
0.0
0.00001
0.0001
0.001
0.01
0.1
1
10
100
Affimer conc (μg/mL)

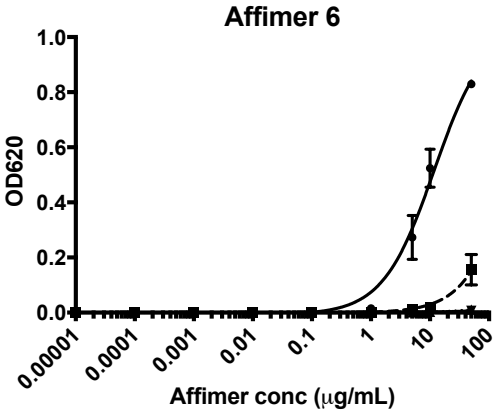
Affimer 6
OD620
1.0
0.8
0.6
0.4
0.2
0.0
0.00001
0.0001
0.001
0.01
0.1
1
10
100
Affimer conc (μg/mL)

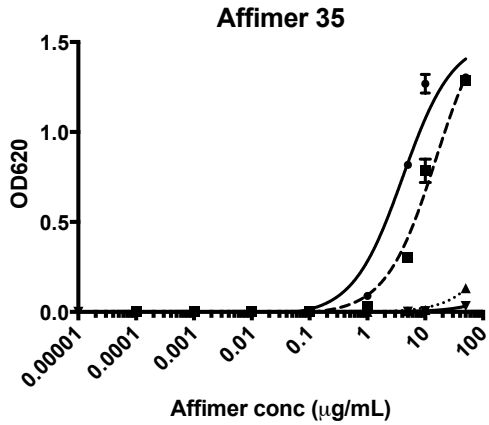
Affimer 35
OD620
1.5
1.0
0.5
0.0
0.00001
0.0001
0.001
0.01
0.1
1
10
100
Affimer conc (μg/mL)

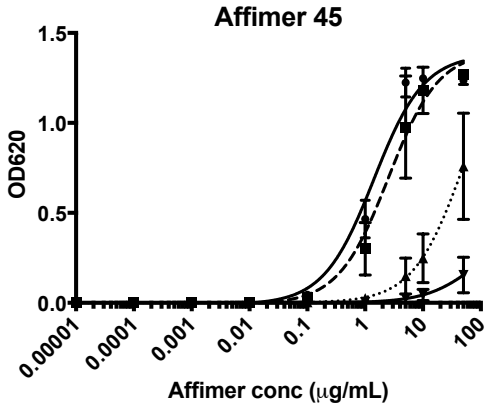
Affimer 45
OD620
1.5
1.0
0.5
0.0
0.00001
0.0001
0.001
0.01
0.1
1
10
100
Affimer conc (μg/mL)

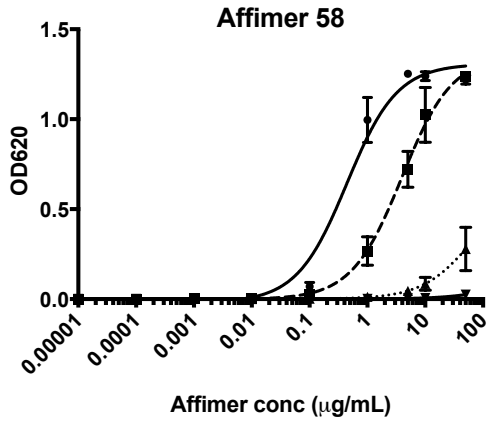
Affimer 58
OD620
1.5
1.0
0.5
0.0
0.00001
0.0001
0.001
0.01
0.1
1
10
100
Affimer conc (μg/mL)

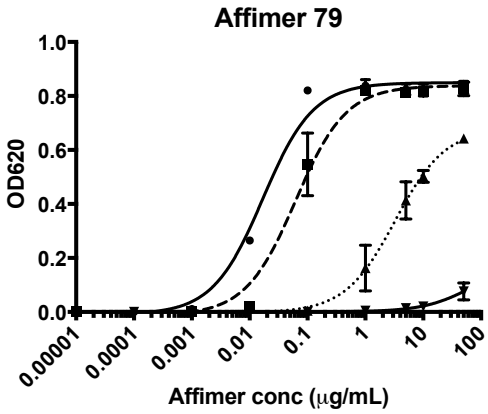
Affimer 79
OD620
1.0
0.8
0.6
0.4
0.2
0.0
0.00001
0.0001
0.001
0.01
0.1
1
10
100
Affimer conc (μg/mL)

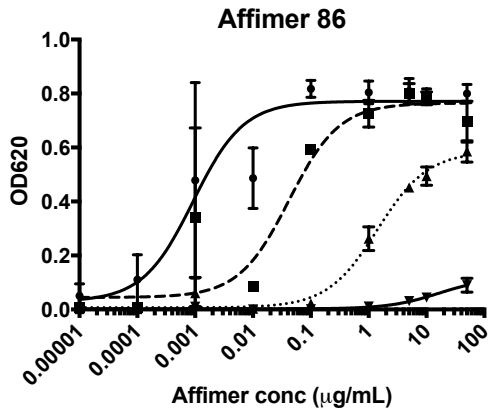
Affimer 86
OD620
1.0
0.8
0.6
0.4
0.2
0.0
0.00001
0.0001
0.001
0.01
0.1
1
10
100
Affimer conc (μg/mL)

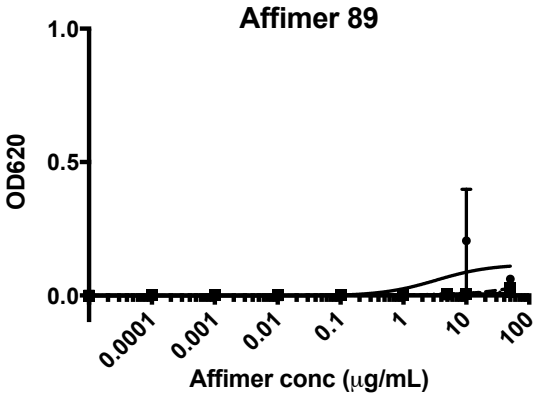
Affimer 89
OD620
1.0
0.5
0.0
0.0001
0.001
0.01
0.1
1
10
100
Affimer conc (μg/mL)

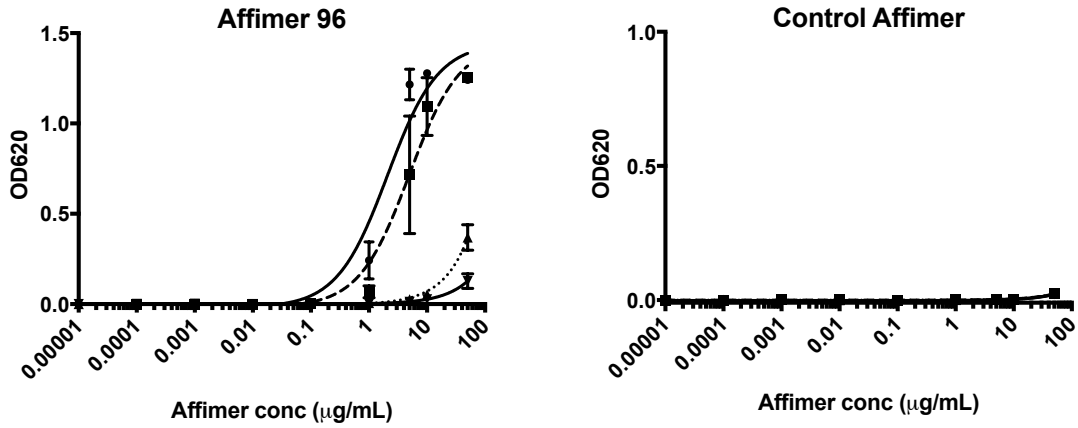

Figure 3.6. TRPV1 Affimer concentration-response ELISA. Affimers were tested for their ability to bind their cognate TRPV1 peptide at a range of concentrations to determine the strength of their binding. The TRPV1 peptide was immobilised on streptavidin-coated plates at a range of concentrations from 20-160 ng/mL. The Affimer clones isolated against the TRPV1 peptide were then incubated at a range of concentration ranging from 0.00001-100 μg/mL. Next, bound Affimer was incubated with an anti-8X His antibody conjugated to HRP. Detection then took place by addition of HRP substrate, TMB. (• = 160 ng/mL target, ■ = 80 ng/mL peptide, ▲ = 40 ng/mL peptide, ▼ = 20 ng/mL peptide).

Affimer clone	K_d against 160 ng/mL peptide ± S. E. M (nM)
Affimer 1	29.62 ± 6.46
Affimer 2	0.92 ± 0.005
Affimer 3	4769 ± NA
Affimer 4	187.8 ± 217.8
Affimer 5	502.1 ± 2,773
Affimer 6	56,396 ± NA
Affimer 35	2,565 ± NA
Affimer 45	176.2 ± 33.69
Affimer 58	40.61 ± 8.38
Affimer 79	1.38 ± 0.154
Affimer 86	0.069 ± 0.038
Affimer 89	114,059 ± NA
Affimer 96	361.5 ± 114.9
Control Affimer	NA

Table 3.4. K_d values of Affimer binding to TRPV1 peptide when immobilised at 160 ng/mL. Units were converted from mg/mL to nM using the equation mg/mL / Affimer molecular weight (Daltons) = concentration (M). Statistical analysis was conducted using GraphPad Prism software. For values that could not be calculated, NA has been displayed instead of a value.

3.2.3 Affimers bind to TRPV1 expressed in mammalian cells

To investigate binding of the identified Affimers to full-length TRPV1, affinity fluorescence staining was performed on TRPV1-expressing U-2 OS cells. Initially, Affimers were incubated on PFA fixed TRPV1-expressing U-2 OS cells however no signal could be observed (**Figure 3.7**). Next, Affimers were incubated on live TRPV1-expressing U-2 OS cells for 20 minutes prior to fixation. Affimer 2 demonstrated the ability to specifically bind to the TRPV1-expressing cells

(green) with no signal detected on a control U-2 OS cell line (**Figure 3.8**). All of the other Affimers did not show staining.

Next, co-staining between Affimer 2 and anti-TRPV1 antibody was conducted. Results demonstrated putatively similar staining patterns for Affimer and antibody (**Figure 3.9**). Again, no binding was observed on a parental U-2 OS cell line. Whilst this result suggests Affimer 2 and the anti-TRPV1 antibody may recognise the same protein, to further confirm this, confocal high-resolution imaging would be required. Furthermore, imaging studies using a competing peptide control would further confirm this result.

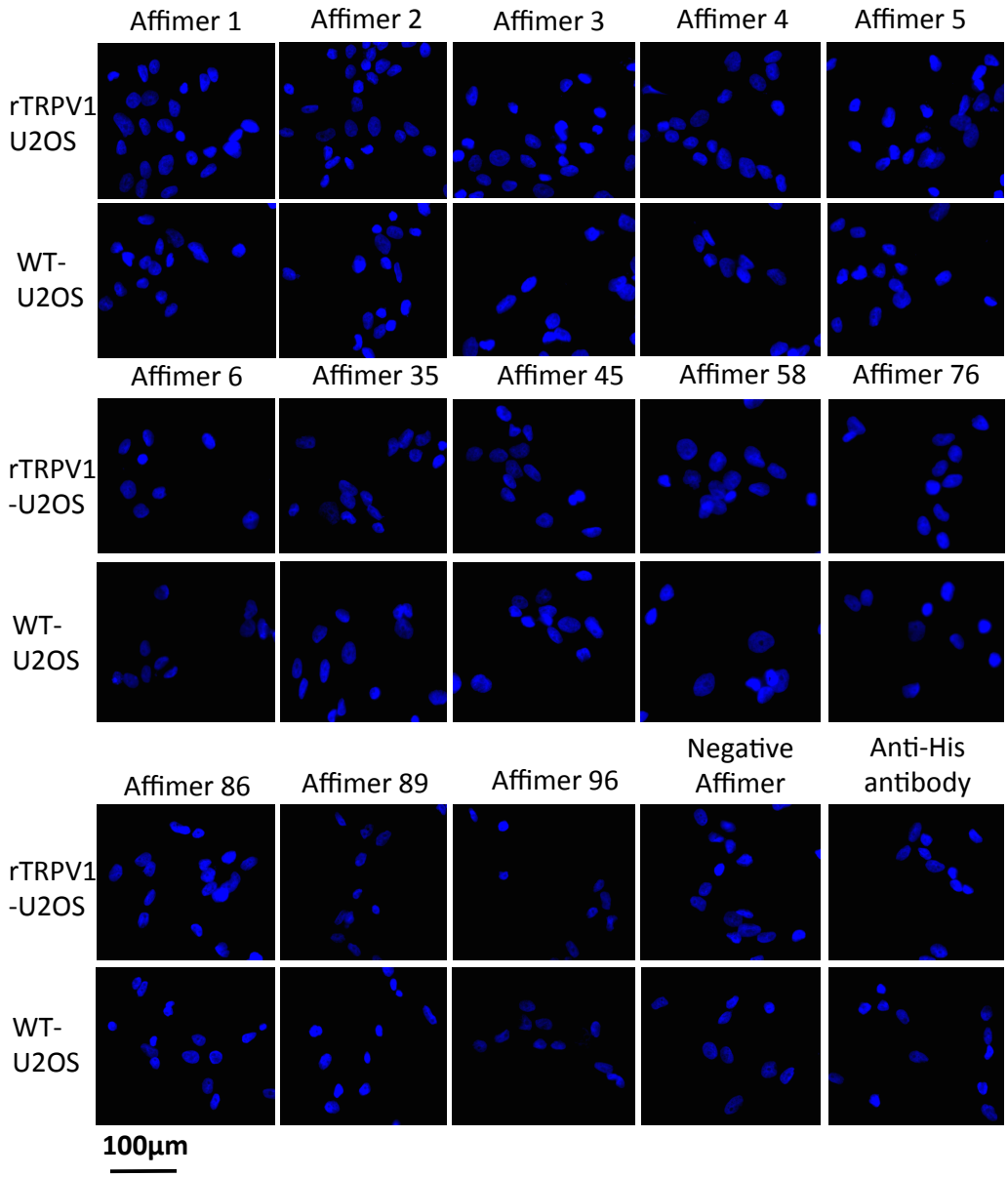

Figure 3.7. Immunocytochemistry against TRPV1-expressing cells in their fixed state. U-2 OS cells transiently expressing rat TRPV1 were plated on to coverslips and fixed using 4% PFA. Affimers were incubated against fixed cells for one hour at room temperature. Affimers were subsequently detected using an anti-8XHis antibody (mouse) and anti-mouse-488 antibody. Coverslips were then mounted on to glass slides using ProLong Diamond anti-fade mounting solution supplemented with DAPI for DNA staining (*blue*).

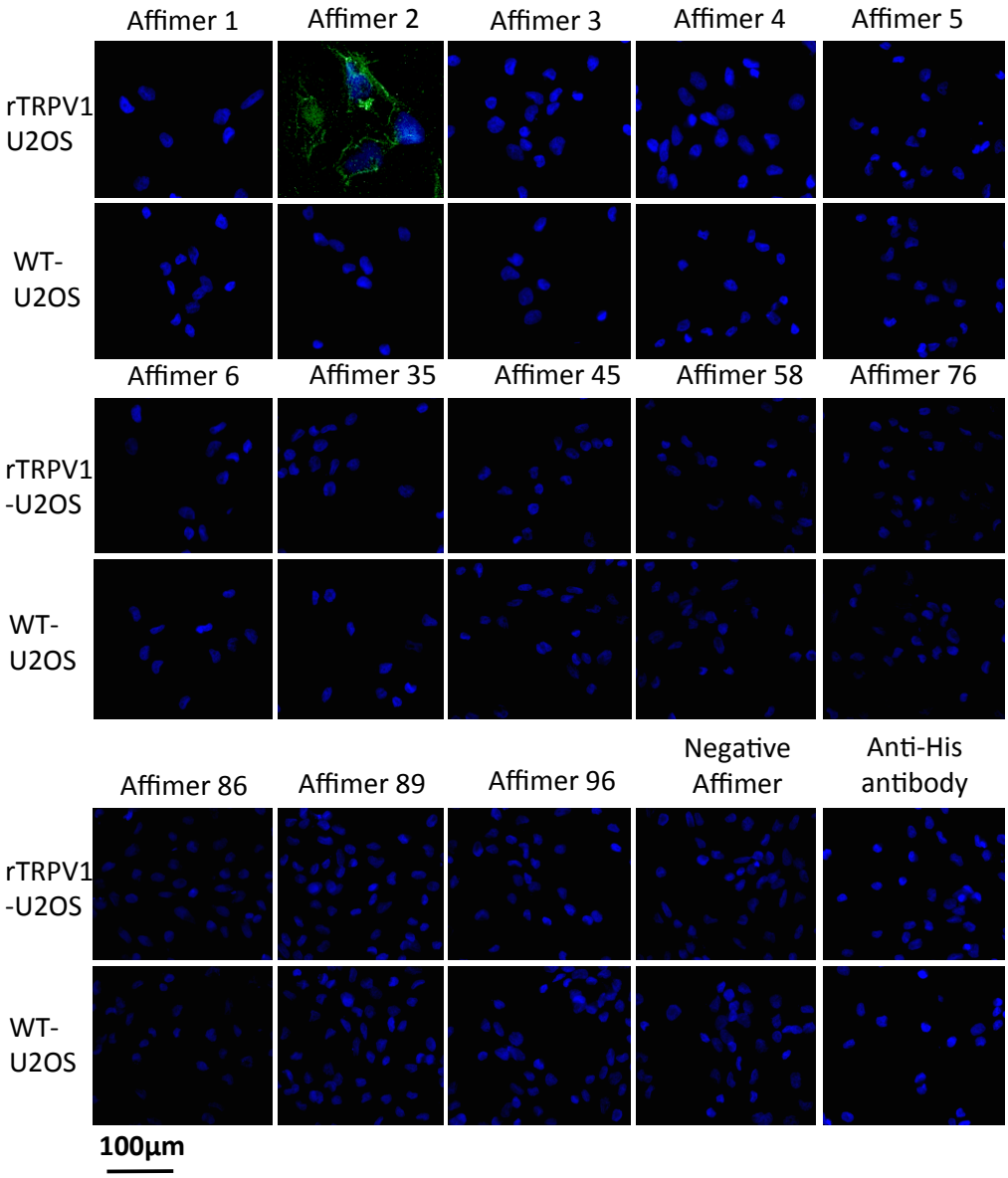

Figure 3.8. Immunocytochemistry against TRPV1-expressing cells in their live state. U-2 OS cells transiently expressing rat TRPV1 were plated on to coverslips and incubated with Affimers for 20 minutes, washed with assay buffer and fixed with 4% PFA. Affimers were subsequently detected using anti-8XHis antibody (mouse) and anti-mouse-488 antibody (*green*). Coverslips were then mounted on to glass slides using ProLong Diamond Antifade mounting solution supplemented with DAPI for DNA staining (*blue*).

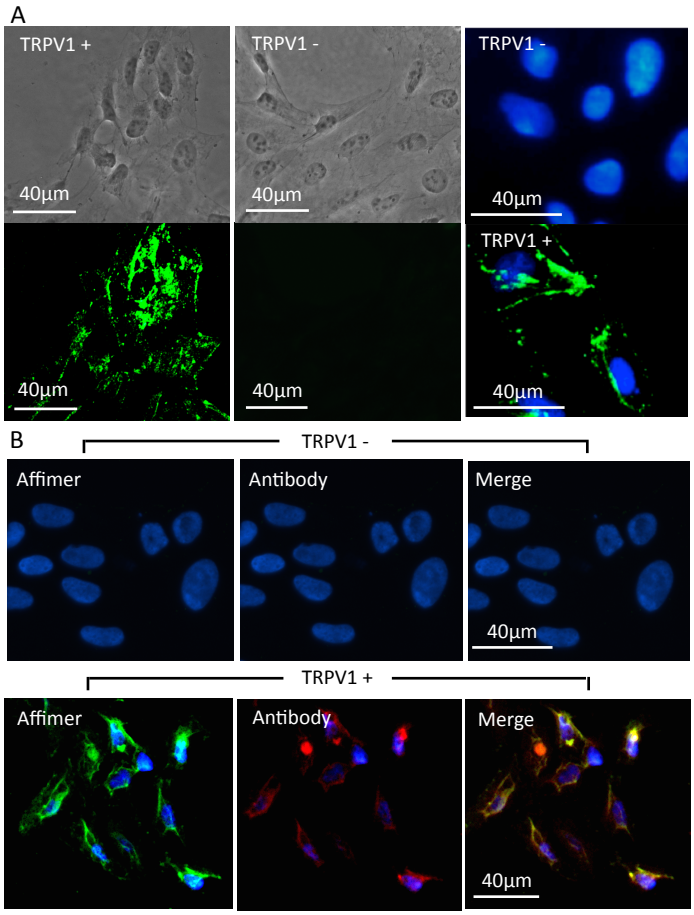

Figure 3.9. Affimer 2 and anti-TRPV1 antibody provide putatively similar staining patterns by immunocytochemistry. A. TRPV1-expressing cells were plated on to coverslips and incubated with Affimer 2 at 5 µg/mL in assay buffer for twenty minutes, washed and fixed using 4% PFA. Cells were permeabilised and then blocked with 1% BSA. Cells were then incubated with an anti-His antibody (mouse) to detect Affimer. Coverslips were then mounted on to glass slides using ProLong Diamond Antifade mounting solution with DAPI (*blue*). B. A non-expressing U-2 OS cell line (TRPV1 -) and a TRPV1-expressing U-2 OS cell line (TRPV1 +) were co-stained with Affimer 2 and an anti-TRPV1 antibody. Cells were prepared as described above. Briefly, Affimer 2 was incubated on cells at 5 µg/mL and then cells were fixed, permeabilised and blocked. Cells were then incubated in anti-TRPV1 antibody (guinea pig) and anti-His antbody (mouse) and then washed. Cells were then incubated in anti-mouse-488 (*green*) and anti-guinea pig-594 antibody (*red*). Cells were mounted to glass slides as described above. Samples were imaged using an EVOS FL imaging system.

3.2.4 Affimers induce positive allosteric modulation of TRPV1

The ability of Affimers to modulate TRPV1 activity was tested by calcium influx assay. Prior to testing of Affimers, the response of TRPV1 to its orthosteric agonist, capsaicin, was assessed. Results demonstrated that TRPV1 responded to capsaicin in a concentration-dependent manner with an EC_{50} of 156 nM calculated, a similar value to that previously reported in the literature (Gavva *et al.* 2004). Furthermore no response against a non-expressing, parental cell line was observed when tested at 1 µM capsaicin (**Figure 3.10**).

Following validation of the TRPV1-expressing cell line, Affimers were tested for their ability to modulate TRPV1. Initially, Affimers were tested for their ability to activate TRPV1 however no response was observed. Next, the ability of Affimers to inhibit TRPV1 was tested. Affimers were pre-incubated on cells at a concentration of 1 µM followed by activation of TRPV1 with capsaicin at the EC_{20} concentration of capsaicin calculated from Figure 3.10 (~40 nM). Despite observing no inhibition in response to TRPV1, results demonstrated that the response of TRPV1 to capsaicin was enhanced. For example, the response of TRPV1 to capsaicin following pre-incubation with Affimer 35 was approximately 60% increased compared to pre-incubation of TRPV1 with the buffer only control. Furthermore, negative control Affimer demonstrated very little change in response (**Figure 3.11**).

Next, the ability of Affimers to shift the EC_{50} curves for capsaicin was assessed by testing the effect of 1 µM Affimer on the response of TRPV1 to a range of capsaicin concentrations (**Figure 3.12**). Results demonstrated that a number of Affimers were able to reduce the EC_{50} concentration of capsaicin, with the most potent Affimers, 35 and 45, able to reduce the EC_{50} of capsaicin by a factor of five (significance = ** <0.01 as measured by student t-test). Again, the negative control Affimer had little effect on capsaicin EC_{50} (**Table 3.5**).

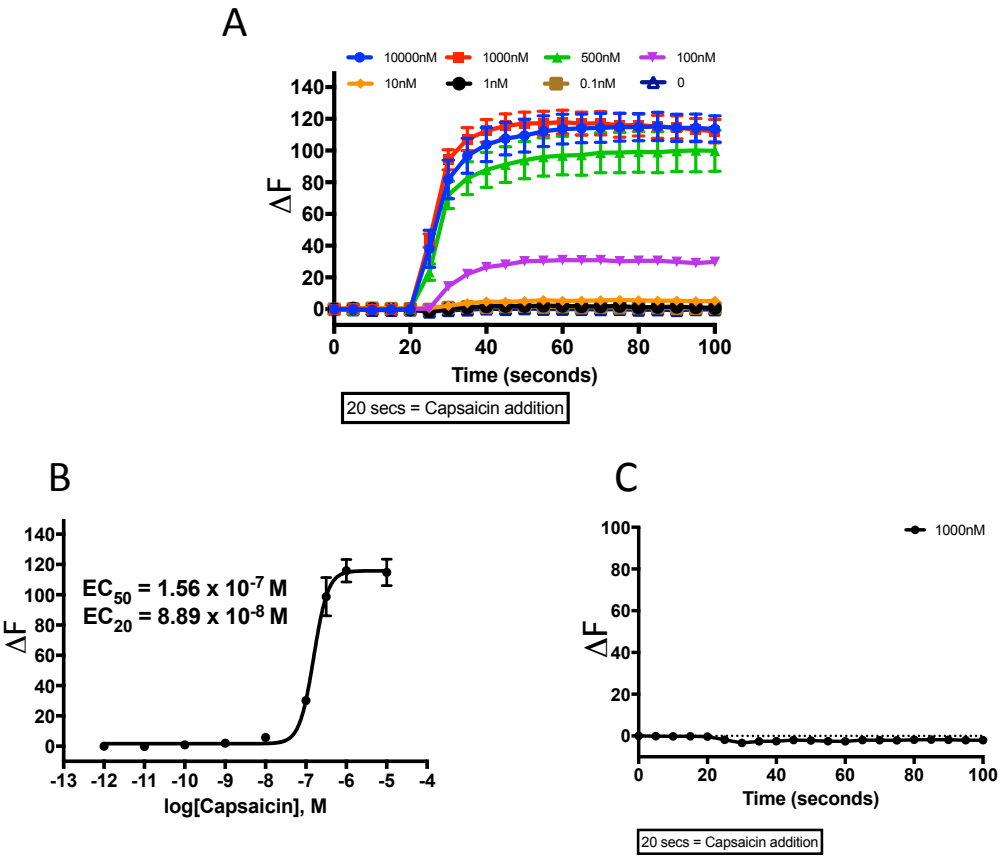

Figure 3.10. Validation of rat TRPV1 activity when transiently expressed in a U-2 OS cell line. A. TRPV1-expressing U-2 OS cells were seeded in to 96 well plates at 50,000 cells per well 24 hours before use. Cells were incubated for one hour with cell-permeable Fluo 4-AM calcium dye. Cells were washed three times with assay buffer and incubated for twenty minutes in assay buffer to enable de-esterification of Fluo 4-AM. Next, cells were loaded on to a FlexStation III multi-well plate reader and the program set to add capsaicin at a range of concentrations after 20 seconds. Cell response was measured for a further 80 seconds. Peak response was then used to assess the response to capsaicin. B. Peak response was used to compile a concentration-response curve. C. The same experiment was also conducted against a TRPV1-negative cell line with response against 1 µM capsaicin (N = 3).

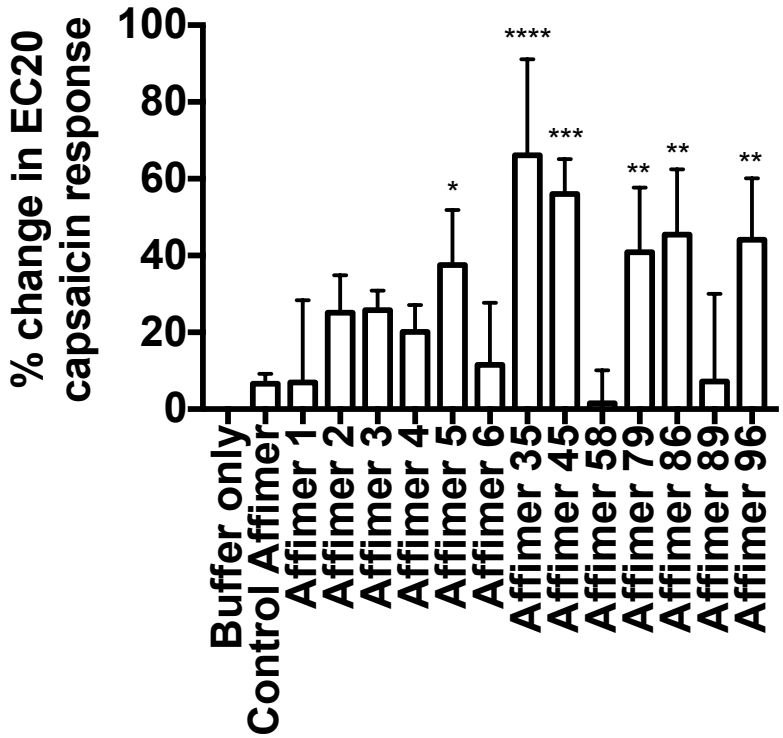

Figure 3.11. Potentiation of TRPV1 response by Affimers when activated by capsaicin at its EC_{20} concentration. TRPV1-expressing U-2 OS cells were plated in to black-walled 96 well plates at 100,000 cells per well and cells were loaded with 1 µM Fluo-4 AM for one hour in the dark. Cells were then washed with assay buffer and incubated with 1 µM of Affimers in assay buffer for 30 min. Cells were then loaded on to a Flexstation III device and 40 nM of capsaicin in assay buffer added to cells. Response to capsaicin was measured for 60 sec. Peak response to capsaicin in the presence of different Affimers was then measured (*Significance measured using ANOVA with multiple comparisons. N = 3, *= <0.1, **= <0.01, ***= <0.001, **** = <0.0001*).

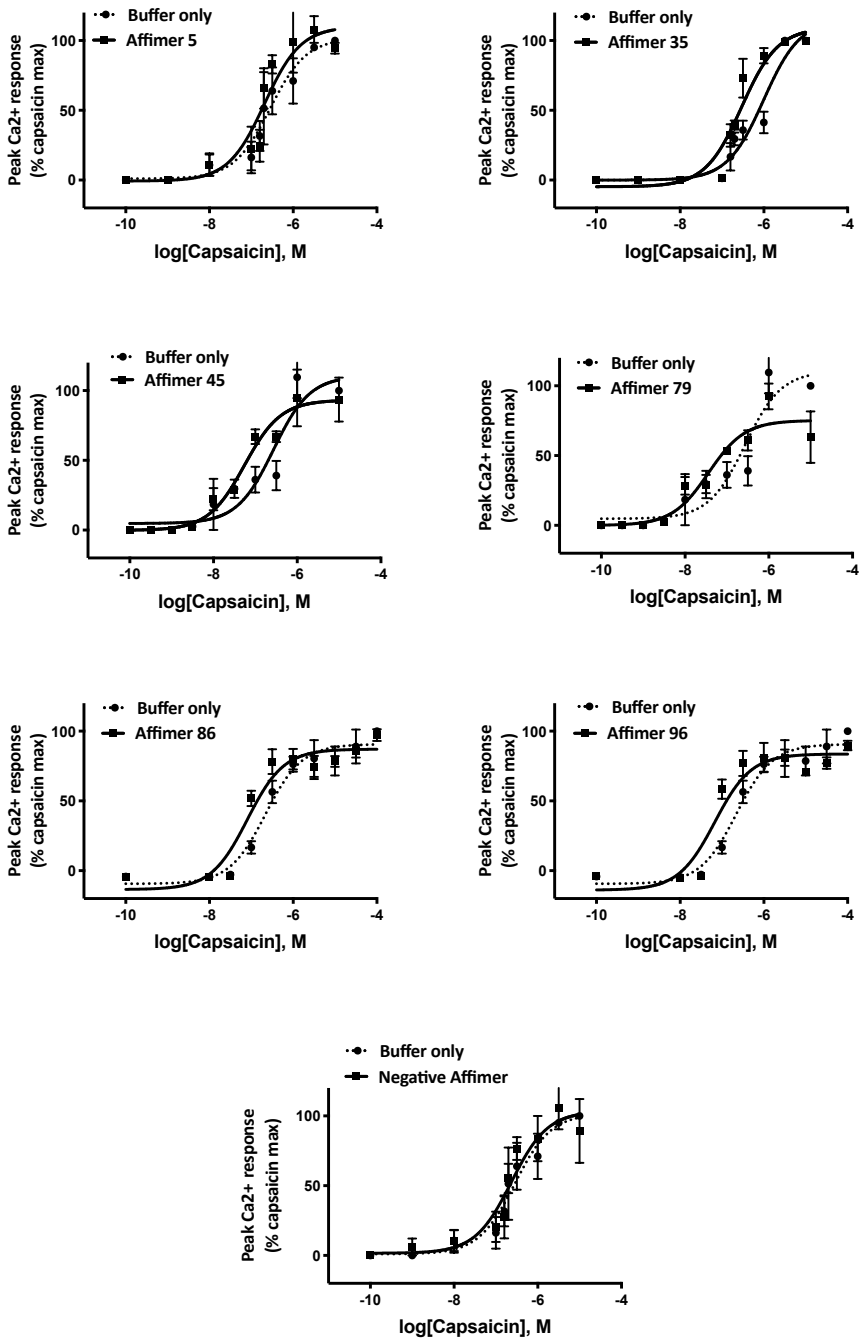

Figure 3.12. Affimer potentiation of TRPV1 response when activated by a range of capsaicin concentrations. Cells expressing TRPV1 were prepared as described in Figure 3.11. Affimers were then incubated on the cells at a concentration of 1 µM in assay buffer for 30 min prior to activation of TRPV1 by a range of capsaicin concentrations using a Flexstation III device. Response was measured for 60 sec and peak response determined. Concentration-response curves were formulated using GraphPad Prism software.

Affimer clone	EC_{50} ± S. E. M (nM)	Significance
Affimer 5	206 ± 10.9	Ns
Affimer 35	45 ± 7.1	**
Affimer 45	55 ± 6.7	**
Affimer 79	36 ± 7.2	**
Affimer 86	80 ± 6.7	**
Affimer 96	67 ± 7.3	**
Negative Affimer	233 ± 11.49	ns

Table 3.5. EC_{50} values for Affimers when tested for potentiation of capsaicin-evoked TRPV1 activation. Statistical analysis was conducted using GraphPad Prism software. *(Significance measured by t-test of EC_{50} values. N = 3. ns – no significant difference, ** = <0.01**).***

As a result of the similarities in amino acid sequence between Affimers and DkTx, it was hypothesised that the inability of Affimers to directly activate TRPV1 may be a result of their lack of bivalency, a property essential for the DkTx activation of TRPV1 (Bohlen *et al.* 2010). One of the most potent Affimers, Affimer 45, was therefore reformatted in to a dimeric Affimer. The DkTx linker region (Lys-Tyr-Lys-Pro-Tyr-Val-Pro-Val-Thr-Thr-Asn) was used to join the two Affimers (**Figure 3.13**). The resulting dimeric Affimer 45 was subsequently expressed in BL21 Star (DE3) cells and protein analysed by SDS PAGE and Coomassie staining (**Figure 3.14**A). Results demonstrated that all expressed protein was dimeric and soluble, migrating to a size of approximately 27 kDa, the expected size of a dimeric Affimer adjoined by the DkTx linker region. Subsequently, the ability of dimeric Affimer 45 to bind the TRPV1 peptide was tested by ELISA in which the Affimer was detected using anti-His antibody (**Figure 3.14**B). Results demonstrated that the dimeric Affimer 45 was still able to detect its cognate peptide to a similar

level as that observed for the monomeric Affimer 45. Next, the ability of dimeric Affimer 45 to directly activate TRPV1 was tested. Results demonstrated that, as with monomeric Affimer 45, no direct activation could be observed (**Figure 3.14**C). Furthermore, similar potentiation was observed with no enhanced effect conferred by the bivalent properties of dimeric Affimer 45 (**Figure 3.14**D). These observations may be a result of the DkTx linker properties being unsuitable to enable accurate extension of the two Affimer 45 molecules over two TRPV1 subunits. It is hypothesised that optimisation of this linker region may provide alterations to the effects conferred by the dimeric Affimer 45.

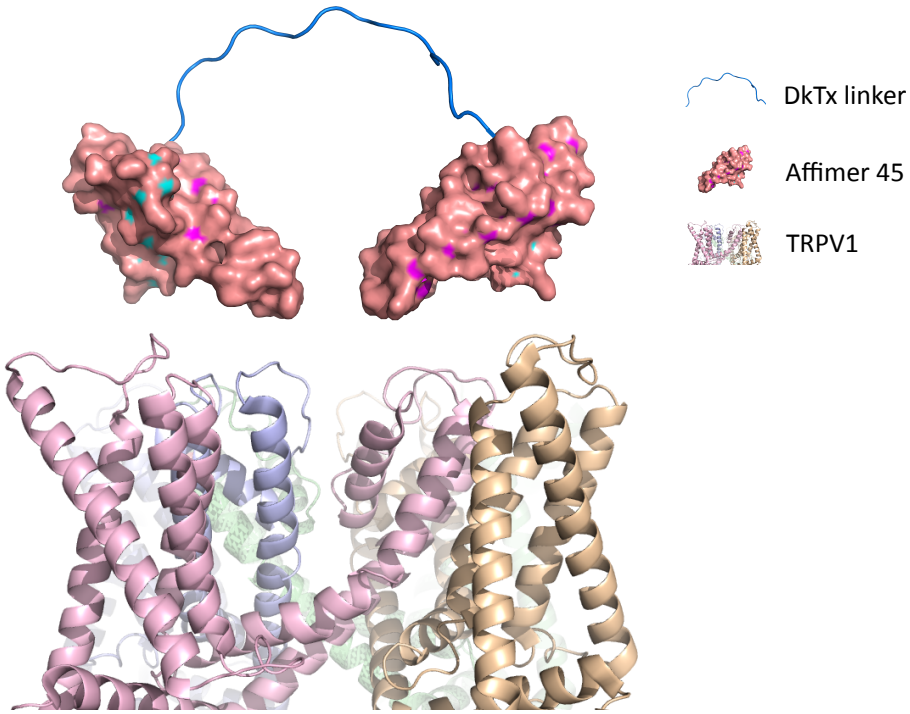

Figure 3.13. Schematic of a dimeric Affimer 45 to test for TRPV1 activating properties. As a result of the inability of Affimer 45 to directly activate TRPV1, an innate property of DkTx, it was postulated that the bivalency essential to DkTx function may confer activating properties on to Affimer 45. To test this, restriction cloning was used to insert the DkTx linker region (Lys-Tyr-Lys-Pro-Tyr-Val-Pro-Val-Thr-Thr-Asn) between two Affimer 45 molecules.

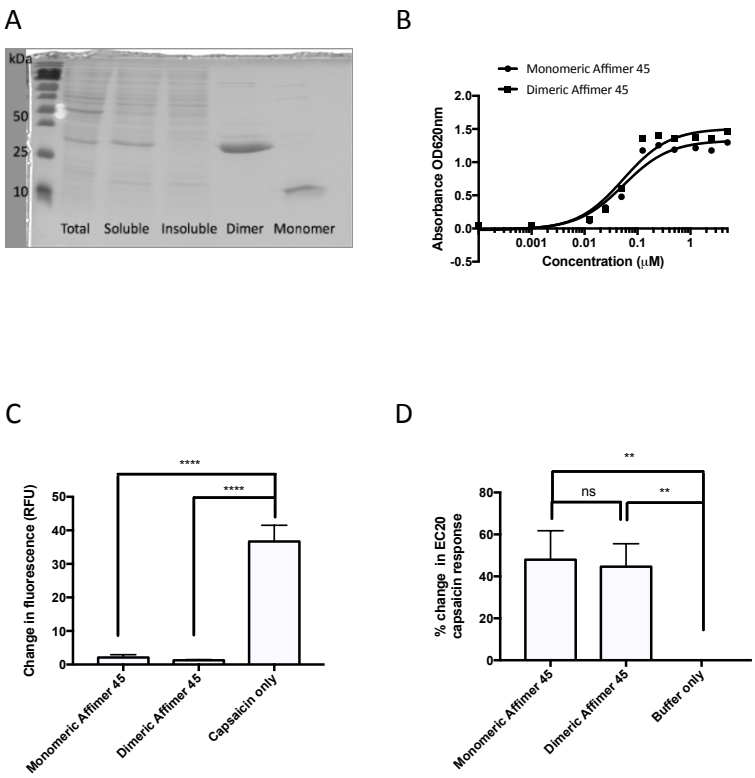

Figure 3.14. Production of a dimeric Affimer 45 to test for its ability to directly activate TRPV1. A dimeric Affimer 45 construct was generated by restriction cloning. A. The dimeric Affimer was expressed in BL21 Star (DE3) cells and purified from the soluble fraction using NiNTA resin. Purified protein was run on a SDS-PAGE gel and analysed by Coomassie staining. B. Binding of the dimeric Affimer 45 to its cognate peptide was tested by ELISA. 1 μM of TRPV1 peptide was immobilised on streptavidin-coated plates for one hour and unbound peptide washed away with PBS-T. Dimeric or monomeric Affimer was then incubated on peptide at a range of concentrations for one hour and then washed with PBS-T. Incubation with anti-8X-His antibody conjugated to HRP was then conducted for one hour with excess antibody washed away with PBS-T. TMB was then added and measured at 620 nm. C. Next, the ability of dimeric Affimer 45 to modulate TRPV1 was tested. Direct activation was tested initially. TRPV1-expressing U-2 OS cells were plated in to black-walled 96-well plates at 100,000 cells per well and then incubated with Fluo-4 AM for one hour. Cells were then washed and loaded on to a FlexStation III multi-well plate reader programmed to add either monomeric or dimeric Affimer after twenty seconds. Capsaicin (1 μM) was also added as a positive control. Peak response was measured and change in response from baseline calculated. D. The same experiment was also conducted however monomeric or dimeric Affimer was pre-incubated on cells prior to their activation by capsaicin.

3.3 Discussion

The work presented in this chapter describes the isolation of Affimer reagents against a synthetic peptide mimicking a region of the TRPV1 ion channel. ELISA was used to confirm binding to the peptide however a significant observation made in this study was the ability of a number of the Affimers to modulate TRPV1 function. Despite their ability to modulate TRPV1 function, only one of these Affimers, Affimer 2, was able to detect TRPV1 by immunocytochemical staining. One potential explanation for this may be that most of the Affimers were unable to access their epitope when the TRPV1 channel was in its closed state. This may also provide an explanation for the inability of Affimers to modulate the function of TRPV1 in the absence of its orthosteric agonist, capsaicin. In the positive allosteric modulation assays, the opening of TRPV1 following capsaicin application may have placed the TRPV1 outer pore domain in a conformation that enabled the Affimers to access their epitope. In a study by Lenter *et al* (1993), a monoclonal antibody, denoted 9EG7, was able to detect $\alpha_4\beta_1$ integrin, but only in its activated form. When in its non-activated form, detection of $\alpha_4\beta_1$ integrin by flow cytometry was not possible. In this study, the 9EG7 antibody was able to block binding between lymphocytes and endothelioma cells, a cell adhesion process mediated by the $\alpha_4\beta_1$ integrins. This blockage took place only following activation of $\alpha_4\beta_1$ integrin with phorbol esters. It was suggested that a conformational change undergone by $\alpha_4\beta_1$ integrins up on activation by phorbol esters resulted in the 9EG7 epitope becoming accessible (Lenter *et al.* 1993). The study described in this thesis may focus its future work on investigating if the TRPV1 epitope targeted by Affimers is indeed inaccessible when TRPV1 is in its closed state. One possible experiment that could be conducted is to activate TRPV1 with capsaicin prior to incubation with Affimers. Their detection could then take place by immunocytochemistry. An alternative method would be to activate TRPV1 with capsaicin and then fix cells for immunocytochemical staining.

Despite the inability of the majority of Affimers to detect TRPV1, Affimer 2 demonstrated putative staining of TRPV1. Further experiments do however need to be conducted to enable accurate conclusions to be drawn. For example,

the use of confocal microscopy and z-stack imaging to confirm co-localisation with an anti-TRPV1 antibody is required. Furthermore, use of a competing peptide to confirm that Affimer 2 is binding to this peptide region of TRPV1 needs to be conducted.

Some of the identified Affimers contained a tryptophan and glycine residue in their first variable region. The presence of these residues in the inhibitory cysteine knot (ICK) loop 1 of the DkTx toxin alongside its similar binding epitope (Bohlen *et al.* 2010), prompted the hypothesis that some of these Affimers may be binding to TRPV1 in a similar manner. Despite this hypothesis, functional effects were different, with DkTx directly activating TRPV1 and Affimers only inducing potentiation following activation by capsaicin. It was hypothesised that, unlike DkTx, the identified Affimers were not able to bind to TRPV1 in a bivalent manner, a configuration that is necessary for DkTx to induce direct activation. As discussed by Bohlen *et al* (Bohlen *et al.* 2010), DkTx binding affinity is greatly reduced when the linker region enabling bivalent binding to TRPV1 is removed. To investigate this hypothesis, Affimer 45 was produced as a dimer with each monomer connected by the DkTx linker region. Dimeric Affimer was then re-tested for its TRPV1 modulation properties. Results demonstrated that dimeric Affimer 45 was still unable to directly activate TRPV1. Future work may investigate the linker region joining the two Affimer proteins, as further optimisation of this region may be required to enable access of each of the Affimers to adjacent TRPV1 subunits. In a study by Danquah et al (2016), dimerization of anti-P2X7 nanobodies via a flexible glycine and serine linker resulted in improved IC_{50} values of the inhibitors to a high picomolar range (Danquah *et al.* 2016). Although it may be possible that the incorrect linker region length or structure may account for the lack of activation by dimeric Affimer, other possibilities also need to be considered. For example, the inability of dimeric Affimer to directly activate TRPV1 may be a result of a lack of phospholipid bilayer interactions, another property that is observed in the interaction between DkTx and TRPV1 (Gao *et al.* 2016).

Despite the inability to induce direct modulation on TRPV1, potentiation of TRPV1 has demonstrated therapeutic applications. For example, the recently

described small molecule potentiator of TRPV1, MRS1477, has shown pain-relieving properties in pre-clinical models (Kaszas *et al.* 2012). Despite the epitope of binding of MRS1477 yet to be defined, it is hypothesised that it binds to the pore-forming TM5 and TM6 regions of TRPV1. Alongside the confirmed TRPV1 epitopes of DkTx and RhTx (**Figure 3.15**), this suggests that this epitope of TRPV1 may be useful for the development of future reagents (Huber *et al.* 2000, Ryu *et al.* 2007, Kaszas *et al.* 2012).

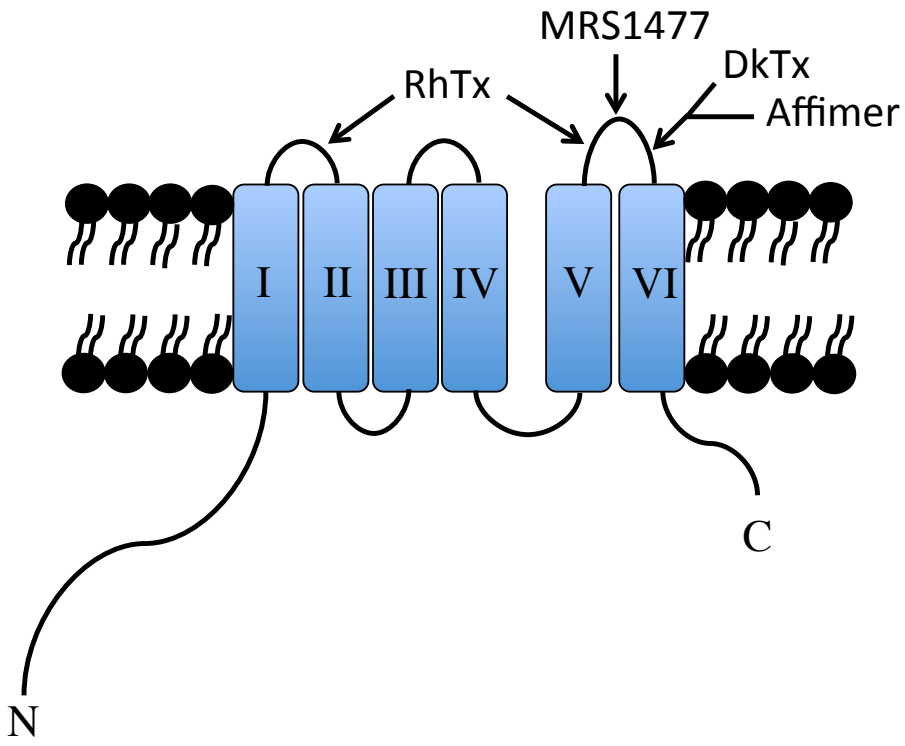

Figure 3.15. Schematic view of a TRPV1 subunit with the binding regions of activating peptide toxins (DkTx, RhTx), a small molecule potentiator, MRS1477 and the Affimers described in this chapter, highlighted.

This study highlights the advantage of using synthetic peptides as targets for phage display screening. Not only does it overcome problems associated with producing membrane proteins, it also enables selection against specific regions of the protein of interest, for example, regions known to be involved in function or ligand binding. This method can also provide tailored selectivity of binding reagents by screening peptides mimicking poorly conserved regions of the protein. Antibodies have been raised against a peptide mimicking a region of

$Na_v1.7$ that demonstrates low similarity with other Nav subtypes. The resulting antibodies were able to detect $Na_v1.7$ with high selectivity (**Lee et al, 2014**). The low homology of the screened peptide region between the TRPV family of proteins suggests possible selectivity of Affimers towards TRPV1, an important feature of therapeutic reagents considering the presence of TRPV channels in a variety of tissues (**Table 3.6**). However, future experiments are required to confirm this hypothesis.

Channel	**Major tissue expression**
TRPV1	Widespread
TRPV2	Lung
TRPV3	Skin, small intestine
TRPV4	CNS, adrenal gland, pancreas, duodenum, testis, placenta
TRPV5	Kidney
TRPV6	Placenta

Table 3.6. Tissue expression of TRPV channel family members. The TRPV channel family members have a wide variety of expression characteristics, with some channels being widely expressed throughout the body such as TRPV1 and others being limited in their expression such as TRPV5.

In addition to being able to select peptides that may confer antibodies with high selectivity, use of synthetic peptides for isolation of antibodies may be required when detection of small changes in amino acid properties are required. For example, almost all phospho-specific antibodies are now raised against synthetic peptides (Lee *et al.* 2016).

Despite providing a number of advantages, screening against peptides also has disadvantages, some of which may be observed in this study. For example, despite isolating a number of Affimer clones able to bind to the peptide, some of these clones were unable to detect the full-length TRPV1 channel in imaging experiments. This may be caused by the presence of protein regions in the full-length channel that are not present during the screening protocol against the peptide.

In conclusion, this chapter describes the identification of Affimer reagents against a peptide mimicking the outer pore domain of the TRPV1 channel. Although further studies are required to confirm detection of full-length TRPV1, preliminary studies suggest that one of these Affimers provides putative staining of TRPV1 by immunocytochemistry, with a number of these Affimers able to enhance the activation of TRPV1 by capsaicin.

Chapter 4

Structural insights into the modulation of TRPV1 by Affimer 45

4 Structural insights into the modulation of TRPV1 by Affimer 45

4.1 Introduction

The identification of Affimer 45 by phage display was previously described, demonstrating its ability to modulate the capsaicin-evoked response of TRPV1. The work described in this chapter explores the structural basis underlying the interaction between Affimer 45 and TRPV1. Site-directed mutagenesis and X-ray crystallography were used to identify the key residues involved in the interaction with results enabling the subsequent generation of an Affimer 45 variant with improved binding properties. Furthermore, the Affimer 45-TRPV1 peptide structural interaction was used to guide the ligand-based *in silico* identification of small molecule modulators of TRPV1.

Recently described structural studies of TRPV1 have identified the outer pore domain as an essential site for activation by a number of toxins including RhTx and DkTx (Bohlen *et al.* 2010, Yang *et al.* 2015). Whilst RhTx interacts with residues towards the posterior region of the TRPV1 outer pore domain, DkTx interacts directly with residues in the region of the TRPV1 outer pore domain screened against with the Affimer library (**Figure 4.1**A).

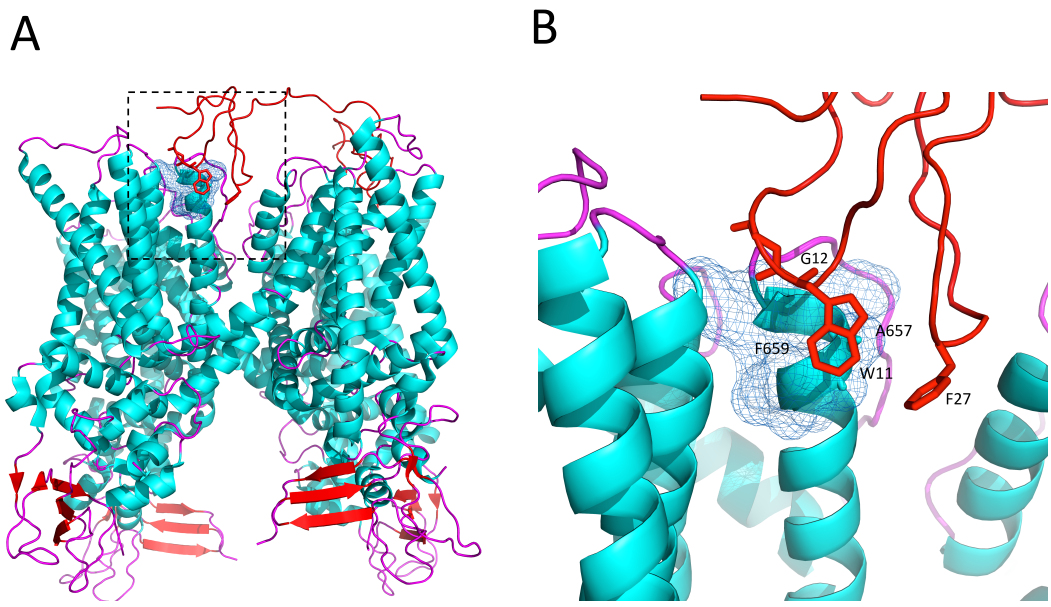

Figure 4.1. The outer pore domain epitope of TRPV1 targeted by the activating toxin, DkTx. A. Crystal structure of DkTx (*red*) in complex with TRPV1 (*cyan*) (5IRX) demonstrating the interaction of DkTx with the outer pore region of TRPV1. B. Zoomed in view of the interaction between the DkTx ICK1 loop and the essential residues of TRPV1 (*blue mesh*) enabling its activation by DkTx (*red ribbon*). DkTx ICK1 has been shown to interact with residues A657 and F659 of the TRPV1 outer pore domain (Gao *et al.* 2016), both residues that are present in the peptide screened against by phage display in our studies to identify Affimer 45. DkTx residues W11 and G12, again, residues observed in the Affimer 45 first variable region, are pivotal to this interaction. The peptide region screened against by phage display in our studies is highlighted using blue mesh.

Mutagenesis studies of the TRPV1 outer pore domain have highlighted a number of residues as being important to the interaction with DkTx (Bohlen *et al.* 2010). When A657 of the TRPV1 outer pore domain was mutated to proline, complete loss of activation by DkTx resulted. Furthermore, mutation of residues F649 and F659 to alanine resulted in a diminished activation of the channel (Bohlen *et al.* 2010). More recently, a structural basis for this interaction has been determined. Close proximity between various DkTx ICK residues with TRPV1 is observed, with an extended tryptophan residue at position 11 of DkTx ICK1 being particularly important (**Figure 4.1**B). This residue appears to associate closely with residues

A657 and F659 of the TRPV1 outer pore domain, both residues, as previously discussed, essential for DkTx-evoked activation of TRPV1. This structure therefore places W11 and G12 in close proximity of the TRPV1 outer pore domain, both residues that can be found in the first variable region of a number of the Affimers identified as TRPV1 modulators (*see previous chapter for sequences*). Despite this, some of the Affimer identified did not contain these tryptophan and glycine residues and it is possible that these Affimers bind to a different part of the TRPV1 peptide screened by phage display.

Based on this observation, it was hypothesised that the conserved tryptophan and glycine residues of Affimer 45 were also essential for the interaction with TRPV1. To test this, site-directed mutagenesis of the Affimer 45 variable regions was conducted to identify the importance of each of the residues to the TRPV1 interaction. Furthermore, X-ray crystallography was used to support the findings from site-directed mutagenesis studies.

To try and further our understanding of the Affimer 45-TRPV1 interaction, an Affimer library was generated based on the residues deemed essential to the interaction to try and find an improved variant of Affimer 45.

The structural data available for TRPV1 has improved vastly in recent years following improvements in cryo-EM, however, the limit of resolution currently remains at 2.9 Å for TRPV1 in complex with its ligands (Gao *et al.* 2016). Owing to the limited resolution, small molecule development using these structures remains difficult. It was therefore hypothesised that by resolving the structure of the Affimer-TRPV1 peptide complex, the design of a small molecule mimetic of the Affimer may be possible. Although biologics have been viewed as competitors to small molecules in the pharmaceutical industry in recent years, their use may complement one another, for example, with biologics being used to identify novel sites on target proteins open to modulation, and small molecules being developed based on these findings and utilised in a clinical setting due to their more favourable pharmacological properties, for example, ability to be administered orally (Hoelder *et al.* 2012, Mocsai *et al.* 2014). In this chapter, the structural interaction between Affimer 45 and its cognate TRPV1 peptide is described. Subsequently, the Affimer 45-TRPV1 peptide crystal

structure is used for the identification of small molecule modulators of TRPV1 (Lawson 2012).

4.2 Results

4.2.1 Site-directed mutagenesis of Affimer 45

To determine which amino acids of the variable regions of Affimer 45 are important for binding to TRPV1, alanine scanning of both variable regions was conducted. Primers were designed (**Table 4.1**) to enable the sequential substitution of each of the Affimer 45 variable region amino acids to an alanine residue (**Table 4.2**). Affimers were produced as previously described and analysed by SDS PAGE and Coomassie staining (**Figure 4.2**). Two clones from mutagenesis studies were tested for ability to express Affimer for each mutant. Next, concentrations were determined for each of the Affimer mutants and concentration normalised to 1 mg/mL (**Table 4.3**).

Primer name	**Primer sequence**	**Tm (^{o}C)**
Affimer 45 VR1.2 Forward	gttgttaaagcgaaagaacagctg**gct**gaaaacacttcggtatgctgacc	67.8
Affimer 45 VR1.2 Reverse	ggtcagcataccgaagttgttttc**agc**cagctgttctttcgctttaacaac	67.8
Affimer 45 VR1.3 Forward	gcgaaagaacagctgttc**gct**aacaacttcggtatgctg	66
Affimer 45 VR1.3 Reverse	cagcataccgaagttgtt**agc**gaacagctgttctttcgc	66
Affimer 45 VR1.4 Forward	aagcgaaagaacagctgttcgaa**gct**aacttcggtatgctgaccatg	67.8
Affimer 45 VR1.4 Reverse	catggtcagcataccgaagtt**agc**ttcgaacagctgttctttcgctt	67.8
Affimer 45 VR1.5 Forward	cgaaagaacagctgttcgaaaac**gct**tcggtatgctgaccatgtac	67.3

Affimer 45 VR1.5 Reverse	gtacatggtcagcataccgaa**agc**gttttcgaacagctgttctttcg	67.3
Affimer 45 VR1.6 Forward	agaacagctgttcgaaaacaac**gct**ggtatgctgaccatgtactacc	67.7
Affimer 45 VR1.6 Reverse	ggtagtacatggtcagcatacc**agc**gttgttttcgaacagctgttct	67.7
Affimer 45 VR1.7 Forward	ctgttcgaaaacaacttc**gct**atgctgaccatgtactac	63.3
Affimer 45 VR1.7 Reverse	gtagtacatggtcagcat**agc**gaagttgttttcgaacag	63.3
Affimer 45 VR1.8 Forward	ctgttcgaaaacaacttcggt**gct**ctgaccatgtactacctgacc	67
Affimer 45 VR1.8 Reverse	ggtcaggtagtacatggtcag**agc**accgaagttgttttcgaacag	67
Affimer 45 VR1.9 Forward	ttcgaaaacaacttcggtatg**gct**accatgtactacctgaccctg	66.6
Affimer 45 VR1.9 Reverse	cagggtcaggtagtacatggt**agc**cataccgaagttgttttcgaa	66.6
Affimer 45 VR2.W Forward	cgaaagtt**gct**gttaaggcaaaactgcaggagttcaa	64.4
Affimer 45 VR2.W Reverse	ttgaactc**agc**cagtttgcacttaacccaaacttttcg	64.4
Affimer 45 VR2.V Forward	cgaaagtttgg**gct**aaggcaaaactgcaggagttcaa	65.5
Affimer 45 VR2.V Reverse	ttgaactcctg**agc**tttgcacttaacccaaacttttcg	65.5
Affimer 45 VR2.K Forward	cgaaagtttgggtt**gct**gcaaaactgcaggagttcaa	65.9

Affimer 45 VR2.K Reverse	ttgaactcctgcag**agc**gcacttaacccaaacttttcg	65.9
Affimer 45 VR2.1 Forward	cgaaagtttgggttaag**gct**aaactgcaggagttcaa	63.8
Affimer 45 VR2.1 Reverse	ttgaactcctgcagttt**agc**cttaacccaaacttttcg	63.8
Affimer 45 VR2.2 Forward	gcgaaagtttgggttaaggca**gct**ctgcaggagttcaaaccggtt	69.7
Affimer 45 VR2.2 Reverse	aaccggtttgaactcctgcag**agc**tgccttaaccccaaactttcgc	69.7

Table 4.1. Site-directed mutagenesis primers. Primers were designed to enable the substitution of Affimer 45 residues with alanine (codon highlighted in bold).

	Variable region one									Variable region two				
WT	A	Q	Q	T	W	W	G	G	I	W	V	K	F	K
VR1.2	A	A	Q	T	W	W	G	G	I	W	V	K	F	K
VR1.3	A	Q	A	T	W	W	G	G	I	W	V	K	F	K
VR1.4	A	Q	Q	A	W	W	G	G	I	W	V	K	F	K
VR1.5	A	Q	Q	T	A	W	G	G	I	W	V	K	F	K
VR1.6	A	Q	Q	T	W	A	G	G	I	W	V	K	F	K
VR1.7	A	Q	Q	T	W	W	A	G	I	W	V	K	F	K
VR1.8	A	Q	Q	T	W	W	G	A	I	W	V	K	F	K
VR1.9	A	Q	Q	T	W	W	G	G	A	W	V	K	F	K
VR2.W	A	Q	Q	T	W	W	G	G	I	A	V	K	F	K
VR2.V	A	Q	Q	T	W	W	G	G	I	W	A	K	F	K
VR2.K	A	Q	Q	T	W	W	G	G	I	W	V	A	F	K
VR2.1	A	Q	Q	T	W	W	G	G	I	W	V	K	A	K
VR2.2	A	Q	Q	T	W	W	G	G	I	W	V	K	F	A

Table 4.2. Sequencing results of Affimer 45 variable regions after site-directed mutagenesis. The alanine substitution is highlighted in red.

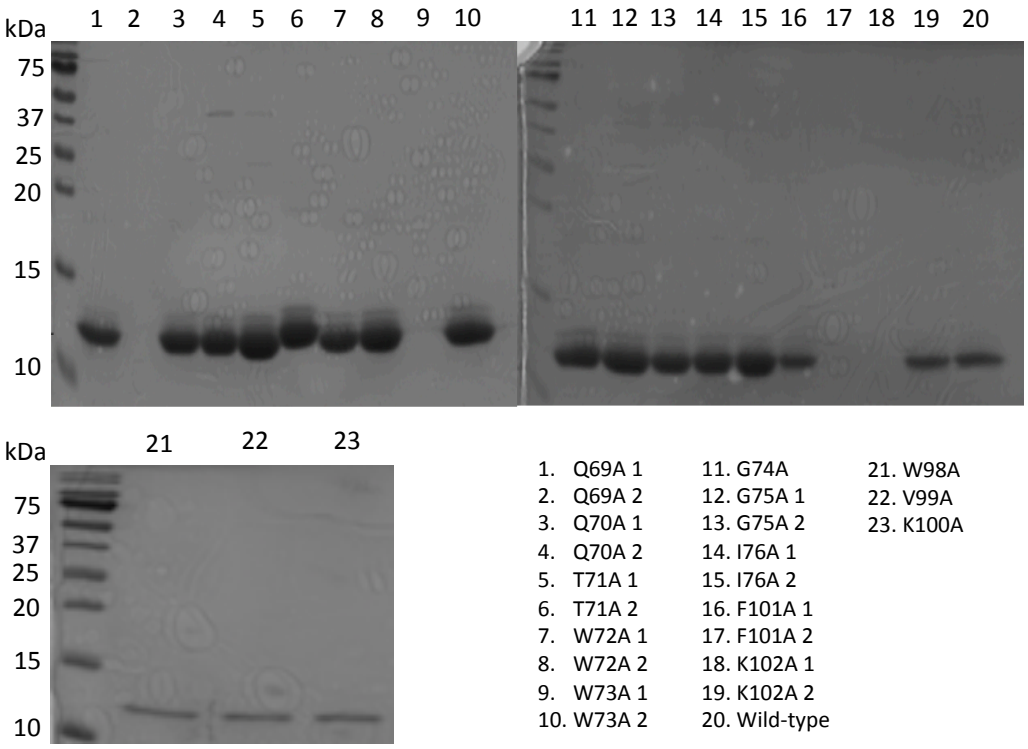

Figure 4.2. Production of Affimer 45 SDM variants and analysis by SDS PAGE. Affimer 45 variants were expressed in *E. coli* BL21 Star (DE3) cells as previously described and protein was then analysed by SDS PAGE. The gel was developed using Coomassie stain. Two single colonies from the site-directed mutagenesis experiment were selected for protein expression.

Affimer	**A280 (mg/mL)**	**Abs 0.1% (= 1 g/L)**	**Concentration (mg/mL)**	**Volume for 1 mg/mL (in 1 mL) (µL)**
Q69A 1	4.236	1.911	2.217	450.1
Q69A 2	-0.012	1.911	-0.006	-
Q70A 1	4.126	1.911	2.159	460.3
Q70A 2	3.989	1.911	2.087	470.9
T71A 1	4.872	1.906	2.556	390.1

T71A 2	4.651	1.906	2.440	400.9
W72A 1	4.232	1.417	2.987	330.5
W72A 2	3.677	1.417	2.595	380.5
W73A 1	-0.008	1.417	-0.006	-
W73A 2	4.666	1.417	3.293	300.4
G74A	4.221	1.898	2.224	440.9
G75A 1	4.891	1.898	2.577	380.8
G75A 2	3.657	1.898	1.927	510.9
I76A 1	3.890	1.908	2.039	490.0
I76A 2	4.201	1.908	2.202	450.4
F101A 1	2.983	1.914	1.559	640.1
F101A 2	-0.001	1.914	0.0005	-
K102A 1	0.012	1.911	0.006	-
K102A 2	3.012	1.911	1.576	630.5
Wild-type	2.789	1.901	1.467	680.2
W98A	1.487	1.417	1.049	1000
V99A	1.980	1.901	1.042	1000
K100A	2.210	1.906	1.159	869.6

Table 4.3. TRPV1 Affimer mutant concentration measurements by Nanodrop spectrophotometry and normalisation to 1 mg/mL for use in binding assays. Absorption coefficients were calculated using the Expasy Protein Parameters online tool.

Next, site-directed mutagenesis was carried out using QuikChange Mutagenesis (Agilent). Although residues W98, V99 and K100 form part of the Affimer scaffold rather than the variable regions, these residues were also mutated to alanine due to their close proximity to the TRPV1 peptide observed by X-ray crystallography (**Figure 4.3**A and B), to be discussed later in this chapter.

Following successful mutagenesis, each of the Affimer 45 mutants was tested by ELISA for their ability to interact with the TRPV1 peptide originally used to identify Affimer 45 from our library. Affimers were incubated at a concentration of 1 µM against 160 ng/mL of biotinylated peptide adsorbed on the surface of a streptavidin-coated plate. Following washing, bound Affimers were detected using an anti-8XHis antibody (HRP-conjugated) followed by addition of TMB substrate. From this initial ELISA, results immediately highlighted the importance of a number of amino acids to the TRPV1 interaction. When the amino acids T71, W73, G74, I76, K100, F101 and K102 were mutated to alanine, binding was completely abolished. When amino acids Q69, W98 and V99 were mutated to alanine, slightly reduced binding was observed (**Figure 4.3**C).

Next, to gain further insights into the level of importance of the variable region residues, Affimer mutants were incubated at a range of concentrations against 160 ng/mL of peptide. Results confirmed observations from the single concentration ELISA, for example, mutants W73A, I76A and K100A were unable to bind to the peptide even when tested at 10 µM. Additionally, Q69A, T71A, G74A, F101A and K102A were only able to bind to the peptide when incubated at higher concentrations suggesting that these residues were also important to the interaction but to a lesser extent. Residues Q70, W72, G75, W98 and V99 were less important to the interaction however W98 appeared to have a reduced maximum level of binding (**Figure 4.4**).

These results suggested that as with the DkTx ICK loops, the tryptophan and glycine residues present in the first variable region of Affimer 45 are essential for the interaction with TRPV1. Furthermore, certain surrounding residues in the Affimer 45 variable regions were also confirmed as essential to the interaction, for example, I76 of variable region one and K100, F101 and K102 of variable region two. These results suggested that in addition to the first

variable region, the second variable region residues were also involved in the interaction. All K_d values have been displayed in **Table 4.4**.

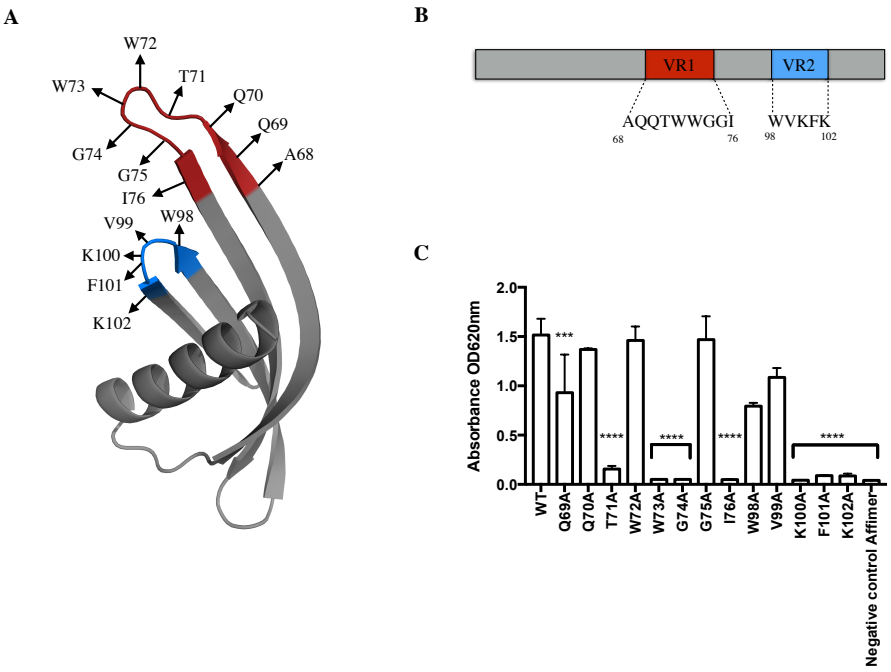

Figure 4.3. ELISA was used to test binding of Affimer 45 mutants to a TRPV1 peptide. A. Crystal structure demonstrating the variable region one (red) and variable region two (blue) residues that were mutated. B. Graphical illustration outlining the variable region one (red) and variable region two (blue) amino acids to be mutated. C. Each amino acid of both variable regions of Affimer 45 was mutated to alanine by QuikChange site-directed mutagenesis. All mutants were tested for their ability to bind their cognate TRPV1 peptide by ELISA. Biotinylated TRPV1 peptide (160 ng/mL) was immobilised on streptavidin-coated plates and then incubated with 1 µM of each of the Affimer mutants. Affimers were detected using an anti-His antibody conjugated to HRP. The addition of HRP substrate, TMB, resulted in a change in colour that was measured at an OD of 620 nm (*N = 3. Statistical analysis conducted using one-way ANOVA with multiple comparisons against wild-type condition; *** = <0.0005, **** = <0.0001*).

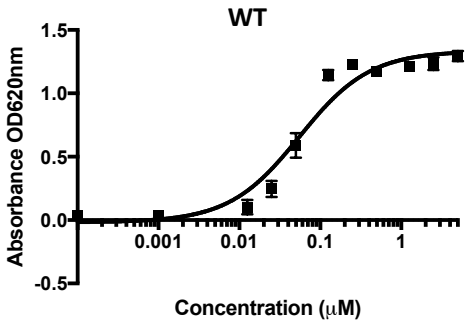
WT
Absorbance OD620nm
1.5
1.0
0.5
0.0
-0.5
0.001
0.01
0.1
1
Concentration (μM)

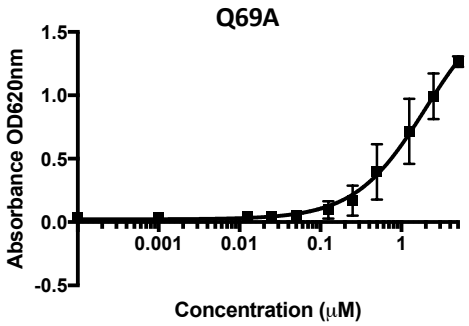
Q69A
Absorbance OD620nm
1.5
1.0
0.5
0.0
-0.5
0.001
0.01
0.1
1
Concentration (μM)

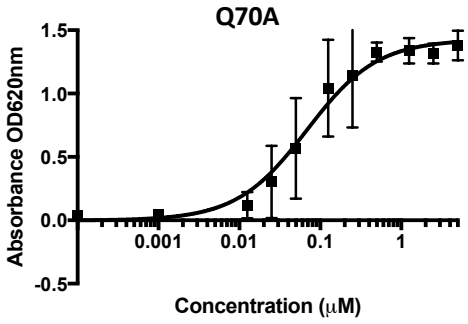
Q70A
Absorbance OD620nm
1.5
1.0
0.5
0.0
-0.5
0.001
0.01
0.1
1
Concentration (μM)

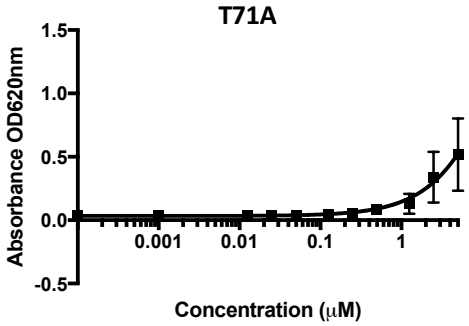
T71A
Absorbance OD620nm
1.5
1.0
0.5
0.0
-0.5
0.001
0.01
0.1
1
Concentration (μM)

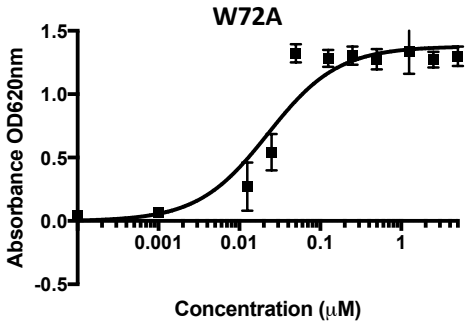
W72A
Absorbance OD620nm
1.5
1.0
0.5
0.0
-0.5
0.001
0.01
0.1
1
Concentration (μM)

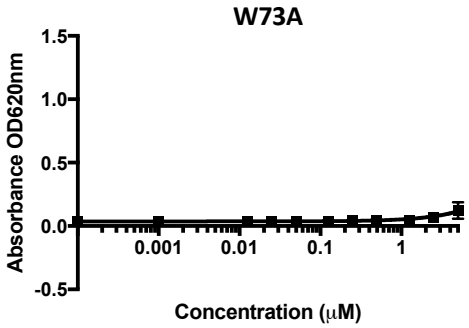
W73A
Absorbance OD620nm
1.5
1.0
0.5
0.0
-0.5
0.001
0.01
0.1
1
Concentration (μM)

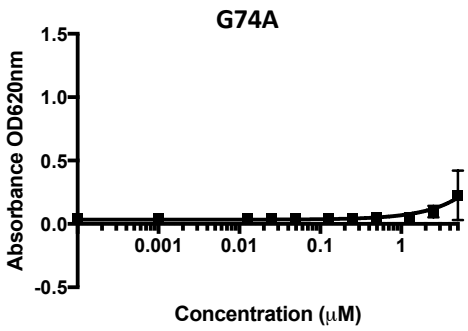
G74A
Absorbance OD620nm
1.5
1.0
0.5
0.0
-0.5
0.001
0.01
0.1
1
Concentration (μM)

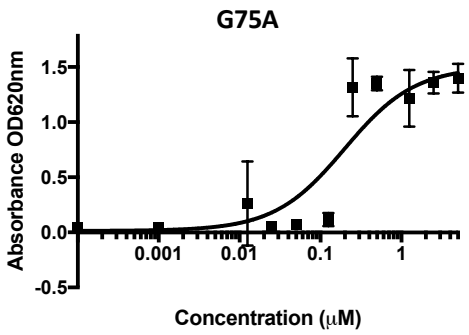
G75A
Absorbance OD620nm
1.5
1.0
0.5
0.0
-0.5
0.001
0.01
0.1
1
Concentration (μM)

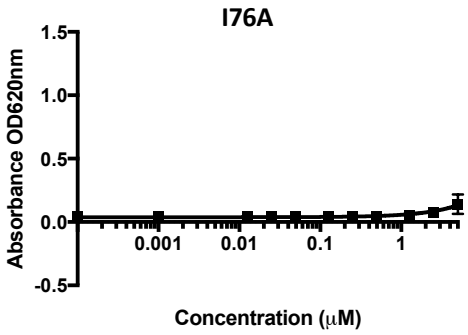
I76A
Absorbance OD620nm
1.5
1.0
0.5
0.0
-0.5
0.001
0.01
0.1
1
Concentration (μM)

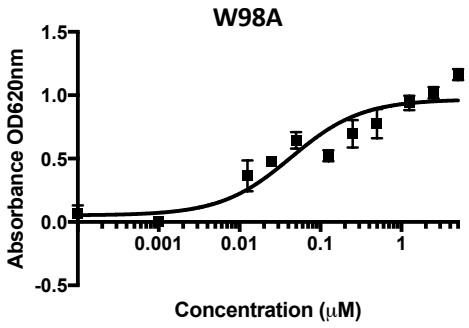
W98A
Absorbance OD620nm
1.5
1.0
0.5
0.0
-0.5
0.001
0.01
0.1
1
Concentration (μM)

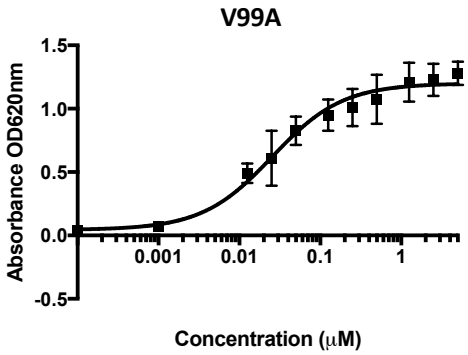
V99A
Absorbance OD620nm
1.5
1.0
0.5
0.0
-0.5
0.001
0.01
0.1
1
Concentration (μM)

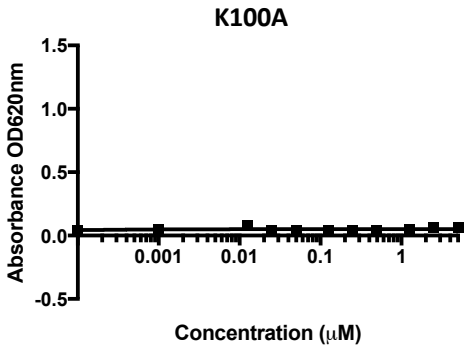
K100A
Absorbance OD620nm
1.5
1.0
0.5
0.0
-0.5
0.001
0.01
0.1
1
Concentration (μM)

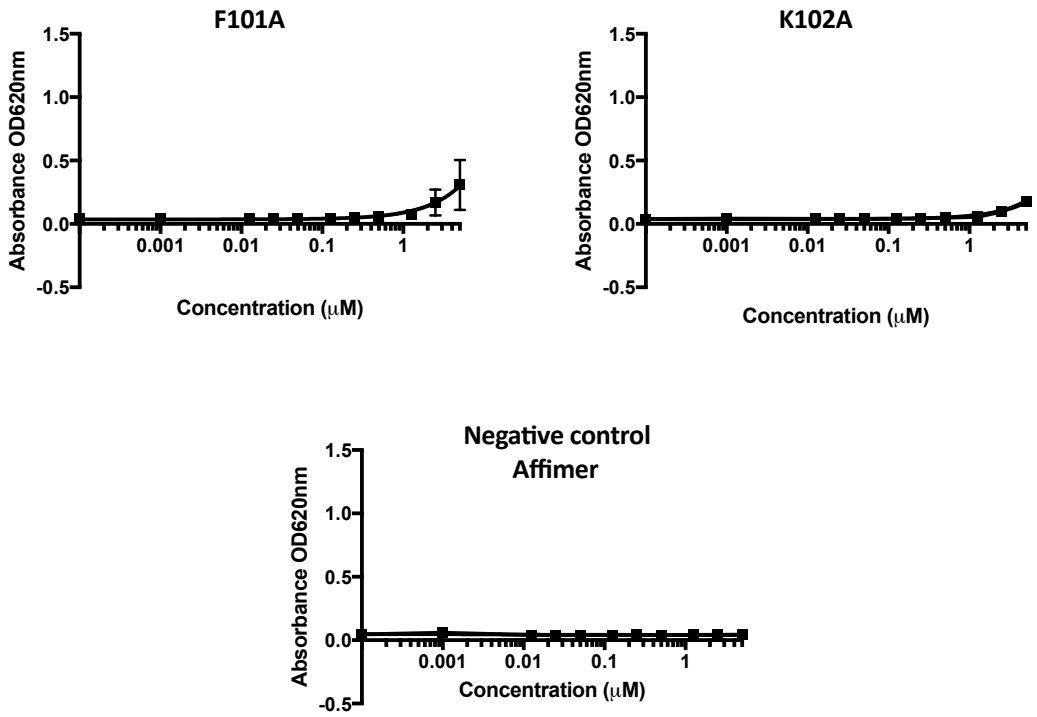

Figure 4.4. Concentration-response ELISA to test the extent to which each of the Affimer 45 mutations disturbed the interaction with TRPV1. TRPV1 peptide was immobilised on streptavidin-coated plates. Affimer 45 mutants were incubated against 160 ng/mL of TRPV1 peptide at a range of concentrations. The Affimers were then detected using a anti-His antibody conjugated to HRP, enabling detection by addition of TMB and measurement at 620 nm.

Affimer variant	**K_d ± S. E. M (nM)**
WT	62 ± 11
Q69A	2,485 ± 2,135
Q70A	77 ± 25
T71A	NA
W72A	26 ± 6
W73A	NA
G74A	NA
G75A	247 ± 132
I76A	NA
W98A	15 ± 5
V99A	20 ± 4
K100A	NA
F101A	NA
K102A	NA
Negative Affimer	NA

Table 4.4. K_d values for Affimer variants tested for binding against immobilised TRPV1 peptide. K_d values are dislayed as nM values however for variants that demonstrated no binding, NA has been displayed instead of a value.

4.2.2 Structural analysis of the Affimer 45-TRPV1 interaction by X-ray crystallography

To investigate the molecular mechanism underlying the Affimer 45-TRPV1 interaction in atomic detail, the Affimer 45-TRPV1 peptide complex was crystallised. To do this, Affimer 45 was produced as recently described and purified using a combination of Ni-NTA resin and size exclusion chromatography (SEC). Results demonstrated an increase in absorbance at 280nm over a number of fractions (**Figure 4.5**A). Analysis of these fractions by SDS PAGE subsequently developed with Coomassie stain demonstrated the presence of Affimer 45 in all of these fractions (**Figure 4.5**B). The fractions were subsequently pooled and incubated with the TRPV1 peptide at a 1:1 molar ratio. The complex was then concentrated to a concentration of 8 mg/mL and used in crystallisation trials. After incubation for 12 hours, a crystal could be observed in the buffer condition composed of 0.1M HEPES, pH 7.5, 2% v/v PEG400, 2M $(NH_4)_2SO_4$ (**Figure 4.6**).

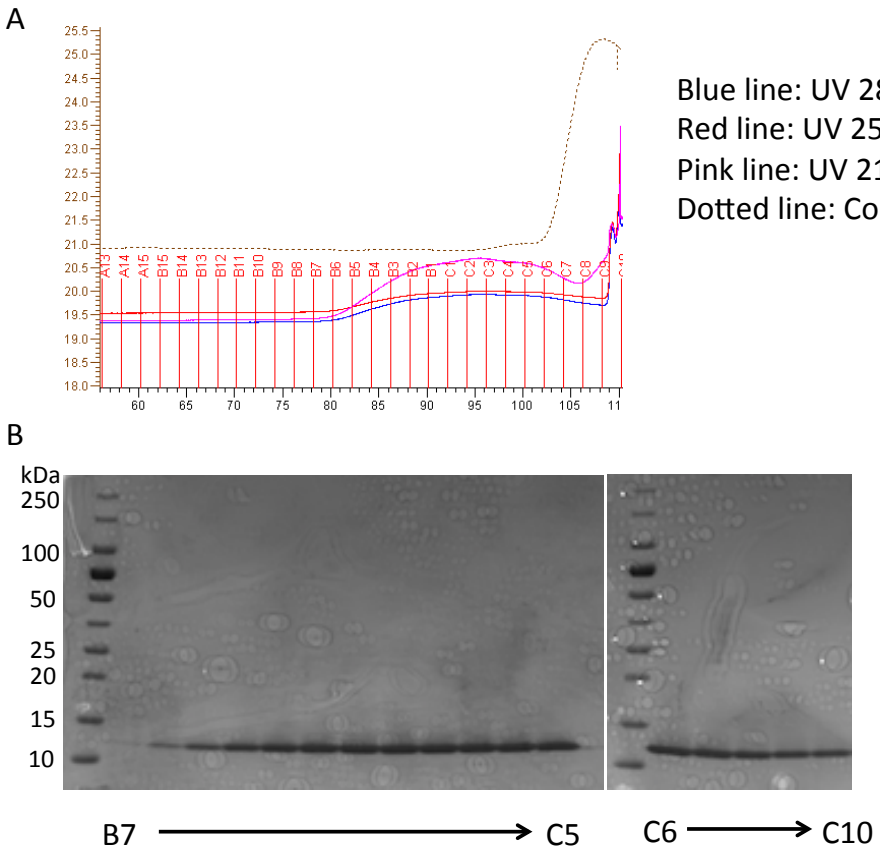

Figure 4.5. Size exclusion chromatography trace (A) and SDS PAGE analysis (B) of protein obtained from eluted fractions. A. Affimer 45 was produced as previously described and purified initially using Ni-NTA resin. Protein was subsequently purified by size exclusion chromatography using a Superdex G75 pre-packed column. The column was buffer exchanged in to PBS and then Affimer protein purified. B. Fractions that corresponded to an increase in absorbance at 280 nm were then analysed by SDS PAGE and Coomassie staining.

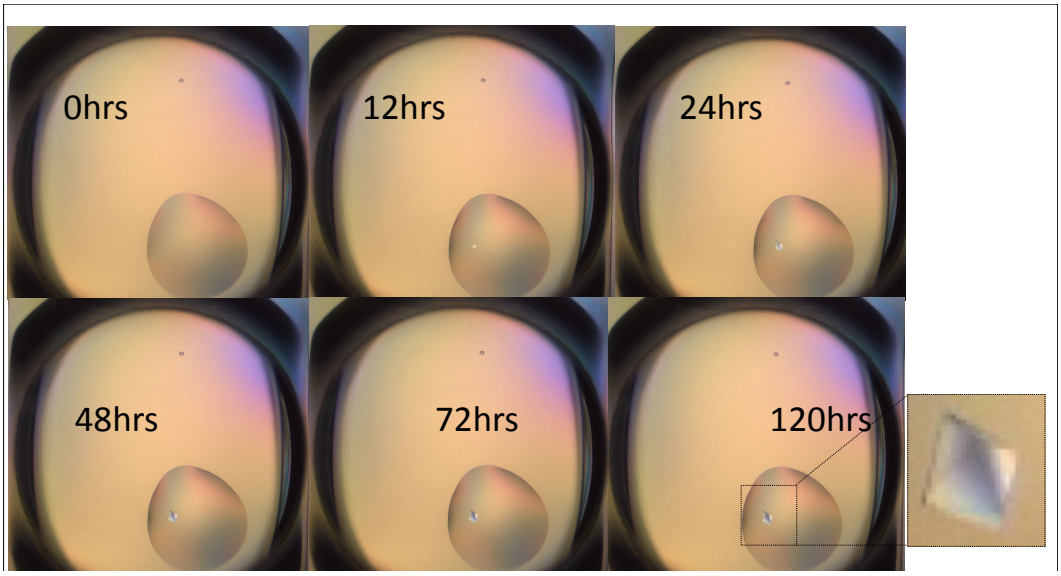

Figure 4.6. An image demonstrating the growth of the crystal used for analysis of the Affimer 45-TRPV1 peptide complex. Crystal trials were set up as previously described with Affimer 45 and the TRPV1 peptide formed as a complex at a 1:1 stoichiometry. Drops were set up using a Douglas Oryx 6 plate loader using NT8 software with drops added at 0.2µl volumes. Imaging took place using Rockimager 1000, Formulatrix. The Affimer 45-TRPV1 peptide complex crystallised in 12 hours in 0.1M HEPES, pH 7.5, 2% v/v PEG400, 2M $(NH_4)_2SO_4$. The resulting crystal diffracted to 2.5Å resolution using beamline IO4 at Diamond Light Source Ltd, Oxford.

The crystal structure (**Figure 4.7**) diffracted to 2.5 Å resolution and contained Affimer 45 and the peptide sequence of the TRPV1 outer pore domain with a 1:1 stoichiometry. Similar to other Affimers (Kyle *et al.* 2015, Hughes *et al.* 2017, Michel *et al.* 2017, Robinson *et al.* 2018), Affimer 45 contained the typical phytocystatin framework (Tiede *et al.* 2014) with a full variable region one of nine amino acids however the second variable region was truncated and contained only two amino acids, a property that is unusual in previously isolated Affimers. This may be a result of the small size of the peptide target. Nevertheless, both variable regions appear to form contacts with the peptide, suggesting the importance of both variable regions to the interaction. Furthermore, amino acids present in the backbone adjacent to variable region two also form hydrophobic contacts with the peptide.

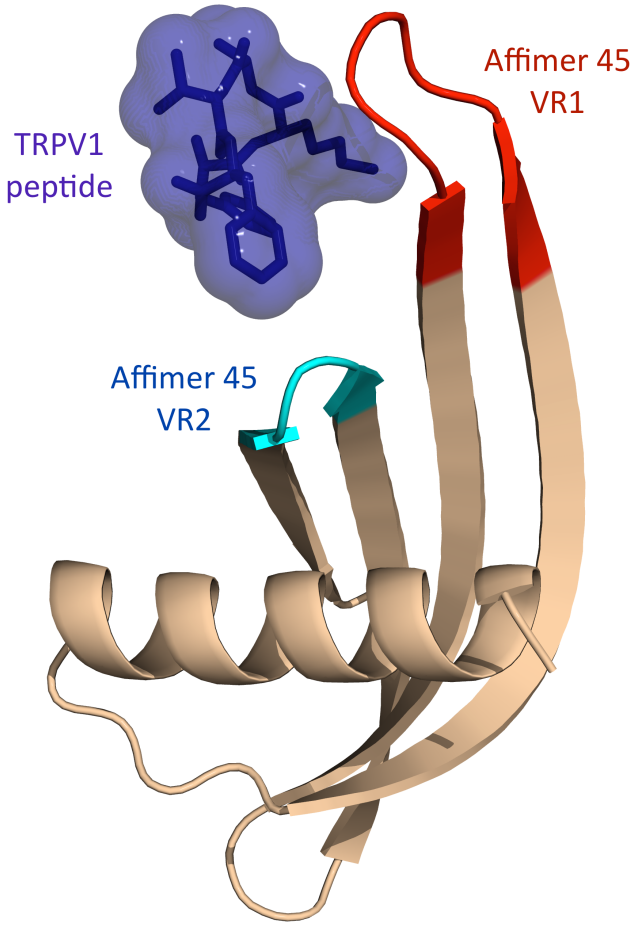

Figure 4.7. Affimer 45 was crystallised in complex with the peptide mimicking a region of the TRPV1 outer pore domain. Affimer 45 was expressed and purified by affinity chromatography followed by gel filtration to obtain the monomeric Affimer 45 protein. Subsequently, Affimer 45 was added to the TRPV1 peptide at a 1:1 molar ratio to form a complex and concentrated to 8 mg/mL. Crystallisation trials were then set up using the NT8 crystallisation system, Formulatrix robotic device with a variety of JCSG commercial buffers (Molecular Dimensions). Imaging took place using Rockimager 1000, Formulatrix. The Affimer 45-TRPV1 peptide complex crystallised in 12 hours in 0.1 M HEPES, pH 7.5, 2% v/v PEG400, 2 M $(NH_4)_2SO_4$. The resulting crystal diffracted to 2.5 Å resolution using beamline IO4 at Diamond Light Source Ltd, Oxford.

The first and second variable regions of Affimer 45 form a number of interactions with the peptide (**Figure 4.8**A). In variable region one, a hydrogen bond is formed between the nitrogen group of the Affimer 45 W72 indole side chain and the

oxygen group of the A13 carbonyl group of the peptide. Another hydrogen bond is formed between the Affimer 45 W73 indole side chain and the peptide K12 carbonyl group. Furthermore, a parallel-displaced π-π interaction can be observed between the aromatic side chains of the Affimer 45 W73 and the peptide F15. In variable region two, a hydrogen bond is formed between the Affimer 45 lysyl side chain of K100 and the peptide F15 carbonyl group. Another μ-μ interaction can also be observed between the aromatic side chains of the Affimer 45 W98 and peptide F11 (**Figure 4.8**A). In addition to hydrophilic interactions, a number of hydrophobic interactions also take place.

The combination of hydrophilic (*blue*) and hydrophobic (*red*) interactions are highlighted in **Figure 4.8**B. Hydrophobic interactions are formed between I76 of Affimer 45 and F11 of the peptide. W73 of Affimer 45 also inserts itself into a hydrophobic region formed by A13 and V14 of the peptide (**Figure 4.8**C). Interestingly, site-directed mutagenesis of Affimer 45 suggested that although W73 is critical for the interaction between Affimer 45 and the TRPV1 peptide, binding was not disturbed by mutation of W72, despite the crystal structure demonstrating contact with the peptide via its indole ring, a property that would be lost when the amino acid is mutated to alanine.

In variable region 2, the Affimer 45-TRPV1 peptide interaction is further stabilised by a polar contact between the lysyl side chain of K100 and the carbonyl group of F15 of the TRPV1 peptide (**Figure 4.8**D). The importance of this residue was also supported by site-directed mutagenesis results. Additionally, a π-π interaction can be observed between Affimer 45 W98 side-chain and the peptide F11 side chain.

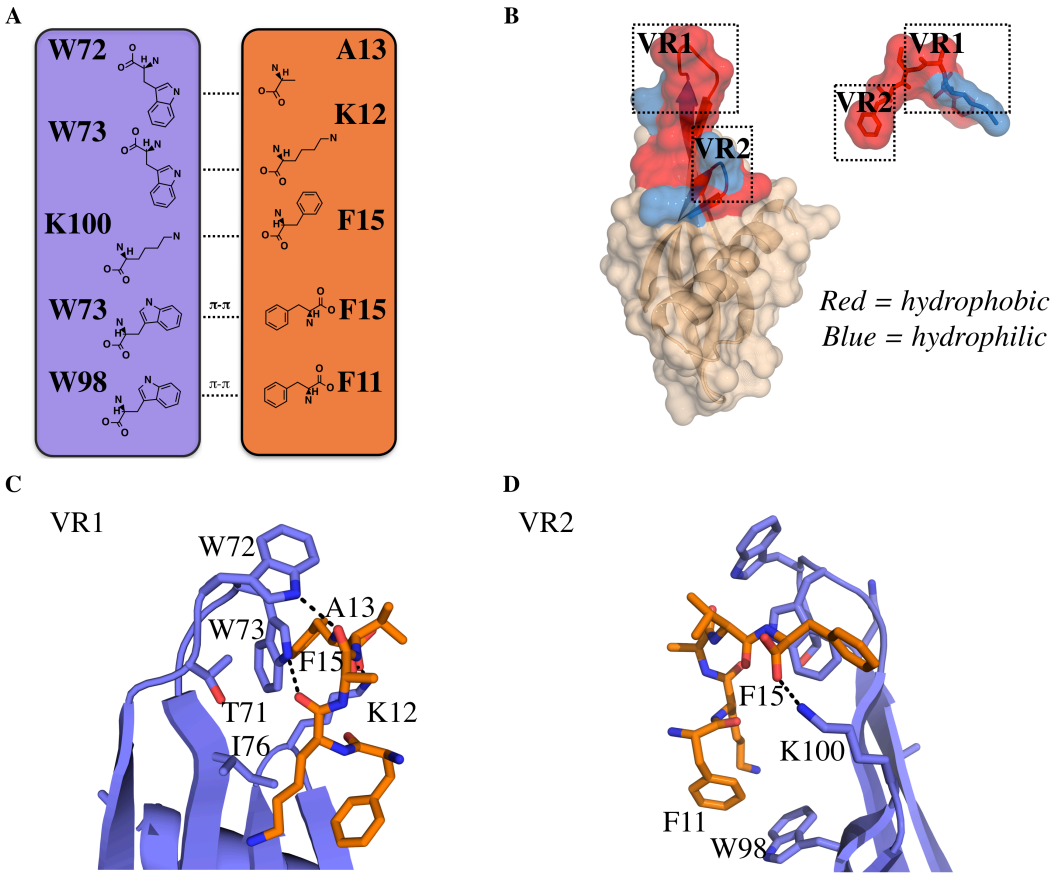

Figure 4.8. Affimer 45 interacts with the TRPV1 peptide using both variable regions. A. The crystal structure between Affimer 45 and the TRPV1 peptide revealed a number of interactions between Affimer 45 (*purple*) and the TRPV1 peptide (*orange*) that are displayed in 2D format. B. A combination of hydrophobic (*red*) and hydrophilic (*blue*) binding interactions are mediated by VR1 and VR2. C. Closer examination of the VR1 interactions identifies specific interactions between various amino acids. D. Variable region two amino acid interactions can also be observed.

By conducting structural alignment between the peptide screened and the full-length TRPV1 channel (**Figure 4.9**A), results suggested that both Affimer 45 and DkTx interact with the same region of TRPV1. However, differences can be observed on the structural constraints placed on this peptide region of the channel (**Figure 4.9**B). These differences may account for functional differences imposed by the two reagents i.e. direct activation by DkTx compared to potentiation by Affimer 45. It is important to stress however, that the lower resolution provided by the TRPV1-DkTx structure (2.9 Å) may in fact be resulting

in the differences observed between the two models with side-chain resolution not as clear.

In addition to the structural data collected for the interaction between DkTx and TRPV1, scanning mutagenesis studies have elucidated the importance of three residues in the outer pore domain of TRPV1 (F649, A657 and F659) for interacting with DkTx (Bohlen *et al.* 2010). The crystal structure of Affimer 45 in complex with the peptide mimicking the outer pore domain of TRPV1 implicates similar residues in the Affimer 45-TRPV1 interaction (**Figure 4.9**C).

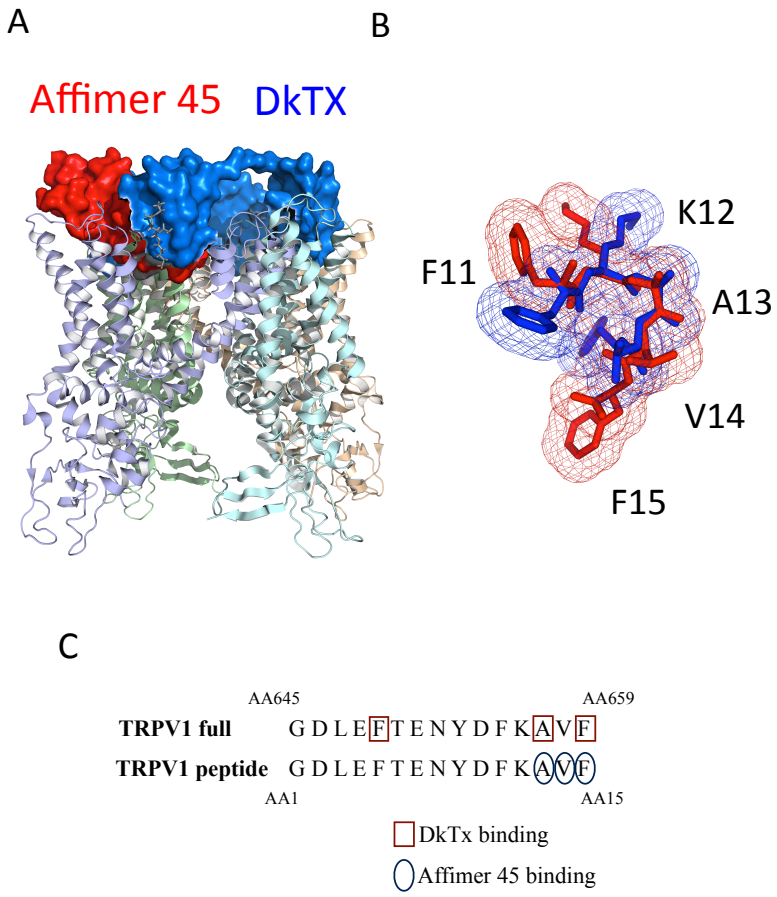

Figure 4.9. Alignment of Affimer 45-TRPV1 peptide crystal structure with DkTx-TRPV1 cryo-EM structure (PDB: 5IRX) demonstrates identical epitope. A. To identify similarities in binding between Affimer 45 and DkTx to TRPV1, a structural alignment was conducted using MacPyMol. Whilst it was already known that Affimer 45 bound to the 5-mer peptide region of the 15-mer peptide it was crystallised in complex with (*red*), the structure of the DkTx-TRPV1 complex (*blue*) reveals that these two molecules demonstrate overlap in their binding region of TRPV1. B. When the binding region is zoomed in, the residues FKAVF are identified as the overlapping binding region. However, structural shifts can be observed between the Affimer bound region (*red mesh*) and DkTx bound region (*blue mesh*). C. The peptide used to isolate Affimer 45 is presented alongside its full-length TRPV1 counterpart with important residues, based on structural studies and scanning mutagenesis, for DkTx (*red boxes*) and Affimer 45 (*blue circles*) binding highlighted.

4.2.3 Affinity maturation of Affimer 45 towards TRPV1

Following elucidation of the binding interaction between Affimer 45 and the TRPV1 peptide, it was decided that based on the importance of the tryptophan and glycine residues of variable region one, alongside their presence in the DkTx toxin, a new library would be generated based around these residues, with surrounding variable region amino acids randomised, to try and identify an Affimer 45 variant with improved binding properties. To do this, splicing by overlap extension PCR was conducted using two PCR fragments (1 and 2). Fragment 1 extended from the DsbA signal sequence to the first variable region whilst the second fragment extended from the first variable region to the *PstI* restriction site incorporating randomised amino acid residues in the first variable region (**Figure 4.10**A and B). This randomisation took place through the use of triplet nucleotides with the exclusion of cysteine and stop codons as previously described for the original generation of the Affimer library (Tiede *et al.* 2014).

After the generation of fragment 1 and fragment 2, SOE PCR was conducted to join the two fragments together to produce a SOE PCR product that runs from the DsbA signal sequence to the *PstI* restriction site, whilst incorporating a 5' *NheI* restriction site. Next, the fragment 1 forward primer and the fragment 2 reverse primer were used in a final reaction that incorporated four rounds of amplification to generate a final amplification product (**Figure 4.10**C). All DNA products were analysed by agarose gel electrophoresis (**Figure 4.10**D).

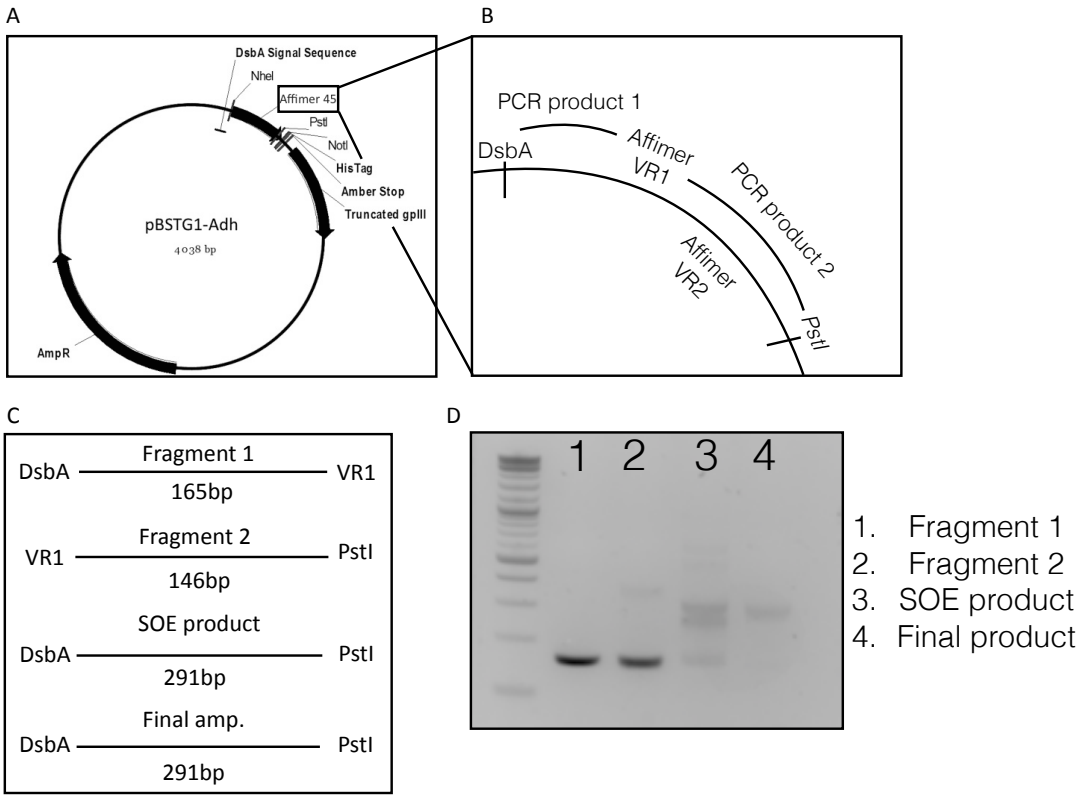

Figure 4.10. Affinity maturation of Affimer 45 to try and improve its affinity towards its cognate TRPV1 peptide was conducted using splicing by overlap extension PCR. A. The final PCR product was cloned into to a pBSTG1-Adh plasmid to enable production of phage pIII coat proteins conjugated to the resulting library of Affimers. B. The first PCR product, termed fragment 1, extended from the DsbA signal sequence to the first Affimer variable region. The second PCR product, termed fragment 2, extended from the first Affimer variable region to the *PstI* restriction site, incorporating the second variable region. C. Finally, the two fragments were joined together by SOE PCR resulting in a product of approximately 300 bp that incorporated Affimer 45 with randomised variable region amino acids surrounding the tryptophan-glycine motif of variable region one. D. Following the initial PCR and subsequent SOE PCR experiments, all products were analysed by agarose gel electrophoresis to confirm correct molecular weight.

After the final PCR product had been generated, it was digested using *NheI* and *PstI* restriction enzymes and ligated in a digested pDHis vector with the same enzymes. The resulting ligation product was transformed into *E. coli* XL1 Blue super competent cells and plated on to LB agar supplemented with carbenicillin. Random colonies were sent for sequencing using a pDHis-specific primer (M13R)

to ensure the successful ligation of SOE product in to the pDHis vector. Results demonstrated a good level of variety in the nine clones sequenced (**Table 4.5**). Subsequently, a larger-scale ligation was set up for the generation of a new library based on the Affimer 45 tryptophan-glycine motif. This library will be termed the Affimer 45(WG) library herein.

Affimer clone	**Variable Region 1**	**Variable Region 2**
Clone 1	MHPRT**WG**LE	**FK**
Clone 2	AQEIR**WG**ER	**FK**
Clone 3	DVNYD**WG**FH	**FK**
Clone 4	NWGID**WG**EH	**FK**
Clone 5	PDAYH**WG**DN	**FK**
Clone 6	FMETF**WG**IM	**FK**
Clone 7	WWNML**WG**PF	**FK**
Clone 8	GVYVS**WG**NG	**FK**
Clone 9	LHQIW**WG**HI	**FK**

Table 4.5. Sequencing results of a selected number of clones from the initial library.

Following the successful generation of a randomised Affimer 45(WG) library, the TRPV1 peptide was screened by phage display. In the first round of biopanning, two rounds of negative selection against a $Na_v1.7$ peptide were conducted followed by positive selection against the TRPV1 peptide with a binding step of 30 minutes conducted. All biopanning rounds were conducted on streptavidin-coated strips. Unbound Affimer phage were washed and the bound Affimer phage eluted using low and high pH steps. Affimer phage were infected in to log-phase ER2738 *E. coli* cells and plated on to LB agar supplemented with carbenicillin. Next, individual clones were tested by phage ELISA. To test for differences in binding between wild-type Affimer 45 and mutants, the concentration of target peptide providing a low response when incubated with wild-type Affimer 45 phage was established so that improvements in binding by mutants could be easily identified (**Figure 4.11**). Results demonstrated the concentration of peptide that resulted in a 50% response was 0.132 µg/mL, or

0.132 µM. As a result, this concentration of peptide was used in all subsequent phage ELISA's.

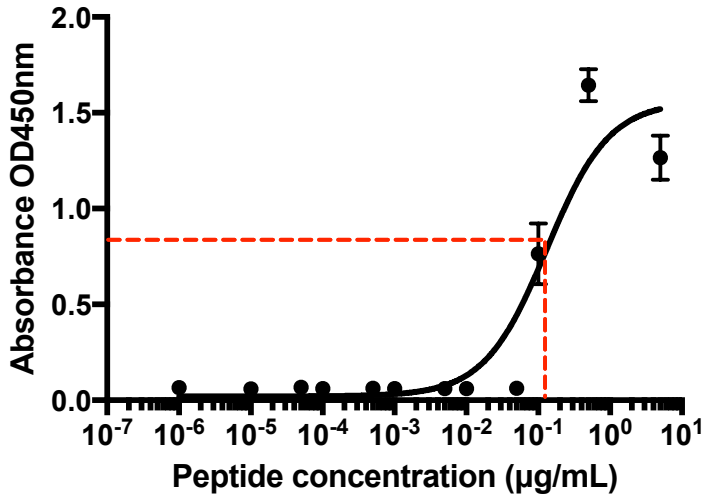

Figure 4.11. Graph showing a concentration response phage ELISA using a constant amount of Affimer 45 phage against a range of TRPV1 peptide concentrations. The concentration of TRPV1 target peptide that would elicit a 50% response (red line) from the Affimer 45 WT was determined by incubating the Affimer 45 WT-pIII against the TRPV1 peptide when immobilised at different concentrations. The TRPV1 peptide was immobilised on streptavidin-coated plates. Excess peptide was washed away and bound peptide incubated with Affimer 45 phage. The Affimer 45 phage was then detected using an anti-Fd antibody conjugated to HRP. Addition of TMB for one min followed by stopping of the reaction with sulphuric acid was followed by measurement at 450 nm.

The concentration of peptide target established that provided a low response by wild-type Affimer 45 phage (0.132 µg/mL) was then used for subsequent phage ELISAs. Phage ELISA of panning round one clones was conducted with a number of clones demonstrating higher levels of binding when compared to the wild-type Affimer 45 (🡻) (**Figure 4.12**A). Sequencing of the binders providing the highest signal revealed the presence of various levels of amino acid enrichment at each of the randomised positions (**Figure 4.12**B). For example, enrichment of a glutamate residue at position Q1.2, a methionine at T1.4, an aspartate or glutamate at W1.5 and a hydrophobic residue at I1.9 could be observed (**Figure 4.12**C).

A

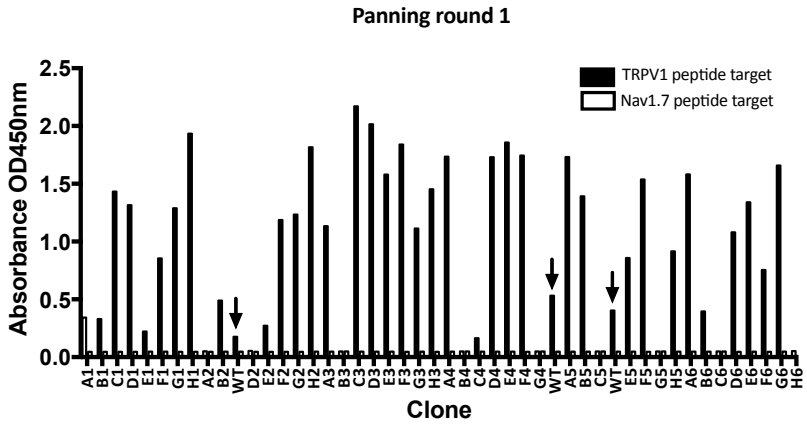

B

Clone	VR1 sequence	Clone	VR1 sequence	Clone	VR1 sequence
C1	RQQMD**WG**TL	D3	VEALN**WG**KF	B5	VEDRH**WG**RM
D1	ISFRD**WG**VL	E3	KFSKA**WG**RM	E5	KEIAN**WG**GI
F1	YNWQD**WG**VL	F3	REFMV**WG**QL	F5	INFTE**WG**AM
G1	SDEMI**WG**RL	G3	WRDTE**WG**ML	H5	LTNRD**WG**II
H1	VFSVE**WG**GM	H3	LKYQE**WG**LL	A6	SQTMV**WG**MM
F2	RREMV**WG**VL	A4	VETLN**WG**RL	D6	SQNMY**WG**VF
G2	VEPVE**WG**FM	D4	QQKVT**WG**AL	E6	NEPFA**WG**MF
H2	MDHAT**WG**KL	E4	NEMMD**WG**AI	F6	SVKME**WG**DL
A3	KAPRT**WG**LL	F4	DEAKD**WG**RI	G6	---------
C3	GETTT**WG**HI	A5	NEDRG**WG**KL		

C

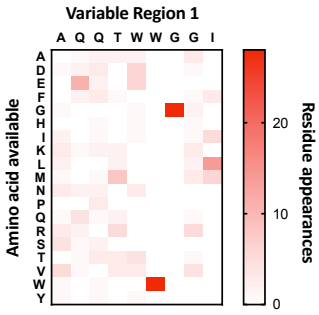

Figure 4.12. Phage ELISA and sequencing results following <u>one round of biopanning</u> against the TRPV1 peptide with the Affimer 45 (WG) library. A. A phage ELISA was conducted as previously described using monoclonal Affimers identified from the screen using the Affimer 45 (WG) library with the wild-type Affimer 45 phage (🡻) included for comparison. B. Clones that demonstrated highest levels of binding were sequenced using an M13R primer. The constant WG residues are highlighted in bold. C. A heat map showing amino acid enrichment at each of the randomised positions with dark red showing high enrichment and white showing no enrichment.

Panning round one phage were advanced in to a second round of biopanning with selection taking place on streptavidin-coated beads using a reduced binding step of ten minutes. Washing was then conducted for either one day or five days, with both durations using either standard conditions or competition against wild-type Affimer 45 (pIII-unconjugated). Random clones were then tested by phage

ELISA with clones sequenced and heat maps generated to identify enrichment of amino acids at the variable region one positions as described in Figure 4.12 (**Figure 4.13**, **Figure 4.14**, **Figure 4.15**, **Figure 4.16**). Common amino acid enrichments could be observed from all methods of selection. For example, negatively charged residue or glutamine at Q1.2, methionine or threonine at T1.4, aspartate, proline or serine at W1.5, lysine or methionine at G1.8 and hydrophobic residue at I1.9. Furthermore, phage ELISA results for Affimer phage isolated from biopanning round two demonstrated that five days of washing in comparison to only one enabled the isolation of more Affimer phage that produced a higher response by ELISA.

A

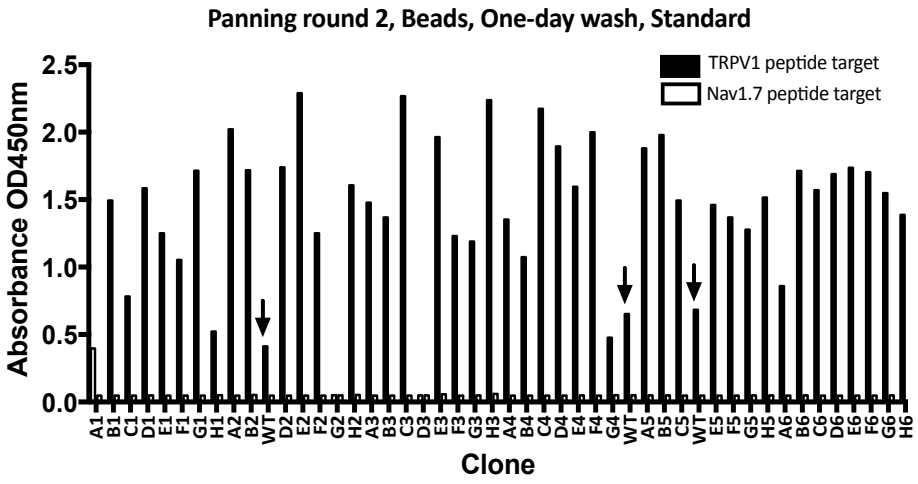

B

Clone	VR1 sequence	Clone	VR1 sequence	Clone	VR1 sequence
A1	PYQTE**WG**IM	A3	YESTA**WG**AI	A5	QQHMD**WG**ML
B1	HEMFS**WG**RF	B3	SSVQK**WG**LF	B5	MEYTH**WG**KM
C1	HYPAT**WG**HL	C3	LEYVP**WG**ML	C5	RNQQD**WG**TL
D1	SDLTM**WG**KL	D3	NRQPF**WG**FY	D5	---------
E1	YMQVD**WG**GM	E3	AFSVD**WG**HL	E5	SEAMN**WG**VV
F1	MHHTH**WG**MM	F3	HYTVD**WG**WL	F5	ADAAS**WG**QL
G1	QEEMT**WG**MF	G3	VINTA**WG**KM	G5	YQELP**WG**GL
H1	NHTTD**WG**VL	H3	RDYVS**WG**LL	H5	IDQTT**WG**MF
A2	AQLTN**WG**KV	A4	RVGTD**WG**MI	A6	ERFYD**WG**VL
B2	TQMMG**WG**SL	B4	SRMHE**WG**RL	B6	KDKME**WG**IL
C2	FQQTD**WG**RM	C4	SPAMD**WG**TL	C6	MDATS**WG**AI
D2	DQLLD**WG**MF	D4	MEAMN**WG**AI	D6	RHMMT**WG**ML
E2	SDQLS**WG**IL	E4	FEAMD**WG**GF	E6	NDFLE**WG**RL
F2	MQIAT**WG**MM	F4	EFAVE**WG**GM	F6	SQAMD**WG**TL
G2	ITWXY**WG**WY	G4	HKLME**WG**RI	G6	SYFVE**WG**RL
H2	---------	H4	TLKTD**WG**KM	H6	EEKQH**WG**NL

C

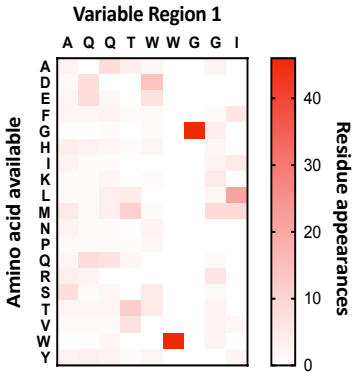

Figure 4.13. Phage ELISA and sequencing results following a second round of biopanning with one day of washing under standard conditions against the TRPV1 peptide with the Affimer 45 (WG) library. A. A phage ELISA was conducted as previously described using monoclonal Affimers identified from the second round of biopanning using the Affimer 45 (WG) library with the wild-type Affimer 45 phage (🡻) included for comparison. B. Clones that demonstrated highest levels of binding were sequenced using an M13R primer. The constant WG residues are highlighted in bold. C. A heat map showing amino acid enrichment at each of the randomised positions with dark red showing high enrichment and white showing no enrichment.

A

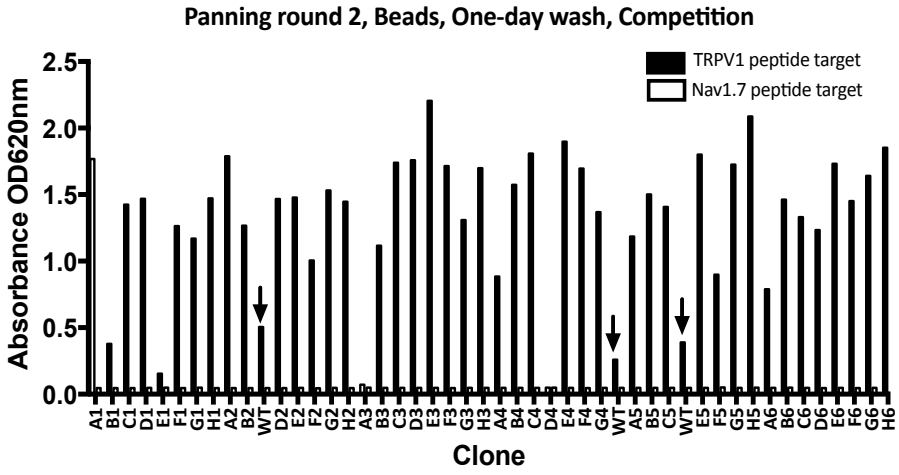

B

Clone	VR1 sequence	Clone	VR1 sequence	Clone	VR1 sequence
A1	KEYTQ**WG**LM	A3	---------	A5	MEFYD**WG**VL
B1	WDYKE**WG**AL	B3	WEHFT**WG**RM	B5	IEKHN**WG**RM
C1	MQTKN**WG**ML	C3	ADQRT**WG**IL	C5	WRLTE**WG**AI
D1	PQLMV**WG**MM	D3	MQYIR**WG**KI	D5	HELPP**WG**LM
E1	KMSMH**WG**DL	E3	HEFFD**WG**RF	E5	IDEMT**WG**KM
F1	HEAHS**WG**MF	F3	YEPMD**WG**VI	F5	FHKTA**WG**ML
G1	HEFKS**WG**VL	G3	ANYVP**WG**AM	G5	KESMQ**WG**MM
H1	GHDKY**WG**VM	H3	RYAQP**WG**VL	H6	SQAMD**WG**TL
A2	MYQMD**WG**AM	A4	AWVVD**WG**MI	A6	MAEVA**WG**MM
B2	TQMMG**WG**SL	B4	MYTKP**WG**LL	B6	IHEMQ**WG**VL
C2	AETVA**WG**GL	C4	MEMMV**WG**RM	C6	THEVG**WG**NL
D2	VELFP**WG**MF	D4	VXYGH**WG**YQ	D6	HWFYS**WG**RL
E2	EQETQ**WG**KM	E4	QEHMP**WG**KF	E6	YTEMA**WG**GL
F2	PLMTD**WG**MM	F4	WEHMP**WG**MF	F6	MHNVE**WG**GL
G2	REQME**WG**AM	G4	AMTTD**WG**KM	G6	SSTTT**WG**MI
H2	TDQRH**WG**HL	H4	VSKMD**WG**MM	H6	---------

C

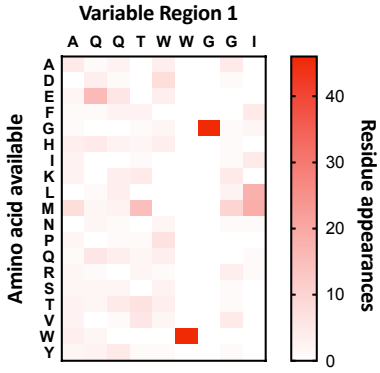

Figure 4.14. Phage ELISA and sequencing results following a second round of biopanning with one day of washing with competition with Affimer 45 wild-type. A. A phage ELISA was conducted as previously described using monoclonal Affimers identified from the second biopanning round using competition with WT Affimer 45 (non-phage). The wild-type Affimer 45 phage (🡻) are included for comparison. B. Clones that demonstrated highest levels of binding were sequenced using an M13R primer. The constant WG residues are highlighted in bold. C. A heat map showing amino acid enrichment at each of the randomised positions with dark red showing high enrichment and white showing no enrichment.

A

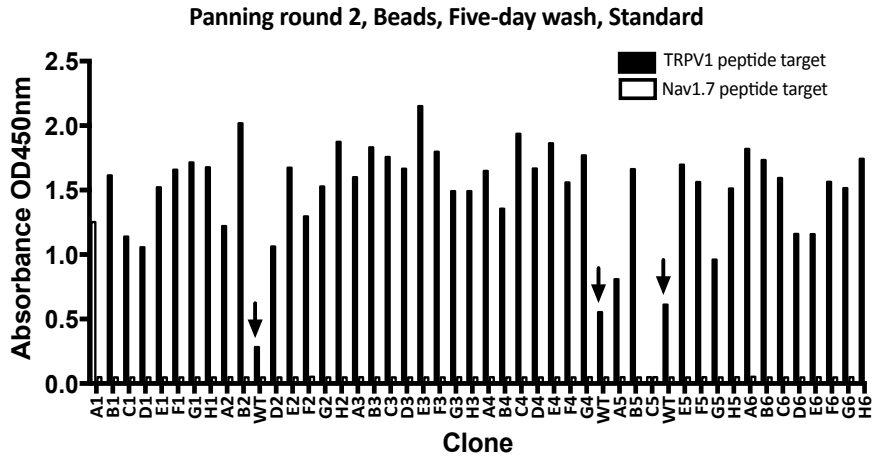

B

Clone	VR1 sequence	Clone	VR1 sequence	Clone	VR1 sequence
A1	LQDTH**WG**KM	A3	VEMVA**WG**ML	A5	MQQQH**WG**VL
B1	SQVQS**WG**QF	B3	SSTTN**WG**LI	B5	MDTMP**WG**MM
C1	TQEMI**WG**RM	C3	AEIRD**WG**RM	C5	---------
D1	YTVMP**WG**AM	D3	MQSME**WG**VL	D5	SQEYG**WG**VL
E1	NQLTQ**WG**KL	E3	AEQMP**WG**VM	E5	KQQMT**WG**AM
F1	LHVTD**WG**LL	F3	PYYTD**WG**MM	F5	TQQTA**WG**MM
G1	HHAVD**WG**LL	G3	HVDVV**WG**RM	G5	QQMTT**WG**VL
H1	QQKMV**WG**MM	H3	TQMMG**WG**SL	H6	EHDVP**WG**LM
A2	MFITQ**WG**RM	A4	ADQRD**WG**KL	A6	TEKMN**WG**DL
B2	HEIMA**WG**KM	B4	HQNFG**WG**KL	B6	SDTME**WG**QL
C2	SEKPT**WG**VL	C4	VYVME**WG**KM	C6	YQEMD**WG**ML
D2	MSETV**WG**VI	D4	RRKMQ**WG**IL	D6	TQHFH**WG**QL
E2	WMTYD**WG**RL	E4	PTLLD**WG**ML	E6	YNEAP**WG**KL
F2	TSYQD**WG**AL	F4	FQFTP**WG**KM	F6	NEFVH**WG**GM
G2	SEMMV**WG**RM	G4	PELMP**WG**VM	G6	HQIFG**WG**RF
H2	SNETS**WG**MM	H4	PERKA**WG**KI	H6	QVEVT**WG**LM

C

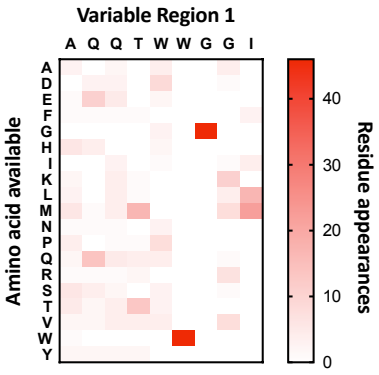

Figure 4.15. Phage ELISA and sequencing results following a <u>second round of biopanning with five days of washing under standard conditions</u>. A. A phage ELISA was conducted as previously described using monoclonal Affimers identified from the second round of biopanning with five days of washing. The wild-type Affimer 45 phage (🡻) is included for comparison. B. Clones that demonstrated highest levels of binding were sequenced using an M13R primer. The constant WG residues are highlighted in bold. C. A heat map showing amino acid enrichment at each of the randomised positions with dark red showing high enrichment and white showing no enrichment.

A

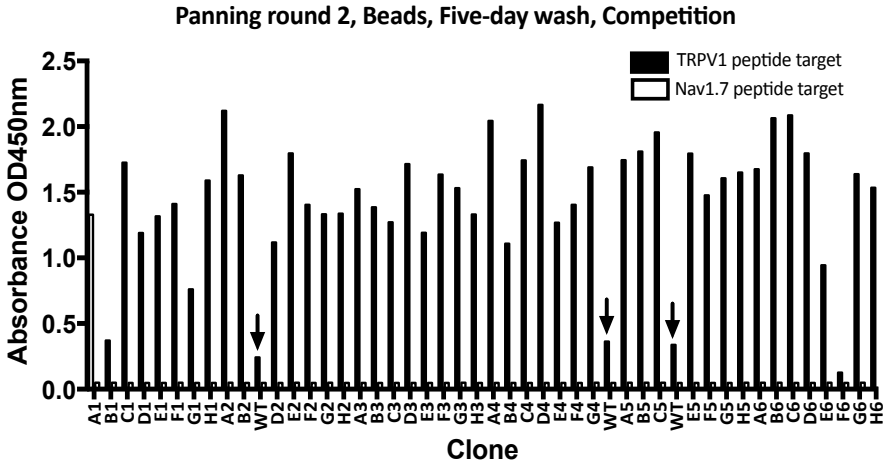

B

Clone	VR1 sequence	Clone	VR1 sequence	Clone	VR1 sequence
A1	MEFQD**WG**VL	A3	MFPVD**WG**ML	A5	QEKRS**WG**ML
B1	LMTTV**WG**MM	B3	ADQLS**WG**KM	B5	SDYVT**WG**RL
C1	MDIVD**WG**KM	C3	PMEMS**WG**VM	C5	HQSMS**WG**RL
D1	MTMQS**WG**MM	D3	EDWTA**WG**KI	D5	YHLTS**WG**AM
E1	WDPKP**WG**ML	E3	IEMAL**WG**MI	E5	AEQMS**WG**TM
F1	NWSKS**WG**RL	F3	PEFVP**WG**VL	F5	PQVTS**WG**IL
G1	KEFFN**WG**VM	G3	KYQTS**WG**AM	G5	YESTA**WG**AI
H1	MNQMS**WG**VM	H3	KHYVD**WG**AM	H5	HEGLH**WG**RF
A2	FEYVK**WG**KM	A4	MEFTS**WG**RM	A6	MQIMK**WG**KM
B2	LWEKE**WG**LL	B4	KELTV**WG**IF	B6	YDLMS**WG**AI
C2	MERTR**WG**KM	C4	WQDLA**WG**KF	C6	KEPTD**WG**MF
D2	AEEVS**WG**TM	D4	IEGTD**WG**KL	D6	HEEQN**WG**RF
E2	LEPTI**WG**KM	E4	---------	E6	HSTMP**WG**KM
F2	TERVT**WG**MI	F4	WRLTE**WG**AI	F6	MVSMQ**WG**KM
G2	QEDTV**WG**RF	G4	REMMP**WG**MM	G6	LHATP**WG**KM
H2	EFVKP**WG**IL	H4	PEHVP**WG**AM	H6	---------

C

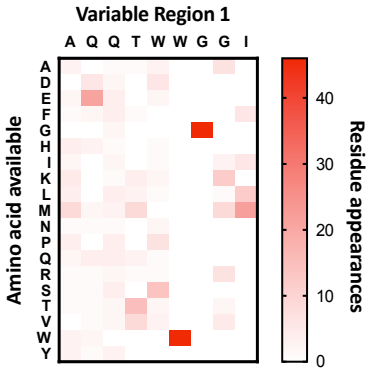

Figure 4.16. Phage ELISA and sequencing results following a second round of biopanning with five days of washing with competition with the Affimer 45 wild-type. A. A phage ELISA was conducted as previously described using monoclonal Affimers identified from the second round of biopanning using competition with WT Affimer 45 (non-phage) and five days of washing. The wild-type Affimer 45 phage (🡻) is included for comparison. B. Clones that demonstrated highest levels of binding were sequenced using an M13R primer. The constant WG residues are highlighted in bold. C. A heat map showing amino acid enrichment at each of the randomised positions with dark red showing high enrichment and white showing no enrichment.

Next, a number of Affimer 45 variants were selected, based on the presence of the above described amino acid enrichments and strength of response when tested by phage ELISA, for sub-cloning and expression independently of the pIII phage coat protein (**Figure 4.17**). These clones were tested for binding against the TRPV1 peptide in ELISA's in which the Affimer 45 variants were incubated against the TRPV1 peptide and a negative control peptide (**Figure 4.18**A). Results demonstrated that all Affimer 45 (WG) variants were able to interact with the TRPV1 peptide with enhanced binding compared to the Affimer 45 WT. Furthermore, none of the Affimers demonstrated non-specific binding to the negative control peptide. Next, Affimer 45(WG) K_d values were established by incubating the TRPV1 peptide with a range of Affimer 45 (WG) variant concentrations (**Figure 4.18**B). Results demonstrated that the majority of Affimer variants were able to bind to the TRPV1 peptide when incubated at lower concentrations than the Affimer 45 WT, with Affimer 45(WG) variants 3 and 9 demonstrating the highest levels of binding. This improvement in binding can be observed from the calculated K_d values (**Table 4.6**), with wild-type Affimer 45 K_d calculated as 257.8 ± 1,174 nM against 40 ng/µL of TRPV1 peptide whilst the highest affinity variants, 3 and 9, having K_d values of 2 ± 0.46 and 6.46 ± 2.23 nM, respectively, calculated.

The proposed structural basis of the improved binding mechanisms of Affimer 45(WG) variants 3 and 9 is hypothesised in **Figure 4.19** .For Affimer 45 (WG) 3, the presence of an aspartate residue at position 72 is likely to enable the formation of a salt bridge with the K12 residue of the peptide (**Figure 4.19**A). Furthermore, the presence of an arginine residue at position 68 is likely to enable an interaction with one of the negatively charged amino acids present at the N-terminus of the peptide (**Figure 4.19**B). The precise bonding between these residues is further highlighted in 2D schematic (**Figure 4.19**C). Affimer 45 (WG) 9 contains a glutamate residue at position 69 that enables the formation of a salt bridge with the lysyl side chain of K12 (**Figure 4.19**D). Again, the presence of a positively charged amino acid at position 68 of Affimer 45 is likely to enable an interaction with a negatively charged residue at the N-terminus of the peptide

(**Figure 4.19**E). Again, these interactions are demonstrated in 2D schematic (**Figure 4.19**F).

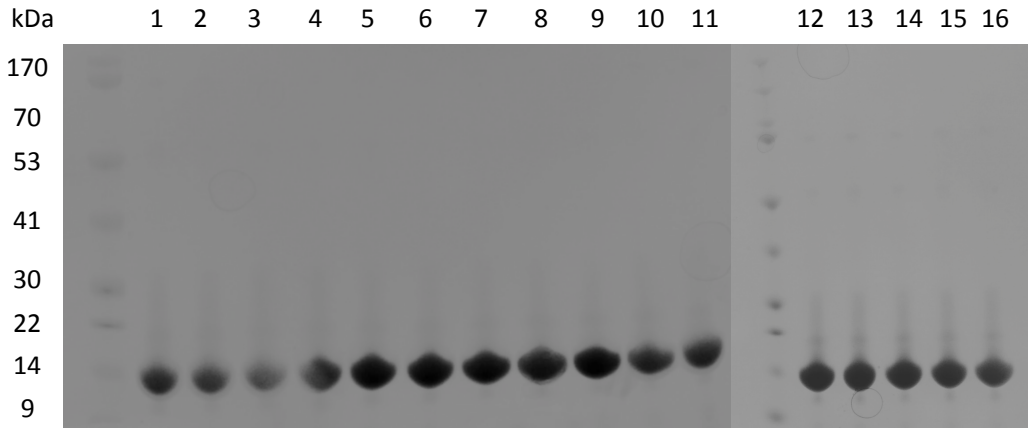

Figure 4.17. Analysis of Affimer 45 (WG) variant proteins by SDS PAGE and Coomassie staining. Following production of Affimer 45 (WG) variants from pET11a in BL21 Star (DE3) cells, concentrations were normalised to 5 mg/mL and then protein analysed by SDS PAGE. Gels were developed with Coomassie stain. Peacock™ Prestained Protein Marker was used.

A

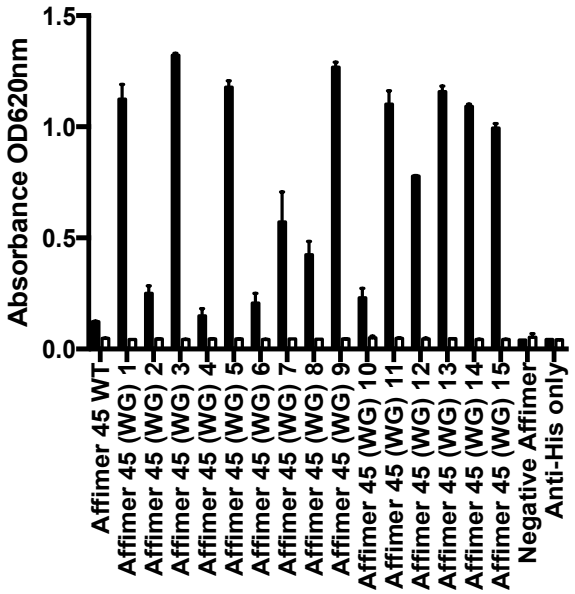
Absorbance OD620nm
1.5
1.0
0.5
0.0
Affimer 45 WT
Affimer 45 (WG) 1
Affimer 45 (WG) 2
Affimer 45 (WG) 3
Affimer 45 (WG) 4
Affimer 45 (WG) 5
Affimer 45 (WG) 6
Affimer 45 (WG) 7
Affimer 45 (WG) 8
Affimer 45 (WG) 9
Affimer 45 (WG) 10
Affimer 45 (WG) 11
Affimer 45 (WG) 12
Affimer 45 (WG) 13
Affimer 45 (WG) 14
Affimer 45 (WG) 15
Negative Affimer
Anti-His only

B

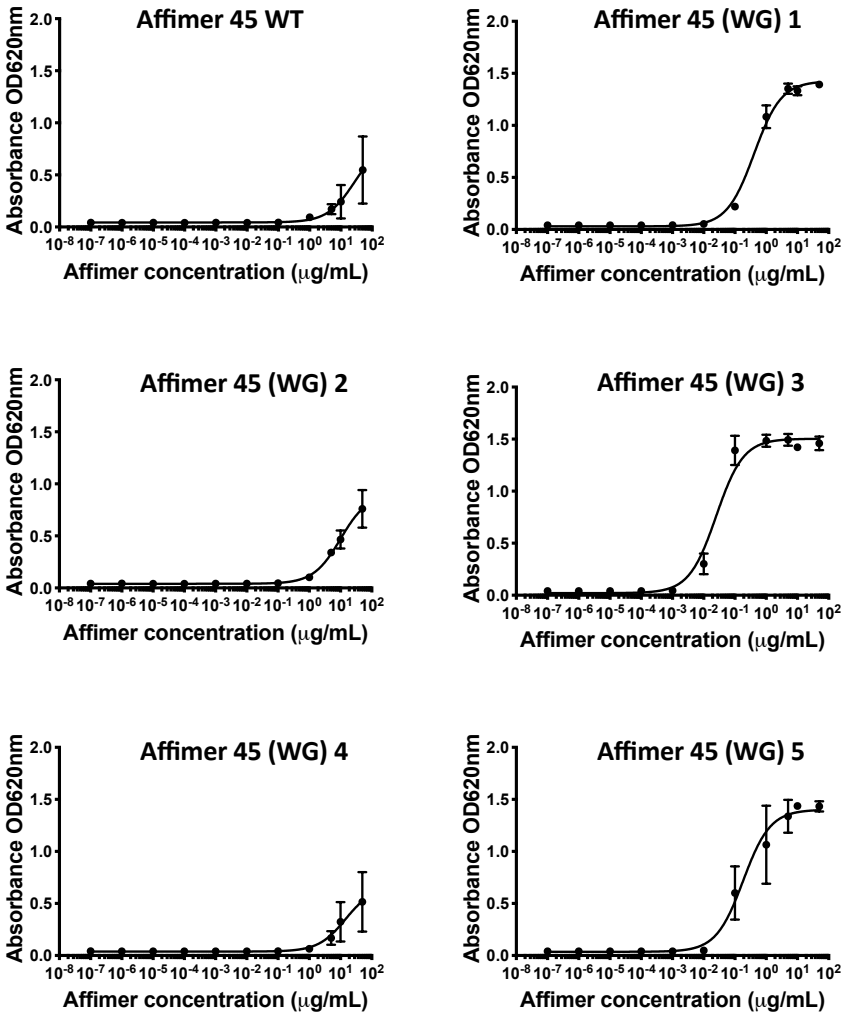
Affimer 45 WT
Affimer 45 (WG) 1
Affimer 45 (WG) 2
Affimer 45 (WG) 3
Affimer 45 (WG) 4
Affimer 45 (WG) 5
Absorbance OD620nm
2.0
1.5
1.0
0.5
0.0
10-8 10-7 10-6 10-5 10-4 10-3 10-2 10-1 100 101 102
Affimer concentration (μg/mL)

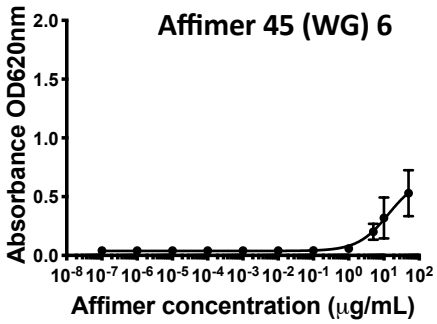
Affimer 45 (WG) 6
Absorbance OD620nm
2.0
1.5
1.0
0.5
0.0
10-8 10-7 10-6 10-5 10-4 10-3 10-2 10-1 100 101 102
Affimer concentration (μg/mL)

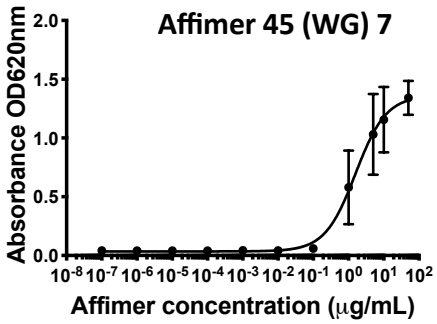
Affimer 45 (WG) 7
Absorbance OD620nm
2.0
1.5
1.0
0.5
0.0
10-8 10-7 10-6 10-5 10-4 10-3 10-2 10-1 100 101 102
Affimer concentration (μg/mL)

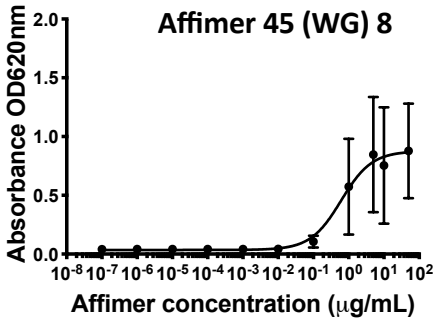
Affimer 45 (WG) 8
Absorbance OD620nm
2.0
1.5
1.0
0.5
0.0
10-8 10-7 10-6 10-5 10-4 10-3 10-2 10-1 100 101 102
Affimer concentration (μg/mL)

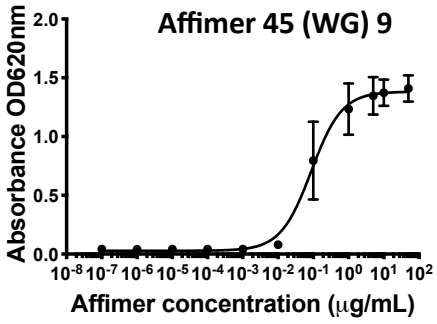
Affimer 45 (WG) 9
Absorbance OD620nm
2.0
1.5
1.0
0.5
0.0
10-8 10-7 10-6 10-5 10-4 10-3 10-2 10-1 100 101 102
Affimer concentration (μg/mL)

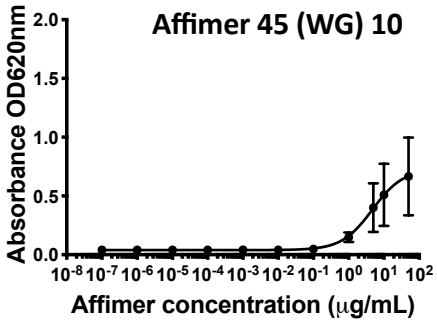
Affimer 45 (WG) 10
Absorbance OD620nm
2.0
1.5
1.0
0.5
0.0
10-8 10-7 10-6 10-5 10-4 10-3 10-2 10-1 100 101 102
Affimer concentration (μg/mL)

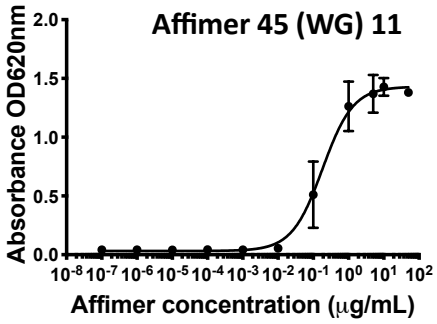
Affimer 45 (WG) 11
Absorbance OD620nm
2.0
1.5
1.0
0.5
0.0
10-8 10-7 10-6 10-5 10-4 10-3 10-2 10-1 100 101 102
Affimer concentration (μg/mL)

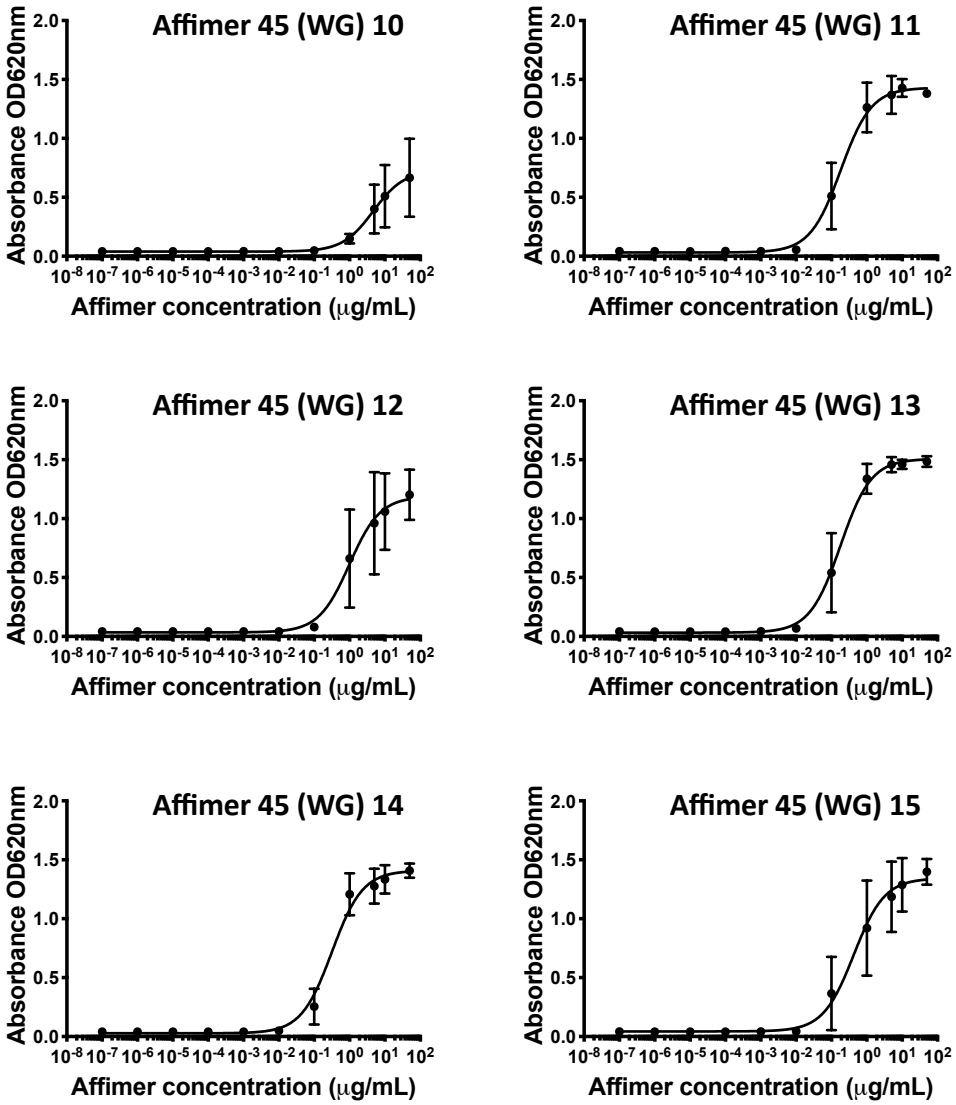

Figure 4.18. Concentration-dependent ELISA's to test for improved binding of Affimer 45 (WG) variants compared to the wild-type Affimer 45. A. Initially, an ELISA was conducted with Affimer 45 (WG) variants being incubated against TRPV1 peptide (*black bars*) and a negative control peptide (*white bars*) (40 ng/mL), at a single concentration of Affimer (10 μg/mL). The Affimer was subsequently detected using an anti-His antibody conjugated to HRP with addition of HRP substrate, TMB, enabling detection at 620 nm. B. Next, concentration-response ELISA's were conducted. Peptide was immobilized as previously and a range of Affimer 45 variant concentrations incubated. Affimers were detected using an anti-His antibody (HRP) following addition of TMB and measurement at 620 nm.

Affimer 45 variant	Variable region one sequence	K_d ± S. E. M against 40 ng/mL peptide (nM)
WT	AQQTWWGGI	257.8 ± 1,174
1	GETTTWGHI	33.53 ± 5.15
2	SDQLSWGIL	759 ± 987
3	RVGTDWGMI	2 ± 0.46
4	HKLMEWGRI	22,216 ± NA
5	RNQQDWGTL	12.61 ± 5.07
6	KESMQWGMM	7,014 ± NA
7	HEIMAWGKM	108 ± 67.61
8	PTLLDWGML	46.15 ± 63.07
9	TEKMNWGDL	6.46 ± 2.23
10	QVEVTWGLM	412.31 ± 790.23
11	FEYVKWGKM	15.07 ± 4.62
12	IEGTDWGKL	64.61 ± 54.76
13	HQSMSWGRL	14.23 ± 3.84
14	YDLMSWGAI	24.38 ± 4.54
15	KEPTDWGMF	25.38 ± 16.15

Table 4.6. K_d values for Affimer 45 (WG) variants when incubated against 40 ng/mL of TRPV1 peptide. All values are displayed as nM however when values could not be calculated, NA is displayed instead.

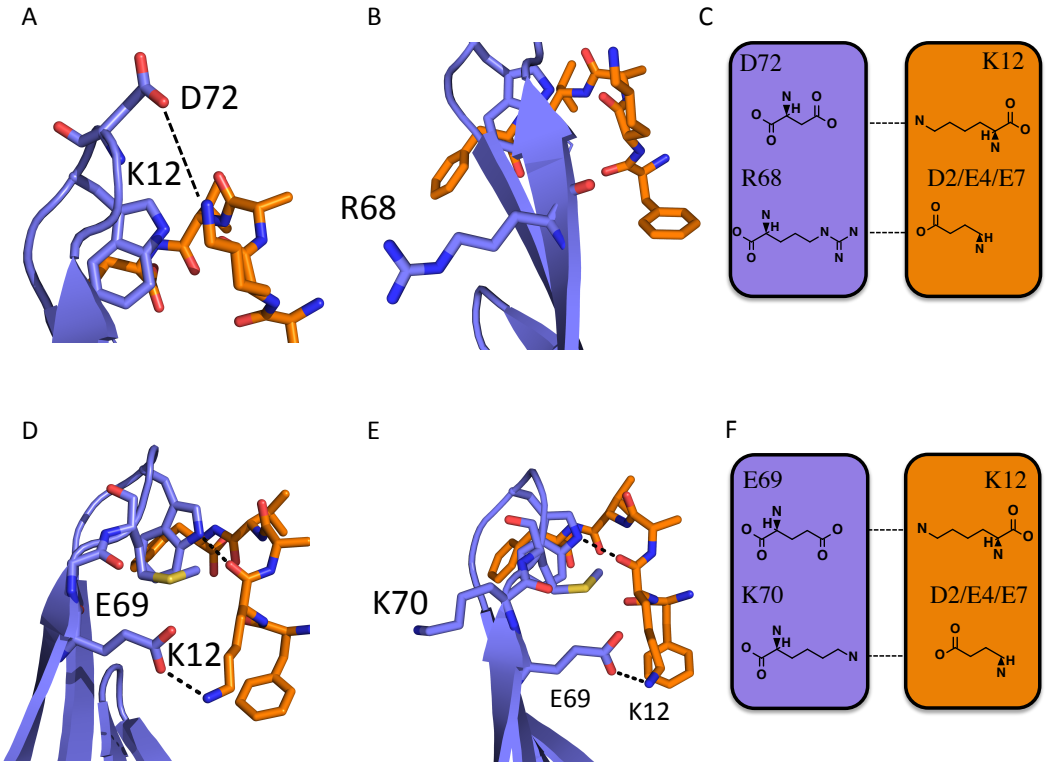

Figure 4.19. Affimer 45 (WG) variants 3 and 9 may demonstrate improved binding to the TRPV1 peptide using enriched negatively and positively charged residues. The structural rationale for the improved binding of the two Affimer 45 (WG) variants with the greatest improvements in binding, Affimers 3 and 9, is presented. Structures were composed using the mutagenesis function on MacPyMol to mutate residues of the wild-type Affimer 45-TRPV1 peptide complex structure solved. Side-chain interactions are shown for Affimer 3 (A and B) with interactions shown in 2D format (C). The side-chain interactions for Affimer 9 are also shown (D and E), again with 2D interactions illustrated (F). Note, interacting residues for R68 and K70 cannot be shown as this region of the peptide target could not be solved during X-ray crystallography.

4.2.4 Identification of Affimer 45 small molecule mimetics

As the structural information provided by the Affimer 45-TRPV1 peptide complex provided improved resolution than TRPV1 structural data currently available (Gao *et al.* 2016), this information was used to screen for small molecules that could mimic the modulatory effects of Affimer 45. To do this, the important amino acids of Affimer 45 involved in peptide binding, as confirmed by site-directed mutagenesis and X-ray crystallography, were used to develop an

Affimer 45 pharmacophore using the shape similarity virtual screening tool, ROCS (OpenEye Scientific). This pharmacophore included the amino acids, Thr71, Trp73 and Ile76 of Affimer 45 VR1 (**Figure 4.20**). The reason these amino acids were selected is a result of their importance demonstrated from site-directed mutagenesis (**Figure 4.3**).

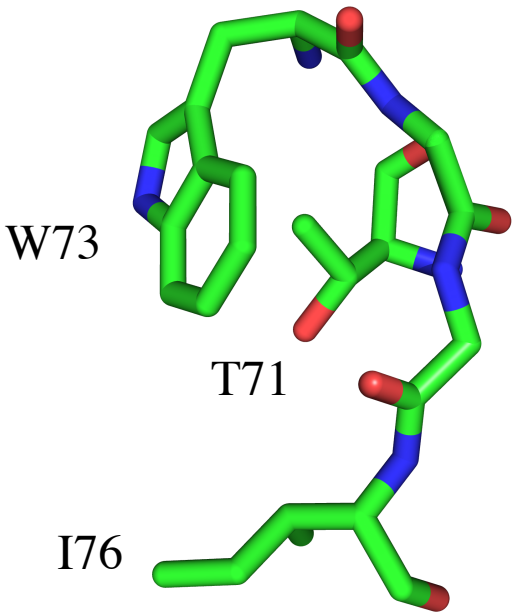

Figure 4.20. Variable region one residues of Affimer 45 essential to the TRPV1 interaction are shown. The Affimer 45 variable region one residues determined as essential to the interaction with the TRPV1 peptide were compiled as a separate molecule using MacPyMol. This molecule was subsequently used to generate a 'pharmacophore' molecule for the identification of small molecule compounds with similar shape. The residues used to develop this pharmacophore were Thr71, Trp73 and Ile76.

The pharmacophore of Affimer 45 was then used to identify compounds of similar shape from a 150,000 compound library established by the Medicinal Chemistry and Chemical Biology department at the University of Leeds, herein referred to as the MCCB library. From this initial screen, 1000 of the most similar compounds were screened against the TRPV1 peptide using PyRx to establish estimated binding affinities. Ideally, the compound library would have been

screened against full-length TRPV1 (Gao *et al.* 2016) however the peptide was selected due to the enhanced resolution obtained in this study. The top scoring 50 compounds were then identified and 47 were tested against TRPV1 using an *in vitro* cell-based assay (**Figure 4.21**). Three of the compounds were unavailable. Results demonstrated that a number of compounds were able to inhibit the response of TRPV1 to capsaicin from which five of the compounds (🡻) were selected for further studies (C36 and C37 were duplicate wells).

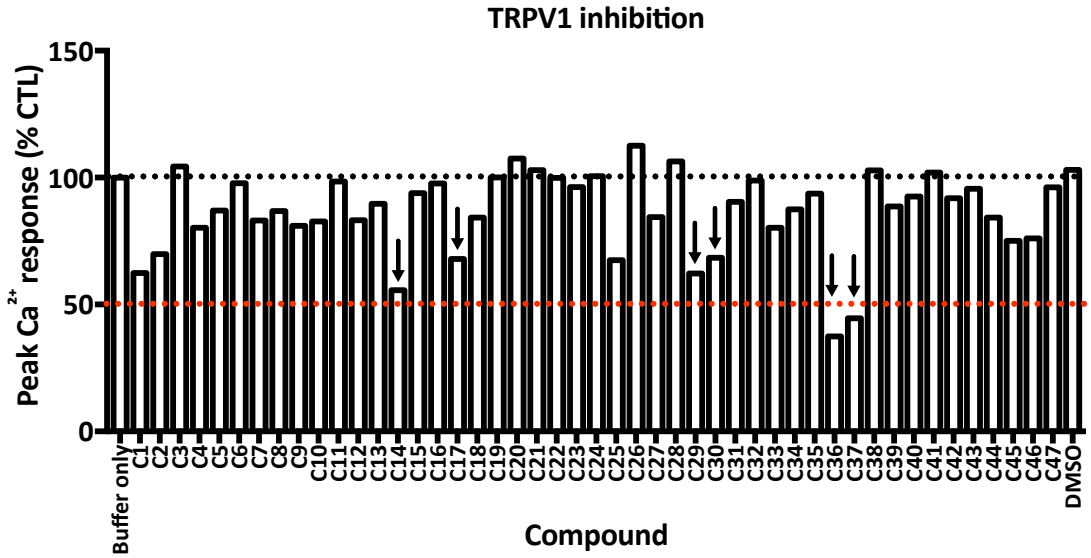

Figure 4.21. *In vitro* cell-based assays to test for TRPV1 inhibition using identified MCCB compounds. Forty-seven of the identified MCCB compounds with similar shape to the Affimer 45 pharmacophore developed were tested for their ability to inhibit TRPV1. TRPV1 expressing cells were plated at 100,000 cells per well in black-walled 96 well plates. Cells were incubated with Fluo-4 AM for one hour and then washed with assay buffer. Cells were incubated with compounds for thirty minutes and then loaded on to a Flexstation III plate reader programmed to add capsaicin after 20 seconds. Capsaicin was added at an EC_{20} concentration (40 nM). Peak responses were measured and calculated as a percentage response to that of a buffer only control, with buffer only control representing 100% response. The black dotted line represents the response observed when buffer only was incubated on cells (denoted 100% response) and the red line represents the 50% of the maximal response.

Next, the five identified compounds (**Figure 4.22**) were advanced in to concentration-response studies with the concentration of compound evoking

50% inhibition of the maximal response established. To do this, each of the compounds was pre-incubated on TRPV1-expressing U-2 OS cells for thirty minutes alongside a DMSO only control, at a range of concentrations. Next, TRPV1 was activated using an EC_{20} concentration of capsaicin (40 nM). Results demonstrated that C14, C17, C29 and C36 were able to inhibit the TRPV1 response in a concentration-dependent manner. Although C14 and C29 only demonstrated a slight response when incubated at higher concentrations (>70μM), C17 and C36 demonstrated 50% inhibition of the maximum capsaicin response when incubated at 54.6 and 68.6 μM respectively (**Figure 4.23**).

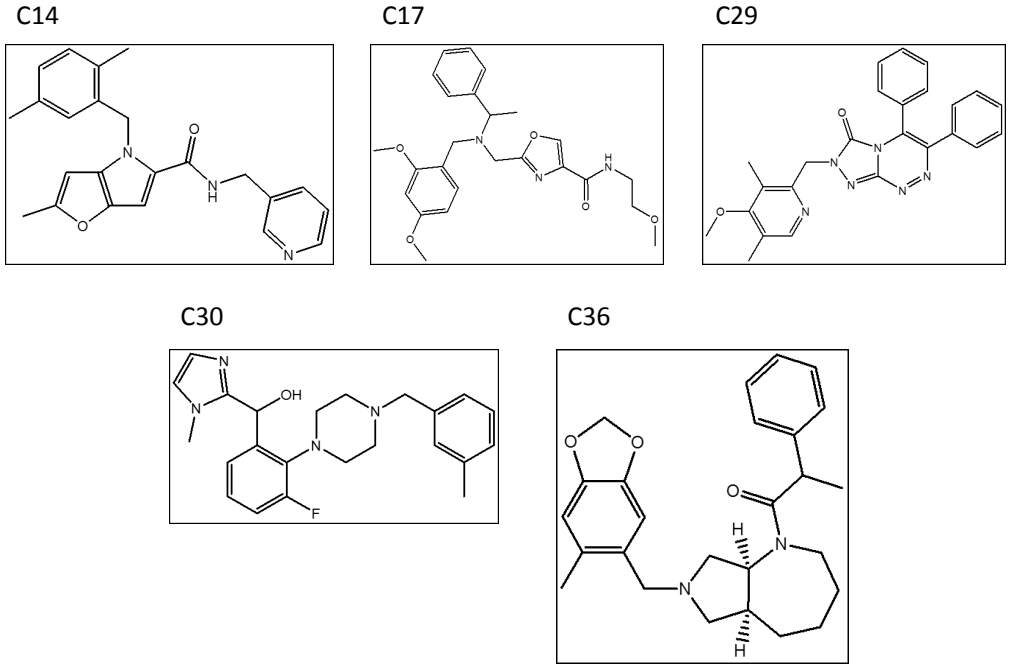

Figure 4.22. Chemical structures of the five MCCB compounds observed to have an inhibitory effect in cell-based studies.

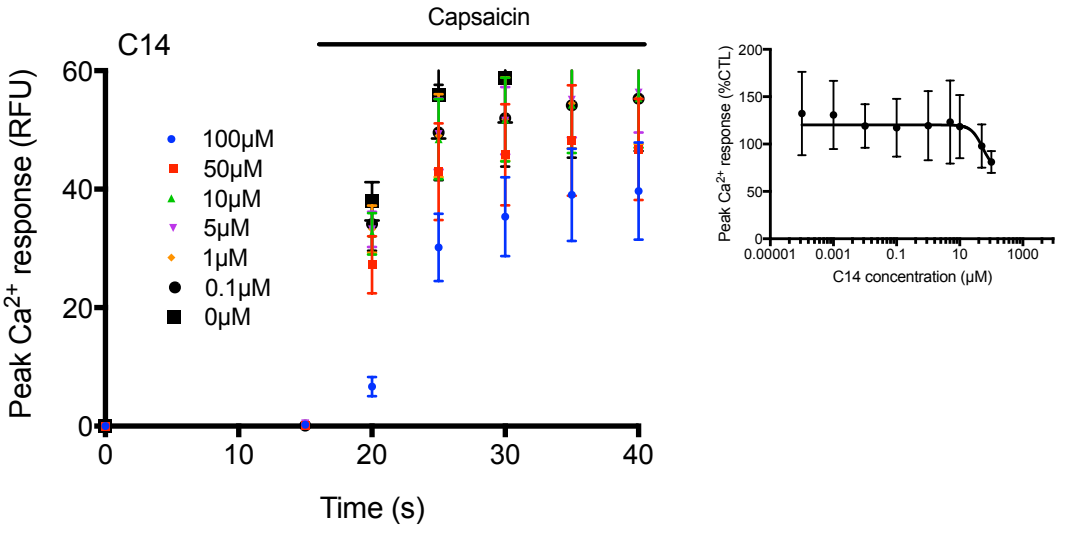
C14
Capsaicin
100μM
50μM
10μM
5μM
1μM
0.1μM
0μM
Peak Ca2+ response (RFU)
Time (s)
Peak Ca2+ response (%CTL)
C14 concentration (μM)

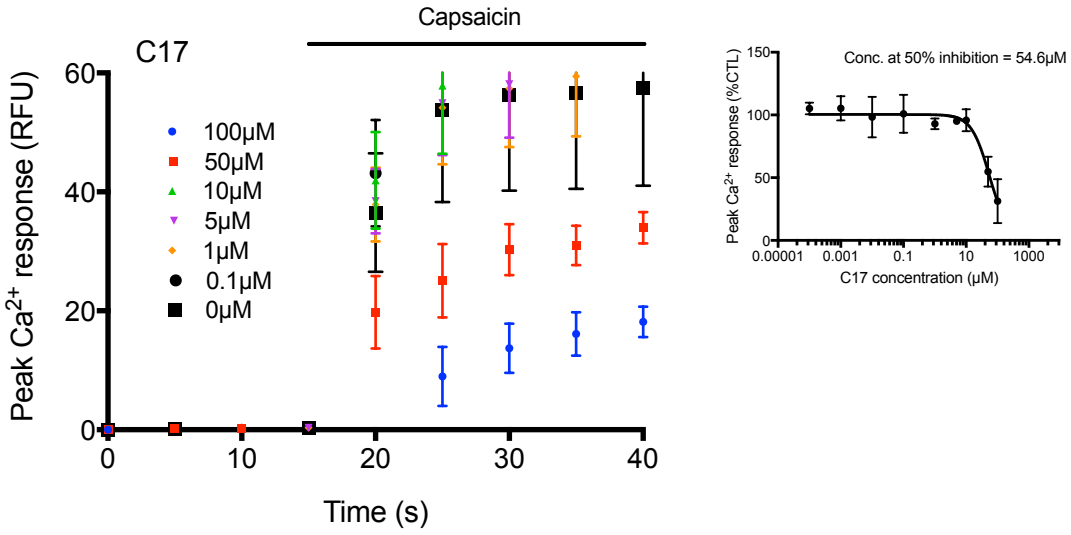
C17
Capsaicin
100μM
50μM
10μM
5μM
1μM
0.1μM
0μM
Peak Ca2+ response (RFU)
Time (s)
Conc. at 50% inhibition = 54.6μM
Peak Ca2+ response (%CTL)
C17 concentration (μM)

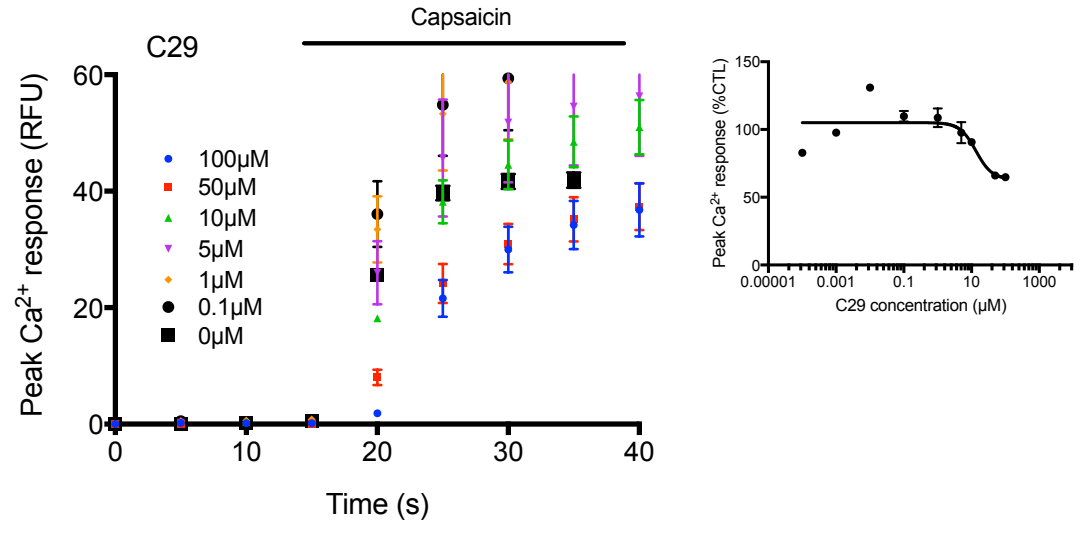
C29
Capsaicin
100μM
50μM
10μM
5μM
1μM
0.1μM
0μM
Peak Ca2+ response (RFU)
Time (s)
Peak Ca2+ response (%CTL)
C29 concentration (μM)

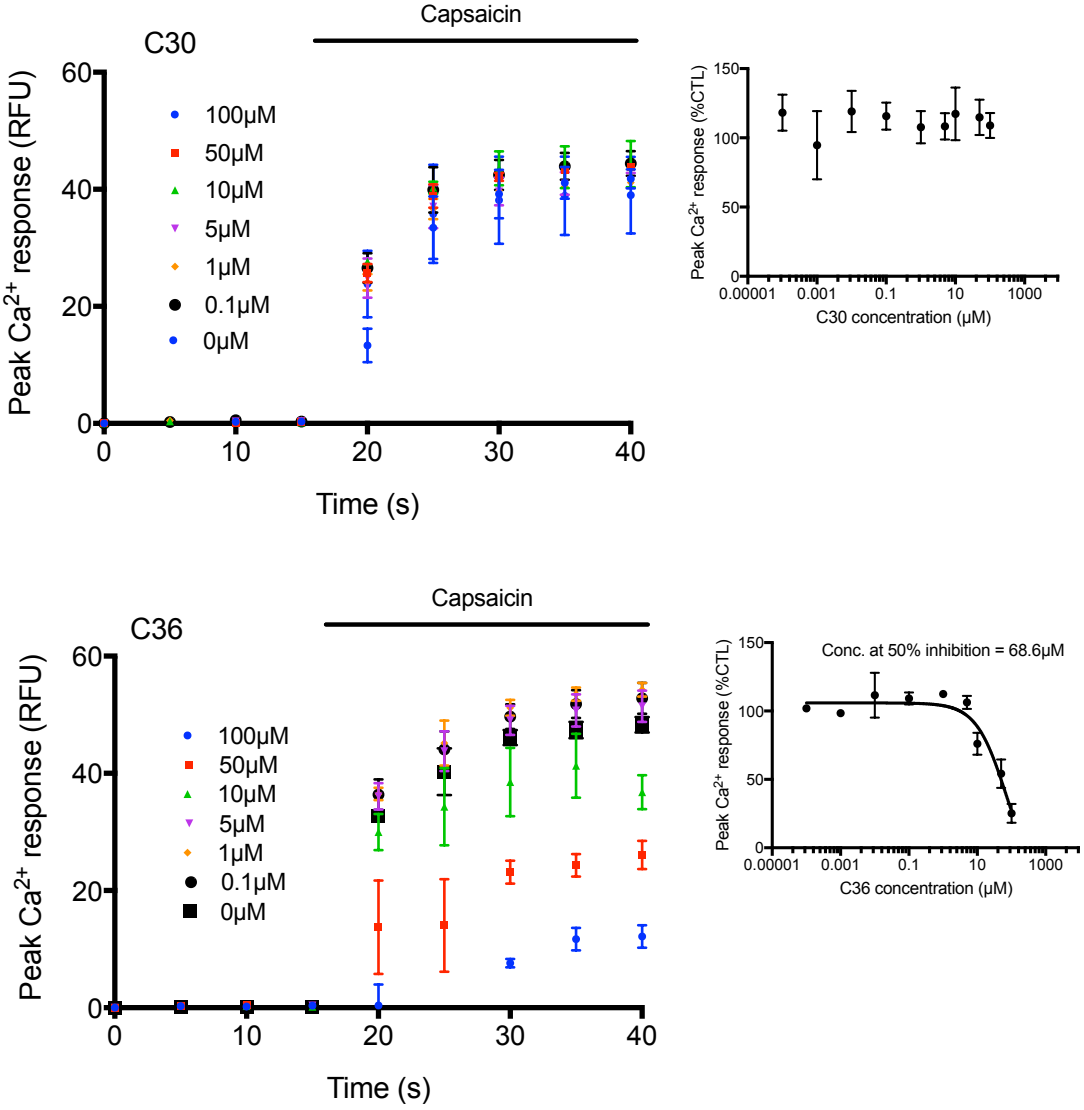
C30
Capsaicin
100μM
50μM
10μM
5μM
1μM
0.1μM
0μM
Peak Ca2+ response (RFU)
Time (s)
Peak Ca2+ response (%CTL)
C30 concentration (μM)
C36
Capsaicin
100μM
50μM
10μM
5μM
1μM
0.1μM
0μM
Peak Ca2+ response (RFU)
Time (s)
Conc. at 50% inhibition = 68.6μM
Peak Ca2+ response (%CTL)
C36 concentration (μM)

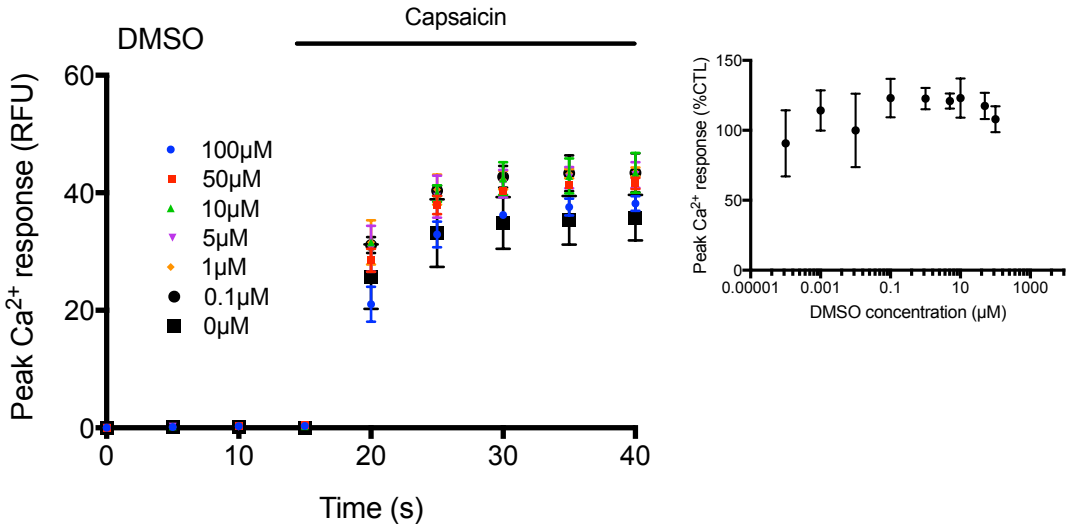

Figure 4.23. Concentration-response studies of the five compounds identified from preliminary TRPV1 inhibition studies. TRPV1 expressing U-2 OS cells were plated at 100,000 cells per well in black-walled 96 well plates. Cells were incubated with Fluo 4-AM for one hour and then washed. Compounds were incubated on TRPV1-expressing cells at a range of concentrations for thirty minutes. Cells were loaded on to a Flexstation III plate reader and TRPV1 was activated by addition of 40 nM capsaicin after 20 sec and response measured for a further 20 sec. Peak response was measured. A concentration-response curve was then produced using GraphPad Prism and concentration of compound eliciting a 50% reduction in maximal response calculated.

4.3 Discussion

The recent structural determination of TRPV1 has provided new insights into its interaction with a variety of ligands at the atomic level (Liao *et al.* 2013, Gao *et al.* 2016). These ligands include both small molecules, such as capsaicin, and peptide toxins, such as DkTx. Despite this, the resolution of these structures is somewhat limited in its use for small molecule drug development. A major reason for this limitation is the resolution of the structures, with the DkTx-bound structure being the highest resolution at 2.9 Å. The structural data is further hindered by the use of C4 symmetry, despite the fact that the DkTx lobes are non-identical. Despite attempts at imposing a more accurate C2 symmetry, data remained insufficient to reveal independent features of the DkTx ICK lobes, features that are likely to be essential for their function (Bae *et al.* 2016). Despite

these limitations, the structure still reveals a number of features, particularly when placed in context with the Affimer 45-TRPV1 peptide structure described in this chapter. The proximity of the W11 and G12 residues of the DkTx ICK1 lobe to the outer pore domain of TRPV1 suggests that the DkTx interaction is similar to the Affimer 45-TRPV1 interaction, due to the proximity of W73 and G74 of Affimer 45 to the same region of TRPV1, alongside the loss of binding by Affimer 45 when these residues are mutated to alanine. Computational studies have also revealed that residues W11, G12, K14 and F27 from ICK1 of DkTx and W53, G54, K56 and F67 of ICK2 of DkTx play an important role in TRPV1 activation. When compared to the structure of the Affimer 45 variable regions, similarities can be observed (**Figure 4.24**).

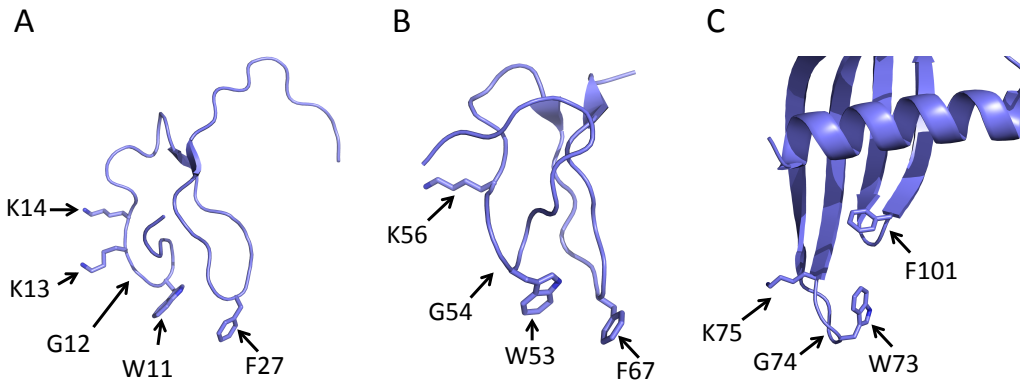

Figure 4.24. Amino acids involved in the TRPV1 interaction are similar between DkTx and Affimer 45. Key amino acids according to computational studies are highlighted for ICK lobes 1 (A) and 2 (B) of DkTx with similarities observed in Affimer 45 variable regions also highlighted (C). Although K75 was not present in the original Affimer 45 identified, this amino acid was enriched during affinity maturation studies.

In this study, the use of directed evolution identified enrichment of various amino acids at positions in the Affimer 45 variable regions. Remarkably, comparison of these amino acids with those found in the DkTx ICK loops provides further similarities, with DkTx containing both the aspartate and lysine residues present at corresponding positions. This observation suggests that the affinity maturation process undertaken in this study has mimicked the natural evolution

process undergone by DkTx over millions of years. Furthermore, the selection of hydrophobic residues surrounded by charged residues is reminiscent of many of the toxins that have evolved to target voltage-gated ion channels through a mixture of channel and lipid bilayer interactions, for example, hanatoxin (Swartz and MacKinnon 1997). Previously, similar methods of affinity maturation have been used to improve the properties of an anti-HER2 DARPin (Zahnd *et al.* 2007). In this study, error-prone PCR was used to mutate nanomolar affinity DARPins in to picomolar affinity binders. Interestingly, the mutations in the improved DARPin differed mainly in its framework residues when compared to its wild-type counterpart, with only two residues different in the variable region residues. This may be useful for future experiments with Affimer 45. Framework residues were identified just outside of the second variable region to be involved in the TRPV1 interaction, however, it is possible that further framework residues are also involved in the interaction, or indeed, could be mutated to take part in the interaction. Alternatively, changes to framework residues could result in subtle changes in conformation that can enable improved binding. Furthermore, increased stringency of the selection procedure could be incorporated to identify Affimer 45 variants with improved binding properties. Improved affinity anti-HER2 DARPins were isolated after 25 days of washing during the selection procedure (Zahnd *et al.* 2007). Directed evolution of Monobodies has also been described. A Monobody targeting the Lyn SH3 domain has undergone directed evolution in which 130-fold enhancements in affinity were reported (Huang *et al.* 2016). In this study, in addition to the incubation of non-biotinylated target protein during the panning procedure to compete away lower affinity Monobody clones, a reduced concentration of biotinylated target protein was also used during the second panning round to enable isolation of only the strongest binding Monobody clones. The study described by Huang et al, 2016, randomised non-crucial amino acids in the binding regions of the isolated Monobody, a similar technique adopted by this study with the anti-TRPV1 Affimer 45. An alternative approach may also be to randomise the crucial amino acids, the rationale behind this approach being that these amino acids are

already known to interact with the target and these contacts may be improved upon.

Whilst biologic-based therapeutics have become firmly established in a clinical setting, the use of biologics as research tools in small molecule drug discovery is still at an early stage. Antibodies and their alternatives have been used to assist the crystallisation of a large repertoire of target proteins, however, their structural interactions have yet to be exploited to identify small molecule compounds that can evoke similar functional effects (Griffin and Lawson 2011). The compounds identified in this study, unlike Affimer 45, resulted in inhibition of TRPV1 rather than potentiation. One explanation for this could be that the small molecules identified contain other points of contact with TRPV1 resulting in a different functional effect. Indeed, studies have previously demonstrated the ability of a single amino acid mutation to convert inhibitory peptides into activators (Brouwer *et al.* 2017). This has also been observed for the platelet-derived growth factor β receptor (PDGFβR) in which the activatory pTM36-4 protein is converted to an inhibitor following substitution of threonine 21 to an asparagine residue. These studies demonstrate the ability to alter activity of protein modulators by small changes in their interactions. An alternative explanation may be that both of the Affimer variable regions are important for potentiation. Despite these hypotheses, further studies are required to determine the binding of the identified small molecules with TRPV1.

Chapter 5

Development of a cell-based phage display protocol for screening membrane proteins

5 Development of a cell-based phage display protocol for screening membrane proteins

5.1 Introduction

Methods for biopanning phage display libraries against soluble, purified protein are well established, however, identifying reagents by phage display is highly dependent on the quality of target, as correct folding and processing of the protein is essential. This can be difficult to achieve for membrane proteins due to the presence of hydrophobic transmembrane domains (Lin and Guidotti 2009). A solution to this problem is screening libraries using whole cells as the target source, thereby maintaining target conformation (Eisenhardt *et al.* 2007, Jones *et al.* 2016). Cell-based biopanning however has many difficulties. For example, the high level of non-relevant proteins at the membrane and propensity for phage coat proteins to interact non-specifically makes the recovery of target specific reagents challenging (Jones *et al.* 2016). Additionally, the low abundance of target protein in comparison to background proteins complicates the biopanning process as large cell populations and increased biopanning rounds can be required for the enrichment of phage towards the protein of interest (Wang *et al.* 2016). Although approaches such as microfluidics has reduced the cell numbers required, this technique provides fresh problems such as optimisation of cell culture within a microfluidic system (Wang *et al.* 2011).

The work described in this chapter focuses on the optimisation of biopanning the Affimer phage library against targets expressed on the extracellular surface of mammalian cells.

5.2 Results

5.2.1 Expression of membrane-bound Herpes Simplex Virus 1 (HSV1) glycoprotein D (gD) target.

The success of previous screens against the recombinant gD protein of HSV1 alongside the ability to express HSV1 gD at the cell surface of mammalian cells prompted its use for the initial optimisation of the cell-based phage display protocol. HSV1 gD cDNA was co-transfected, alongside eGFP-encoding cDNA, into cell lines (HEK293 and CHO) to be used for cell-based phage display. Forty-

eight hours after transfection, GFP levels were assessed by fluorescent microscopy. Approximately 50% of cells were transfected and despite optimisation, levels could not be increased, therefore cell-based biopanning was conducted.

5.2.2 Cell-based biopanning against HSV1 gD.

Previously, a screen had been conducted against soluble HSV1 gD using the Affimer library with a number of specific binders isolated. The success of this screen alongside the availability of a mammalian expression vector encoding the expression of HSV1 gD at the extracellular surface, provided an ideal platform to develop a cell-based biopanning protocol. Furthermore, as HSV1 gD is not normally expressed by mammalian cells, the ability to remove Affimers that bind to other target proteins at the cell surface was possible.

Initially, a HEK293 cell line not expressing HSV1 gD was incubated for one hour with an Affimer phage library that had been enriched against soluble HSV1 gD protein for three rounds of biopanning. The unbound phage were subsequently incubated on a HEK293 cell line expressing HSV1 gD. After one hour of incubation, cells were washed with assay buffer and bound phage eluted using a mixture of low and high pH buffers, infected into *E. coli* ER2738 cells and plated on to LB agar supplemented with carbenicillin. The same procedure was also conducted for a parental HEK293 cell line not expressing HSV1 gD. A substantial increase in Affimer recovery was observed from HSV1 gD-expressing cells in comparison to the non-expressing cell line, suggesting the ability of Affimer reagents to detect membrane-bound HSV1 gD, a conclusion further validated by cell-based phage ELISA (**Figure 5.1**). This provided promise that cells could be used to display proteins for screening by phage display.

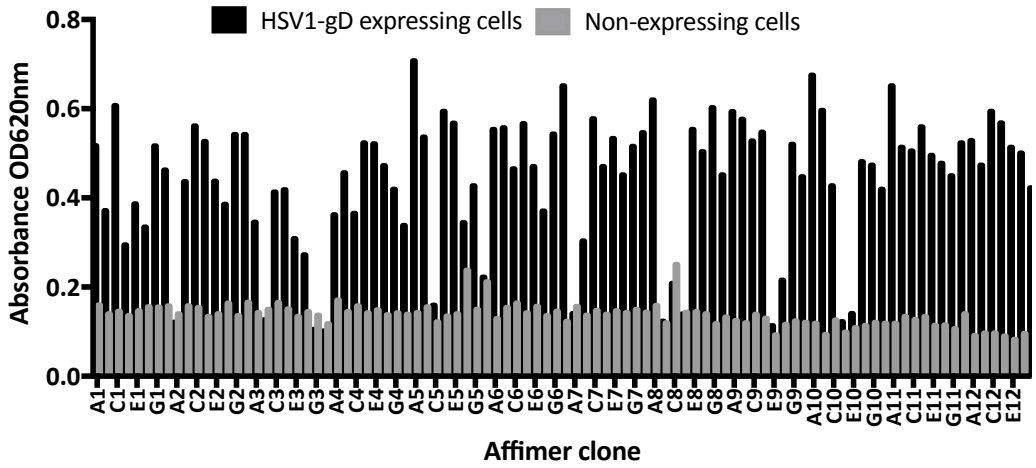

Figure 5.1. Phage ELISA showing binding of Affimer phage to HSV1 gD-expressing cells following isolation against recombinant protein. Affimer phage isolated from phage display against recombinant HSV1 gD protein were screened by phage ELISA against HSV1 gD-expressing cells (black) and non-expressing parental cells (grey). Cells expressing HSV1 gD were plated in to 32 wells of a 96 well plate. In addition, non-expressing parental cells were plated in to another 32 wells of a 96 well plate. Approximately 100,000 cells per well were plated and grown overnight until a confluence of 100% was reached. Cells were then fixed with 4% PFA and blocked with 2x Casein blocking buffer. Affimer phage were incubated on cells for one hour and then unbound phage washed away. Bound phage were detected with an anti-Fd antibody conjugated to HRP using TMB substrate and measurement at 620 nm.

Following the success of the cell-based biopanning approach using a library of Affimers enriched against soluble protein, the approach was further optimised for use with a naïve Affimer library. This optimisation made use of a solution-based panning strategy, identical in nature to that of the screen conducted with our enriched library, with the addition of two negative selection stages against non-expressing cell lines (**Figure 5.2**). Furthermore, each biopanning round made use of alternating cell lines (HEK293 and CHO), a step used to provide alternative 'background' proteins for a more stringent panning procedure. In addition to using a naïve Affimer library, libraries that had been enriched against recombinant HSV1 gD for either one, two or three biopanning rounds were also introduced at various stages of the naïve screen as a positive control. For example, the 'Enriched P1' library had undergone one biopanning round against

soluble HSV1 gD, 'Enriched P2' library had undergone two biopanning rounds against soluble HSV1 gD, and so on. Furthermore, the final biopanning round, round seven, was conducted under two conditions, with both cells in suspension (T25) and adherent cells (6WP), panned against.

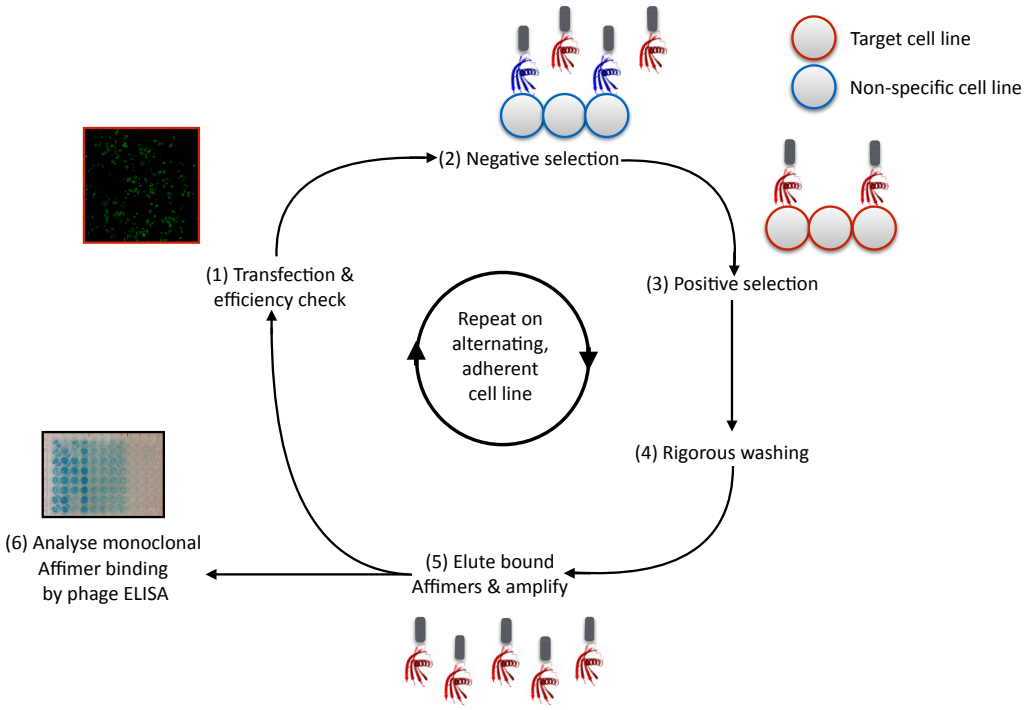

Figure 5.2. Methodology used for the biopanning of membrane-based targets using the Affimer phage display library. (1) The target gene was transfected in to the cell line with a GFP-expressing vector to ensure successful transfection of cells. (2) The Affimer phage display library was incubated on a parental cell line not expressing the target protein to remove any Affimer phage binding to non-target proteins from the positive selection procedure. (3) The Affimer phage not bound to the parental cell line were then incubated on the target-expressing cell line. (4) A stringent washing step was conducted with PBS buffer to remove any unbound Affimer phage still remaining in the selection process. (5) Affimer phage bound to target protein were eluted from the cells with a mixture of low and high pH buffers and then grown in *E. coli* for progression in to a subsequent round of biopanning, on an alternate cell line. (6) After biopanning has resulted in enrichment of Affimer phage against cells expressing the target protein (compared to the non-expressing cells), monoclonal Affimers are tested for binding to the target-expressing cells by cell-based phage ELISA.

After seven biopanning rounds, a significant increase in Affimer clones binding to HSV1-gD expressing cells compared to a non-expressing cell line was observed, suggesting enrichment of HSV1 gD-binding Affimers (**Table 5.1**). In the seventh round of biopanning, selection against adherent cells enabled improved stringency of washing by removing centrifugation steps to recover cells. The introduction of this adherent cell biopanning round enabled a larger difference in recovery of phage from the HSV1 gD-expressing cell line compared to the non-expressing cell line. Furthermore, use of the Affimer libraries that had been selected against soluble HSV1 gD protein enabled the enrichment of phage against HSV1-gD expressing cells in fewer rounds. The number of rounds required was dependent on the number of rounds of biopanning conducted against soluble protein (**Table 5.1**), for example, one round of panning against soluble protein enabled enrichment against cell-based target after two rounds whilst three rounds of panning against soluble protein enabled enrichment against cell-based target in a single round.

To confirm binding by monoclonal Affimers, ninety-six clones that had been isolated after seven panning rounds were tested for binding by cell-based phage-ELISA. A high number of clones able to bind specifically to a HSV1 gD-expressing cell line were observed (**Figure 5.3**).

Round 1	**Naïve**					
Positive	15,500					
Negative	4,800					
Round 2	**Naive**	**Enriched (P1)**				
Positive	10,200	4,100				
Negative	4,100	6,400				
Round 3	**Naive**	**Enriched (P1)**	**Enriched (P2)**			
Positive	412	1,060	776			
Negative	484	1,040	820			
Round 4	**Naive**	**Enriched (P1)**	**Enriched (P2)**	**Enriched (P3)**		
Positive	26	17	42	156		
Negative	29	2	0	0		
Round 5	**Naive**	**Enriched (P1)**	**Enriched (P2)**	**Enriched (P3)**	**Enriched (P4)**	
Positive	325	64	152	357	36,700	
Negative	90	5	15	3	0	
Round 6	**Naive**	**Enriched (P1)**	**Enriched (P2)**	**Enriched (P3)**	**Enriched (P4)**	**Enriched (P5)**
Positive	18,000	320,000	100,000	32,000	36,000	400,000
Negative	3,000	3,400	2,100	200	0	1,800
Round 7	**Naïve 6WP**	**Naïve T25**				
Positive	200,000	300,000				
Negative	6,400	60,600				

Table 5.1. Colony counts to enable comparison of phage recovery using either a naïve library or libraries with various levels of enrichment against soluble protein. Naïve libraries used for selection had undergone no biopanning rounds against soluble protein. Enriched (P1) had been enriched against soluble protein for one panning round, enriched (P2) had been enriched against soluble protein for two rounds and so on.

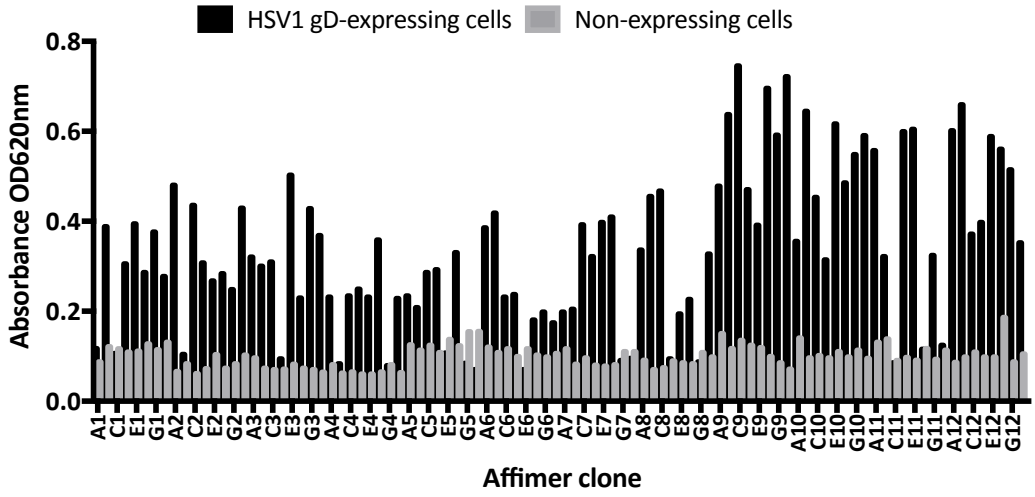

Figure 5.3. Phage ELISA showing binding of Affimer phage to HSV1 gD expressing cells following isolation after seven rounds of biopanning against cells. Affimer phage isolated from biopanning round seven against HSV1 gD expressing cells were screened by phage ELISA against HSV1 gD-expressing cells (black) and non-expressing parental cells (grey). Cells expressing HSV1 gD were plated in to 32 wells of a 96 well plate. In addition, non-expressing parental cells were plated in to another 32 wells of a 96 well plate. Approximately 100,000 cells per well were plated and grown overnight until a confluence of 100% was reached. Cells were then fixed with 4% PFA and blocked with 2x Casein blocking buffer. Affimer phage were incubated on cells for one hour and then unbound phage washed away. Binding of the phage was detected with an anti-Fd antibody conjugated to HRP using TMB substrate and measurement at 620 nm.

Despite being able to identify Affimers against HSV1 gD using the seven-round biopanning protocol, the observation made in the seventh panning round, that adherent cells enabled improvement in enrichment, was used to try and reduce the time and reagents, for example cell numbers, required for biopanning. As a result, a new protocol was devised in which a solution step was used in the first panning round for increased target number and to enrich phage followed by two rounds of biopanning on alternating, adherent cell lines, with ten washing steps each to reduce background binding. This reformatted biopanning protocol enabled the identification of HSV1-gD specific Affimer reagents within three panning rounds (**Figure 5.4**), with verification of HSV1 gD-specific binding validated by cell-based phage ELISA (**Figure 5.5**). However, phage ELISA results

from this shorter screening strategy were not as consistent as results obtained from the previous strategy and therefore it is likely that although binders can be identified in a shorter time-frame, the increased biopanning rounds used previously is likely to enable better removal of 'poorer' binders.

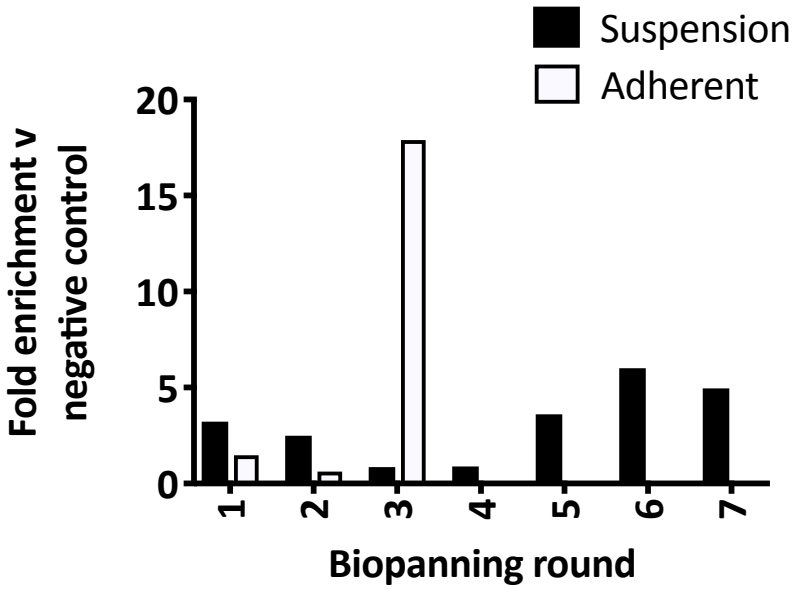

Figure 5.4. Comparison of enrichment of bound Affimer phage when screened against cells in suspension or when adherent. Affimer phage were screened against cells expressing HSV1 gD when in suspension and when adherent. Briefly, cells were plated in to two T75 flasks and when at a confluence of approximately 60% were transfected with DNA encoding HSV1 gD protein. Forty eight hours after transfections cells were panned against. For one set of cells, phage (in assay buffer) were added directly to the T75 flask (adherent) whilst for the other set of cells, trypsinisation took place and cells were resuspended in assay buffer (in solution). Phage were then added. Adherent cells were washed six times with assay buffer to remove unbound phage and bound phage were then eluted using low and high pH methods. The same washing and elution procedure was followed for cells in solution however cell recovery between washes was required by centrifugation. The recovery of Affimer phage from both HSV1 gD expressing and parental cells from each biopanning round was then measured and fold enrichment calculated.

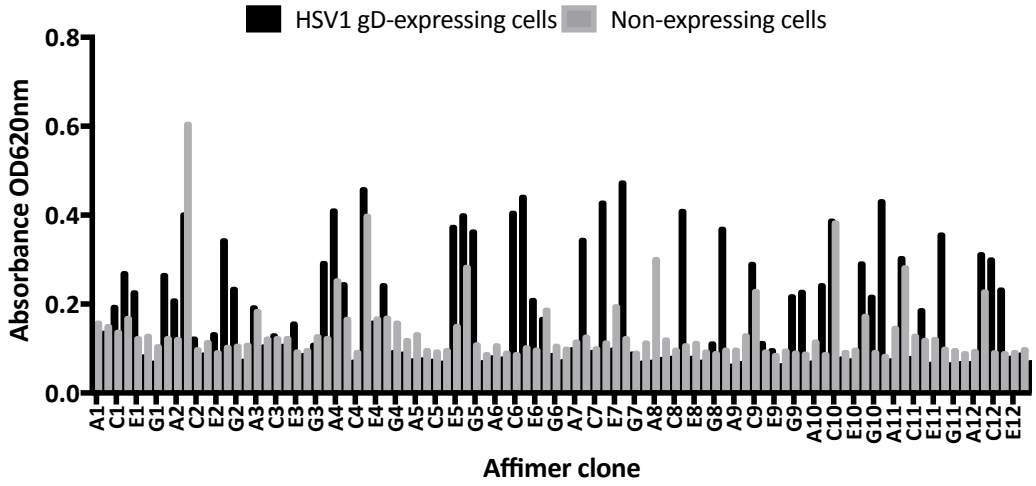

Figure 5.5. Phage ELISA showing binding of Affimers to HSV1 gD-expressing cells following isolation after three rounds of biopanning. Affimer phage isolated after three biopanning rounds against HSV1 gD protein expressed at the cell surface were screened by phage ELISA against HSV1 gD-expressing cells (black) and non-expressing parental cells (grey). Cells expressing HSV1 gD were plated in to 32 wells of a 96 well plate. In addition, non-expressing parental cells were plated in to another 32 wells of a 96 well plate. Approximately 100,000 cells per well were plated and grown overnight until a confluence of 100% was reached. Cells were then fixed with 4% PFA and blocked with 2x Casein blocking buffer. Affimer phage were incubated on cells for one hour and then unbound phage washed away. Binding of the phage was detected with an anti-Fd antibody conjugated to HRP using TMB substrate and measurement at 620 nm.

All clones that demonstrated specific binding to the HSV1-gD expressing cells were sequenced from the seven and three-round approaches however only a single clone was identified from each of the biopanning protocols. Furthermore, only two clones were identified from the initial screen that panned using phage enriched against soluble protein. Despite this, the variable regions demonstrated large similarities (**Table 5.2**). Both clones shared a 'Q--PPW' motif in variable region one and a 'S-LHSL' motif in variable region two. Furthermore, slight similarities could be detected between clones recovered from the naïve screen and the screen conducted with phage already enriched against soluble protein. For example, a 'SL' motif was shared between the Affimers recovered from the naïve screen and Affimer$_{HSV1\text{-}gD\text{-}Enrich1}$ and a 'QR' motif between Affimer$_{HSV1\text{-}gD\text{-}Naive3}$ and Affimer$_{HSV1\text{-}gD\text{-}Enrich1}$.

Af-HSV1 gD	**Variable region 1**	**Variable region 2**
Affimer$_{HSV1\text{-}gD\text{-}Enrich1}$	KEAVSLFPM	DQREYNIEW
Affimer$_{HSV1\text{-}gD\text{-}Enrich2}$	AIQPWIIME	HYPGLVYIQ
Affimer$_{HSV1\text{-}gD\text{-}Naïve7}$	T**Q**DK**PPW**EH	**S**F**LHSL**VQR
Affimer$_{HSV1\text{-}gD\text{-}Naïve3}$	H**Q**RA**PPW**HA	**S**P**LHSL**LDL

Table 5.2. Affimer variable regions for HSV1 gD-binding Affimers from both enriched and naïve libraries. Similarities between naïve Affimer variable regions are highlighted in bold whilst similarities between enriched and naïve clones are underlined.

5.2.3 Further characterisation of HSV1 gD Affimer clones.

To validate that the Affimer clones were able to bind HSV1-gD-expressing cell lines independently of the pIII-phage coat protein all identified Affimers were sub-cloned in to pET11a and produced fused to a His tag as previously described. Produced Affimers were analysed by SDS PAGE and Coomassie staining (**Figure 5.6**). Next concentrations were measured by Nanodrop spectrophotometry and normalised to 10μM (**Table 5.3**).

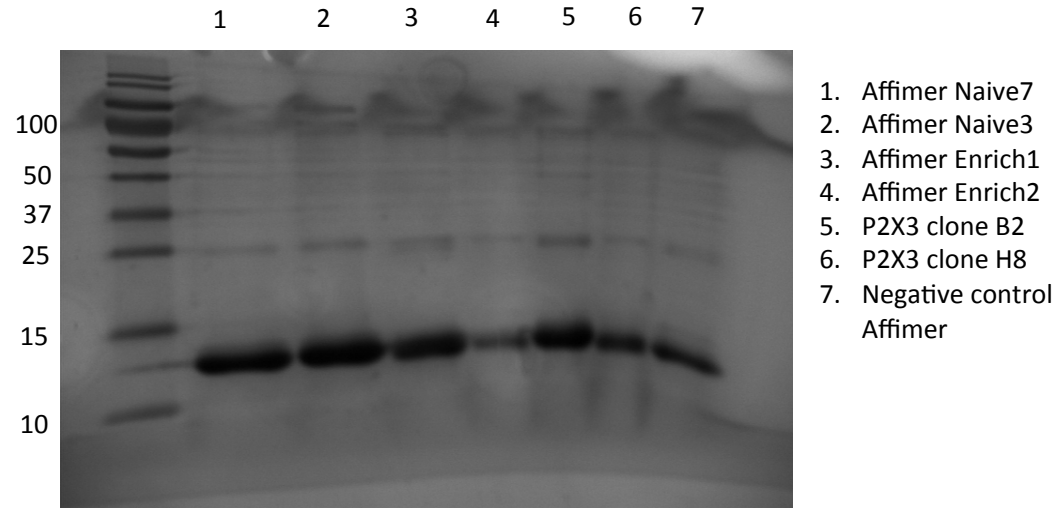

Figure 5.6. Analysis of anti-HSV1 gD Affimers and anti-P2X3 Affimers by SDS PAGE and Coomassie staining. Affimers that were identified against HSV1 gD protein by cell-based phage display were produced as previously described. Furthermore, Affimers identified against P2X3 protein, to be described later in this chapter, were also produced. All purified proteins were analysed by SDS PAGE gel and Coomassie staining.

Affimer	**A280**	**Abs 0.1% (= 1 g/L)**	**Concentration (mg/mL)**	**Concentration (µM)**	**Volume for 10 µM in 1 mL (µL)**
Naive7	3.389	1.233	2.749	211	47
Naive3	4.267	1.247	3.422	263	38
Enrich1	3.982	1.347	2.956	227	44
Enrich2	1.890	1.476	1.280	98	102
P2X3 clone B2	3.672	1.249	2.940	226	44
P2X3 clone H8	2.213	1.897	1.167	90	111

Negative control Affimer	2.445	1.645	1.486	114	88

Table 5.3. HSV1 gD Affimer concentration measurements by Nanodrop spectrophotometry and normalisation to 10 µM for use in binding assays. Absorption coefficients were calculated using the Expasy Protein Parameters online tool.

Next, ELISA confirmed target-specific binding to a HSV1 gD-expressing cell line (**Figure 5.7**A). Additionally, to control for transfection artefacts, a P2X transfected cell line was tested with only background levels of binding observed (**Figure 5.7**B).

To further probe this interaction, the Affimer showing greatest binding by protein ELISA, Affimer$_{HSV1\text{-}gD\text{-}Naive3}$, was confirmed to bind selectively to a HSV1 gD-expressing cell line by affinity fluorescence (**Figure 5.7**C).

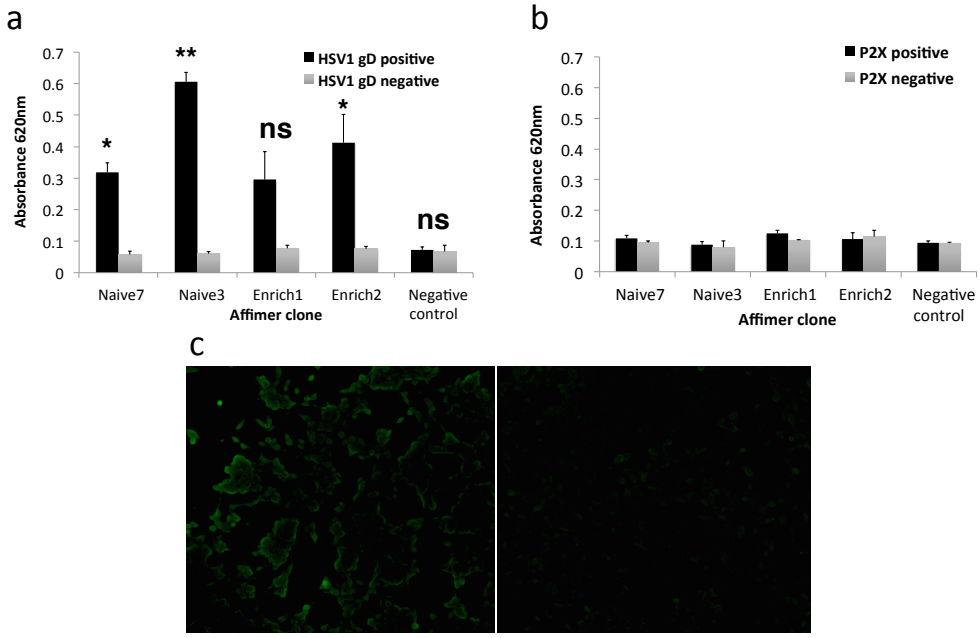

Figure 5.7. Validation of HSV1 gD-specific Affimer binding to their target by ELISA and ICC. Anti-HSV1 gD monoclonal Affimers from both naïve and enriched libraries were tested for binding to CHO cells expressing HSV1 gD at the membrane. A. CHO cells expressing HSV1 gD were plated at 100,000 cells per well to 96 well plates and incubated for 24 hours. Once confluence had reached 100%, cells were fixed with 4% PFA. Affimers were incubated on fixed cells at a concentration of 1 µM for one hour. Affimer was detected by incubation with anti-His conjugated to HRP and addition of TMB. Measurement was conducted at 620 nm. Affimer incubation was also conducted

on a non-expressing, parental cell line. B. Cells expressing a negative control P2X ion channel were plated at 100,000 cells per well in a 96 well plate. Cells were prepared in the same way as HSV1 gD expressing cells. Affimers were then incubated on cells for one hour and detected using an anti-His antibody conjugated with HRP and addition of TMB. C. HSV1 gD expressing cells (*left*) and non-expressing cells (*right*) were plated on to coverslips and grown to approximately 80% confluence and fixed with 4% PFA. The Affimer that demonstrated the greatest OD at 620 nm during ELISA, 'Enrich2', was incubated on cells for one hour and then unbound Affimer washed away. Anti-His (Rabbit) antibody was incubated on cells for one hour and excess washed away. Anti-Rabbit-488 antibody was incubated on cells for one hour and excess washed away. Coverslips were mounted on to glass slides using ProLong Antifade mounting solution and imaged using an EVOS FL cell imaging system (Thermo Scientific). *Error bars show S.E.M. values*. *N = 3, Naive7 t-test p-value = 0.02, Naive3 t-test p-value = 0.0027, Enrich1 t-test p-value = 0.14, Enrich2 t-test p-value = 0.06.*

5.2.4 Using the optimised cell-based phage display protocol to screen ion channel targets.

The cell-based phage display protocol optimised against HSV1 gD was used to screen against an ion channel implicated in chronic pain, P2X3.

Following three rounds of biopanning, a slight amplification in phage recovered from P2X3-expressing cells (~four-fold) was observed and thus single Affimer clones were tested for binding by cell-based phage ELISA. Results demonstrated that only two Affimer clones could bind to P2X3-expressing cells compared to the non-expressing control cells (**Figure 5.8**). Nevertheless, the identified Affimers (🡻) were tested for binding independently of the pIII-coat protein. To do this, the Affimer coding region was sub-cloned in to a pET11a vector enabling the pIII-independent expression of the identified Affimers. The reason this was conducted was to improve expression levels of Affimer. The ELISA was conducted by incubating the Affimers against cells expressing the P2X3 protein followed by detection of the Affimers using an anti-His antibody. However, results indicated that despite the binding of a positive control 'cell-based' anti-HSV1 gD Affimer to HSV1 gD-expressing cells (with little binding to P2X3-expressing cells), the isolated P2X3 Affimers were unable to specifically

identify P2X3-expressing cells. Furthermore, high levels of binding to the HSV1 gD-expressing cells was observed for clone H8 (**Figure 5.9**).

Due to potential problems encountered when screening P2X3, for example the cell death (Apicella and Fabbretti 2012) and potential rapid internalisation of the receptor (Vacca *et al.* 2009), a different ion channel, TRPV1, was used. TRPV1 had already been screened via a peptide mimotope from which Affimers able to recognise the full-length channel had been identified, discussed in chapter 3 (Tiede *et al.* 2017), demonstrating the Affimer library contained binders that could recognise this ion channel. Despite this, the small extracellular regions presented by this channel were likely to make it a challenging target. Results demonstrated that despite showing enrichment of phage against a TRPV1-expressing cell line based on colonies counted, monoclonal Affimers able to specifically recognise a TRPV1-expressing cell line could not be identified by cell-based phage ELISA (**Figure 5.10**). One possibility for this may be inability of the detection antibodies to gain access to the bound phage when present at the membrane surface. However, this would need to be tested further for accurate conclusion to be made. Additionally, the presence of the pIII coat protein may be hindering access to the target protein. To test for this possibility, a cell-based ELISA was conducted to detect TRPV1 using a previously validated Affimer (Affimer 2) that targets TRPV1, described in chapter 3 (Tiede *et al.* 2017). In this ELISA, the ability of the Affimer, both pIII conjugated and unconjugated, to bind its target on cells was assessed. Results demonstrated that although the Affimer was able to recognise its target when expressed independently of the pIII-coat protein, when in its pIII-conjugated state, binding was no longer able to take place. Furthermore, a clear increase in non-specific binding can be observed (**Figure 5.11**).

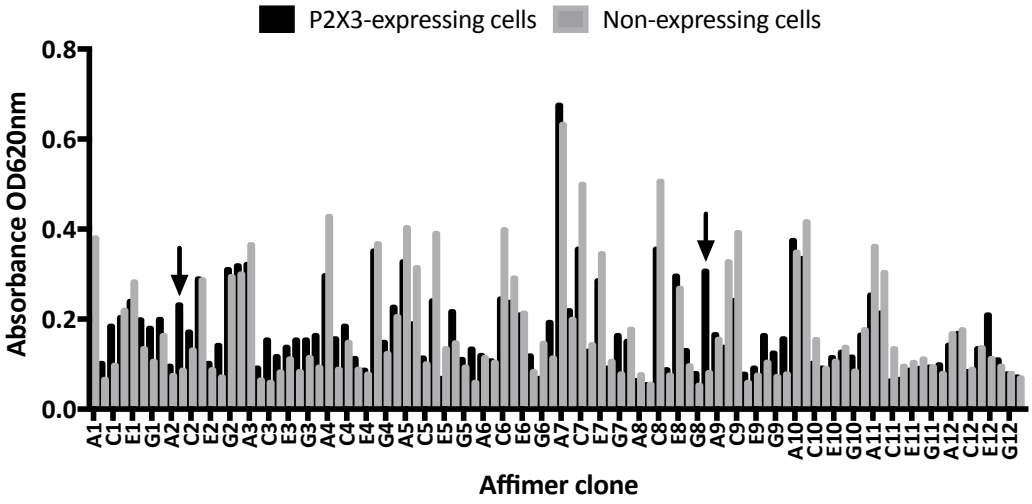

Figure 5.8. Phage ELISA showing binding by Affimers isolated from three rounds of biopanning against P2X3 expressing cells. Affimer phage isolated after three biopanning rounds against P2X3 protein expressed at the cell surface were screened by phage ELISA against P2X3-expressing cells (black) and non-expressing parental cells (grey). Cells expressing P2X3 were plated into 32 wells of a 96 well plate. In addition, non-expressing parental cells were plated into another 32 wells of a 96 well plate. Approximately 100,000 cells per well were plated and grown overnight until a confluence of 100% was reached. Cells were then fixed with 4% PFA and blocked with 2x Casein blocking buffer. Affimer phage were incubated on cells for one hour and then unbound phage washed away. Binding of the phage was detected with an anti-Fd antibody conjugated to HRP using TMB substrate and measurement at 620 nm.

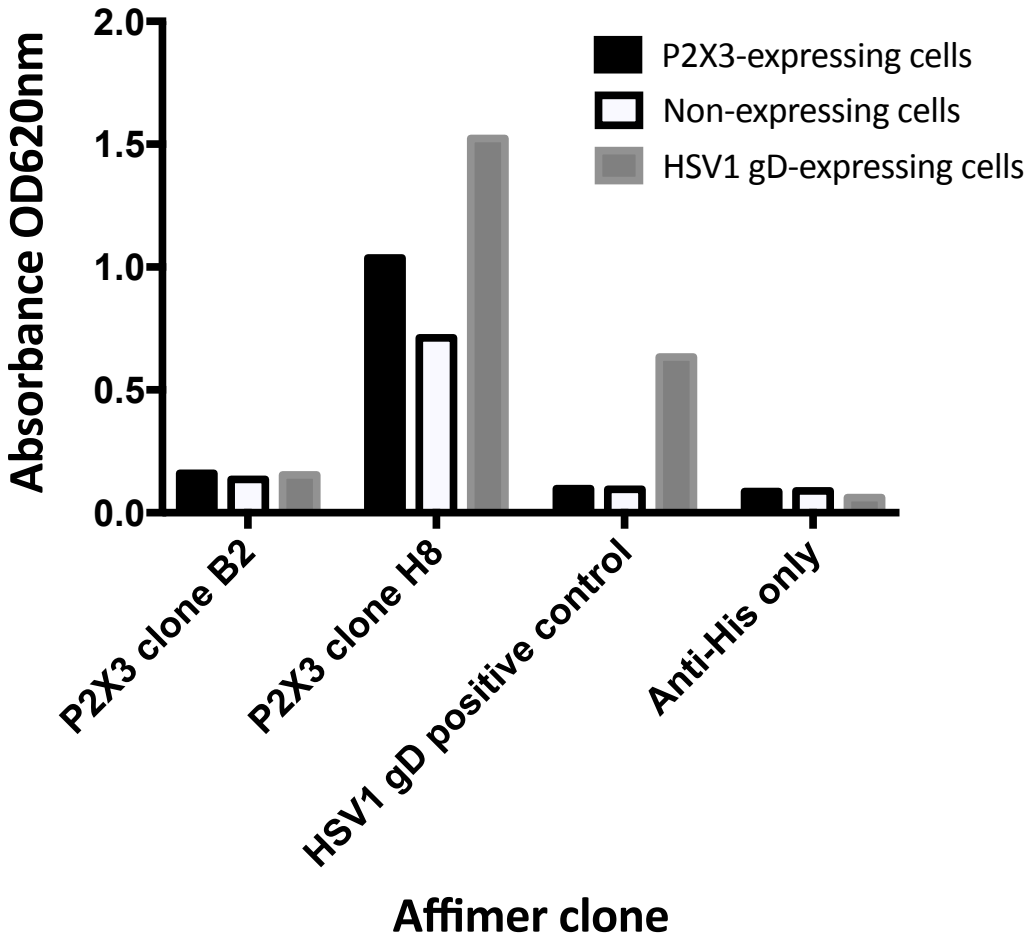

Figure 5.9. ELISA testing binding of Affimer clones B2 and H8 to P2X3 expressing cells. Cells expressing P2X3 (black) were plated into 32 wells of a 96 well plate. In addition, non-expressing parental cells (white) and HSV1 gD expressing cells (grey) were plated into another 32 wells of a 96 well plate each. Approximately 100,000 cells per well were plated and grown overnight until a confluence of 100% was reached. Cells were then fixed with 4% PFA and blocked with 2x Casein blocking buffer. P2X3 Affimer clones B2 and H8 were incubated on cells at a concentration of 1 µM for one hour. Bound Affimers were detected with an anti-His antibody conjugated to HRP using TMB substrate and measurement at 620 nm. In addition, an Affimer clone isolated from the HSV1 gD screen and an anti-His antibody only were used as positive and negative controls respectively.

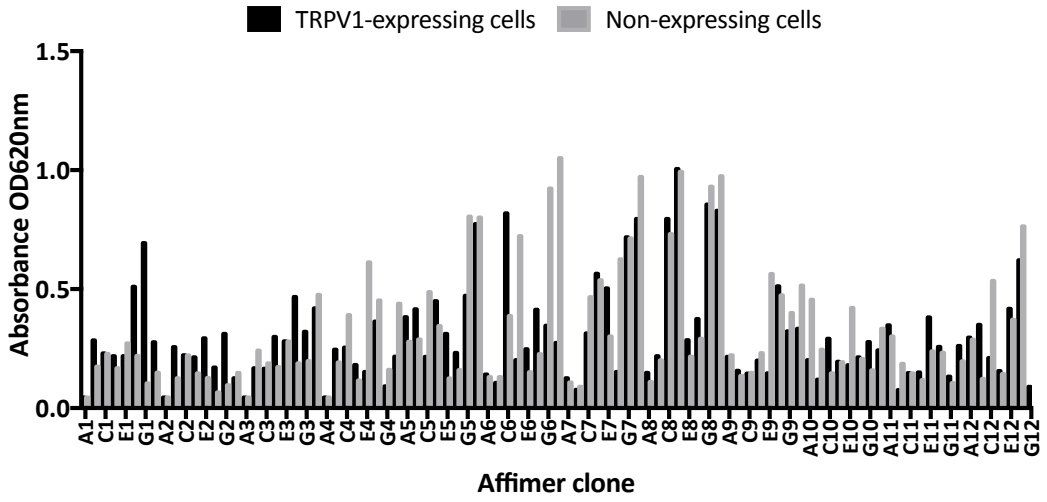

Figure 5.10. Phage ELISA showing binding of Affimer phage isolated after three rounds of biopanning against TRPV1 expressing cells. Affimer phage isolated after three biopanning rounds against TRPV1 protein expressed at the cell surface were screened by phage ELISA against TRPV1-expressing cells (black) and non-expressing parental cells (grey) Cells expressing TRPV1 were plated in to 32 wells of a 96 well plate. In addition, non-expressing parental cells were plated into another 32 wells of a 96 well plate. Approximately 100,000 cells per well were plated and grown overnight until a confluence of 100% was reached. Cells were then fixed with 4% PFA and blocked with 2x Casein blocking buffer. Affimer phage were incubated on cells for one hour and then unbound phage washed away. Binding of the phage was detected with an anti-Fd antibody conjugated to HRP using TMB substrate and measurement at 620 nm.

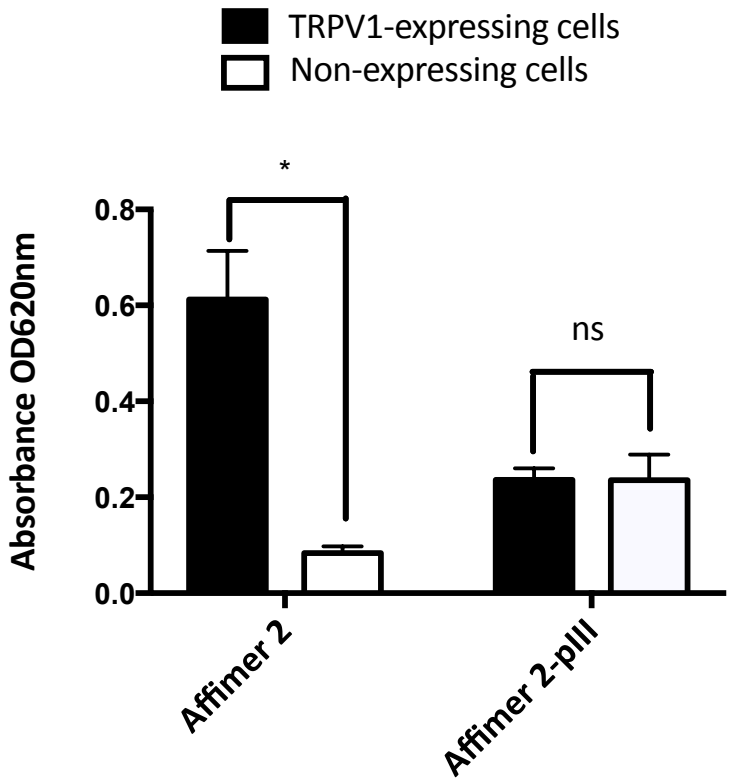

Figure 5.11. Phage ELISA to test for binding to TRPV1-expressing cells by TRPV1 Affimer 2 when expressed with or without the pIII coat protein. Affimer 2 isolated against a TRPV1 peptide and subsequently shown to bind to TRPV1 expressed at the cell surface was tested for binding to TRPV1 by ELISA when expressed with and without the pIII coat protein (Tiede *et al.* 2017). Affimer 2 was screened by phage ELISA against TRPV1-expressing (black) and non-expressing parental cells (white). Approximately 100,000 cells were plated in to wells of a 96 well plate and grown overnight until a confluence of 100% was reached. Cells were then fixed with 4% PFA and blocked with 2x Casein blocking buffer. Affimer 2 was incubated on cells for one hour and then unbound Affimer washed away. Binding of the Affimer was detected with an anti-His antibody conjugated to HRP using TMB substrate and measurement at 620 nm. *Statistical analysis was performed by t-test, N = 3. * = 0.05*

.

5.3 Discussion

This chapter reports a cell-based biopanning approach used to identify Affimer reagents able to recognise the membrane protein, HSV1 gD, within three rounds of biopanning. In addition to the relatively quick identification of binders, the use of two rounds of biopanning against adherent cell lines at a population of only 1.2 x 10^6 makes the approach more suitable when cell numbers are low or in demand, for example, when harvested from tissues.

Although the optimised approach requires small cell numbers for screening, the target expression on positive cell lines still requires careful management. A number of efforts have been made to try and analyse the population of target protein at the cell membrane, for example by conjugating it to GFP (Jones *et al.* 2016). However, binding reagents identified against GFP-conjugated membrane proteins cannot necessarily be applied to their non-conjugated counterparts as previous studies have demonstrated the ability of GFP-tagging to alter protein conformation and trafficking (Ataka and Pieribone 2002). As a result, our study expresses target proteins independently of a marker protein to measure transfection efficiency, a method used routinely (Kovala *et al.* 2000).

Another essential aspect of cell-based biopanning is the removal of non-specific phage by stringent washing steps, a difficult process when cell maintenance is required. A number of cell-based biopanning strategies have utilised cells in solution with centrifugation steps separating washes, however cell loss associated with this approach limits the viable number of washing steps (Eisenhardt *et al.* 2007, Yoon *et al.* 2012, Jones *et al.* 2016). By utilising adherent cells however, increased stringency of washing provides much faster identification of HSV1 gD-specific Affimers.

Analysis of sequencing data demonstrates high homology between HSV1 gD Affimer clones isolated from the naïve library screens. For example, the presence of a Q—PPW motif in variable region one and a S-LHSL motif in variable region two (**Table 5.2**). Furthermore, slight similarity can be observed between the Affimer clones recovered from the naïve and enriched libraries. For example,

Affimer$_{HSV1\text{-}gD\text{-}Enrich1}$ contains the 'SL' motif in variable region one and a 'QR' motif that can also be found in the naïve library Affimer clones (**Table 5.2**, *underlined*). Despite recovery Affimers with similar sequences from both the seven- and three-round protocols, as well as similarities between enriched and naïve library clones, the recovery of only two unique Affimer clones from the naïve library screen suggests that the ability to recover clone variants often observed when screening against purified protein is limited. One possible explanation for this may be the poor access to potential binding regions caused by features of the cell membrane, for example other proteins and phospholipids. This may result in reduced variation of binding Affimers, as fewer sites on the target protein are accessible. This observation has also been made in other cell-based phage display techniques (Jones *et al.* 2016). A further possibility may be that whilst screening against soluble target, high levels of antigen are available and as a result, lower affinity clones can be recovered from the library. When screening against cell-based target on the other hand, the lower level of target density in comparison may result in only the highest affinity clones being recovered. Nevertheless, the high homology observed between Affimer$_{HSV1\text{-}gD\text{-}naive7}$ and Affimer$_{HSV1\text{-}gD\text{-}naive3}$ suggests that the HSV1 gD epitope is likely identical. Further testing by ELISA and ICC confirmed HSV1-gD specific binding.

Although the method described in this chapter most likely works with single-pass membrane proteins with large extracellular domains, for example, the HSV1 gD extracellular domain is 314 amino acids in length, the presence of non-specific proteins at the cell membrane may interfere with biopanning against smaller targets. Indeed, use of the optimised protocol against two ion channel targets, P2X3 and TRPV1, failed to identify Affimers towards these proteins. The difficulty when screening membrane proteins with poorly accessible epitopes could be observed by testing a pre-validated TRPV1-specific Affimer (Tiede *et al.* 2017). When tested in its pIII-conjugated and unconjugated form for binding against TRPV1 expressed at the cell membrane, it was observed that the presence of the pIII coat protein hindered access of the Affimer to its TRPV1 epitope present in the outer pore domain. One experiment that could be

conducted to test for this is to use a full-length pIII coat protein rather than the currently truncated protein used. This result further suggests the advantage of the small size of the Affimer reagent when targeting cryptic epitopes.

The cell-based biopanning approach described provides a method for identifying Affimer reagents against inert membrane-based targets with large extracellular domains. A number of advantages over current protocols are described including the low cell numbers and low number of biopanning rounds required. These advantages make screening of targets less laborious and cheaper. Whilst the method is likely to work most successfully against membrane proteins with large extracellular domains, proteins with smaller extracellular domains are likely to be more troublesome. Despite this, examples are available in which antibodies raised against recombinant proteins mimicking regions of ion channels are able to detect their cognate, full-length proteins (Lee *et al.* 2014). The small molecular size of the Affimer scaffold should complement this ability to detect epitopes present within tight binding pockets. Indeed, chapter three of this thesis describes the ability of Affimers to detect an epitope present in the pore domain of TRPV1 (Tiede *et al.* 2017).

Chapter 6

The identification of Affimer reagents against P2X3, a major drug target for chronic pain

6 The identification of Affimer reagents against P2X3, a major drug target for chronic pain

6.1 Introduction

As previously discussed, a number of disorders resulting in chronic pain are caused by mutations to ion channel genes however ion channels are also found to be involved in chronic pain via altered expression at the afferent fibres of nociceptive sensory neurons (Serrano *et al.* 2012). The ATP-gated P2X3 ion channel demonstrates enhanced expression in chronic pain and as a result has been identified as a major analgesic drug target (Xu and Huang 2002, Xiang *et al.* 2008). Indeed, P2X3 inhibition has demonstrated pain-relieving properties in murine models (Honore *et al.* 2002). Many of the P2X3-specific reagents that are currently undergoing clinical testing are chemical compounds, with Afferent Pharmaceuticals' AF-219 entering phase II for the treatment of chronic cough (Abdulqawi *et al.* 2015). A number of drawbacks associated with small molecule drugs have been frequently described, such as their lack of selectivity, leading academic and industrial researchers to explore biologics for targeting ion channels, with functional P2X3 antibodies and toxins being reported in the past decade (Grishin *et al.* 2010, Shcherbatko *et al.* 2016).

In addition to the search for therapeutic reagents, ligands that can be used for studying ion channels, by immunocytochemistry (ICC) for example, are highly sought (Chen *et al.* 2012). Although conjugation of ion channels to fluorescent proteins has been explored as a method for studying their behaviour, such 'fluorescent tagging' has the potential for altering protein architecture and properties thus making its use questionable (Maue 2007). The high affinity of toxins for ion channels has also been exploited to develop them as imaging tools, however, despite recent progress; difficulties in producing these proteins limit their practicality (Ondrus *et al.* 2012, Bartok *et al.* 2015). Furthermore, their selectivity can sometimes limit their use. Although antibodies remain the gold standard for bioimaging, issues with variability and specificity have been reported (Baker 2015, Bradbury and Pluckthun 2015). Additionally, introducing antibodies into the reducing environment of the cytoplasm can be difficult,

limiting their use for studying ion channels in their dynamic state (Marschall *et al.* 2011). Indeed, the P2X family of ion channels are known to undergo a variety of trafficking processes (**Figure 6.1**). Furthermore, various family members are predominantly expressed at intracellular compartments, with P2X6 expressed at the endoplasmic reticulum (Ormond *et al.* 2006), making live cell studies difficult. More recently, alternative binding proteins able to overcome some issues associated with antibodies whilst retaining their binding capabilities have been explored for studying ion channels. However, whilst examples of inhibitors (Danquah *et al.* 2016) and crystallisation chaperones (Stockbridge *et al.* 2015) are available, their use as ion channel imaging tools is limited. For this reason, antibodies remain the most commonly marketed reagent for this application.

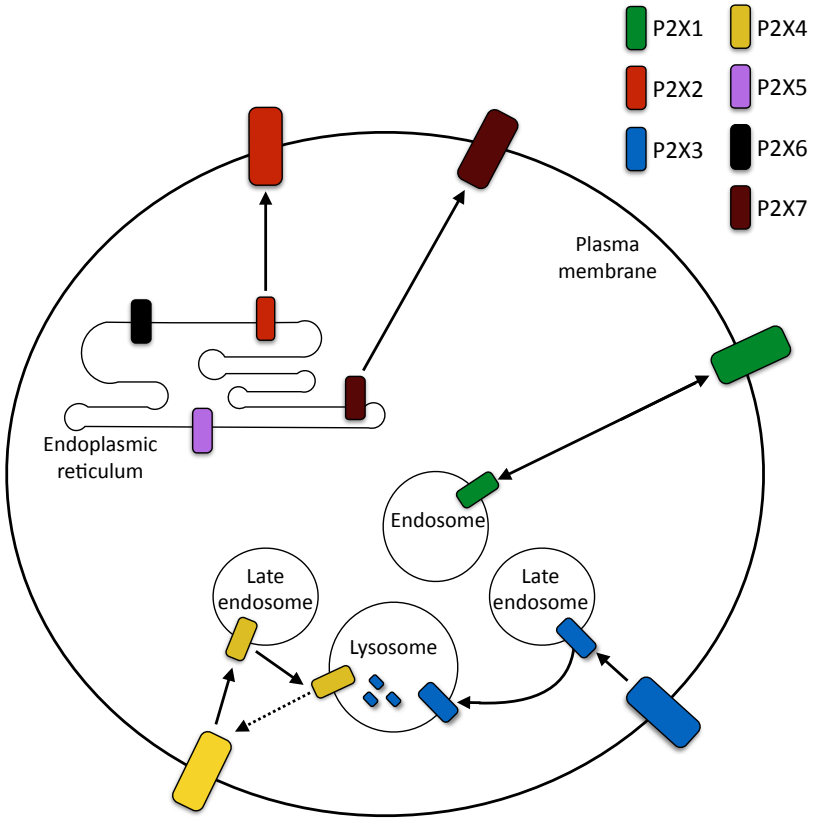

Figure 6.1. Trafficking and processing of the P2X family of ion channels. The P2X family of ion channels consists of seven members that each have different trafficking properties and as a result are localised to different cellular compartments. P2X5 and P2X6 predominantly remain localised to the endoplasmic reticulum however variants can become localised at the plasma membrane, for example, P2X6/P2X2 heteromers. P2X2 and P2X7 are stably expressed at the cell surface and traffic slowly through the secretory pathway. P2X1 rapidly cycles between the cell surface and endosomes. P2X3 is continuously trafficked to the late endosomes and lysosomes where it is degraded. P2X4 is continuously cycled between the cell surface, late endosomes and lysosomes whilst avoiding degradation (*Adapted from (Robinson and Murrell-Lagnado 2013)*).

In this chapter, the isolation of P2X3-specific reagents from our Affimer phage display library is presented. A combination of recombinant P2X3 extracellular domain (ECD) protein expressed in both bacterial and mammalian systems was used for screening by phage display, with final validation conducted by immunocytochemistry (ICC) on trimeric P2X3 over-expressed on various cell lines.

6.2 Results

6.2.1 Expression and characterisation of P2X3 extracellular domain (ECD) segments in *E. coli*

P2X3 ECD segments (**Figure 6.2**) were expressed in BL21 Star (DE3) *E. coli* cells and protein solubilised using 8 M urea and subsequently refolded by sequential dilution of urea by dialysis. Protein from individual cellular compartments was analysed by SDS PAGE and Coomassie staining (**Figure 6.3**A). P2X3 ECD segments L44-T155, T155-N317 and L44-N317 showed an apparent molecular mass of 17, 25 and 35 kDa, which is relatively close to their theoretical values of 15.5, 21.8 and 34.1 kDa, respectively. Results did however demonstrate that following protein re-folding, a contaminating protein of approximately 37 kDa could be observed for each protein that was purified.

Next, the expressed proteins were characterised by circular dichroism (CD) for assessing the presence of secondary structure. The CD spectra of P2X3 ECD L44-T155 demonstrated α-helical structure and segments T155-N317 and L44-N317 favoured a mixed α-helical and β-sheet population. When compared to structural models of the recently crystallised P2X3 from *Homo sapiens* (**Figure 6.4**A and B, PDB: 5SVJ), these results suggest that correct folding of segments L44-N317 and T155-N317 of P2X3 ECD may have taken place. The lack of β-sheet structure present in L44-T155 suggests that this segment may not have folded in a manner similar to that of the full-length protein, possibly a result of becoming too truncated, resulting in the loss of amino acids that interact to help form this secondary structure. For this reason, no further studies were conducted on segment L44-T155.

To further probe folding of P2X3 ECD segments L44-N317 and T155-N317, binding to their cognate ligand, ATP, was examined by fluorescence polarisation (FP) (**Figure 6.5**A). Briefly, a fluorescent analogue of ATP, MANT-ATP, would be expected to have a fast rate of tumbling when unbound. On addition of the P2X3 ECD, binding would result in slower tumbling that can be measured as an increase in polarisation. On incubation of P2X3 ECD L44-N317 with MANT-ATP, an increase in polarisation of 79.54 ± 12.64 (S.D) was observed whilst addition of P2X3 ECD segment T155-N317 demonstrated an increase in polarisation of only 21.12 ± 12.60 (S.D), a smaller increase in polarisation, as expected due to its truncated structure. Results were normalised to a negative control protein, SUMO, and student t-test analysis between P2X3 ECD L44-N317 and SUMO, as well as P2X3 ECD T155-N317 and SUMO were conducted, demonstrating *p*-values of 0.002 and 0.02, respectively (**Figure 6.5**B). Next, the ability of the full length P2X3 ECD (L44-N317) to bind ATP in a concentration-dependent manner was assessed (**Figure 6.5**C). Results demonstrated that as the concentration of P2X3 ECD L44-N317 increased, change in polarisation when compared to a buffer only control also increased. Collectively, results from CD and FP experiments suggest that expressed P2X3 ECD segments can be expressed in this format to produce accurately folded protein for incorporating into phage display screens with the Affimer library.

6.2.2 Expression and purification of P2X3 ECD chimera's in HEK293 cells

The high disulphide bond content and glycosylation sites present in the P2X3 ECD prompted the expression of the P2X3 ECD in a mammalian expression system. To do this, the P2X3 ECD open reading frame was cloned in to a variety of OPPF-UK pOPIN vectors to enable expression of hP2X3 ECD conjugated to a variety of fusion proteins. These vectors included; pOPINTTGneo-3c-Fc, pOPINTTGneo-3c-CD4 and pOPINTTGneo-3c-HALO7 for expression of Fc, CD4 and HALO chimera's respectively. In addition, hP2X3 ECD was expressed alone by cloning into pOPINTTGneo. Cloning was conducted by In-Fusion^{TM} cloning (Berrow *et al.* 2009). Protein yield was compared by western blot analysis in lysed cells (*Left*, **Figure 6.3**C) and secreted protein in media (*Right*, **Figure 6.3**C). Expression in

HEK293 cells provides protein that is likely to resemble the native P2X3 receptor ECD due to the presence of the required machinery for posttranslational modifications, particularly with the high disulphide bond (five) and N-linked glycosylation (four sites) profile of the P2X3 ECD. Multiple bands present for each of the proteins in the western blot suggested that glycosylation had taken place.

```
L44-T155      MASMLHEKAYQVRDTAIESSVVTKVKGSGLYANRVMDVSDYVTPPQGTSVFVIITKMIVT 60
T155-N317     ------------------------------------------------------------ 0
L44-N317      MASMLHEKAYQVRDTAIESSVVTKVKGSGLYANRVMDVSDYVTPPQGTSVFVIITKMIVT 60


L44-T155      ENQMQGFCPESEEKYRCVSDSQCGPERLPGGGILTGRCVNYSSVLRTCEIQGWCPTAAAH 120
T155-N317     ----------------------------------------------------MASMTEVDT 9
L44-N317      ENQMQGFCPESEEKYRCVSDSQCGPERLPGGGILTGRCVNYSSVLRTCEIQGWCPTEVDT 120
                                                                  . * .

L44-T155      HHHHHHH-------------------------------------------------- 127
T155-N317     VETPIMMEAENFTIFIKNSIRFPLFNFEKGNLLPNLTARDMKTCRFHPDKDPFCPILRVG 69
L44-N317      VETPIMMEAENFTIFIKNSIRFPLFNFEKGNLLPNLTARDMKTCRFHPDKDPFCPILRVG 180
                .

L44-T155      ------------------------------------------------------------ 127
T155-N317     DVVKFAGQDFAKLARTGGVLGIKIGWVCDLDKAWDQCIPKYSFTRLDSVSEKSSVSPGYN 129
L44-N317      DVVKFAGQDFAKLARTGGVLGIKIGWVCDLDKAWDQCIPKYSFTRLDSVSEKSSVSPGYN 240


L44-T155       -------------------------------------------------   127
T155-N317      FRFAKYYKMENGSEYRTLLKAFGIRFDVLVYGNAGKFNAAAHHHHHHHH   178
L44-N317       FRFAKYYKMENGSEYRTLLKAFGIRFDVLVYGNAGKFNAAAHHHHHHHH   289
```

Figure 6.2. Aligned amino acid sequence of the open reading frames of the human P2X3 ion channel ECD segments cloned in to a pET11a expression vector. C-terminal octahistidine tag is included in the sequence. L44-N317 represents the full-length ECD of human P2X3 whilst L44-T155 and T155-N317 represent two truncated segments of the human P2X3 ECD. Sequence alignments were prepared using Clustal Omega.

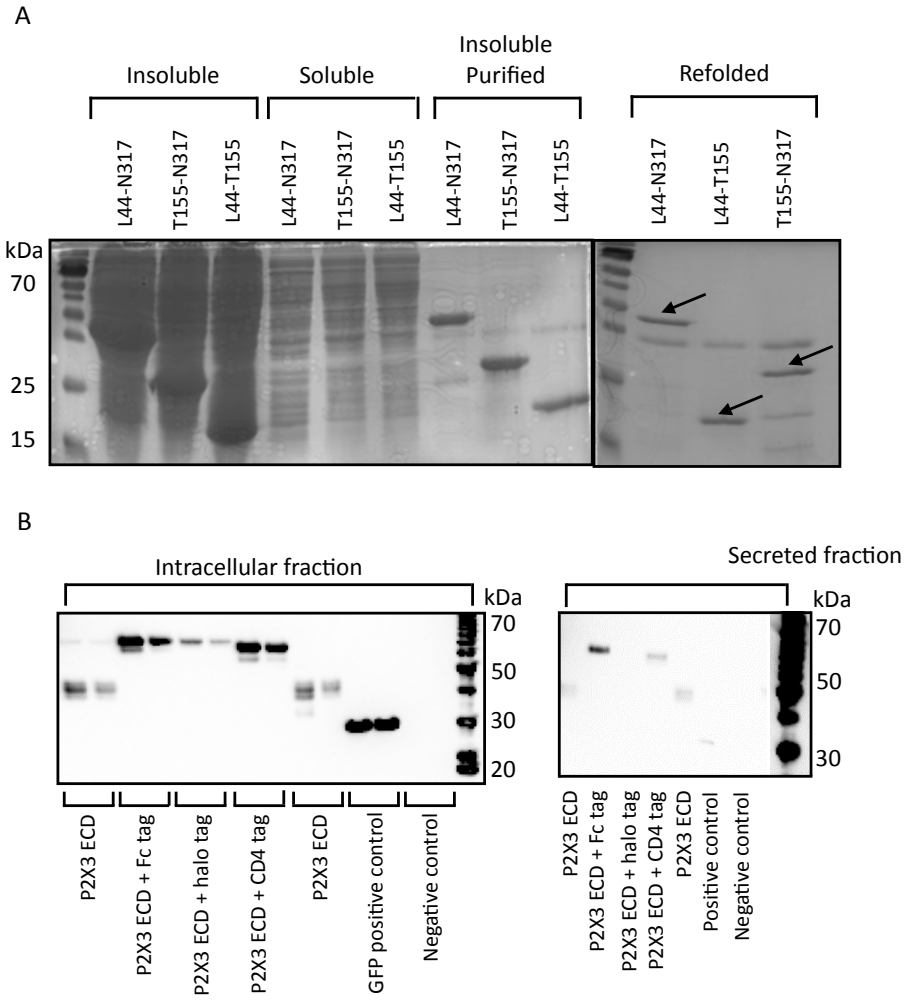

Figure 6.3. P2X3 ECD segments were expressed in *E. coli* (A) and HEK293 cells (B). A. SDS PAGE analysis of insoluble, soluble, purified (from the insoluble fraction) and refolded P2X3 protein. *Segment theoretical MW; P2X3 ECD L44-N317. 34.1 kDa, P2X3 EC T155-N317. 21.8 kDa, P2X3 EC L44-T155. 15.5 kDa.* B. Western blot analysis of intracellular and secreted P2X3 protein expressed with various fusion partners including Fc, halo and CD4. Protein was detected using an anti-His antibody conjugated to HRP and detected using TMB. A GFP positive control and non-His tagged negative control were included.

A

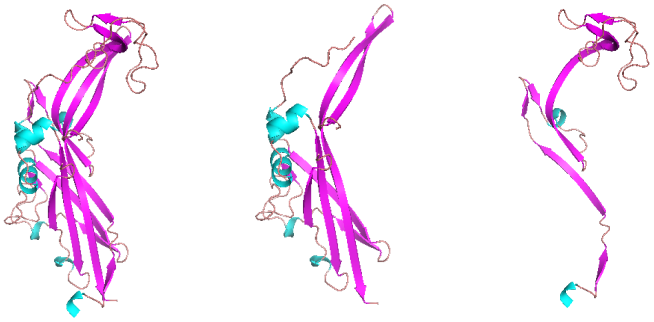

L44-N317 T155-N317 L44-T155

B

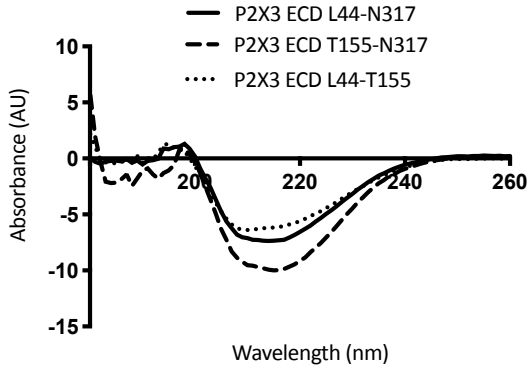

Figure 6.4. Characterisation of P2X3 ECD secondary structure by circular dichroism (CD). A. Crystal structure of human P2X3 (PDB:5SVJ). B. CD traces for P2X3 segment L44-T155 (dots), P2X3 segment T155-N317 (dashes) and P2X3 segment L44-N317 (line).

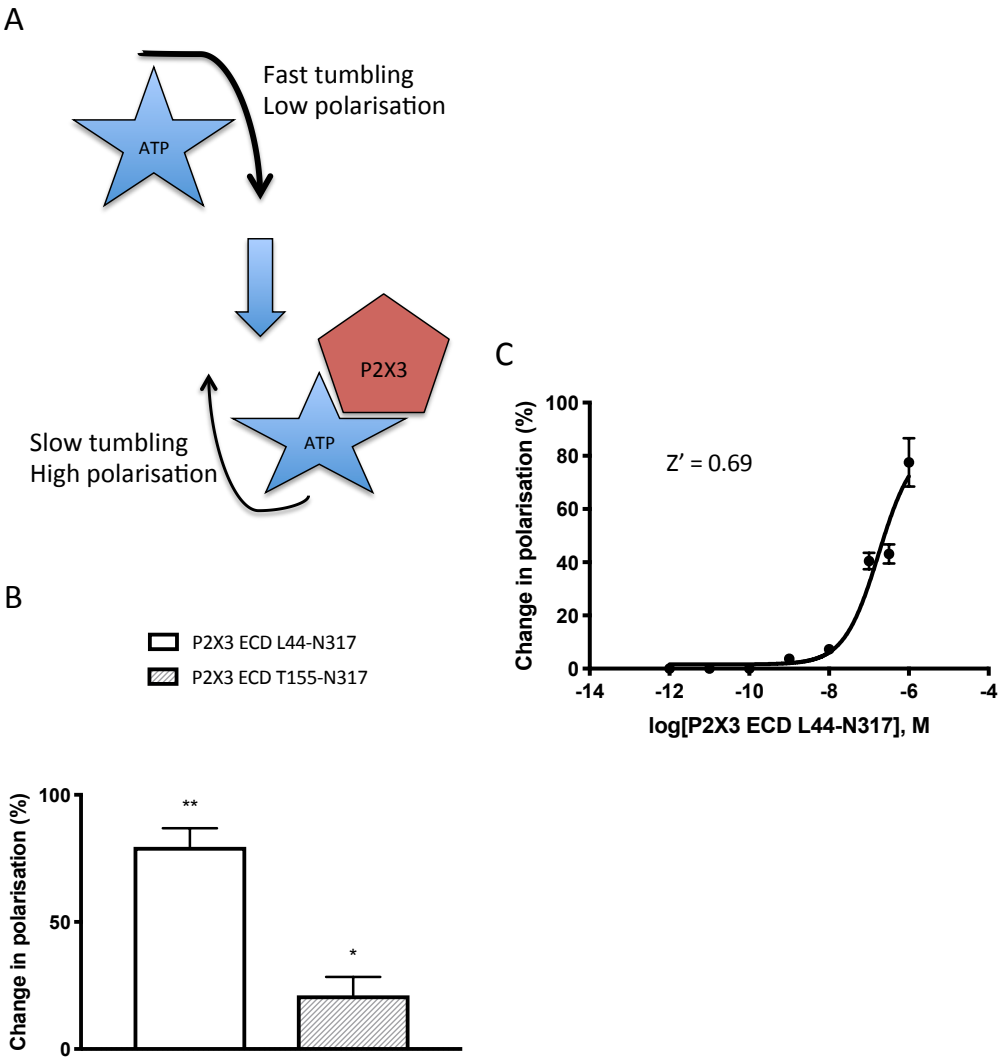

Figure 6.5. Characterisation of P2X3 ECD tertiary structure by fluorescence polarisation. A. P2X3 ECD was assessed for its ability to bind its cognate ligand, ATP, conjugated to a MANT fluorophore by FP. In this assay, the binding of P2X3 ECD to MANT-ATP would be expected to result in increased polarisation. B. Initially, 1 µM of P2X3 ECD L44-N317 and T155-N317 were each mixed with 1 µM MANT-ATP and incubated with gentle agitation in the dark for thirty minutes. Next, fluorescence polarisation was measured using a Tecan Spark plate reader (Tecan Life Sciences) measured at absorption and emission wavelengths of 356/448 nm *(N = 3, L44-N317 t-test p-value = 0.00225, T155-N317 t-test p-value = 0.02).* C. Subsequently, a range of P2X3 ECD L44-N317 concentrations were incubated with 1 µM MANT-ATP for thirty minutes in the dark with gentle agitation. Fluorescence polarisation was measured using a Tecan Spark plate reader at absorption and emission wavelengths of 356 and 448 nm respectively (*Z' factor 0.69*).

6.2.3 P2X3 ECD phage display

Expressed P2X3 ECD L44-N317 protein was purified and biotinylated using EZ-Link NHS-SS-Biotin according to previously reported methods (Tiede *et al.* 2014). The naïve Affimer library was enriched against P2X3 ECD L44-N317 for three rounds of biopanning. A final round of selection was then conducted against biotinylated P2X3 ECD-Fc chimeric protein expressed in HEK293 cells. Ninety-six monoclonal Affimers were tested by phage ELISA against both P2X3 ECD L44-N317 from bacteria and P2X3 ECD-Fc from mammalian cells with a hit rate of ~20% observed. The sequencing of all P2X3-specific clones revealed fifteen unique Affimers (**Table 6.1**) with a variety of binding affinities estimated by phage ELISA (**Figure 6.6**). Affimers that showed strong binding by phage ELISA (Affimers 1, 4 and 7) share sequence similarity with each other (highlighted in bold in **Table 6.1**).

Affimer^{P2X3} clone	Variable region 1	Variable region 2
1	DTGH**IYY**YH	WM**T**YK**KL**LA
2	NFESLYGPY	FQFTHHITR
3	EINFQLPSG	LPNFYQAFY
4	**WQA**A**VY**YK**Q**	WPHFMDDDR
5	QYYGIYGPW	YVFYKAKSK
6	AIGYTYYRH	KGGMSHNYF
7	**WQS**D**LY**LP**Q**	HKDR**T**ME**KI**
8	VVQWDDFIP	PGYLFGNYV
9	IYSAKYTMY	YIHQGRKSK
10	KIYPEVWEI	SAMRSANNQ
11	DFNGDSIIH	RLIYLGWHR
12	SIDSDWLPI	DAMMYGRFF
13	VRYLYGFTY	ARHNLFENT
14	VRQQWGMTF	TALENEQYI
15	WQWGIYGPW	HALKEPGVP

Table 6.1. Affimer sequences identified from recombinant P2X3 ECD screen

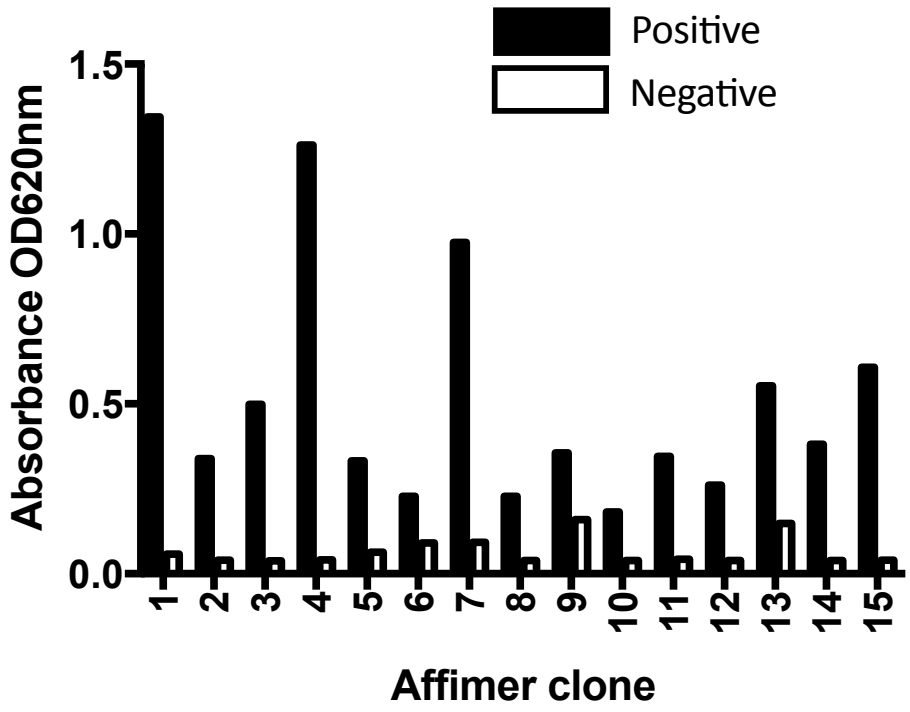

Figure 6.6. Phage ELISA showing binding of P2X3 Affimer clones to recombinant P2X3 ECD-Fc protein. Phage display was used to screen purified P2X3 ECD L44-N317 using our Affimer library for three rounds of selection against protein expressed in bacteria with a final round of selection conducted against chimeric P2X3 ECD-Fc protein expressed in mammalian cells. Isolated clones were then tested by phage ELISA for binding against recombinant P2X3 ECD-Fc protein. Recombinant protein was biotinylated and immobilised on wells of a streptavidin-coated plate. Affimer phage were then incubated on P2X3 ECD-Fc for one hour and unbound Affimer phage washed away. Bound Affimer phage were then detected with anti-Fd antibody conjugated to HRP. Addition of TMB and measurement at 620 nm then took place.

6.2.4 Human P2X3 immunocytochemistry

Following isolation of Affimers that were able to bind P2X3 ECD protein expressed in both bacterial and mammalian systems, it was important to confirm the ability of Affimers to recognise full-length, trimeric P2X3 expressed in cells. To do this, a 1321N1 cell line stably expressing human P2X3 (hP2X3) was used to investigate the ability of Affimers to recognise the full-length hP2X3 channel by immunocytochemistry. Affimers were produced as previously described. Protein concentration was measured by Nanodrop spectrophotometry and actual concentration calculated using Abs 0.1% (= 1 g/L). Protein was normalised to 3 mg/mL and analysed by SDS PAGE and Coomassie staining (**Figure 6.7**).

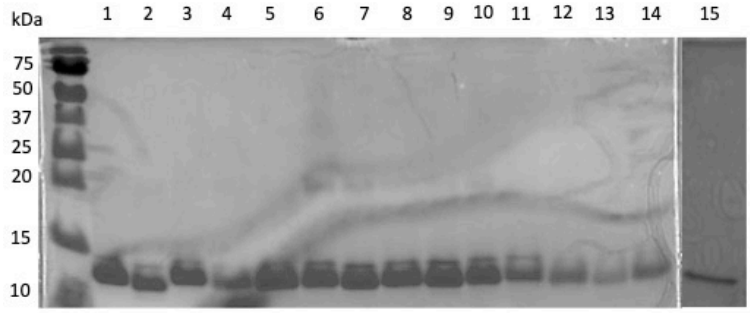

1. Affimer 1
2. Affimer 2
3. Affimer 3
4. Affimer 4
5. Affimer 5
6. Affimer 6
7. Affimer 7
8. Affimer 8
9. Affimer 9
10. Affimer 10
11. Affimer 11
12. Affimer 12
13. Affimer 13
14. Affimer 14
15. Affimer 15

Figure 6.7. Analysis of anti-P2X3 Affimer proteins by SDS PAGE and Coomassie staining. Affimers were produced as previously described and then purified protein was analysed using SDS PAGE. The gel was developed using Coomassie stain.

Next, Affimers were tested against hP2X3 when fixed using PFA however results demonstrated that none of the Affimers were able to recognise hP2X3. In contrast, an anti-P2X3 antibody was able to stain hP2X3-expressing 1321N1 cells whilst resulting in no signal on parental 1321N1 cells (**Figure 6.8**). The inability of Affimers to recognise fixed hP2X3 may be a result of cross-linking caused by the fixation method, resulting in loss of conformation to the target epitope. To test this, Affimers were added to live cells prior to fixation. Results demonstrated that whilst the majority of Affimers provided no signal on the parental 1321N1

cell line, Affimers 1 and 7 were able to detect a protein present in hP2X3-expressing cells that was not present in the parental cells (**Figure 6.9**). The remaining Affimers showed no binding to P2X3 expressed in mammalian cells that could be differentiated from that observed against parental cells.

Staining observed for Affimers 1 and 7 appeared to be particularly punctate, possibly a result of the constitutive internalisation of P2X3 to the endosome-lysosome pathway reported to take place (Vacca *et al.* 2009). Another possibility is that Affimers are themselves initiating this internalisation, a phenomenon that has been observed with antibodies raised against P2X3 (Shcherbatko *et al.* 2016). Further studies would be required to confirm this however. Nevertheless, results demonstrated that Affimers raised against the recombinant P2X3 ECD protein were able to recognise full-length hP2X3, with observed staining similar to that produced by a commercially available anti-P2X3 antibody (**Figure 6.9**, *final panel*).

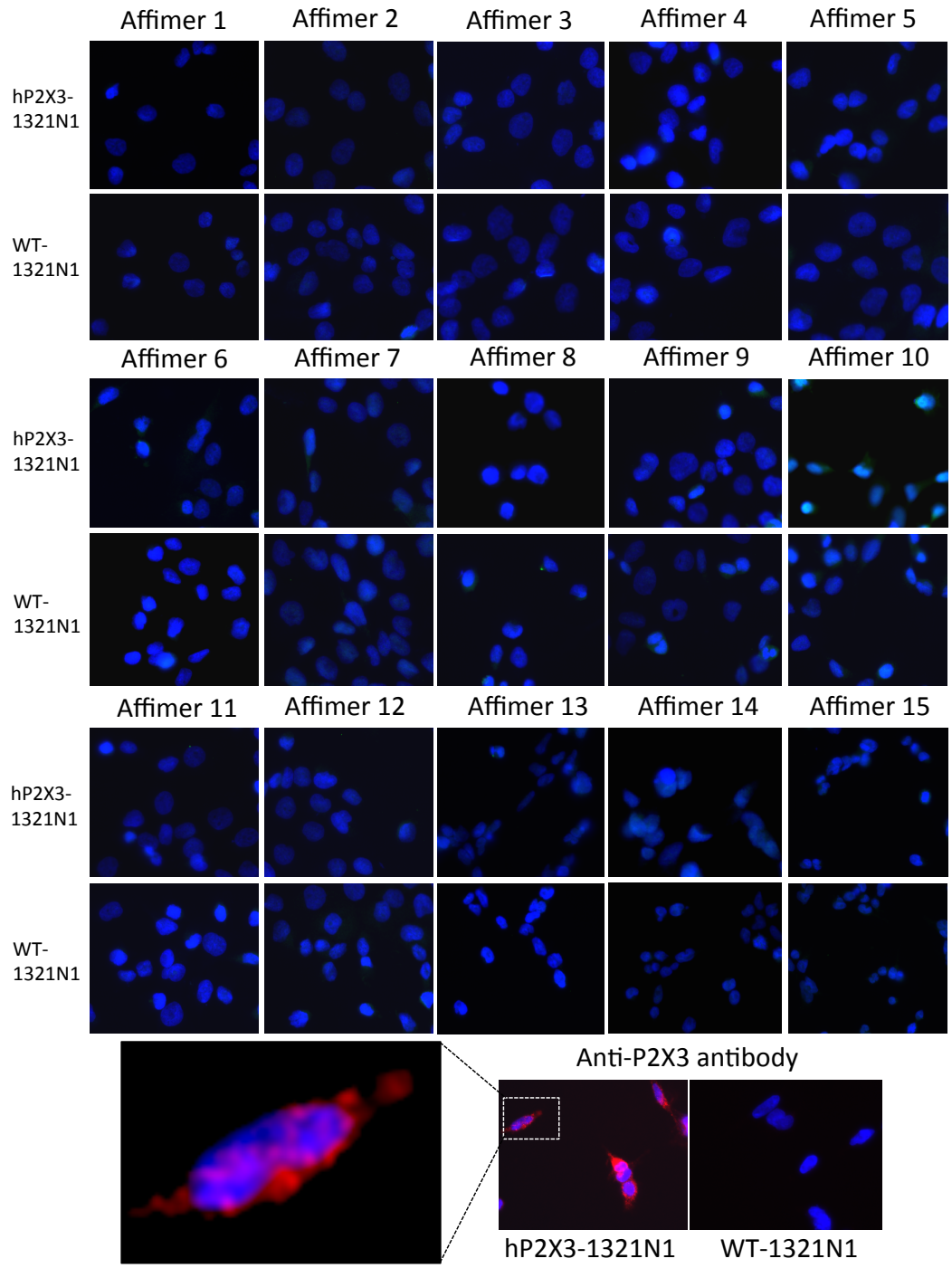

Figure 6.8. Human P2X3 immunocytochemistry against fixed cells. Human P2X3-expressing 1321N1 cells were seeded on to cover slips and then fixed with 4% PFA. Cells were then permeabilised with 0.1% Triton X100 for 20 minutes and blocked with 1% milk. Cells were then incubated with Affimers 1-15 or anti-P2X3 antibody for one hour at room temperature with gentle agitation. Next, detection of Affimer was conducted using anti-6X His antibody (mouse) followed by anti-mouse-488. Anti-P2X3 antibody (rabbit) was detected using a fluorophore conjugated anti-rabbit antibody.

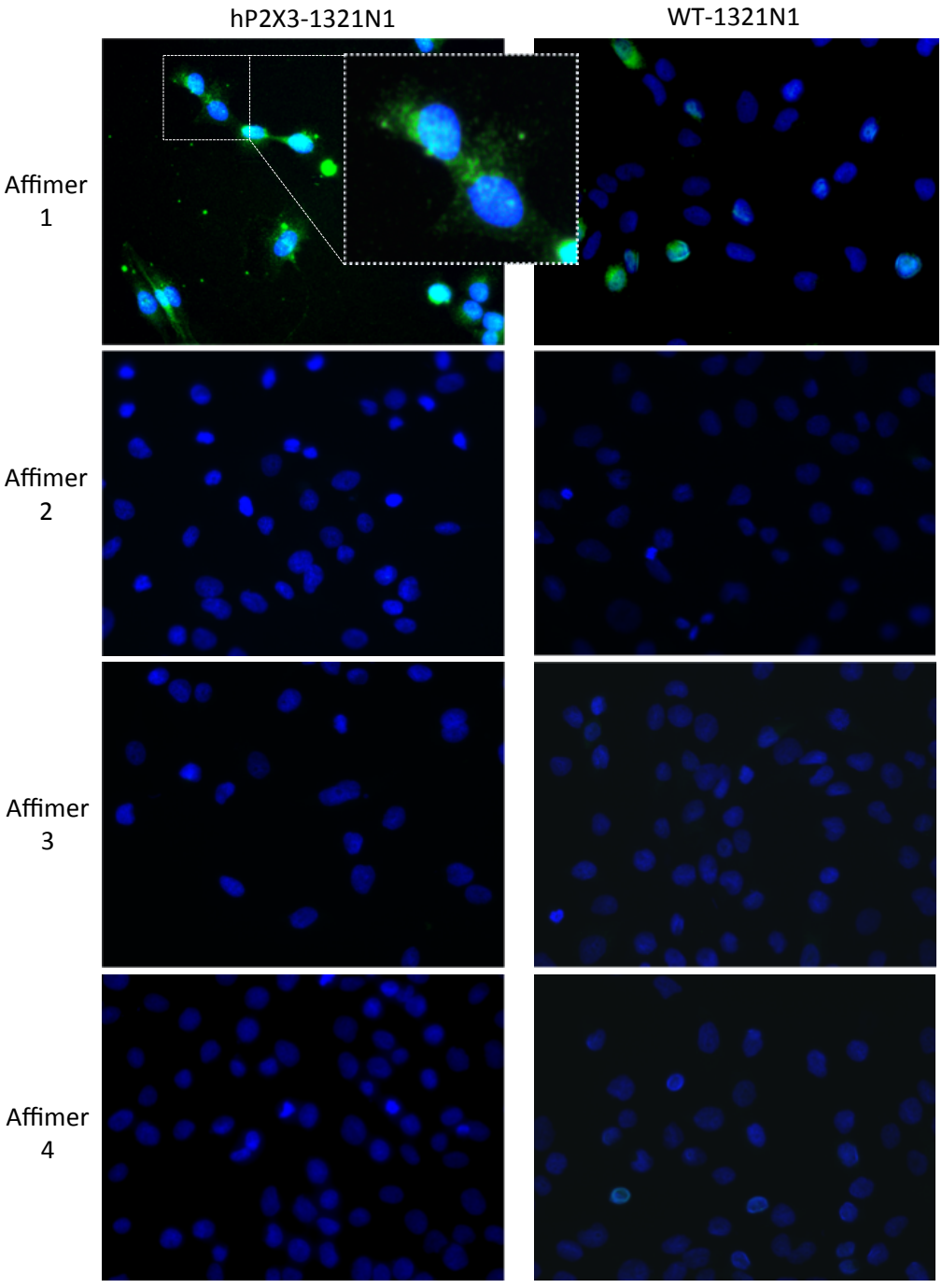
hP2X3-1321N1
WT-1321N1
Affimer 1
Affimer 2
Affimer 3
Affimer 4

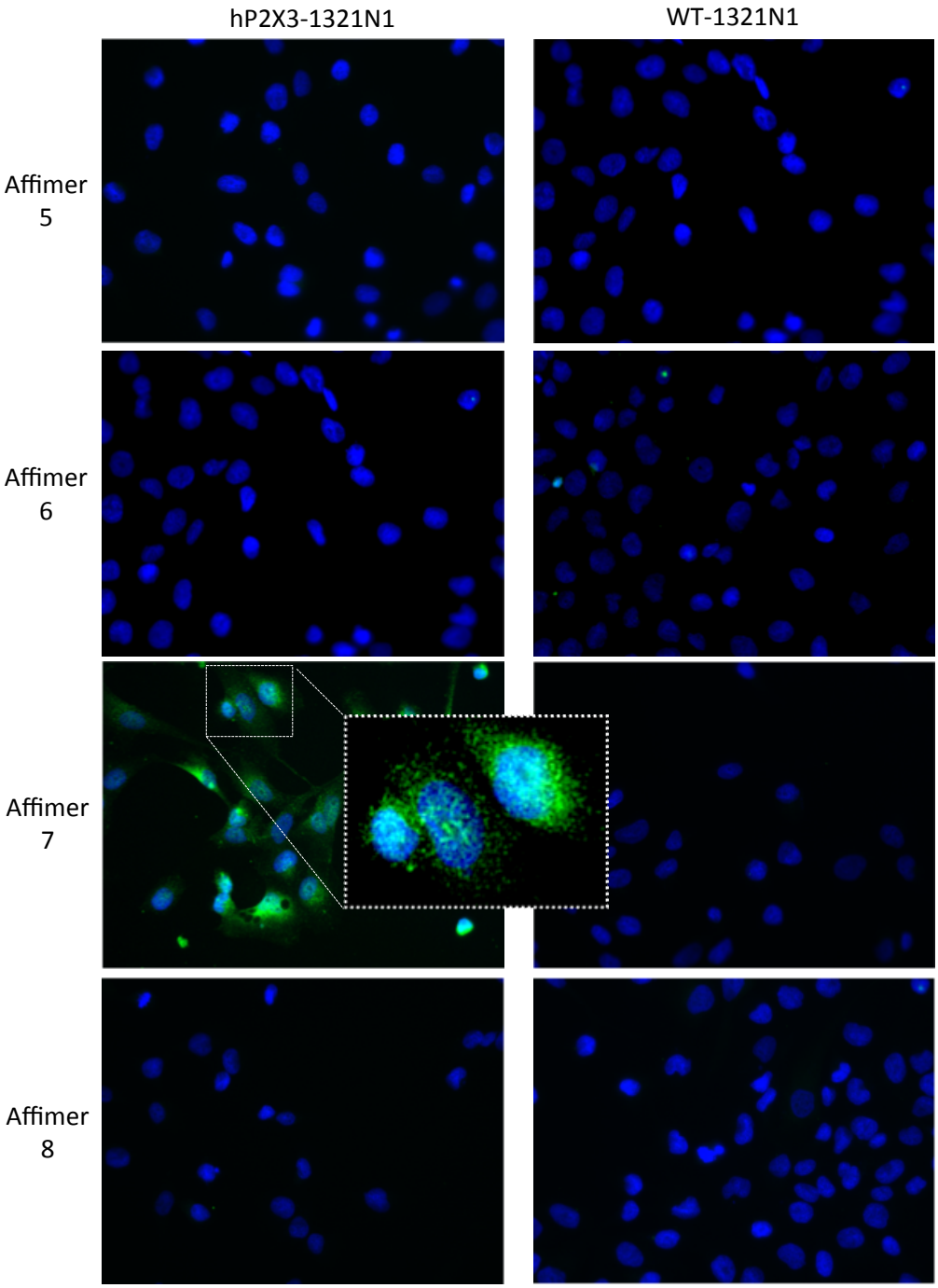
hP2X3-1321N1
WT-1321N1
Affimer 5
Affimer 6
Affimer 7
Affimer 8

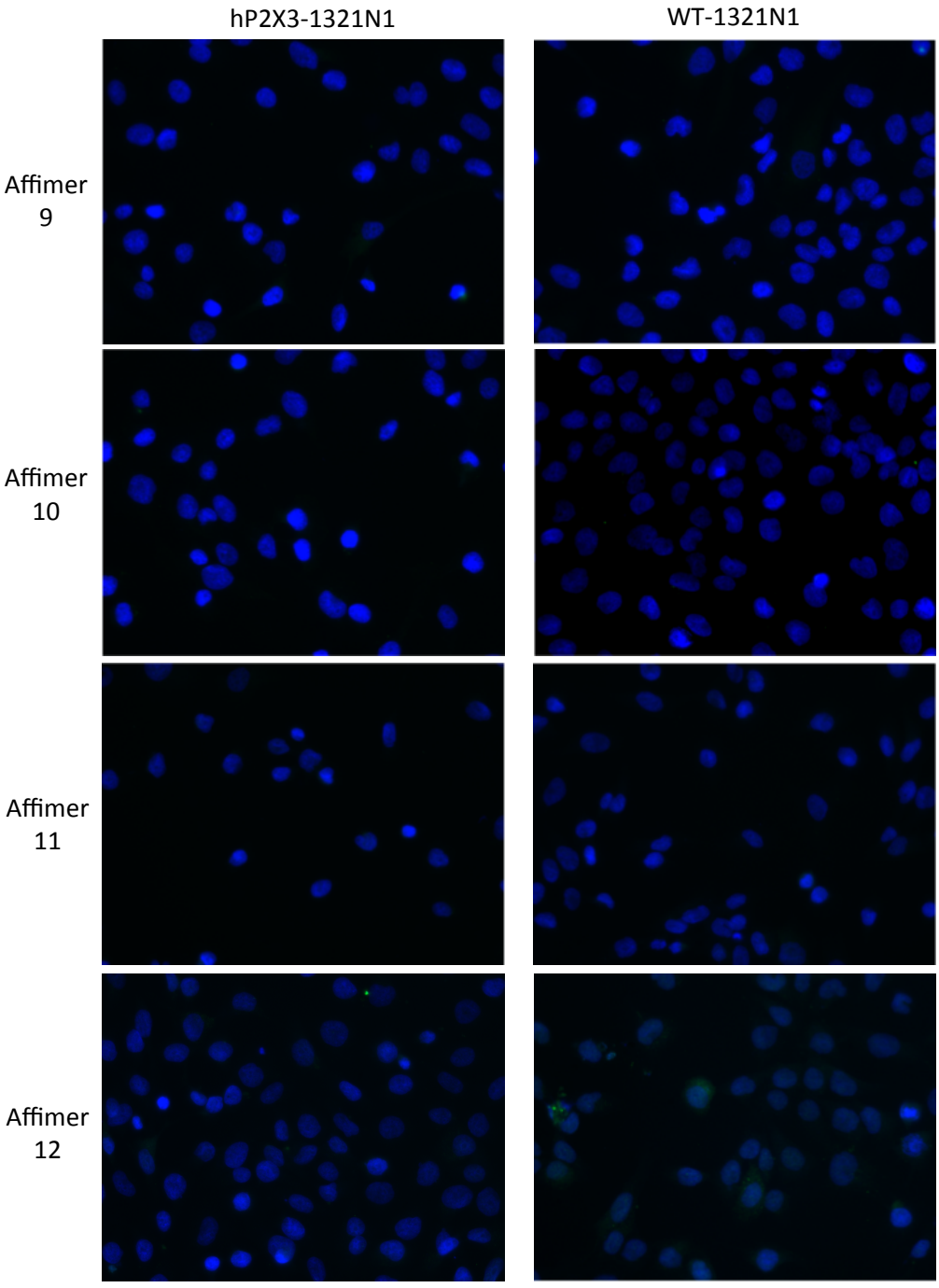
hP2X3-1321N1
WT-1321N1
Affimer 9
Affimer 10
Affimer 11
Affimer 12

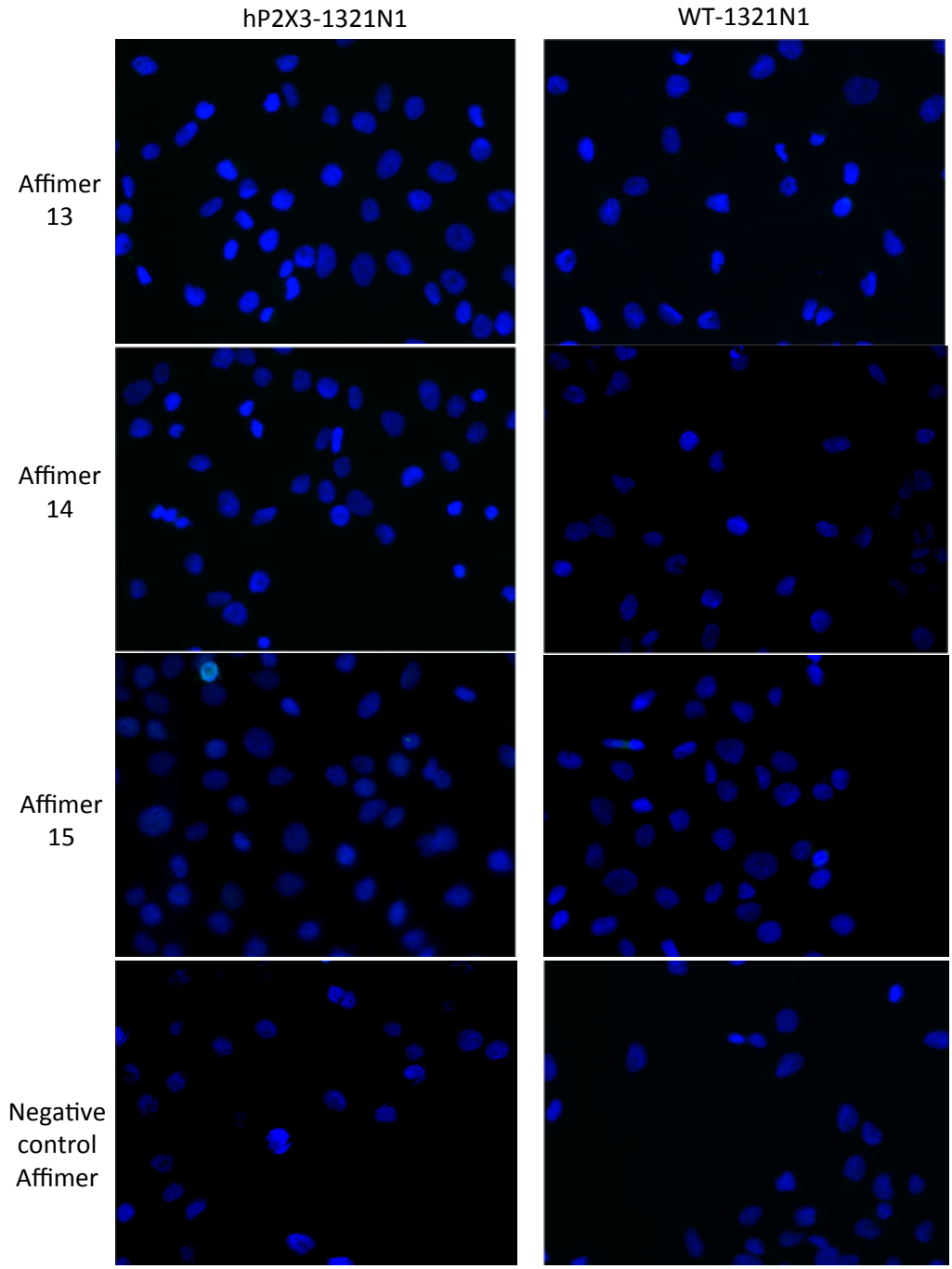
hP2X3-1321N1
WT-1321N1
Affimer 13
Affimer 14
Affimer 15
Negative control Affimer

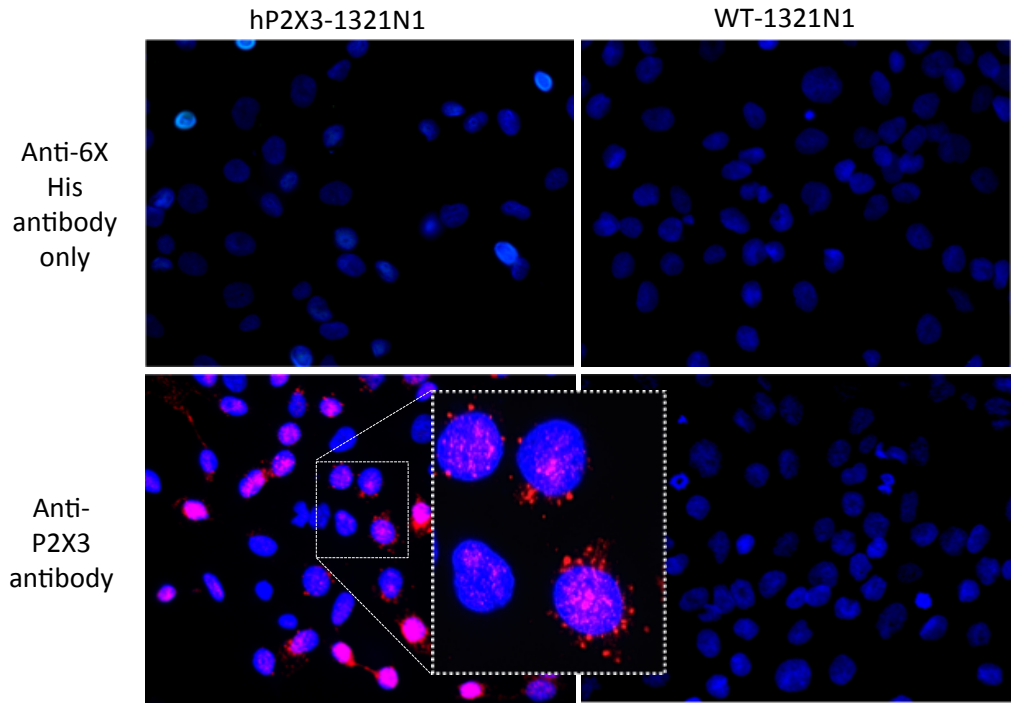

Figure 6.9. Human P2X3 immunocytochemistry against live cells. Human P2X3-expressing 1321N1 cells were seeded on to cover slips and then incubated with Affimers 1-15 for twenty minutes at room temperature with gentle agitation. Cells were subsequently washed with assay buffer three times and fixed using 4% PFA. Cells were permeabilised with 0.1% Triton X100 in PBS and blocked for 30 minutes with 1% milk in PBS. Detection of Affimer was conducted using anti-6X His antibody (mouse) followed by anti-mouse antibody conjugated to Alexa Fluor-488. P2X3 was stained separately using a commercially available antibody that was detected using a secondary antibody conjugated to a 594-fluorophore.

Next, this similarity between Affimers and antibody was further probed by co-staining. Results demonstrated that whilst staining was similar, differences could be observed (**Figure 6.10**). This may be a result of alterations in target protein at the stage of staining, for example, Affimers are added to target in its live state almost thirty minutes before the addition of antibody to the cells in their fixed state. The rapid cycling of P2X3 between the plasma membrane and the endosome-lysosome pathway further increases the possibility that P2X3 is present in different cellular compartments (Vacca *et al.* 2009). Another explanation may be a result of the differences in size of the detecting reagent, with Affimers almost ten times smaller than the anti-P2X3 antibody.

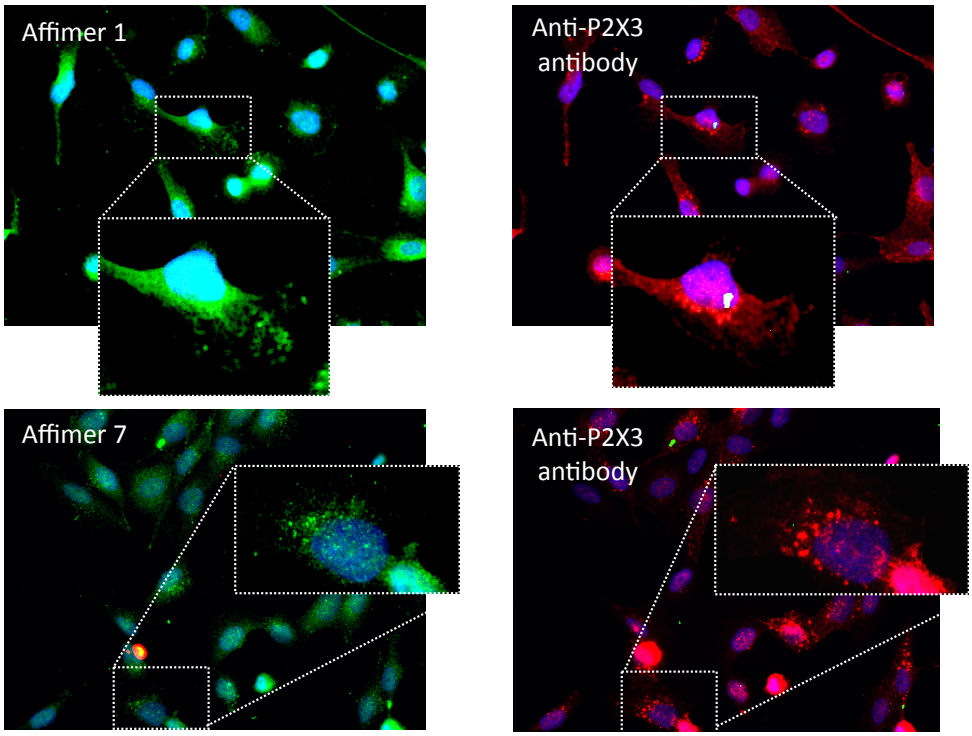

Figure 6.10. Co-staining of hP2X3 using Affimers 1 and 7 alongside anti-P2X3 antibody. A hP2X3-expressing 1321N1 cell line was stained as previously with Affimers however this time co-staining with an anti-P2X3 antibody was conducted. This took place by incubating Affimer-stained cells (green) with anti-P2X3 antibody once in their fixed, permeabilised state. Anti-P2X3 antibody was then detected by secondary antibody conjugated to Alexa Fluor 594 (red).

6.2.5 Rat P2X3 immunocytochemistry

Next, the ability of Affimers to detect rat P2X3 (rP2X3) was investigated. To test this, HEK293 cells stably expressing rP2X3 was used for immunocytochemistry studies. Again, rP2X3 was initially stained in its fixed state with similar results to those observed against hP2X3, with none of the Affimers able to recognise fixed rP2X3 (**Figure 6.11**). Subsequently, the ability of Affimers to recognise live rP2X3 was tested. To do this, a rP2X3-expressing HEK293 cell line was stained with Affimers and anti-P2X3 antibody. Results demonstrated that the majority of Affimers were unable to specifically detect rP2X3, however Affimers 1 and 7 were able to detect the presence of a protein available for binding in the rP2X3 stable cells compared to a non-expressing parental cell line (**Figure 6.12**). Again, Affimers 1 and 7 demonstrated similar staining to that of an anti-P2X3 antibody (**Figure 6.12**, *final panel*).

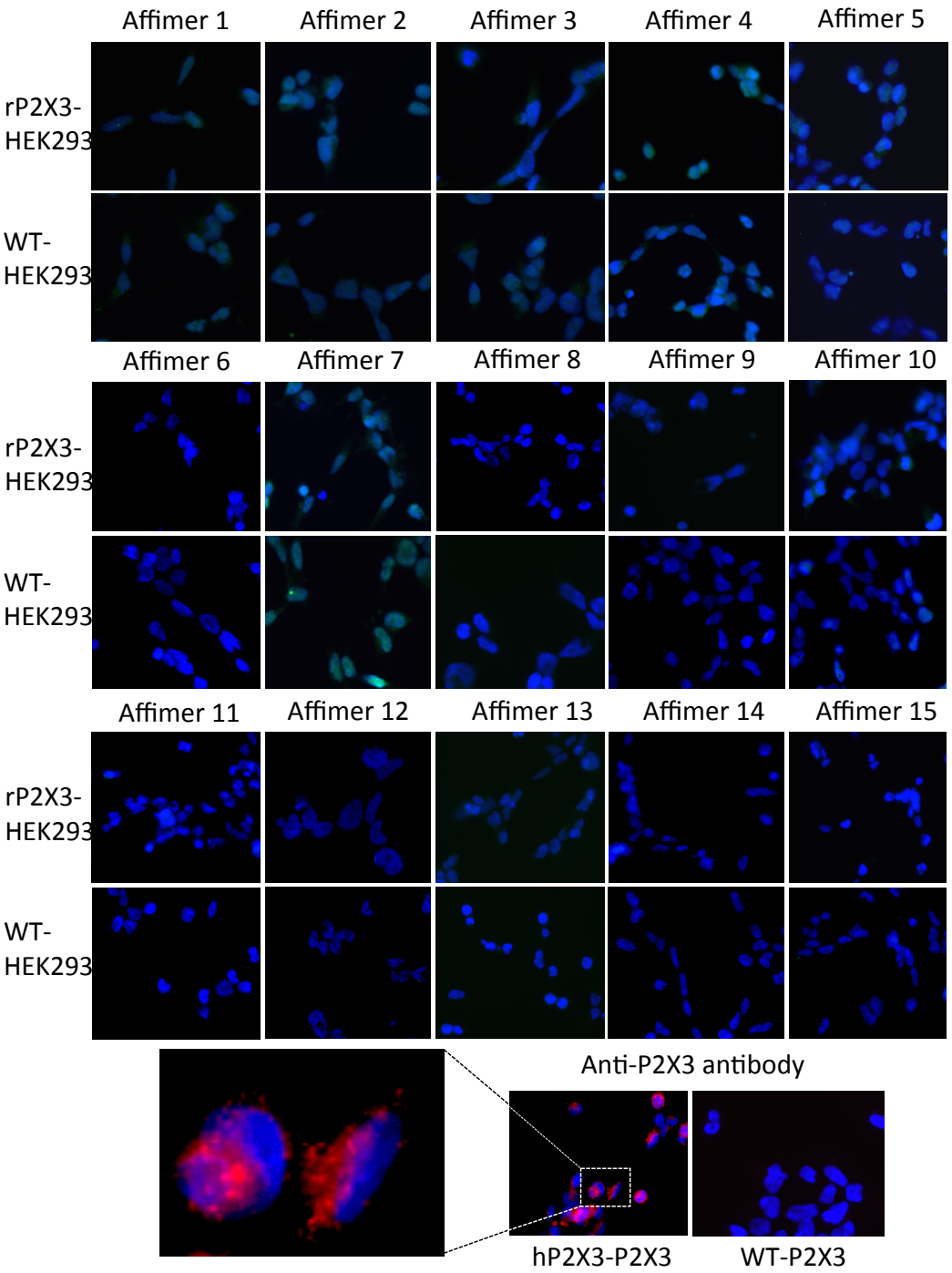

Figure 6.11. Rat P2X3 immunocytochemistry against fixed cells. Rat P2X3-expressing HEK293 cells were seeded on to cover slips and then fixed with 4% PFA. Cells were then permeabilised with 0.1% Triton X100 in PBS for 20 minutes and blocked with 1% milk in PBS. Cells were then incubated with Affimers 1-15 or anti-P2X3 antibody for one hour at room temperature with gentle agitation. Next, detection of Affimer was conducted using anti-6X His antibody (mouse) followed by anti-mouse antibody conjugated to Alexa Fluor 488. Anti-P2X3 antibody (rabbit) was detected using a fluorophore conjugated anti-rabbit antibody.

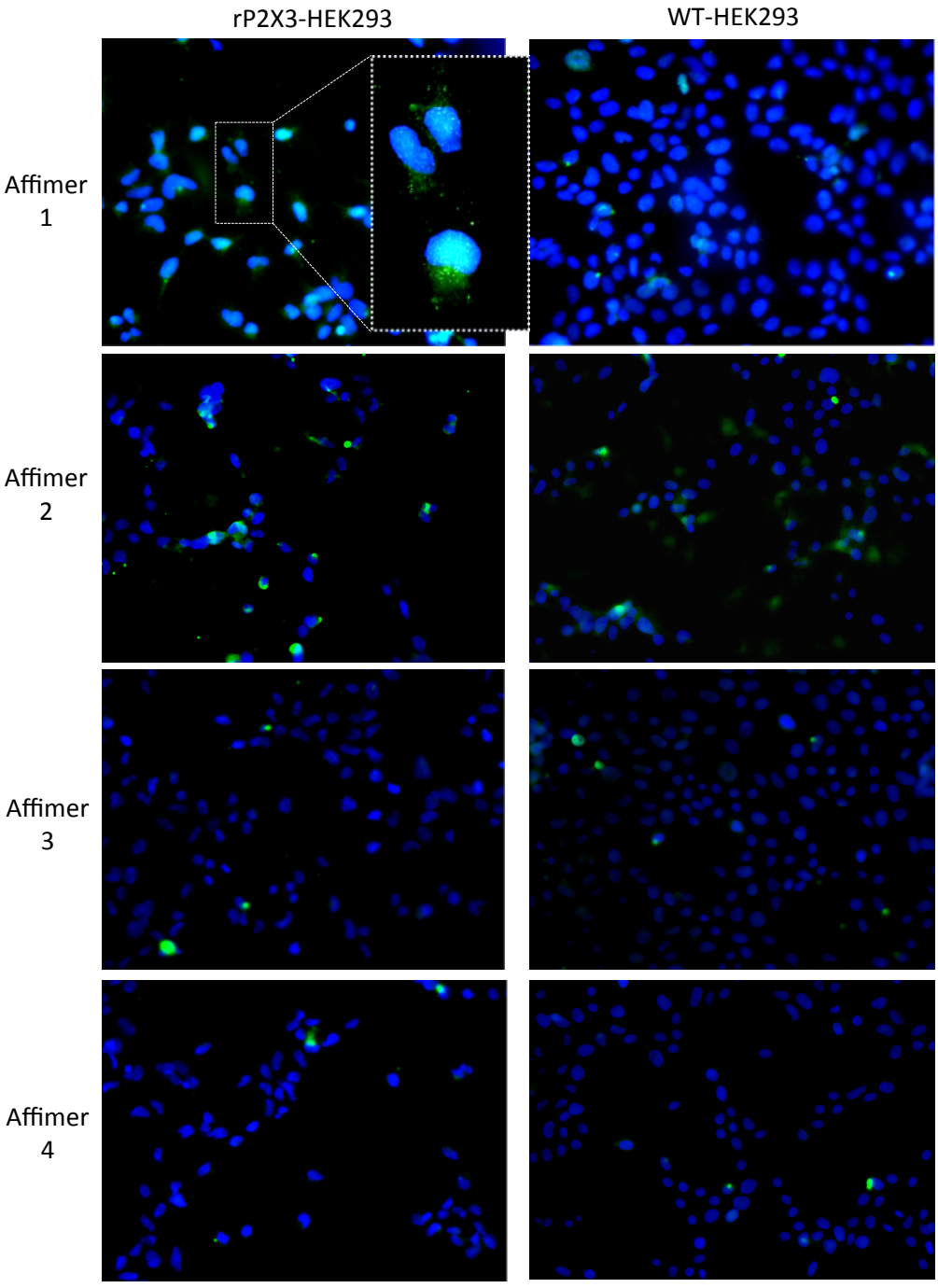
rP2X3-HEK293
WT-HEK293
Affimer 1
Affimer 2
Affimer 3
Affimer 4

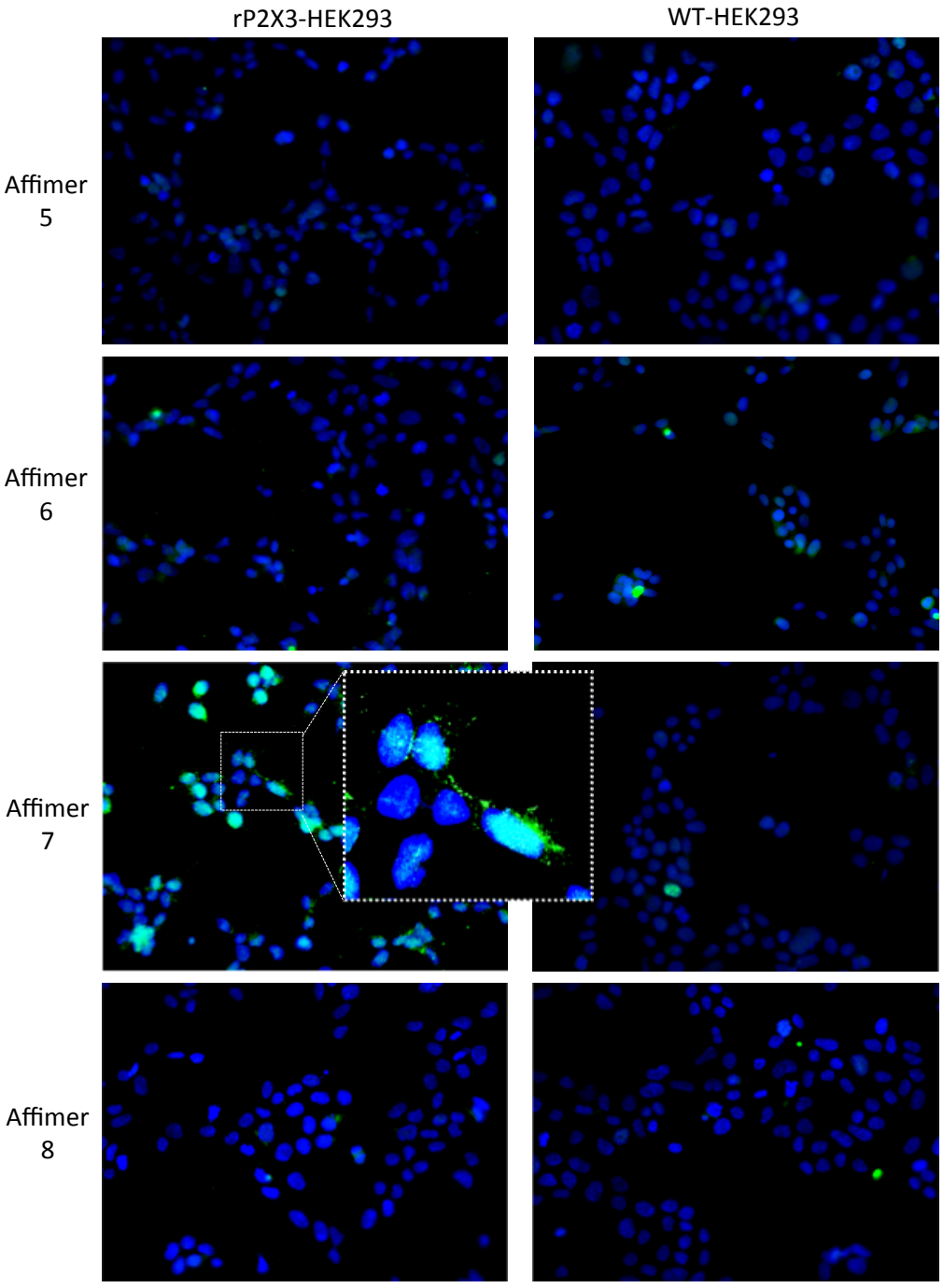
rP2X3-HEK293
WT-HEK293
Affimer 5
Affimer 6
Affimer 7
Affimer 8

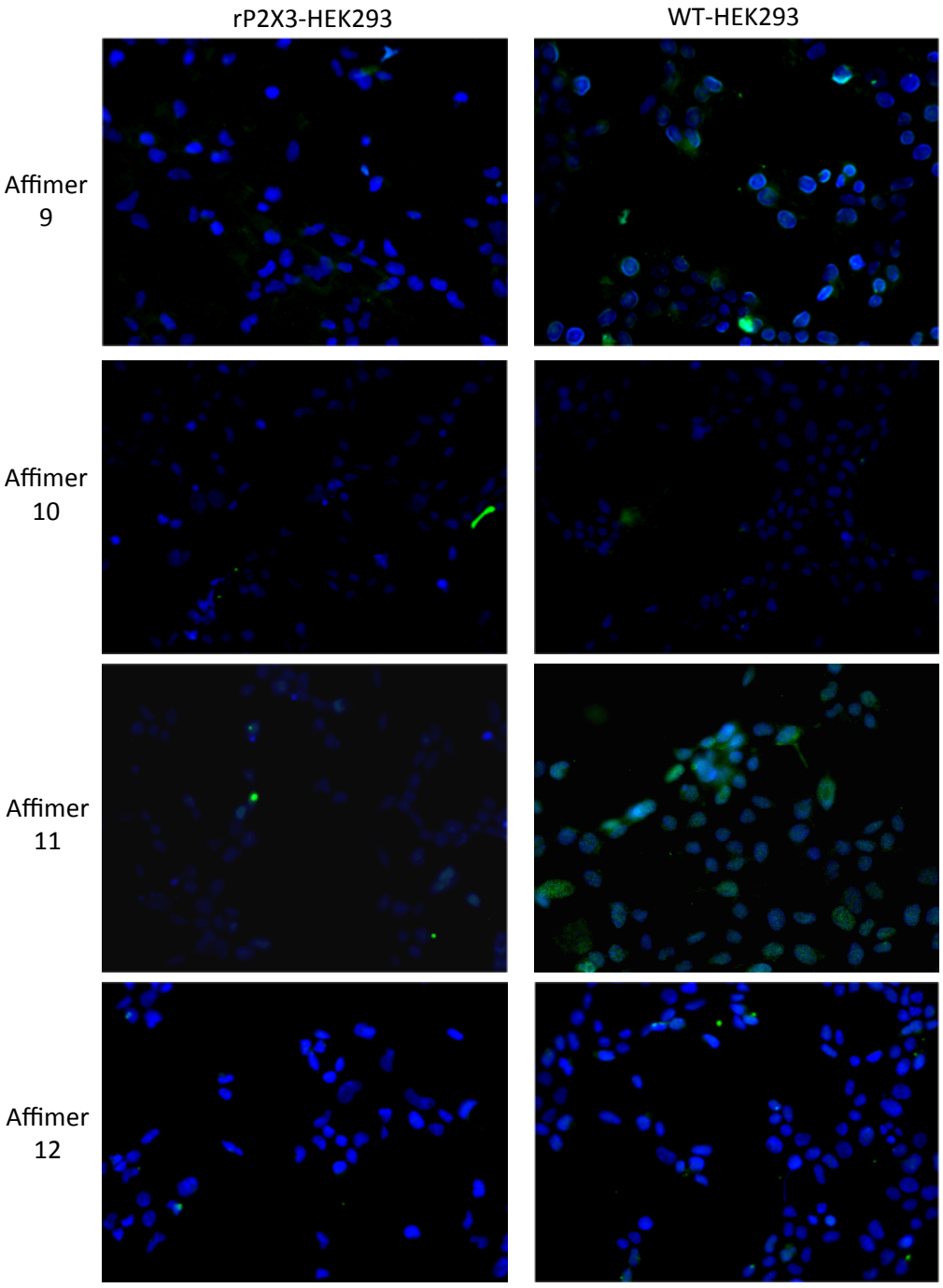
rP2X3-HEK293
WT-HEK293
Affimer 9
Affimer 10
Affimer 11
Affimer 12

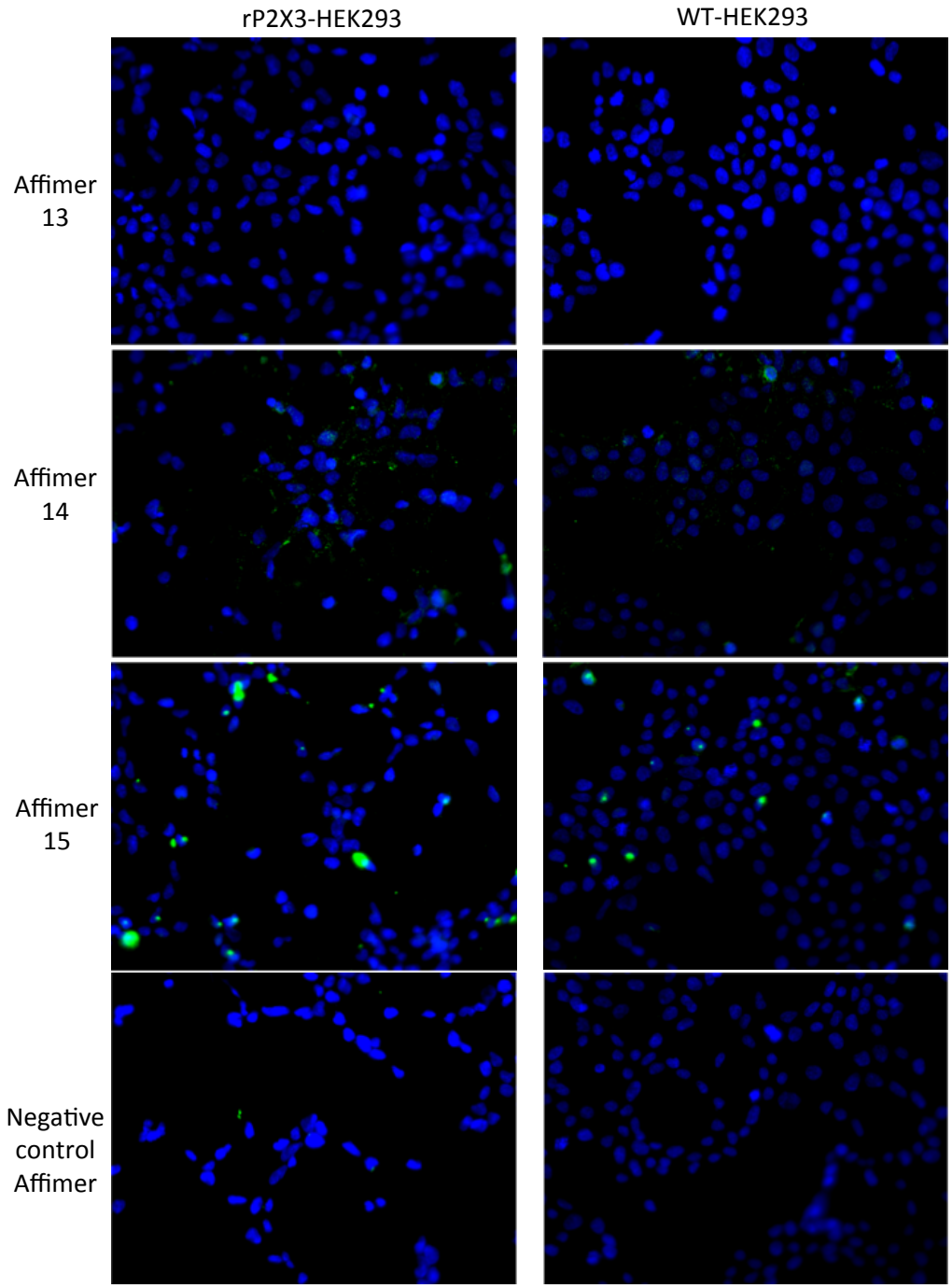
rP2X3-HEK293
WT-HEK293
Affimer 13
Affimer 14
Affimer 15
Negative control Affimer

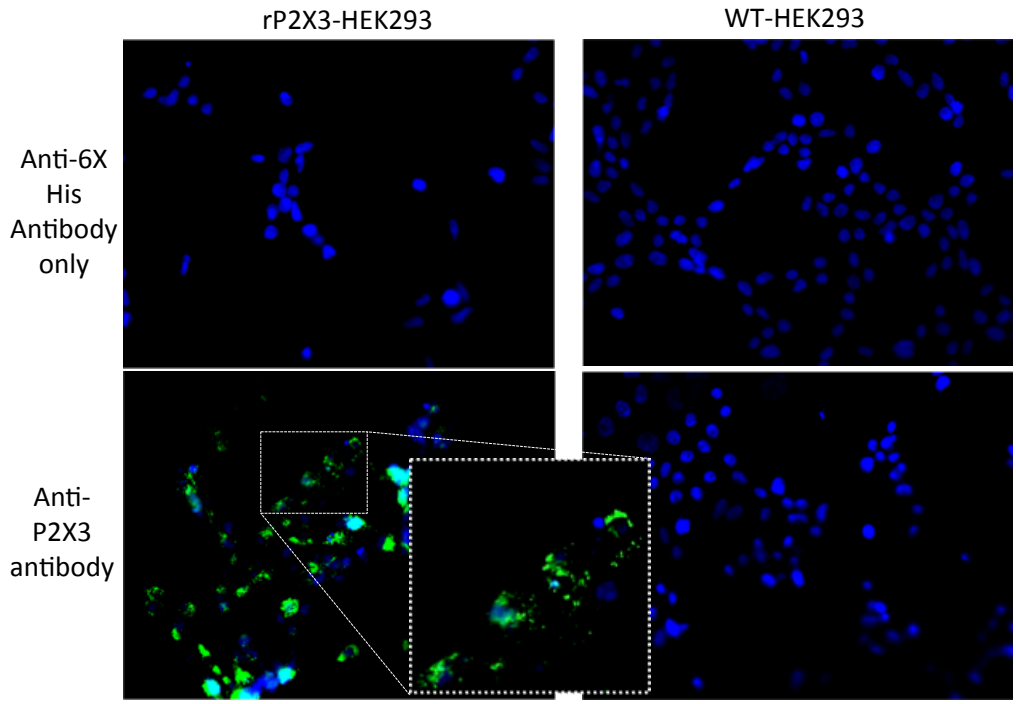

Figure 6.12. Rat P2X3 immunocytochemistry against live cells. Affimer and antibody were incubated on cells separately using the method described in Figure 6.8. Briefly, 1 µM of Affimer was incubated on cells in their live state for twenty minutes followed by washing with assay buffer. Cells were then fixed with 4% PFA and permeabilised using 0.1% Triton-X100 in PBS. Cells were then blocked in 1% milk in PBS. Cells were incubated in mouse anti-His antibody and antibody detected using anti-mouse-488 antibody. In addition, separate cells were stained using anti-P2X3 antibody (rabbit) that was detected using an anti-rabbit antibody conjugated to Alexa Fluor 488.

Subsequently, similarity in staining between Affimer and antibody was investigated for Affimers that specifically stained rP2X3-expressing cells (Affimers 1 and 7) (**Figure 6.13**). Results demonstrated a clear punctate staining pattern for both Affimer and antibody that appeared to overlap in regions suggesting co-localisation. However, staining appeared slightly different for each reagent. This difference may be a result of target epitope properties, as previously described. In additional experiments, no recognition of closely-related P2X family members, P2X2 and P2X7, could be observed (**Figure 6.13**, *far right*).

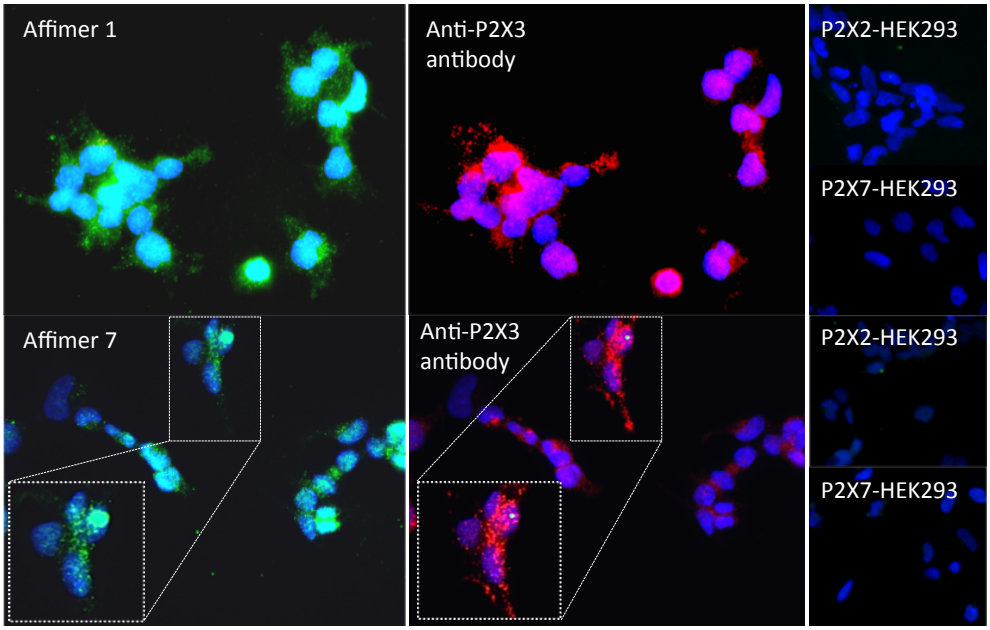

Figure 6.13. Co-staining of rP2X3 using Affimers 1 and 7 alongside anti-P2X3 antibody. Live cells were incubated with Affimers for twenty minutes prior to washing. Cells were then fixed and permeabilised before incubation with an anti-P2X3 antibody for one hour. Affimer was then detected using an anti-His antibody whilst anti-P2X3 was detected using a species-specific fluorescently labelled secondary antibody. In additional experiments, Affimers and anti-P2X3 antibody were also incubated on HEK293 cells stably expressing P2X2 and P2X7 ion channels (*far right panels*).

The ability of Affimers 1 and 7 to recognise both human and rat P2X3, an unsurprising observation considering the high homology between proteins (**Figure 6.14**), may yet prove useful for clinical studies if functional effects are elucidated in future experiments.

```
Human      MNCISDFFTYETTKSVVVKSWTIGIINRVVQLLIISYFVGWVFLHEKAYQVRDTAIESSV    60
Rat        MNCISDFFTYETTKSVVVKSWTIGIINRAVQLLIISYFVGWVFLHEKAYQVRDTAIESSV    60
           ****************************.******************************

Human      VTKVKGSGLYANRVMDVSDYVTPPQGTSVFVIITKMIVTENQMQGFCPESEEKYRCVSDS    120
Rat        VTKVKGFGRYANRVMDVSDYVTPPQGTSVFVIITKMIVTENQMQGFCPENEEKYRCVSDS    120
           ****** * ****************************************.**********

Human      QCGPERLPGGGILTGRCVNYSSVLRTCEIQGWCPTEVDTVETPIMMEAENFTIFIKNSIR    180
Rat        QCGPERFPGGGILTGRCVNYSSVLRTCEIQGWCPTEVDTVEMPIMMEAENFTIFIKNSIR    180
           ******:********************************* ******************

Human      FPLFNFEKGNLLPNLTARDMKTCRFHPDKDPFCPILRVGDVVKFAGQDFAKLARTGGVLG    240
Rat        FPLFNFEKGNLLPNLTDKDIKRCRFHPEKAPFCPILRVGDVVKFAGQDFAKLARTGGVLG    240
           **************** :*:* *****:* ******************************

Human      IKIGWVCDLDKAWDQCIPKYSFTRLDSVSEKSSVSPGYNFRFAKYYKMENGSEYRTLLKA    300
Rat        IKIGWVCDLDKAWDQCIPKYSFTRLDGVSEKSSVSPGYNFRFAKYYKMENGSEYRTLLKA    300
           **************************.*********************************

Human      FGIRFDVLVYGNAGKFNIIPTIISSVAAFTSVGVGTVLCDIILLNFLKGADQYKAKKFEE    360
Rat        FGIRFDVLVYGNAGKFNIIPTIISSVAAFTSVGVGTVLCDIILLNFLKGADHYKARKFEE    360
           ************************************************:***:****

Human      VNETTLKIAALTNPVYPSDQTTAEKQSTDSGAFSIGH   397
Rat        VTETTLKGTASTNPVFASDQATVEKQSTDSGAYSIGH   397
           *.***** :* ****: ***:*.*********:****
```

Figure 6.14. Sequence alignment of human and rat P2X3 prepared using Clustal Omega. A * is used to highlight sequence similarities.

6.3 Discussion

Binding reagents for targeting ion channels are highly sought for academic research as well as therapeutic use. Although antibodies have been successfully used for these purposes (Shcherbatko *et al.* 2016), various drawbacks have led to the development of alternative binding reagents (Bedford *et al.* 2017). However, the production of reagents towards ion channels is hindered by the difficulty in generating suitable proteins for screening. These problems have been confronted by a number of screening protocols such as screening target epitopes on intact mammalian cells or even present within tissues by *in vivo* phage display (Arap *et al.* 2002). The disadvantages of these methods however are similar to those encountered by classic hybridoma strategies as they are prone to unspecific binding to the abundance of antigens present in the display environment (Buchwalow *et al.* 2011, Wu *et al.* 2016). An alternative method for screening against membrane proteins is to assemble them in to artificial bilayers, such as nanoscale phospholipid bilayers, called nanodiscs (Pavlidou *et al.* 2013). This method brings various limitations of its own, for example, ensuring correct orientation of the membrane protein for presenting the extracellular region for phage display (Denisov and Sligar 2016). One method that can be used to ensure extracellular targeting is to screen against recombinant fragments of the ion channel extracellular regions, a method used previously for antibody generation by hybridoma technology (Jones *et al.* 2010, Lee *et al.* 2014).

In this chapter, a novel method for the identification of binding reagents against P2X3 is described. P2X3 has been validated as a major target for chronic pain disorders (Xu and Huang 2002, Xiang *et al.* 2008), targeting of which has shown promise in the clinic, with Afferent Pharmaceuticals' AF219 advancing to phase II of clinical trials (Abdulqawi *et al.* 2015). Additionally antibodies have started to show promise for targeting P2X3 channels, with Shcherbatko *et al* (2016) raising a panel of monoclonal antibodies against the full-length P2X3 receptor with a number of varied functional effects (Shcherbatko *et al.* 2016). Small molecules and antibodies each have their own drawbacks however, for example, poor selectivity and large molecular weight, respectively (Chames *et al.*

2009, Huggins *et al.* 2012). Affimer binding proteins could potentially overcome these issues due to their proven ability to distinguish between closely related proteins (Tiede *et al.* 2017) and relatively small molecular size when compared to antibodies.

In this work, a bacterial expression system was initially used to produce P2X3 ECD protein at a yield sufficient enough to screen against with our library. Expressing extracellular domains of ion channels has been reported previously by Hang et al (2000) in which segments of the α1 subunit of $GABA_A$ were expressed and shown to bind their ligand, benzodiazepine (BZD) (Hang *et al.* 2000). The presence of ordered α-helical and β-sheet structure in the P2X3 domain (Mansoor *et al.* 2016) provided initial validation that the expressed ECD protein may have been folded in a manner similar to the full-length, membrane-bound P2X3 ECD (**Figure 6.4**). To further analyse protein folding, the ability of P2X3 ECD segments to bind ATP, a native ligand of P2X3, was probed using a fluorescently labelled ATP analogue, MANT-ATP, in a FP assay (**Figure 6.5**). Although previous studies have demonstrated the ATP-binding site to be present within intersubunit domains of trimeric hP2X3 (Bodnar *et al.* 2011, Mansoor *et al.* 2016), our study suggests that the presence of a single domain can provide low affinity binding to ATP, an observation made from the high concentration of ATP required for a noticeable change in polarisation. This poor affinity would be expected considering the lack of two subunits that provide the binding site for ATP. In comparison to a handgrip model, the loss of neighbouring subunits, representing fingers of a hand, may still allow retention of a lower affinity binding, or grip. Indeed, studies have demonstrated that the mutagenesis of the nucleotide-binding domains can maintain ATP sensitivity, however even high concentrations of ATP (300 μM) were no longer able to saturate the receptor (Riedel *et al.* 2012). Further work has demonstrated the ability of $GABA_A$ α1 subunits expressed in bacteria to bind their native ligand, benzodiazepine (Xue *et al.* 1998, Hang *et al.* 2000, Shi *et al.* 2003). Another possibility in this study is that the individual P2X3 ECD segments are interacting with each other to form trimers and the ATP-binding site is in fact being produced via inter-subunit connectivity, thus providing the low level ATP interaction, a phenomenon

demonstrated by the closely-related rat P2X2 monomeric extracellular domains (Kim *et al.* 1997). In future experiments, this could be investigated by analysing the produced P2X3 ECD by size exclusion chromatography. This work suggests the possibility that bacterial expression of the P2X3 ion channel ECD can be carried out to an extent in which it is able to bind its native ligand, albeit, at a low level.

During the phage display procedure against P2X3, the presence of a contaminating protein in each purification of approximately 37kDa prompted a secondary screening step against mammalian produced P2X3 ectodomain protein. This validation took place against mammalian expressed P2X3 ECD conjugated to the Fc portion of an antibody (for improved solubility). The ability of Affimers to recognise mammalian-expressed P2X3 ECD further consolidated the possibility that accurate epitope had been expressed in bacteria and that identified Affimers were able to bind protein expressed in both systems. Subsequently, the ability of Affimers to identify full-length, trimeric P2X3 was investigated by immunocytochemistry. Initially, Affimers were tested for binding against P2X3 on cells fixed with 4% PFA however no signal could be detected against human or rat P2X3. When tested against P2X3 in its live state however, Affimers 1 and 7 demonstrated a P2X3-specific signal, indicated by only binding to cells when expressing P2X3. Although no obvious sequence similarity could be observed between the two Affimers, the suggested binding strengths observed from phage ELISA (**Figure 6.6**) may point to the recognition being a result of affinity, with only Affimers 1, 4 and 7 demonstrating an OD620 nm of >0.9. Interestingly, Affimer 4 was not able to recognise full-length P2X3 despite appearing stronger than Affimer 7 at binding, a characteristic that may be explained by the sequence similarity of the Affimers. Whilst Affimer 4 shares a variable region one WQΦ-ΦY--Q motif with Affimer 7, its second variable region shares no similarity (or very little) to either Affimer 1 or 7, yet Affimer 1 and 7 share a second variable region motif, T—KL (**Table 6.1**). Thus the second variable region of Affimer 4 may be causing impaired binding to full-length P2X3, for example, by recognising a region of the ion channel present in the intersection between two subunits.

In addition to the surge in interest surrounding P2X3 reagents for therapeutic use (Abdulqawi *et al.* 2015, Cully 2016, Jung *et al.* 2017), efforts have been made to expand the catalogue of reagents that can be used as imaging tools (Shcherbatko *et al.* 2016). Currently, the majority of imaging reagents on the market, namely antibodies, are raised against the C-terminal intracellular loop of P2X3. This provides two drawbacks; live cell imaging is not possible as antibodies can not be introduced across the cell membrane unless it is fixed and permeabilised, and additionally, the large size of antibodies limits their use in super-resolution microscopy.

In addition to targeting the extracellular domain of P2X3, the Affimers described in this chapter could be used in future experiments for live cell imaging due to their ability to fold in the reducing environment of the cytosol. Anti-F-actin Affimers have demonstrated the ability to bind to F-actin in live cells (Lopata *et al.* 2018). Furthermore, the small size of Affimers may yet provide advantages for imaging P2X3 by super-resolution microscopy, with examples of their success in this technique already published (Bedford *et al.* 2017, Tiede *et al.* 2017, Lopata *et al.* 2018, Schlichthaerle *et al.* 2018).

Whilst these Affimers are yet to be tested in functional assays, their ability to recognise both human and rat variants of P2X3 provides a property that may prove useful in the later stages of their development, for example, if validated in pre-clinical rodent models. Furthermore, their ability to selectively bind P2X3 with no recognition of P2X2 or P2X7 expressing cell lines (**Figure 6.13**, *inset*) further improves their therapeutic potential due to the different tissue localisation of P2X family members (Khakh *et al.* 2001) (**Table 6.2**).

P2X family member	Tissue localisation	Reference
P2X1	Smooth muscle, platelets	(Vial and Evans 2000, Hechler *et al.* 2003)
P2X2	Sensory epithelium, auditory neurons	(Housley *et al.* 1999)
P2X3	CNS	(Chen *et al.* 1995)
P2X4	CNS, blood vessels	(Soto *et al.* 1996, Stokes *et al.* 2017)
P2X5	Epithelium, gastrointestinal tract	(Groschel-Stewart *et al.* 1999, Ruan and Burnstock 2005)
P2X6	Kidney	(de Baaij *et al.* 2016)
P2X7	Epithelium, hematopoietic cells, CNS	(Groschel-Stewart *et al.* 1999, Sperlagh and Illes 2014)

Table 6.2. Tissue localisation of P2X family members.

In conclusion, this chapter describes the production and characterisation of recombinant P2X3 ECD protein for screening purposes, with subsequent identification and characterisation of Affimer reagents. The ability of Affimers to recognise trimeric P2X3 expressed heterologously also makes them potentially useful for studying the trafficking and endocytotic processing of P2X3 (Vacca *et al.* 2009). In addition, future studies may yet reveal a functional impact of the reagent, providing insights in to P2X3 modulation.

7 Discussion

This thesis describes the identification of Affimer reagents that are able to detect and modulate the ion channels, TRPV1 and P2X3. A number of problems cause difficulties in studying ion channels, for example, their hydrophobic membrane segments can cause aggregation when trying to produce protein for screening purposes. This presents problems for isolating biologics by methods such as phage display. Furthermore, the heterogeneous nature of membrane proteins can cause problems when trying to express a large population of homogeneous proteins for X-ray crystallography (White 2004). As a result, identifying small molecules by *in silico* screening is difficult as high-resolution data of the target protein is required. The work described in this thesis explores ways at improving both of these areas of ion channel drug discovery. In addition to investigating methods for the identification of Affimer reagents against ion channels, the use of Affimers in structural studies to guide the identification of small molecules is described.

In the first part of this study, a synthetic TRPV1 peptide was used in phage display screens for the isolation of Affimer reagents. The screened peptide mimicked a region of the outer pore domain of TRPV1 and a number of Affimer reagents were isolated that could modulate the full-length TRPV1 channel in the presence of capsaicin. Furthermore, one of these Affimers was able to detect TRPV1 by immunocytochemistry. The next part of this study focused on the optimisation of a cell-based phage display method. Despite the inability to detect ion channel proteins using this method, the method was used for isolating Affimers against the membrane protein, HSV1 gD. The final part of this study explored the production of recombinant P2X3 extracellular domain in various organisms followed by its use in Affimer phage display screens. Some of the Affimer reagents isolated were able to recognise the full-length P2X3 when expressed in mammalian cell lines.

In addition to exploring methods for the isolation of Affimer reagents against ion channels, this is the first study to investigate the use of non-antibody binding proteins for their use in designing small molecule mimetics towards ion

channels. One of the anti-TRPV1 Affimers that demonstrated the ability to potentiate TRPV1 response to capsaicin was crystallised in complex with its cognate peptide. The resulting crystal structure was used to screen for small molecule mimetics of this Affimer. Although this screen identified compounds that were able to modulate the TRPV1 ion channel, further work would be required to optimise the current compounds to enhance their potency. Additionally, studies are required to allow clear understanding of why their mechanism of action appears different to that observed for the Affimer from which they were designed. This work is likely to require structural studies of the identified small molecule in complex with the TRPV1 channel. Such structural information may then improve the compound identification and optimisation process.

7.1 Developing phage display methods for screening ion channel targets

A number of methods have been used to produce recombinant ion channel proteins for screening purposes. Recently, the overexpression of ion channels on *Tetrahymena thermophila* cells has been exploited by TetraGenetics in a technology termed TetraExpress^{TM} to enable drug discovery and the structure-based design of small molecules. Recently, an anti $K_v1.3$ nanobody was identified using this technique (Bednenko *et al.* 2018). An alternative method that has been used for the generation of antibodies against $Na_v1.7$ is the immunisation of animals with synthetic peptides mimicking the VSD of the channel protein (Lee *et al.* 2014). The study described in this thesis used a synthetic peptide mimicking a region of TRPV1 for the isolation of Affimer reagents by phage display.

During the TRPV1 peptide screen, the region of TRPV1 that the peptide mimicked was the outer pore domain. This region was selected based on previous studies in which the TRPV1 toxin, DkTx, has been identified to bind at this region resulting in the channels activation (Bohlen *et al.* 2010). Furthermore, based on the crystal structure of TRPV1 (Gao *et al.* 2016), this region was expected to allow access to the Affimer. A number of studies have investigated the use of synthetic peptides for generating antibodies that are able to inhibit ion channels. Miller *et al* (2014) isolated antibodies against the extracellular pore

loop of TRPM8 that were able to act as antagonists of the channel (Miller *et al.* 2014). Yang *et al* (2012) also identified $K_V1.3$ channel blockers using a similar technique in which rabbits were immunized using a peptide mimicking the pore region of the channel (Yang *et al.* 2012).

Other studies have also selected for binding reagents by screening against synthetic peptides. Koduvayur *et al* have recently described the generation of recombinant antibodies towards rat $GABA_A$ by selecting against peptides designed to mimic extracellular regions of the rat α1 and β2 $GABA_A$ subunits. The reagents identified in this study were able to recognise fully folded $GABA_A$ receptors expressed in *Xenopus laevis* oocytes and also native $GABA_A$ expressed in mouse retina (Koduvayur *et al.* 2014). Boshuizen *et al* adopted a similar technique to identify monoclonal antibodies able to bind to the human CXC chemokine receptor 2 (Boshuizen, 2014). In this study, structured peptides mimicking the ligand binding sites for CXC chemokine receptor 2 were screened against using a monoclonal antibody library. Isolated antibodies resulted in inhibition of the IL-8 and Gro-2 induced β-arrestin recruitment, a process driven by the CXC chemokine receptor 2. In a study conducted by Bagheri *et al* (2017), ScFv phage display libraries were selected against peptides mimicking a region of the extracellular domain of 4-1BB, a surface glycoprotein in the tumour necrosis factor receptor family that has been identified as a promising target in the treatment of cancer (Bagheri *et al.* 2017). The anti-41BB antibodies identified in this study enhanced surface CD69 expression and interleukin 2 production in stimulated CCRF-CEM cells, confirming agonistic effects of the identified antibodies. These studies all demonstrate the advantages of designing peptides as antigens for screening against. For example, being able to select regions of proteins that have specific ligand binding functions and so selecting for reagents that are likely to affect function of the desired protein target. However, in future studies that adopt this approach, it should also be noted that a number of disadvantages of screening peptides are present. For example, although binding reagents may be isolated against the screened peptide, these reagents may not necessarily recognise the full-length protein, due to conformational changes or inability to access the peptide region. In our study, only one of the identified

Affimers was able to detect full-length TRPV1 expressed at the surface of U-2 OS cells by immunocytochemical methods (Tiede *et al.* 2017). However, a number of the Affimers resulted in modulation of the channel in a functional assay, suggesting that binding was taking place. This modulation did however only take place in the presence of capsaicin, an agonist that opens the TRPV1 channel pore. It could therefore be suggested that the Affimers are only able to bind to the peptide region of TRPV1 following conformational change induced by capsaicin, allowing for access of Affimers to the pore. Future studies may focus on investigating this hypothesis. For example, capsaicin could be incorporated in to the immunocytochemical staining method. A potential reason for one of the Affimers to detect TRPV1 by immunocytochemical methods in the absence of capsaicin may be a result of its binding mode, with a binding orientation enabling access being adopted by this Affimer. Future work may focus on studying how this Affimer interacts with TRPV1, for example, elucidation of the complex of this Affimer with the full-length TRPV1 channel could be studied by cryo-EM.

Other studies may focus on optimisation of the Affimer cell staining protocol. For example, a different labelling strategy could be used. Previous observations have shown that detection of Affimer binding using an anti-His antibody is not always possible, with the His-tag sometimes occluded from binding. An alternative approach during ICC studies may be to directly conjugate the Affimer to a fluorophore, removing the need for a secondary detection antibody. Additionally, the inability of Affimers to bind to TRPV1 in fixed cells suggests that an alternative fixation method may be required. A recently described fixative, glyoxal (Richter *et al.* 2018), has shown promise when used for cell staining with Affimers as an alternative to PFA. Furthermore, although characterised by ICC studies, the use of this reagent in other detection methods such as western blot and immunoprecipitation still need to be optimised.

Despite the structure of TRPV1 in complex with DkTx being available, the resolution of 2.9 Å limits the ability to identify side chain interactions required for structure-guided drug design. It was hypothesised that the improved resolution of the structure in this study of Affimer 45 in complex with a peptide region of TRPV1 known to be amenable to functional modulation would allow for

the development of small molecules that could modulate TRPV1. A number of methods have been developed to try and stabilise proteins for crystallisation, such as forming co-complexes with ligands, or crystallisation chaperones. Although native antibodies are unsuitable as crystallisation chaperones due to their flexible linker region and bivalent mode of binding, a number of their fragments have been used to introduce stability in to target proteins structure for crystallography (Tormo *et al.* 1994, Hunte and Michel 2002). In addition to antibody fragments, a number of alternative scaffolds have been used for stabilising target proteins for structural studies including Affibodies and DARPins (Tolmachev *et al.* 2007, Sennhauser and Grutter 2008).

Although this thesis describes the identification of small molecule compounds that can modulate TRPV1, the observed effects were different to those of the Affimer they were designed to mimic. A potential explanation for this could be that the identified compounds are able to bind to TRPV1 with more or slightly different contact points to Affimer 45. As previously discussed, studies demonstrated the ability of a single amino acid mutation to convert peptides from inhibitors to activators (Brouwer *et al.* 2017). Alternatively, both of the Affimer 45 variable regions may be necessary to induce potentiation. In addition to future work on Affimer 45, such as variable region shuffling and deletions, to elucidate the importance of each variable region to the interaction with TRPV1 at the cell surface, future work may focus on improving the potency of the identified compounds. A method that could be used is to introduce more contact points between the compound and TRPV1. This method however has various difficulties. For example, to expand the small molecule contact points with TRPV1, a high resolution structure of TRPV1 would be required so that the compounds identified can be docked on to their correct epitope, from which increased contacts could be inserted and then compounds synthesised for *in vitro* testing.

Despite identifying Affimer 45 variants that were able to bind to the TRPV1 peptide with higher affinity, cell-based studies using these Affimers could not be conducted due to a shortage of time. Future studies could therefore look in to the improved functional effects that these Affimer 45 variants evoke.

Subsequent structural studies with these improved Affimer 45 variants could also result in identification of small molecules with improved functional properties. Another aspect of this work that could be studied would be to expand the number of amino acids of Affimer 45 that are mutated during the directed evolution procedure. Zahnd et al (2007) found that by mutation in the framework residues of an anti-HER2 DARPin altered this DARPin from a low nanomolar binder to a high picomolar binder (Zahnd *et al.* 2007). Therefore mutagenesis of Affimer 45 framework residues may provide useful information.

The next part of this study describes the production of the P2X3 ectodomain accompanied by the identification of Affimer reagents that were able to putatively detect P2X3 by immunocytochemistry. Currently, the majority of antibodies commercially available against P2X3 are raised against the intracellular C-terminus (Abcam; ab10269 and ab75453) and as a result, can only be used for staining of P2X3 when cells and tissues are fixed and permeabilised. The Affimers identified in this study therefore hold the advantage of being useful for studying P2X3 in its dynamic state. As a result, the trafficking behaviour of P2X3 can be studied. One study that described the production of antibodies against P2X3 immunised mice with full-length recombinant human P2X3 protein expressed by mammalian cells (Shcherbatko *et al.* 2016). The isolated antibodies were able to label P2X3 expressed on cells in their live state with inhibition of the receptor observed, a result of antibody-mediated internalisation of P2X3. In our study, incubation of P2X3-expressing cells with two of the Affimers isolated by phage display did appear to result in staining of intracellular structures. Future studies may firstly investigate whether this staining is a result of P2X3 internalisation and secondly, if such internalisation is driven by Affimers. To do this, staining of P2X3 at the cell membrane could be conducted against P2X3-expressing cells both treated and untreated with Affimer to elucidate whether the presence of Affimer drives P2X3 internalisation. In addition, staining of subcellular compartments could be used. The small size of the described Affimers may also be useful for super-resolution imaging of P2X3. An anti-HER4 Affimer has already shown its use in this technique (Tiede *et al.* 2017). More

recently, anti-actin Affimers have been combined with the technique termed DNA-PAINT for use in super-resolution microscopy (Schlichthaerle *et al.* 2018).

In this study, the generation of the P2X3 ectodomain was quite challenging. Bacterial production of the P2X3 ectodomain resulted in only insoluble protein and therefore re-folding was required. Following re-folding of the protein, a contaminating protein of ~37kDa could be observed in all conditions. Despite this, different CD results were observed, suggesting that the characteristics could be attributed to the P2X3 ECD protein produced. For example, lack of β-sheet structure observed in L44-T155, despite the presence of the contaminating protein, suggested that this structure being present in T155-N317 and L44-N317 was a result of the P2X3 ECD proteins themselves. Nevertheless, P2X3 ECD folding was further investigated by fluorescence polarisation. Previously, studies have reported on the production of $GABA_A$ receptor α-1 subunit ectodomain with correct folding confirmed by ligand binding assays. In this study, the use of a fluorescence polarisation assay confirmed benzodiazepine binding (Hang *et al.* 2000). Binding affinity was observed to be in the micromolar range rather than the nanomolar affinity observed between native $GABA_A$ receptors and benzodiazepine, a similar observation that we made in our study with micromolar binding between the produced P2X3 ectodomain and ATP measured – much higher than the affinity reported between ATP and trimeric, native P2X3 receptors.

Despite this confirmation of P2X3 structure from circular dichroism and fluorescence polarisation, the high level of glycosylation undergone by the native P2X3 ectodomain prompted the expression of the P2X3 ectodomain by mammalian cells to ensure Affimers were able to recognise glycosylated receptor. To improve the production of the P2X3 ectodomain in mammalian cells, a number of fusion proteins were used for conjugating to the P2X3 ectodomain. Previous studies have demonstrated improvements in the soluble expression of IL-13Rα-2 ectodomain when fused to the Fc region of human IgG (Davis *et al.* 2000). Following expression of a P2X3-Fc fusion protein in HEK293 cells, the phage clones isolated against the P2X3 protein produced in bacteria were taken through a final round of biopanning against mammalian produced

P2X3-Fc protein. After observing enrichment, individual clones were tested for binding against the P2X3-Fc protein with results demonstrating selective binding. Future studies may investigate the production of ion channel domains with a signal peptide for secretion to the periplasmic space, thus allowing for correct folding. This may remove the need to refold protein from inclusion bodies. The use of a signal peptide has been used for the bacterial production of the HIV integral membrane protein Vpu (Deb *et al.* 2017). In this study, the DNA encoding the Vpu membrane protein was cloned downstream of a PelB signal peptide which enabled the successful expression and purification of this otherwise difficult-to-express protein.

Despite the elucidation of the human P2X3 structure at high resolution (Mansoor *et al.* 2016) shortly after the production of the P2X3 ectodomain protein described in this study, the technique of producing ion channel ectodomains for use in structural studies might be useful. This technique has already been described for solving the extracellular domain structures of a nicotinic acetylcholine receptor (nAChR) (Smit *et al.* 2001) and a pentameric ligand-gated ion channel (pLGIC) from *Gloeobacter violaceus* (Nury *et al.* 2010). Furthermore, studying the structural interaction between Affimers and the P2X3 ectodomain may be useful. Prior to this however, future studies should focus on identifying any functional effects of the anti-P2X3 Affimers. Despite conducting preliminary testing to identify any functional properties of the Affimers, a shortage of time prevented complete testing. In these tests, Affimers were analysed for inhibitory and activatory effects by short incubation periods on P2X3-expressing cells. Results however demonstrated no effect. Future work may look in to longer incubation periods of Affimers with P2X3 before testing activity. Previous studies have demonstrated that despite observing no inhibitory activity of antibodies when incubated on P2X3 for 20 minutes, when this incubation period was extended to 20 hours, full inhibition could be observed by only 0.3 μM of antibody. In contrast, another antibody in the same study was able to inhibit the response of P2X3 to ATP when incubated on the receptor for only 20 minutes. This demonstrates the complexity of investigating the functional effects of binding reagents against P2X3 (Shcherbatko *et al.* 2016). If

indeed the isolated Affimers do not evoke a functional effect, subsequent screening strategies to try and identify functional Affimers may be required. Such screening strategies may incorporate the use of P2X3 protein in its ATP-bound form for example. By negatively selecting against the P2X3 protein in its unbound state, Affimer reagents able to bind specifically to P2X3 in its ATP-bound conformation could be identified. This could provide the advantage of identifying high affinity Affimers that can displace ATP from its binding site, preventing ATP-induced activation. Alternatively, this method may allow isolation of Affimer reagents that can bind to the pore region of P2X3 in its ATP-bound conformation. Such Affimers may act as channel pore blockers. Screening for binding reagents towards proteins in specific conformations has been conducted previously. ScFvs specific for the GTP-bound form of the GTPase Rab6 were isolated by selecting against the GTP-bound Rab6 (Nizak *et al.* 2003).

In the final part of this study, the development of a method for screening against membrane proteins in their native environment – the cell membrane, is described. In this study, the protein target HSV1 gD was selected as a model protein for two reasons. Firstly, the recombinant protein had been previously screened against using the Affimer library and thus it was already known that Affimers that were able to bind to HSV1 gD were present in the library. Secondly, the HSV1 gD extracellular domain is approximately 300 amino acids and thus of similar size to a number of ligand gated ion channel extracellular domains, therefore by optimising a protocol suitable for screening HSV1 gD, many of the ligand-gated ion channels could potentially be screened against using the same protocol. Following an initial screen using an Affimer library that had been enriched against recombinant HSV1 gD protein, the next step was to develop a protocol that could identify Affimer reagents from a naïve library. A number of studies have developed protocols for screening phage display libraries against mammalian cells. Many of these protocols require large numbers of cells that can be difficult to obtain when in limited supply, for example, when harvested from tissues. The method described in this thesis uses only a small number of cells in a 6-well plate. Furthermore, removal of centrifugation steps during the wash phase reduces cell loss during washing. Finally, fixation of cells using

paraformaldehyde during the phage ELISA enabled washing using a robotic plate washer, therefore increasing reproducibility of the procedure. A number of alternative protocols have been described including screening against cells in solution using centrifugation steps (Shimoni *et al.* 2013). In the study described in this thesis, alternating cell lines were also utilised between biopanning rounds to present the phage pools to a variety of background proteins to help reduce the number of non-specific phage in the phage pool. This technique has also been described by Jones *et al* (Jones *et al.* 2016).

Despite the use of the optimised screening strategy for identifying Affimers against HSV1 gD, subsequent screens against the ion channels, P2X3 and TRPV1 were unsuccessful in isolating Affimers. This may have been caused by a number of factors. For example, when screening against TRPV1, a protein with small extracellular loops, steric hindrance may have resulted from the presence of the truncated pIII phage coat protein conjugated to the Affimers during the phage display screen. This possibility was studied by ELISA in which Affimer 2, despite being able to bind TRPV1 (Tiede *et al.* 2017) was no longer able to do so when expressed as a pIII fusion (**Figure 5.11**). Further investigation in to the conjugation between Affimer and pIII coat protein may provide improved success when screening against cell-based targets. This may include use of a linker region between the Affimer and pIII or the use of a full-length pIII instead of a truncated pIII protein. These alterations could enable improved access of the Affimers to cell-based epitopes.

7.2 Affimers for use in structural studies

A number of Affimers have been crystallised in complex with their target proteins (Hughes *et al.* 2017, Michel *et al.* 2017, Robinson *et al.* 2018). The information gained from these studies, as previously mentioned, can be used for a number of purposes. In addition to the design of small molecule modulators that have more favourable pharmacological properties than Affimers, the information can be used to further improve on the properties of the Affimer itself by conducting mutagenesis studies to enhance the contact points between the Affimer and its target protein, thereby enhancing affinity.

Affimers that are able to inhibit the formation of SUMO-dependent protein-protein interactions have been isolated from the Affimer library with the molecular interaction between inhibitory Affimers and SUMO solved at high resolution (Hughes *et al.* 2017). This structural data enabled the mechanisms of selectivity of the Affimers for SUMO1 and SUMO2/3 to be understood in greater detail. Interestingly, two of the anti-SUMO Affimers isolated contained the amino acid residues (I/V) DLT in their variable regions, a consensus sequence shared with SUMO-interacting motifs (SIM's). Furthermore, some of the other Affimers isolated shared part of this consensus sequence. Finally, for one of the anti-SUMO1 Affimers, the second variable region was absent altogether. Both of these observations are also made in the work reported in this thesis, with the anti-TRPV1 Affimers containing a consensus WG sequence in variable region one that is found in DkTx, an anti-TRPV1 toxin. Additionally, the second variable region of anti-TRPV1 Affimers is truncated in the majority of clones. This demonstrates the ability to isolate Affimer reagents from the synthetic phage display library that are similar to protein ligands that have been generated in nature, suggesting the high level of complexity of the Affimer library. It also demonstrates the potential that a library containing only a single variable region may have in future experiments. This Affimer may provide advantages over the current Affimer as screening of smaller target proteins or access to binding pockets may be improved.

The structural interaction between anti-Ubiquitin Affimers and distinct ubiquitin (Ub) linkages has also been solved at high resolution, with Affimers bound to K6 and K33 Ub linkages solved at 2.5 and 2.8 Å resolution respectively (Michel *et al.* 2017). The structures solved demonstrated a similar mode of interaction to those observed between Ub and naturally occurring ubiquitin binding domains (UBD's), again demonstrating the ability to isolate Affimers that mimic naturally occurring proteins. This study also demonstrated improvements in binding following dimerization of Affimers, an experiment conducted for the anti-TRPV1 Affimer. In this study, the generation of a dimerized anti-TRPV1 Affimer demonstrated no improved binding characteristics towards the synthetic peptide by ELISA and also demonstrated no obvious improvement in ion channel

modulation. However, this may be a result of the linker region inserted between the two Affimer monomers. Despite choosing this linker region based on its presence in the DkTx toxin, the different sizes of the Affimers to the DkTx ICK may result in the requirement of a different linker length, work that still needs to be optimised.

The identification of anti-FcγRIIIa Affimers that were able to either directly inhibit function or modulate function allosterically along with their crystal structures demonstrated the difference in binding mode (Robinson *et al.* 2018). In this study, the Affimers were isolated against the FcγRIIIa ectodomain with functional effects observed against the full-length receptor, a similar screening method utilised for the anti-P2X3 Affimers described in this thesis. Furthermore, the screened ectodomain had been treated with glycosylase, demonstrating the ability of isolating Affimer reagents against non-glycosylated protein that are then able to recognise glycosylated protein. Additionally, SPR studies of isolated Affimers against glycosylated FcγRIIIa ectodomain and non-glycosylated ectodomain demonstrated little difference in binding affinity.

These studies all demonstrate the use of Affimer reagents as modulators of protein-protein interactions. The isolation of such Affimers coupled with the structural interaction at atomic resolution provides the ability to improve interactions to further improve the functional effect of the Affimer. Alternatively, as is described in this thesis, the structural interaction could be used to design different modulators altogether. The anti-TRPV1 Affimers isolated in this study have demonstrated preliminary data suggesting that the functional interaction between Affimers and their cognate ligand can indeed be exploited for the design of small molecule modulators of the target protein. Further work is required to build on this in terms of improving the effects of the identified small molecule compounds.

7.3 Conclusion

Affimer reagents have been described that demonstrate putative staining of the ion channels TRPV1 and P2X3 by immunocytochemical methods. Furthermore, modulation of TRPV1 function is induced by a number of the anti-TRPV1 Affimers

isolated. However, a number of opportunities have been highlighted for future experiments. Importantly, these experiments are required to further investigate some results that despite providing possible explanations for remain somewhat confounding. For example, the inability of some Affimers to detect TRPV1 by immunocytochemistry yet induce TRPV1 potentiation in functional assays.

Possibly the most exciting result of this study is the elucidation of the interaction between Affimer 45 and a TRPV1 peptide at atomic resolution. Future work with this Affimer may yet provide greater insights in to mechanisms of TRPV1 modulation. Finally, the compounds identified based on this interaction demonstrated *in vitro* functional effects. Further optimisation of these compounds may yield extremely useful reagents for studying TRPV1 function.

In all, this study demonstrates the potential of Affimer reagents in detecting and modulating ion channel function, with structural studies providing a mechanistic insight into such modulation.

8 References

(1999). Combinatorial Chemistry & High throughput Screening, Bentham Science Publishers.

Abdulqawi, R., R. Dockry, K. Holt, G. Layton, B. G. McCarthy, A. P. Ford and J. A. Smith (2015). "P2X3 receptor antagonist (AF-219) in refractory chronic cough: a randomised, double-blind, placebo-controlled phase 2 study." Lancet **385**(9974): 1198-1205.

Abraham, N., M. Healy, L. Ragnarsson, A. Brust, P. F. Alewood and R. J. Lewis (2017). "Structural mechanisms for alpha-conotoxin activity at the human alpha3beta4 nicotinic acetylcholine receptor." Sci Rep **7**: 45466.

Ackerman, M. J., J. J. Schroeder, R. Berry, D. J. Schaid, C. J. Porter, V. V. Michels and S. N. Thibodeau (1998). "A novel mutation in KVLQT1 is the molecular basis of inherited long QT syndrome in a near-drowning patient's family." Pediatr Res **44**(2): 148-153.

Ahuja, S., S. Mukund, L. Deng, K. Khakh, E. Chang, H. Ho, S. Shriver, C. Young, S. Lin, J. P. Johnson, Jr., P. Wu, J. Li, M. Coons, C. Tam, B. Brillantes, H. Sampang, K. Mortara, K. K. Bowman, K. R. Clark, A. Estevez, Z. Xie, H. Verschoof, M. Grimwood, C. Dehnhardt, J. C. Andrez, T. Focken, D. P. Sutherlin, B. S. Safina, M. A. Starovasnik, D. F. Ortwine, Y. Franke, C. J. Cohen, D. H. Hackos, C. M. Koth and J. Payandeh (2015). "Structural basis of Nav1.7 inhibition by an isoform-selective small-molecule antagonist." Science **350**(6267): aac5464.

Ai, T., Y. Fujiwara, K. Tsuji, H. Otani, S. Nakano, Y. Kubo and M. Horie (2002). "Novel KCNJ2 mutation in familial periodic paralysis with ventricular dysrhythmia." Circulation **105**(22): 2592-2594.

Akai, J., N. Makita, H. Sakurada, N. Shirai, K. Ueda, A. Kitabatake, K. Nakazawa, A. Kimura and M. Hiraoka (2000). "A novel SCN5A mutation associated with idiopathic ventricular fibrillation without typical ECG findings of Brugada syndrome." FEBS Lett **479**(1-2): 29-34.

Anand, P. and K. Bley (2011). "Topical capsaicin for pain management: therapeutic potential and mechanisms of action of the new high-concentration capsaicin 8% patch." Br J Anaesth **107**(4): 490-502.

Andelfinger, G., A. R. Tapper, R. C. Welch, C. G. Vanoye, A. L. George, Jr. and D. W. Benson (2002). "KCNJ2 mutation results in Andersen syndrome with sex-specific cardiac and skeletal muscle phenotypes." Am J Hum Genet **71**(3): 663-668.

Andolfo, I., R. Russo, F. Manna, B. E. Shmukler, A. Gambale, G. Vitiello, G. De Rosa, C. Brugnara, S. L. Alper, L. M. Snyder and A. Iolascon (2015). "Novel Gardos channel mutations linked to dehydrated hereditary stomatocytosis (xerocytosis)." Am J Hematol **90**(10): 921-926.

Andres-Enguix, I., L. Shang, P. J. Stansfeld, J. M. Morahan, M. S. Sansom, R. G. Lafreniere, B. Roy, L. R. Griffiths, G. A. Rouleau, G. C. Ebers, Z. M. Cader and S. J. Tucker (2012). "Functional analysis of missense variants in the TRESK (KCNK18) K channel." Sci Rep **2**: 237.

Antzelevitch, C., G. D. Pollevick, J. M. Cordeiro, O. Casis, M. C. Sanguinetti, Y. Aizawa, A. Guerchicoff, R. Pfeiffer, A. Oliva, B. Wollnik, P. Gelber, E. P. Bonaros,

Jr., E. Burashnikov, Y. Wu, J. D. Sargent, S. Schickel, R. Oberheiden, A. Bhatia, L. F. Hsu, M. Haissaguerre, R. Schimpf, M. Borggrefe and C. Wolpert (2007). "Loss-of-function mutations in the cardiac calcium channel underlie a new clinical entity characterized by ST-segment elevation, short QT intervals, and sudden cardiac death." Circulation **115**(4): 442-449.
Apicella, L. and E. Fabbretti (2012). "P2X3 receptor expression by HEK cells conditions their survival." Purinergic Signal **8**(2): 295-300.
Arap, W., M. G. Kolonin, M. Trepel, J. Lahdenranta, M. Cardo-Vila, R. J. Giordano, P. J. Mintz, P. U. Ardelt, V. J. Yao, C. I. Vidal, L. Chen, A. Flamm, H. Valtanen, L. M. Weavind, M. E. Hicks, R. E. Pollock, G. H. Botz, C. D. Bucana, E. Koivunen, D. Cahill, P. Troncoso, K. A. Baggerly, R. D. Pentz, K. A. Do, C. J. Logothetis and R. Pasqualini (2002). "Steps toward mapping the human vasculature by phage display." Nat Med **8**(2): 121-127.
Ataka, K. and V. A. Pieribone (2002). "A genetically targetable fluorescent probe of channel gating with rapid kinetics." Biophys J **82**(1 Pt 1): 509-516.
Baconguis, I., C. J. Bohlen, A. Goehring, D. Julius and E. Gouaux (2014). "X-ray structure of acid-sensing ion channel 1-snake toxin complex reveals open state of a Na(+)-selective channel." Cell **156**(4): 717-729.
Bae, C., C. Anselmi, J. Kalia, A. Jara-Oseguera, C. D. Schwieters, D. Krepkiy, C. Won Lee, E. H. Kim, J. I. Kim, J. D. Faraldo-Gomez and K. J. Swartz (2016). "Structural insights into the mechanism of activation of the TRPV1 channel by a membrane-bound tarantula toxin." Elife **5**.
Bagheri, S., M. Yousefi, E. Safaie Qamsari, F. Riazi-Rad, M. Abolhassani, V. Younesi, R. Dorostkar, A. A. Movassaghpour and Z. Sharifzadeh (2017). "Selection of single chain antibody fragments binding to the extracellular domain of 4-1BB receptor by phage display technology." Tumour Biol **39**(3): 1010428317695924.
Baker, M. (2015). "Reproducibility crisis: Blame it on the antibodies." Nature **521**(7552): 274-276.
Banerjee, A., A. Lee, E. Campbell and R. Mackinnon (2013). "Structure of a pore-blocking toxin in complex with a eukaryotic voltage-dependent K(+) channel." Elife **2**: e00594.
Bao, L., A. M. Rapin, E. C. Holmstrand and D. H. Cox (2002). "Elimination of the BK(Ca) channel's high-affinity Ca(2+) sensitivity." J Gen Physiol **120**(2): 173-189.
Barel, O., S. A. Shalev, R. Ofir, A. Cohen, J. Zlotogora, Z. Shorer, G. Mazor, G. Finer, S. Khateeb, N. Zilberberg and O. S. Birk (2008). "Maternally inherited Birk Barel mental retardation dysmorphism syndrome caused by a mutation in the genomically imprinted potassium channel KCNK9." Am J Hum Genet **83**(2): 193-199.
Bartok, A., K. Feher, A. Bodor, K. Rakosi, G. K. Toth, K. E. Kover, G. Panyi and Z. Varga (2015). "An engineered scorpion toxin analogue with improved Kv1.3 selectivity displays reduced conformational flexibility." Sci Rep **5**: 18397.
Battistini, S., S. Stenirri, M. Piatti, C. Gelfi, P. G. Righetti, R. Rocchi, F. Giannini, N. Battistini, G. C. Guazzi, M. Ferrari and P. Carrera (1999). "A new CACNA1A gene mutation in acetazolamide-responsive familial hemiplegic migraine and ataxia." Neurology **53**(1): 38-43.
Bech-Hansen, N. T., M. J. Naylor, T. A. Maybaum, W. G. Pearce, B. Koop, G. A. Fishman, M. Mets, M. A. Musarella and K. M. Boycott (1998). "Loss-of-function

mutations in a calcium-channel alpha1-subunit gene in Xp11.23 cause incomplete X-linked congenital stationary night blindness." Nat Genet **19**(3): 264-267.
Bedford, R., C. Tiede, R. Hughes, A. Curd, M. J. McPherson, M. Peckham and D. C. Tomlinson (2017). "Alternative reagents to antibodies in imaging applications." Biophys Rev.
Bednenko, J., R. Harriman, L. Marien, H. M. Nguyen, A. Agrawal, A. Papoyan, Y. Bisharyan, J. Cardarelli, D. Cassidy-Hanley, T. Clark, D. Pedersen, Y. Abdiche, W. Harriman, B. van der Woning, H. de Haard, E. Collarini, H. Wulff and P. Colussi (2018). "A multiplatform strategy for the discovery of conventional monoclonal antibodies that inhibit the voltage-gated potassium channel Kv1.3." MAbs **10**(4): 636-650.
Bendahhou, S., E. Fournier, D. Sternberg, G. Bassez, A. Furby, C. Sereni, M. R. Donaldson, M. M. Larroque, B. Fontaine and J. Barhanin (2005). "In vivo and in vitro functional characterization of Andersen's syndrome mutations." J Physiol **565**(Pt 3): 731-741.
Beneski, D. A. and W. A. Catterall (1980). "Covalent labeling of protein components of the sodium channel with a photoactivable derivative of scorpion toxin." Proc Natl Acad Sci U S A **77**(1): 639-643.
Benson, D. W., D. W. Wang, M. Dyment, T. K. Knilans, F. A. Fish, M. J. Strieper, T. H. Rhodes and A. L. George, Jr. (2003). "Congenital sick sinus syndrome caused by recessive mutations in the cardiac sodium channel gene (SCN5A)." J Clin Invest **112**(7): 1019-1028.
Bergeron, Z. L. and J. P. Bingham (2012). "Scorpion toxins specific for potassium (K+) channels: a historical overview of peptide bioengineering." Toxins (Basel) **4**(11): 1082-1119.
Berrow, N. S., D. Alderton and R. J. Owens (2009). "The precise engineering of expression vectors using high-throughput In-Fusion PCR cloning." Methods Mol Biol **498**: 75-90.
Berrow, N. S., D. Alderton, S. Sainsbury, J. Nettleship, R. Assenberg, N. Rahman, D. I. Stuart and R. J. Owens (2007). "A versatile ligation-independent cloning method suitable for high-throughput expression screening applications." Nucleic Acids Res **35**(6): e45.
Binz, H. K., M. T. Stumpp, P. Forrer, P. Amstutz and A. Pluckthun (2003). "Designing repeat proteins: well-expressed, soluble and stable proteins from combinatorial libraries of consensus ankyrin repeat proteins." J Mol Biol **332**(2): 489-503.
Bittner, S., N. Bobak, M. Feuchtenberger, A. M. Herrmann, K. Gobel, R. W. Kinne, A. J. Hansen, T. Budde, C. Kleinschnitz, O. Frey, H. P. Tony, H. Wiendl and S. G. Meuth (2011). "Expression of K2P5.1 potassium channels on CD4+ T lymphocytes correlates with disease activity in rheumatoid arthritis patients." Arthritis Res Ther **13**(1): R21.
Bodnar, M., H. Wang, T. Riedel, S. Hintze, E. Kato, G. Fallah, H. Groger-Arndt, R. Giniatullin, M. Grohmann, R. Hausmann, G. Schmalzing, P. Illes and P. Rubini (2011). "Amino acid residues constituting the agonist binding site of the human P2X3 receptor." J Biol Chem **286**(4): 2739-2749.

Bohlen, C. J., A. Priel, S. Zhou, D. King, J. Siemens and D. Julius (2010). "A bivalent tarantula toxin activates the capsaicin receptor, TRPV1, by targeting the outer pore domain." Cell **141**(5): 834-845.
Bourne, Y., T. T. Talley, S. B. Hansen, P. Taylor and P. Marchot (2005). "Crystal structure of a Cbtx-AChBP complex reveals essential interactions between snake alpha-neurotoxins and nicotinic receptors." EMBO J **24**(8): 1512-1522.
Bowman, C. L., P. A. Gottlieb, T. M. Suchyna, Y. K. Murphy and F. Sachs (2007). "Mechanosensitive ion channels and the peptide inhibitor GsMTx-4: history, properties, mechanisms and pharmacology." Toxicon **49**(2): 249-270.
Bradbury, A. and A. Pluckthun (2015). "Reproducibility: Standardize antibodies used in research." Nature **518**(7537): 27-29.
Braga, R. C., V. M. Alves, M. F. Silva, E. Muratov, D. Fourches, A. Tropsha and C. H. Andrade (2014). "Tuning HERG out: antitarget QSAR models for drug development." Curr Top Med Chem **14**(11): 1399-1415.
Brain, S. D. (2011). "TRPV1 and TRPA1 channels in inflammatory pain: elucidating mechanisms." Ann N Y Acad Sci **1245**: 36-37.
Brouwer, J. M., P. Lan, A. D. Cowan, J. P. Bernardini, R. W. Birkinshaw, M. F. van Delft, B. E. Sleebs, A. Y. Robin, A. Wardak, I. K. Tan, B. Reljic, E. F. Lee, W. D. Fairlie, M. J. Call, B. J. Smith, G. Dewson, G. Lessene, P. M. Colman and P. E. Czabotar (2017). "Conversion of Bim-BH3 from Activator to Inhibitor of Bak through Structure-Based Design." Mol Cell **68**(4): 659-672 e659.
Brown, D. C., M. J. Iadarola, S. Z. Perkowski, H. Erin, F. Shofer, K. J. Laszlo, Z. Olah and A. J. Mannes (2005). "Physiologic and antinociceptive effects of intrathecal resiniferatoxin in a canine bone cancer model." Anesthesiology **103**(5): 1052-1059.
Browne, D. L., S. T. Gancher, J. G. Nutt, E. R. Brunt, E. A. Smith, P. Kramer and M. Litt (1994). "Episodic ataxia/myokymia syndrome is associated with point mutations in the human potassium channel gene, KCNA1." Nat Genet **8**(2): 136-140.
Buchwalow, I., V. Samoilova, W. Boecker and M. Tiemann (2011). "Non-specific binding of antibodies in immunohistochemistry: fallacies and facts." Sci Rep **1**: 28.
Bulman, D. E., K. A. Scoggan, M. D. van Oene, M. W. Nicolle, A. F. Hahn, L. L. Tollar and G. C. Ebers (1999). "A novel sodium channel mutation in a family with hypokalemic periodic paralysis." Neurology **53**(9): 1932-1936.
Carrera, P., M. Piatti, S. Stenirri, L. M. Grimaldi, E. Marchioni, M. Curcio, P. G. Righetti, M. Ferrari and C. Gelfi (1999). "Genetic heterogeneity in Italian families with familial hemiplegic migraine." Neurology **53**(1): 26-33.
Caterina, M. J., M. A. Schumacher, M. Tominaga, T. A. Rosen, J. D. Levine and D. Julius (1997). "The capsaicin receptor: a heat-activated ion channel in the pain pathway." Nature **389**(6653): 816-824.
Catterall, W. (2011). Voltage-gated calcium channels, Cold Spring Harbour Perspectives in Biology.
Catterall, W. A. (1995). "Structure and function of voltage-gated ion channels." Annu Rev Biochem **64**: 493-531.

Chames, P., M. Van Regenmortel, E. Weiss and D. Baty (2009). "Therapeutic antibodies: successes, limitations and hopes for the future." Br J Pharmacol **157**(2): 220-233.
Chatelain, F. C., D. Bichet, D. Douguet, S. Feliciangeli, S. Bendahhou, M. Reichold, R. Warth, J. Barhanin and F. Lesage (2012). "TWIK1, a unique background channel with variable ion selectivity." Proc Natl Acad Sci U S A **109**(14): 5499-5504.
Chen, C. C., A. N. Akopian, L. Sivilotti, D. Colquhoun, G. Burnstock and J. N. Wood (1995). "A P2X purinoceptor expressed by a subset of sensory neurons." Nature **377**(6548): 428-431.
Chen, R., A. Robinson, D. Gordon and S. H. Chung (2011). "Modeling the binding of three toxins to the voltage-gated potassium channel (Kv1.3)." Biophys J **101**(11): 2652-2660.
Chen, X. Q., B. Wang, C. Wu, J. Pan, B. Yuan, Y. Y. Su, X. Y. Jiang, X. Zhang and L. Bao (2012). "Endosome-mediated retrograde axonal transport of P2X3 receptor signals in primary sensory neurons." Cell Res **22**(4): 677-696.
Chen, Y., J. Lu, H. Pan, Y. Zhang, H. Wu, K. Xu, X. Liu, Y. Jiang, X. Bao, Z. Yao, K. Ding, W. H. Lo, B. Qiang, P. Chan, Y. Shen and X. Wu (2003). "Association between genetic variation of CACNA1H and childhood absence epilepsy." Ann Neurol **54**(2): 239-243.
Chen, Y. H., S. J. Xu, S. Bendahhou, X. L. Wang, Y. Wang, W. Y. Xu, H. W. Jin, H. Sun, X. Y. Su, Q. N. Zhuang, Y. Q. Yang, Y. B. Li, Y. Liu, H. J. Xu, X. F. Li, N. Ma, C. P. Mou, Z. Chen, J. Barhanin and W. Huang (2003). "KCNQ1 gain-of-function mutation in familial atrial fibrillation." Science **299**(5604): 251-254.
Cho, Y. S., C. H. Chen, C. Hu, J. Long, R. T. Ong, X. Sim, F. Takeuchi, Y. Wu, M. J. Go, T. Yamauchi, Y. C. Chang, S. H. Kwak, R. C. Ma, K. Yamamoto, L. S. Adair, T. Aung, Q. Cai, L. C. Chang, Y. T. Chen, Y. Gao, F. B. Hu, H. L. Kim, S. Kim, Y. J. Kim, J. J. Lee, N. R. Lee, Y. Li, J. J. Liu, W. Lu, J. Nakamura, E. Nakashima, D. P. Ng, W. T. Tay, F. J. Tsai, T. Y. Wong, M. Yokota, W. Zheng, R. Zhang, C. Wang, W. Y. So, K. Ohnaka, H. Ikegami, K. Hara, Y. M. Cho, N. H. Cho, T. J. Chang, Y. Bao, A. K. Hedman, A. P. Morris, M. I. McCarthy, D. Consortium, T. C. Mu, R. Takayanagi, K. S. Park, W. Jia, L. M. Chuang, J. C. Chan, S. Maeda, T. Kadowaki, J. Y. Lee, J. Y. Wu, Y. Y. Teo, E. S. Tai, X. O. Shu, K. L. Mohlke, N. Kato, B. G. Han and M. Seielstad (2012). "Meta-analysis of genome-wide association studies identifies eight new loci for type 2 diabetes in east Asians." Nat Genet **44**(1): 67-72.
Christophersen, I. E., M. S. Olesen, B. Liang, M. N. Andersen, A. P. Larsen, J. B. Nielsen, S. Haunso, S. P. Olesen, A. Tveit, J. H. Svendsen and N. Schmitt (2013). "Genetic variation in KCNA5: impact on the atrial-specific potassium current IKur in patients with lone atrial fibrillation." Eur Heart J **34**(20): 1517-1525.
ClinicalTrials.gov. (2014). "Resiniferatoxin to Treat Severe Pain Associated With Advanced Cancer; NCT00804154." 2015.
Colombo, C., M. Delvecchio, C. Zecchino, M. F. Faienza, L. Cavallo, F. Barbetti, E. Early Onset Diabetes Study Group of the Italian Society of Paediatric and Diabetology (2005). "Transient neonatal diabetes mellitus is associated with a recurrent (R201H) KCNJ11 (KIR6.2) mutation." Diabetologia **48**(11): 2439-2441.
Coutelier, M., I. Blesneac, A. Monteil, M. L. Monin, K. Ando, E. Mundwiller, A. Brusco, I. Le Ber, M. Anheim, A. Castrioto, C. Duyckaerts, A. Brice, A. Durr, P. Lory

and G. Stevanin (2015). "A Recurrent Mutation in CACNA1G Alters Cav3.1 T-Type Calcium-Channel Conduction and Causes Autosomal-Dominant Cerebellar Ataxia." Am J Hum Genet **97**(5): 726-737.
Cox, J. J., J. Sheynin, Z. Shorer, F. Reimann, A. K. Nicholas, L. Zubovic, M. Baralle, E. Wraige, E. Manor, J. Levy, C. G. Woods and R. Parvari (2010). "Congenital insensitivity to pain: novel SCN9A missense and in-frame deletion mutations." Hum Mutat **31**(9): E1670-1686.
Cully, M. (2016). "Deal watch: Merck bets on purine receptor revival." Nat Rev Drug Discov **15**(8): 525.
Curtis, B. M. and W. A. Catterall (1984). "Purification of the calcium antagonist receptor of the voltage-sensitive calcium channel from skeletal muscle transverse tubules." Biochemistry **23**(10): 2113-2118.
Curtis, B. M. and W. A. Catterall (1986). "Reconstitution of the voltage-sensitive calcium channel purified from skeletal muscle transverse tubules." Biochemistry **25**(11): 3077-3083.
D'Avanzo, N., S. J. Lee, W. W. Cheng and C. G. Nichols (2013). "Energetics and location of phosphoinositide binding in human Kir2.1 channels." J Biol Chem **288**(23): 16726-16737.
Danquah, W., C. Meyer-Schwesinger, B. Rissiek, C. Pinto, A. Serracant-Prat, M. Amadi, D. Iacenda, J. H. Knop, A. Hammel, P. Bergmann, N. Schwarz, J. Assuncao, W. Rotthier, F. Haag, E. Tolosa, P. Bannas, E. Boue-Grabot, T. Magnus, T. Laeremans, C. Stortelers and F. Koch-Nolte (2016). "Nanobodies that block gating of the P2X7 ion channel ameliorate inflammation." Sci Transl Med **8**(366): 366ra162.
Davis, R., K. Schooley, B. Rasmussen, J. Thomas and P. Reddy (2000). "Effect of PDI overexpression on recombinant protein secretion in CHO cells." Biotechnol Prog **16**(5): 736-743.
Dawson, R. J., J. Benz, P. Stohler, T. Tetaz, C. Joseph, S. Huber, G. Schmid, D. Hugin, P. Pflimlin, G. Trube, M. G. Rudolph, M. Hennig and A. Ruf (2012). "Structure of the acid-sensing ion channel 1 in complex with the gating modifier Psalmotoxin 1." Nat Commun **3**: 936.
de Baaij, J. H., A. Kompatscher, D. H. Viering, C. Bos, R. J. Bindels and J. G. Hoenderop (2016). "P2X6 Knockout Mice Exhibit Normal Electrolyte Homeostasis." PLoS One **11**(6): e0156803.
De Schepper, H. U., B. Y. De Winter, L. Van Nassauw, J. P. Timmermans, A. G. Herman, P. A. Pelckmans and J. G. De Man (2008). "TRPV1 receptors on unmyelinated C-fibres mediate colitis-induced sensitization of pelvic afferent nerve fibres in rats." J Physiol **586**(21): 5247-5258.
de Wet, H. and P. Proks (2015). "Molecular action of sulphonylureas on KATP channels: a real partnership between drugs and nucleotides." Biochem Soc Trans **43**(5): 901-907.
Deb, A., W. A. Johnson, A. P. Kline, B. J. Scott, L. R. Meador, D. Srinivas, J. M. Martin-Garcia, K. Dorner, C. R. Borges, R. Misra, B. G. Hogue, P. Fromme and T. S. Mor (2017). "Bacterial expression, correct membrane targeting and functional folding of the HIV-1 membrane protein Vpu using a periplasmic signal peptide." PLoS One **12**(2): e0172529.

Dedek, K., B. Kunath, C. Kananura, U. Reuner, T. J. Jentsch and O. K. Steinlein (2001). "Myokymia and neonatal epilepsy caused by a mutation in the voltage sensor of the KCNQ2 K+ channel." Proc Natl Acad Sci U S A **98**(21): 12272-12277.
del Camino, D. and G. Yellen (2001). "Tight steric closure at the intracellular activation gate of a voltage-gated K(+) channel." Neuron **32**(4): 649-656.
Dellisanti, C. D., Y. Yao, J. C. Stroud, Z. Z. Wang and L. Chen (2007). "Crystal structure of the extracellular domain of nAChR alpha1 bound to alpha-bungarotoxin at 1.94 A resolution." Nat Neurosci **10**(8): 953-962.
Denier, C., A. Ducros, A. Durr, B. Eymard, B. Chassande and E. Tournier-Lasserve (2001). "Missense CACNA1A mutation causing episodic ataxia type 2." Arch Neurol **58**(2): 292-295.
Denisov, I. G. and S. G. Sligar (2016). "Nanodiscs for structural and functional studies of membrane proteins." Nat Struct Mol Biol **23**(6): 481-486.
Dhaka, A., V. Uzzell, A. E. Dubin, J. Mathur, M. Petrus, M. Bandell and A. Patapoutian (2009). "TRPV1 is activated by both acidic and basic pH." J Neurosci **29**(1): 153-158.
Dib-Hajj, S. D., A. M. Rush, T. R. Cummins, F. M. Hisama, S. Novella, L. Tyrrell, L. Marshall and S. G. Waxman (2005). "Gain-of-function mutation in Nav1.7 in familial erythromelalgia induces bursting of sensory neurons." Brain **128**(Pt 8): 1847-1854.
Dillon, D. G., R. Bogdan, J. Fagerness, A. J. Holmes, R. H. Perlis and D. A. Pizzagalli (2010). "Variation in TREK1 gene linked to depression-resistant phenotype is associated with potentiated neural responses to rewards in humans." Hum Brain Mapp **31**(2): 210-221.
Diochot, S., A. Baron, L. D. Rash, E. Deval, P. Escoubas, S. Scarzello, M. Salinas and M. Lazdunski (2004). "A new sea anemone peptide, APETx2, inhibits ASIC3, a major acid-sensitive channel in sensory neurons." EMBO J **23**(7): 1516-1525.
Diochot, S., A. Baron, M. Salinas, D. Douguet, S. Scarzello, A. S. Dabert-Gay, D. Debayle, V. Friend, A. Alloui, M. Lazdunski and E. Lingueglia (2012). "Black mamba venom peptides target acid-sensing ion channels to abolish pain." Nature **490**(7421): 552-555.
Donaldson, M. R., J. L. Jensen, M. Tristani-Firouzi, R. Tawil, S. Bendahhou, W. A. Suarez, A. M. Cobo, J. J. Poza, E. Behr, J. Wagstaff, P. Szepetowski, S. Pereira, T. Mozaffar, D. M. Escolar, Y. H. Fu and L. J. Ptacek (2003). "PIP2 binding residues of Kir2.1 are common targets of mutations causing Andersen syndrome." Neurology **60**(11): 1811-1816.
Donger, C., I. Denjoy, M. Berthet, N. Neyroud, C. Cruaud, M. Bennaceur, G. Chivoret, K. Schwartz, P. Coumel and P. Guicheney (1997). "KVLQT1 C-terminal missense mutation causes a forme fruste long-QT syndrome." Circulation **96**(9): 2778-2781.
Doyle, D. A., J. Morais Cabral, R. A. Pfuetzner, A. Kuo, J. M. Gulbis, S. L. Cohen, B. T. Chait and R. MacKinnon (1998). "The structure of the potassium channel: molecular basis of K+ conduction and selectivity." Science **280**(5360): 69-77.
Du, W., J. F. Bautista, H. Yang, A. Diez-Sampedro, S. A. You, L. Wang, P. Kotagal, H. O. Luders, J. Shi, J. Cui, G. B. Richerson and Q. K. Wang (2005). "Calcium-sensitive potassium channelopathy in human epilepsy and paroxysmal movement disorder." Nat Genet **37**(7): 733-738.

Eid, S. R. (2009). TRPV1 Antagonists: are they too hot to handle? 3rd Annual Pain Therapeutics Summit in Summit, Summit, New Jersey.
Eid, S. R., E. D. Crown, E. L. Moore, H. A. Liang, K. C. Choong, S. Dima, D. A. Henze, S. A. Kane and M. O. Urban (2008). "HC-030031, a TRPA1 selective antagonist, attenuates inflammatory- and neuropathy-induced mechanical hypersensitivity." Mol Pain **4**: 48.
Eisenhardt, S. U., M. Schwarz, N. Bassler and K. Peter (2007). "Subtractive single-chain antibody (scFv) phage-display: tailoring phage-display for high specificity against function-specific conformations of cell membrane molecules." Nat Protoc **2**(12): 3063-3073.
Ellis, S. B., M. E. Williams, N. R. Ways, R. Brenner, A. H. Sharp, A. T. Leung, K. P. Campbell, E. McKenna, W. J. Koch, A. Hui and et al. (1988). "Sequence and expression of mRNAs encoding the alpha 1 and alpha 2 subunits of a DHP-sensitive calcium channel." Science **241**(4873): 1661-1664.
Enna, S. J. and K. E. McCarson (2006). "The role of GABA in the mediation and perception of pain." Adv Pharmacol **54**: 1-27.
Enyedi, P. and G. Czirjak (2010). "Molecular background of leak K+ currents: two-pore domain potassium channels." Physiol Rev **90**(2): 559-605.
Es-Salah-Lamoureux, Z., D. F. Steele and D. Fedida (2010). "Research into the therapeutic roles of two-pore-domain potassium channels." Trends Pharmacol Sci **31**(12): 587-595.
Escayg, A. and A. L. Goldin (2010). "Sodium channel SCN1A and epilepsy: mutations and mechanisms." Epilepsia **51**(9): 1650-1658.
Fainzilber, M., J. C. Lodder, R. C. van der Schors, K. W. Li, Z. Yu, A. L. Burlingame, W. P. Geraerts and K. S. Kits (1996). "A novel hydrophobic omega-conotoxin blocks molluscan dihydropyridine-sensitive calcium channels." Biochemistry **35**(26): 8748-8752.
Feng, Z. P., J. Hamid, C. Doering, G. M. Bosey, T. P. Snutch and G. W. Zamponi (2001). "Residue Gly1326 of the N-type calcium channel alpha 1B subunit controls reversibility of omega-conotoxin GVIA and MVIIA block." J Biol Chem **276**(19): 15728-15735.
Ferreira Junior, W. A., A. J. Zaharenko, K. Kazuma, G. Picolo, V. P. Gutierrez, J. C. de Freitas, K. Konno and Y. Cury (2017). "Peripheral 5-HT3 Receptors Are Involved in the Antinociceptive Effect of Bunodosine 391." Toxins (Basel) **10**(1).
Fertleman, C. R., M. D. Baker, K. A. Parker, S. Moffatt, F. V. Elmslie, B. Abrahamsen, J. Ostman, N. Klugbauer, J. N. Wood, R. M. Gardiner and M. Rees (2006). "SCN9A mutations in paroxysmal extreme pain disorder: allelic variants underlie distinct channel defects and phenotypes." Neuron **52**(5): 767-774.
Fischer, A., B. Schmid, D. Ellinghaus, M. Nothnagel, K. I. Gaede, M. Schurmann, S. Lipinski, P. Rosenstiel, G. Zissel, K. Hohne, M. Petrek, V. Kolek, S. Pabst, C. Grohe, J. Grunewald, M. Ronninger, A. Eklund, L. Padyukov, C. Gieger, H. E. Wichmann, A. Nebel, A. Franke, J. Muller-Quernheim, S. Hofmann and S. Schreiber (2012). "A novel sarcoidosis risk locus for Europeans on chromosome 11q13.1." Am J Respir Crit Care Med **186**(9): 877-885.
Flinspach, M., Q. Xu, A. D. Piekarz, R. Fellows, R. Hagan, A. Gibbs, Y. Liu, R. A. Neff, J. Freedman, W. A. Eckert, M. Zhou, R. Bonesteel, M. W. Pennington, K. A. Eddinger, T. L. Yaksh, M. Hunter, R. V. Swanson and A. D. Wickenden (2017).

"Insensitivity to pain induced by a potent selective closed-state Nav1.7 inhibitor." Sci Rep **7**: 39662.
Forrer, P., H. K. Binz, M. T. Stumpp and A. Pluckthun (2004). "Consensus design of repeat proteins." Chembiochem **5**(2): 183-189.
Frenzel, A., M. Hust and T. Schirrmann (2013). "Expression of recombinant antibodies." Front Immunol **4**: 217.
Freudenthal, B., D. Kulaveerasingam, L. Lingappa, M. A. Shah, L. Brueton, E. Wassmer, M. Ognjanovic, N. Dorison, M. Reichold, D. Bockenhauer, R. Kleta and A. A. Zdebik (2011). "KCNJ10 mutations disrupt function in patients with EAST syndrome." Nephron Physiol **119**(3): p40-48.
Friedrich, C., S. Rinne, S. Zumhagen, A. K. Kiper, N. Silbernagel, M. F. Netter, B. Stallmeyer, E. Schulze-Bahr and N. Decher (2014). "Gain-of-function mutation in TASK-4 channels and severe cardiac conduction disorder." EMBO Mol Med **6**(7): 937-951.
Friend, K. L., D. Crimmins, T. G. Phan, C. M. Sue, A. Colley, V. S. Fung, J. G. Morris, G. R. Sutherland and R. I. Richards (1999). "Detection of a novel missense mutation and second recurrent mutation in the CACNA1A gene in individuals with EA-2 and FHM." Hum Genet **105**(3): 261-265.
Fuentealba, J., B. Munoz, G. Yevenes, G. Moraga-Cid, C. Perez, L. Guzman, J. M. Rigo and L. G. Aguayo (2011). "Potentiation and inhibition of glycine receptors by tutin." Neuropharmacology **60**(2-3): 453-459.
Galvez, A., G. Gimenez-Gallego, J. P. Reuben, L. Roy-Contancin, P. Feigenbaum, G. J. Kaczorowski and M. L. Garcia (1990). "Purification and characterization of a unique, potent, peptidyl probe for the high conductance calcium-activated potassium channel from venom of the scorpion Buthus tamulus." J Biol Chem **265**(19): 11083-11090.
Gao, Y., E. Cao, D. Julius and Y. Cheng (2016). "TRPV1 structures in nanodiscs reveal mechanisms of ligand and lipid action." Nature **534**(7607): 347-351.
Garcia-Valdes, J., F. Z. Zamudio, L. Toro and L. D. Possani (2001). "Slotoxin, alphaKTx1.11, a new scorpion peptide blocker of MaxiK channels that differentiates between alpha and alpha+beta (beta1 or beta4) complexes." FEBS Lett **505**(3): 369-373.
Gavva, N. R., L. Klionsky, Y. Qu, L. Shi, R. Tamir, S. Edenson, T. J. Zhang, V. N. Viswanadhan, A. Toth, L. V. Pearce, T. W. Vanderah, F. Porreca, P. M. Blumberg, J. Lile, Y. Sun, K. Wild, J. C. Louis and J. J. Treanor (2004). "Molecular determinants of vanilloid sensitivity in TRPV1." J Biol Chem **279**(19): 20283-20295.
Ge, J., A. Sun, V. Paajanen, S. Wang, C. Su, Z. Yang, Y. Li, S. Wang, J. Jia, K. Wang, Y. Zou, L. Gao, K. Wang and Z. Fan (2008). "Molecular and clinical characterization of a novel SCN5A mutation associated with atrioventricular block and dilated cardiomyopathy." Circ Arrhythm Electrophysiol **1**(2): 83-92.
Geron, M., A. Hazan and A. Priel (2017). "Animal Toxins Providing Insights into TRPV1 Activation Mechanism." Toxins (Basel) **9**(10).
Glaudemans, B., J. van der Wijst, R. H. Scola, P. J. Lorenzoni, A. Heister, A. W. van der Kemp, N. V. Knoers, J. G. Hoenderop and R. J. Bindels (2009). "A missense mutation in the Kv1.1 voltage-gated potassium channel-encoding gene KCNA1 is

linked to human autosomal dominant hypomagnesemia." J Clin Invest **119**(4): 936-942.
Glogowska, E., K. Lezon-Geyda, Y. Maksimova, V. P. Schulz and P. G. Gallagher (2015). "Mutations in the Gardos channel (KCNN4) are associated with hereditary xerocytosis." Blood **126**(11): 1281-1284.
Glowatzki, E., G. Fakler, U. Brandle, U. Rexhausen, H. P. Zenner, J. P. Ruppersberg and B. Fakler (1995). "Subunit-dependent assembly of inward-rectifier K+ channels." Proc Biol Sci **261**(1361): 251-261.
Gloyn, A. L., C. Diatloff-Zito, E. L. Edghill, C. Bellanne-Chantelot, S. Nivot, R. Coutant, S. Ellard, A. T. Hattersley and J. J. Robert (2006). "KCNJ11 activating mutations are associated with developmental delay, epilepsy and neonatal diabetes syndrome and other neurological features." Eur J Hum Genet **14**(7): 824-830.
Gloyn, A. L., J. Siddiqui and S. Ellard (2006). "Mutations in the genes encoding the pancreatic beta-cell KATP channel subunits Kir6.2 (KCNJ11) and SUR1 (ABCC8) in diabetes mellitus and hyperinsulinism." Hum Mutat **27**(3): 220-231.
Goldin, A. L., R. L. Barchi, J. H. Caldwell, F. Hofmann, J. R. Howe, J. C. Hunter, R. G. Kallen, G. Mandel, M. H. Meisler, Y. B. Netter, M. Noda, M. M. Tamkun, S. G. Waxman, J. N. Wood and W. A. Catterall (2000). "Nomenclature of voltage-gated sodium channels." Neuron **28**(2): 365-368.
Gonzalez-Reyes, L. E., T. P. Ladas, C. C. Chiang and D. M. Durand (2013). "TRPV1 antagonist capsazepine suppresses 4-AP-induced epileptiform activity in vitro and electrographic seizures in vivo." Exp Neurol **250**: 321-332.
Gotti, C., F. Clementi, A. Fornari, A. Gaimarri, S. Guiducci, I. Manfredi, M. Moretti, P. Pedrazzi, L. Pucci and M. Zoli (2009). "Structural and functional diversity of native brain neuronal nicotinic receptors." Biochem Pharmacol **78**(7): 703-711.
Griffin, L. and A. Lawson (2011). "Antibody fragments as tools in crystallography." Clin Exp Immunol **165**(3): 285-291.
Grishin, E. V., G. A. Savchenko, A. A. Vassilevski, Y. V. Korolkova, Y. A. Boychuk, V. Y. Viatchenko-Karpinski, K. D. Nadezhdin, A. S. Arseniev, K. A. Pluzhnikov, V. B. Kulyk, N. V. Voitenko and O. O. Krishtal (2010). "Novel peptide from spider venom inhibits P2X3 receptors and inflammatory pain." Ann Neurol **67**(5): 680-683.
Groen, J., A. F. van Rootselaar, S. M. van der Salm, B. R. Bloem and M. Tijssen (2011). "A new familial syndrome with dystonia and lower limb action myoclonus." Mov Disord **26**(5): 896-900.
Groenewegen, W. A., M. Firouzi, C. R. Bezzina, S. Vliex, I. M. van Langen, L. Sandkuijl, J. P. Smits, M. Hulsbeek, M. B. Rook, H. J. Jongsma and A. A. Wilde (2003). "A cardiac sodium channel mutation cosegregates with a rare connexin40 genotype in familial atrial standstill." Circ Res **92**(1): 14-22.
Groschel-Stewart, U., M. Bardini, T. Robson and G. Burnstock (1999). "Localisation of P2X5 and P2X7 receptors by immunohistochemistry in rat stratified squamous epithelia." Cell Tissue Res **296**(3): 599-605.
Grosskreutz, J., S. Quasthoff, M. Kuhn and P. Grafe (1996). "Capsaicin blocks tetrodotoxin-resistant sodium potentials and calcium potentials in unmyelinated C fibres of biopsied human sural nerve in vitro." Neurosci Lett **208**(1): 49-52.

Gui, J., B. Liu, G. Cao, A. M. Lipchik, M. Perez, Z. Dekan, M. Mobli, N. L. Daly, P. F. Alewood, L. L. Parker, G. F. King, Y. Zhou, S. E. Jordt and M. N. Nitabach (2014). "A tarantula-venom peptide antagonizes the TRPA1 nociceptor ion channel by binding to the S1-S4 gating domain." Curr Biol **24**(5): 473-483.
Guida, S., F. Trettel, S. Pagnutti, E. Mantuano, A. Tottene, L. Veneziano, T. Fellin, M. Spadaro, K. Stauderman, M. Williams, S. Volsen, R. Ophoff, R. Frants, C. Jodice, M. Frontali and D. Pietrobon (2001). "Complete loss of P/Q calcium channel activity caused by a CACNA1A missense mutation carried by patients with episodic ataxia type 2." Am J Hum Genet **68**(3): 759-764.
Gupta, K., M. Zamanian, C. Bae, M. Milescu, D. Krepkiy, D. C. Tilley, J. T. Sack, V. Yarov-Yarovoy, J. I. Kim and K. J. Swartz (2015). "Tarantula toxins use common surfaces for interacting with Kv and ASIC ion channels." Elife **4**: e06774.
Gurnett, C. A., M. De Waard and K. P. Campbell (1996). "Dual function of the voltage-dependent Ca2+ channel alpha 2 delta subunit in current stimulation and subunit interaction." Neuron **16**(2): 431-440.
Guy, H. R. and P. Seetharamulu (1986). "Molecular model of the action potential sodium channel." Proc Natl Acad Sci U S A **83**(2): 508-512.
Haider, S., A. I. Tarasov, T. J. Craig, M. S. Sansom and F. M. Ashcroft (2007). "Identification of the PIP2-binding site on Kir6.2 by molecular modelling and functional analysis." EMBO J **26**(16): 3749-3759.
Hakim, M. A., W. Jiang, L. Luo, B. Li, S. Yang, Y. Song and R. Lai (2015). "Scorpion Toxin, BmP01, Induces Pain by Targeting TRPV1 Channel." Toxins (Basel) **7**(9): 3671-3687.
Hamers-Casterman, C., T. Atarhouch, S. Muyldermans, G. Robinson, C. Hamers, E. B. Songa, N. Bendahman and R. Hamers (1993). "Naturally occurring antibodies devoid of light chains." Nature **363**(6428): 446-448.
Han, S., H. Yi, S. J. Yin, Z. Y. Chen, H. Liu, Z. J. Cao, Y. L. Wu and W. X. Li (2008). "Structural basis of a potent peptide inhibitor designed for Kv1.3 channel, a therapeutic target of autoimmune disease." J Biol Chem **283**(27): 19058-19065.
Hang, J., H. Shi, D. Li, Y. Liao, D. Lian, Y. Xiao and H. Xue (2000). "Ligand binding and structural properties of segments of GABAA receptor alpha 1 subunit overexpressed in Escherichia coli." J Biol Chem **275**(25): 18818-18823.
Harstall, C. O., M (2003). "How prevalent is chronic pain?" PAIN: Clinical Updates **11**(2).
Hechler, B., N. Lenain, P. Marchese, C. Vial, V. Heim, M. Freund, J. P. Cazenave, M. Cattaneo, Z. M. Ruggeri, R. Evans and C. Gachet (2003). "A role of the fast ATP-gated P2X1 cation channel in thrombosis of small arteries in vivo." J Exp Med **198**(4): 661-667.
Heginbotham, L., Z. Lu, T. Abramson and R. MacKinnon (1994). "Mutations in the K+ channel signature sequence." Biophys J **66**(4): 1061-1067.
Hejtmancik, J. F., X. Jiao, A. Li, Y. V. Sergeev, X. Ding, A. K. Sharma, C. C. Chan, I. Medina and A. O. Edwards (2008). "Mutations in KCNJ13 cause autosomal-dominant snowflake vitreoretinal degeneration." Am J Hum Genet **82**(1): 174-180.
Hemara-Wahanui, A., S. Berjukow, C. I. Hope, P. K. Dearden, S. B. Wu, J. Wilson-Wheeler, D. M. Sharp, P. Lundon-Treweek, G. M. Clover, J. C. Hoda, J. Striessnig, R. Marksteiner, S. Hering and M. A. Maw (2005). "A CACNA1F mutation identified

in an X-linked retinal disorder shifts the voltage dependence of Cav1.4 channel activation." Proc Natl Acad Sci U S A **102**(21): 7553-7558.
Heron, S. E., H. Khosravani, D. Varela, C. Bladen, T. C. Williams, M. R. Newman, I. E. Scheffer, S. F. Berkovic, J. C. Mulley and G. W. Zamponi (2007). "Extended spectrum of idiopathic generalized epilepsies associated with CACNA1H functional variants." Ann Neurol **62**(6): 560-568.
Heurteaux, C., N. Guy, C. Laigle, N. Blondeau, F. Duprat, M. Mazzuca, L. Lang-Lazdunski, C. Widmann, M. Zanzouri, G. Romey and M. Lazdunski (2004). "TREK-1, a K+ channel involved in neuroprotection and general anesthesia." EMBO J **23**(13): 2684-2695.
Heurteaux, C., G. Lucas, N. Guy, M. El Yacoubi, S. Thummler, X. D. Peng, F. Noble, N. Blondeau, C. Widmann, M. Borsotto, G. Gobbi, J. M. Vaugeois, G. Debonnel and M. Lazdunski (2006). "Deletion of the background potassium channel TREK-1 results in a depression-resistant phenotype." Nat Neurosci **9**(9): 1134-1141.
Hey, T., E. Fiedler, R. Rudolph and M. Fiedler (2005). "Artificial, non-antibody binding proteins for pharmaceutical and industrial applications." Trends Biotechnol **23**(10): 514-522.
Hibell, A. D., E. J. Kidd, I. P. Chessell, P. P. Humphrey and A. D. Michel (2000). "Apparent species differences in the kinetic properties of P2X(7) receptors." Br J Pharmacol **130**(1): 167-173.
Hibino, H., A. Inanobe, K. Furutani, S. Murakami, I. Findlay and Y. Kurachi (2010). "Inwardly rectifying potassium channels: their structure, function, and physiological roles." Physiol Rev **90**(1): 291-366.
Hille, B. (2001). Ion Channels of Excitable Membranes. Sunderland, MA, U.S.A, Sinauer Associates, Inc.
Hodgkin, A. L. and A. F. Huxley (1952). "A quantitative description of membrane current and its application to conduction and excitation in nerve." J Physiol **117**(4): 500-544.
Hodgkin, A. L., A. F. Huxley and B. Katz (1952). "Measurement of current-voltage relations in the membrane of the giant axon of Loligo." J Physiol **116**(4): 424-448.
Hoelder, S., P. A. Clarke and P. Workman (2012). "Discovery of small molecule cancer drugs: successes, challenges and opportunities." Mol Oncol **6**(2): 155-176.
Hoffmann, T., L. K. Stadler, M. Busby, Q. Song, A. T. Buxton, S. D. Wagner, J. J. Davis and P. Ko Ferrigno (2010). "Structure-function studies of an engineered scaffold protein derived from stefin A. I: Development of the SQM variant." Protein Eng Des Sel **23**(5): 403-413.
Holmgren, M., K. S. Shin and G. Yellen (1998). "The activation gate of a voltage-gated K+ channel can be trapped in the open state by an intersubunit metal bridge." Neuron **21**(3): 617-621.
Hone, A. J., D. Servent and J. M. McIntosh (2018). "alpha9-containing nicotinic acetylcholine receptors and the modulation of pain." Br J Pharmacol **175**(11): 1915-1927.
Honore, P., J. Mikusa, B. Bianchi, H. McDonald, J. Cartmell, C. Faltynek and M. F. Jarvis (2002). "TNP-ATP, a potent P2X3 receptor antagonist, blocks acetic acid-induced abdominal constriction in mice: comparison with reference analgesics." Pain **96**(1-2): 99-105.

Hoogenboom, H. R., A. D. Griffiths, K. S. Johnson, D. J. Chiswell, P. Hudson and G. Winter (1991). "Multi-subunit proteins on the surface of filamentous phage: methodologies for displaying antibody (Fab) heavy and light chains." Nucleic Acids Res **19**(15): 4133-4137.
Hoshi, T., W. N. Zagotta and R. W. Aldrich (1990). "Biophysical and molecular mechanisms of Shaker potassium channel inactivation." Science **250**(4980): 533-538.
Housley, G. D., R. Kanjhan, N. P. Raybould, D. Greenwood, S. G. Salih, L. Jarlebark, L. D. Burton, V. C. Setz, M. B. Cannell, C. Soeller, D. L. Christie, S. Usami, A. Matsubara, H. Yoshie, A. F. Ryan and P. R. Thorne (1999). "Expression of the P2X(2) receptor subunit of the ATP-gated ion channel in the cochlea: implications for sound transduction and auditory neurotransmission." J Neurosci **19**(19): 8377-8388.
Huang, C. L., S. Feng and D. W. Hilgemann (1998). "Direct activation of inward rectifier potassium channels by PIP2 and its stabilization by Gbetagamma." Nature **391**(6669): 803-806.
Huang, L., Q. Zhang, S. Li, L. Guan, X. Xiao, J. Zhang, X. Jia, W. Sun, Z. Zhu, Y. Gao, Y. Yin, P. Wang, X. Guo, J. Wang and Q. Zhang (2013). "Exome sequencing of 47 chinese families with cone-rod dystrophy: mutations in 25 known causative genes." PLoS One **8**(6): e65546.
Huang, R., P. Fang, Z. Hao and B. K. Kay (2016). "Directed Evolution of a Highly Specific FN3 Monobody to the SH3 Domain of Human Lyn Tyrosine Kinase." PLoS One **11**(1): e0145872.
Huber, I., E. Wappl, A. Herzog, J. Mitterdorfer, H. Glossmann, T. Langer and J. Striessnig (2000). "Conserved Ca2+-antagonist-binding properties and putative folding structure of a recombinant high-affinity dihydropyridine-binding domain." Biochem J **347 Pt 3**: 829-836.
Huber, T., D. Steiner, D. Rothlisberger and A. Pluckthun (2007). "In vitro selection and characterization of DARPins and Fab fragments for the co-crystallization of membrane proteins: The Na(+)-citrate symporter CitS as an example." J Struct Biol **159**(2): 206-221.
Huggins, D. J., W. Sherman and B. Tidor (2012). "Rational approaches to improving selectivity in drug design." J Med Chem **55**(4): 1424-1444.
Hughes, D. J., C. Tiede, N. Penswick, A. A. Tang, C. H. Trinh, U. Mandal, K. Z. Zajac, T. Gaule, G. Howell, T. A. Edwards, J. Duan, E. Feyfant, M. J. McPherson, D. C. Tomlinson and A. Whitehouse (2017). "Generation of specific inhibitors of SUMO-1- and SUMO-2/3-mediated protein-protein interactions using Affimer (Adhiron) technology." Sci Signal **10**(505).
Hunte, C. and H. Michel (2002). "Crystallisation of membrane proteins mediated by antibody fragments." Curr Opin Struct Biol **12**(4): 503-508.
Ishii, T. M., C. Silvia, B. Hirschberg, C. T. Bond, J. P. Adelman and J. Maylie (1997). "A human intermediate conductance calcium-activated potassium channel." Proc Natl Acad Sci U S A **94**(21): 11651-11656.
Jancso, G., E. Kiraly and A. Jancso-Gabor (1977). "Pharmacologically induced selective degeneration of chemosensitive primary sensory neurones." Nature **270**(5639): 741-743.

Jarvis, M. F., E. C. Burgard, S. McGaraughty, P. Honore, K. Lynch, T. J. Brennan, A. Subieta, T. Van Biesen, J. Cartmell, B. Bianchi, W. Niforatos, K. Kage, H. Yu, J. Mikusa, C. T. Wismer, C. Z. Zhu, K. Chu, C. H. Lee, A. O. Stewart, J. Polakowski, B. F. Cox, E. Kowaluk, M. Williams, J. Sullivan and C. Faltynek (2002). "A-317491, a novel potent and selective non-nucleotide antagonist of P2X3 and P2X2/3 receptors, reduces chronic inflammatory and neuropathic pain in the rat." Proc Natl Acad Sci U S A **99**(26): 17179-17184.

Jay, S. D., S. B. Ellis, A. F. McCue, M. E. Williams, T. S. Vedvick, M. M. Harpold and K. P. Campbell (1990). "Primary structure of the gamma subunit of the DHP-sensitive calcium channel from skeletal muscle." Science **248**(4954): 490-492.

Jen, J., J. Wan, M. Graves, H. Yu, A. F. Mock, C. J. Coulin, G. Kim, Q. Yue, D. M. Papazian and R. W. Baloh (2001). "Loss-of-function EA2 mutations are associated with impaired neuromuscular transmission." Neurology **57**(10): 1843-1848.

Jen, J., Q. Yue, S. F. Nelson, H. Yu, M. Litt, J. Nutt and R. W. Baloh (1999). "A novel nonsense mutation in CACNA1A causes episodic ataxia and hemiplegia." Neurology **53**(1): 34-37.

Jensen, M. O., V. Jogini, D. W. Borhani, A. E. Leffler, R. O. Dror and D. E. Shaw (2012). "Mechanism of voltage gating in potassium channels." Science **336**(6078): 229-233.

Jiang, Y., A. Lee, J. Chen, M. Cadene, B. T. Chait and R. MacKinnon (2002). "The open pore conformation of potassium channels." Nature **417**(6888): 523-526.

Johannes, C. B., T. K. Le, X. Zhou, J. A. Johnston and R. H. Dworkin (2010). "The prevalence of chronic pain in United States adults: results of an Internet-based survey." J Pain **11**(11): 1230-1239.

Joiner, W. J., L. Y. Wang, M. D. Tang and L. K. Kaczmarek (1997). "hSK4, a member of a novel subfamily of calcium-activated potassium channels." Proc Natl Acad Sci U S A **94**(20): 11013-11018.

Jones, M. L., M. A. Alfaleh, S. Kumble, S. Zhang, G. W. Osborne, M. Yeh, N. Arora, J. J. Hou, C. B. Howard, D. Y. Chin and S. M. Mahler (2016). "Targeting membrane proteins for antibody discovery using phage display." Sci Rep **6**: 26240.

Jones, M. L., T. Seldon, M. Smede, A. Linville, D. Y. Chin, R. Barnard, S. M. Mahler, D. Munster, D. Hart, P. P. Gray and T. P. Munro (2010). "A method for rapid, ligation-independent reformatting of recombinant monoclonal antibodies." J Immunol Methods **354**(1-2): 85-90.

Jongbloed, R. J., A. A. Wilde, J. L. Geelen, P. Doevendans, C. Schaap, I. Van Langen, J. P. van Tintelen, J. M. Cobben, G. C. Beaufort-Krol, J. P. Geraedts and H. J. Smeets (1999). "Novel KCNQ1 and HERG missense mutations in Dutch long-QT families." Hum Mutat **13**(4): 301-310.

Jost, C., J. Schilling, R. Tamaskovic, M. Schwill, A. Honegger and A. Pluckthun (2013). "Structural basis for eliciting a cytotoxic effect in HER2-overexpressing cancer cells via binding to the extracellular domain of HER2." Structure **21**(11): 1979-1991.

Jouvenceau, A., L. H. Eunson, A. Spauschus, V. Ramesh, S. M. Zuberi, D. M. Kullmann and M. G. Hanna (2001). "Human epilepsy associated with dysfunction of the brain P/Q-type calcium channel." Lancet **358**(9284): 801-807.

Juang, J. M., T. P. Lu, L. C. Lai, C. C. Ho, Y. B. Liu, C. T. Tsai, L. Y. Lin, C. C. Yu, W. J. Chen, F. T. Chiang, S. F. Yeh, L. P. Lai, E. Y. Chuang and J. L. Lin (2014). "Disease-

targeted sequencing of ion channel genes identifies de novo mutations in patients with non-familial Brugada syndrome." Sci Rep **4**: 6733.
Julius, D. (2013). "TRP channels and pain." Annu Rev Cell Dev Biol **29**: 355-384.
Jung, H. J., P. I. Kim, S. K. Lee, C. W. Lee, Y. J. Eu, D. G. Lee, Y. E. Earm and J. I. Kim (2006). "Lipid membrane interaction and antimicrobial activity of GsMTx-4, an inhibitor of mechanosensitive channel." Biochem Biophys Res Commun **340**(2): 633-638.
Jung, Y. H., Y. O. Kim, H. Lin, J. H. Cho, J. H. Park, S. D. Lee, J. Bae, K. M. Kang, Y. G. Kim, A. N. Pae, H. Ko, C. S. Park, M. H. Yoon and Y. C. Kim (2017). "Discovery of Potent Antiallodynic Agents for Neuropathic Pain Targeting P2X3 Receptors." ACS Chem Neurosci **8**(7): 1465-1478.
Jurkat-Rott, K., N. Mitrovic, C. Hang, A. Kouzmekine, P. Iaizzo, J. Herzog, H. Lerche, S. Nicole, J. Vale-Santos, D. Chauveau, B. Fontaine and F. Lehmann-Horn (2000). "Voltage-sensor sodium channel mutations cause hypokalemic periodic paralysis type 2 by enhanced inactivation and reduced current." Proc Natl Acad Sci U S A **97**(17): 9549-9554.
Kanumilli S, G. R., Stafford S, Hogg D, Kozlowski R. (2005). "In vitro assay for identifying modulators of Cav channel 1 subunit interactions." J. Physiol.: 568.
Kaszas, K., J. M. Keller, C. Coddou, S. K. Mishra, M. A. Hoon, S. Stojilkovic, K. A. Jacobson and M. J. Iadarola (2012). "Small molecule positive allosteric modulation of TRPV1 activation by vanilloids and acidic pH." J Pharmacol Exp Ther **340**(1): 152-160.
Khakh, B. S., G. Burnstock, C. Kennedy, B. F. King, R. A. North, P. Seguela, M. Voigt and P. P. Humphrey (2001). "International union of pharmacology. XXIV. Current status of the nomenclature and properties of P2X receptors and their subunits." Pharmacol Rev **53**(1): 107-118.
Kim, J. I., M. Takahashi, A. Ogura, T. Kohno, Y. Kudo and K. Sato (1994). "Hydroxyl group of Tyr13 is essential for the activity of omega-conotoxin GVIA, a peptide toxin for N-type calcium channel." J Biol Chem **269**(39): 23876-23878.
Kim, M., O. J. Yoo and S. Choe (1997). "Molecular assembly of the extracellular domain of P2X2, an ATP-gated ion channel." Biochem Biophys Res Commun **240**(3): 618-622.
Kiss, L., J. LoTurco and S. J. Korn (1999). "Contribution of the selectivity filter to inactivation in potassium channels." Biophys J **76**(1 Pt 1): 253-263.
Kobori, A., N. Sarai, W. Shimizu, Y. Nakamura, Y. Murakami, T. Makiyama, S. Ohno, K. Takenaka, T. Ninomiya, Y. Fujiwara, S. Matsuoka, M. Takano, A. Noma, T. Kita and M. Horie (2004). "Additional gene variants reduce effectiveness of beta-blockers in the LQT1 form of long QT syndrome." J Cardiovasc Electrophysiol **15**(2): 190-199.
Koduvayur, S. P., H. A. Gussin, R. Parthasarathy, Z. Hao, B. K. Kay and D. R. Pepperberg (2014). "Generation of recombinant antibodies to rat GABAA receptor subunits by affinity selection on synthetic peptides." PLoS One **9**(2): e87964.
Kohler, M., B. Hirschberg, C. T. Bond, J. M. Kinzie, N. V. Marrion, J. Maylie and J. P. Adelman (1996). "Small-conductance, calcium-activated potassium channels from mammalian brain." Science **273**(5282): 1709-1714.

Koide, A., C. W. Bailey, X. Huang and S. Koide (1998). "The fibronectin type III domain as a scaffold for novel binding proteins." J Mol Biol **284**(4): 1141-1151.
Koide, A., J. Wojcik, R. N. Gilbreth, R. J. Hoey and S. Koide (2012). "Teaching an old scaffold new tricks: monobodies constructed using alternative surfaces of the FN3 scaffold." J Mol Biol **415**(2): 393-405.
Kors, E. E., A. Melberg, K. R. Vanmolkot, E. Kumlien, J. Haan, R. Raininko, R. Flink, H. B. Ginjaar, R. R. Frants, M. D. Ferrari and A. M. van den Maagdenberg (2004). "Childhood epilepsy, familial hemiplegic migraine, cerebellar ataxia, and a new CACNA1A mutation." Neurology **63**(6): 1136-1137.
Kovala, A. T., K. A. Harvey, P. McGlynn, G. Boguslawski, J. G. Garcia and D. English (2000). "High-efficiency transient transfection of endothelial cells for functional analysis." FASEB J **14**(15): 2486-2494.
Kucheryavykh, L. Y., Y. V. Kucheryavykh, M. Inyushin, Y. M. Shuba, P. Sanabria, L. A. Cubano, S. N. Skatchkov and M. J. Eaton (2009). "Ischemia Increases TREK-2 Channel Expression in Astrocytes: Relevance to Glutamate Clearance." Open Neurosci J **3**: 40-47.
Kummer, L., C. W. Hsu, O. Dagliyan, C. MacNevin, M. Kaufholz, B. Zimmermann, N. V. Dokholyan, K. M. Hahn and A. Pluckthun (2013). "Knowledge-based design of a biosensor to quantify localized ERK activation in living cells." Chem Biol **20**(6): 847-856.
Kwan, K. Y., J. M. Glazer, D. P. Corey, F. L. Rice and C. L. Stucky (2009). "TRPA1 modulates mechanotransduction in cutaneous sensory neurons." J Neurosci **29**(15): 4808-4819.
Kyle, H. F., K. F. Wickson, J. Stott, G. M. Burslem, A. L. Breeze, C. Tiede, D. C. Tomlinson, S. L. Warriner, A. Nelson, A. J. Wilson and T. A. Edwards (2015). "Exploration of the HIF-1alpha/p300 interface using peptide and Adhiron phage display technologies." Mol Biosyst **11**(10): 2738-2749.
Lacroix-Fralish, M. L. and J. S. Mogil (2009). "Progress in genetic studies of pain and analgesia." Annu Rev Pharmacol Toxicol **49**: 97-121.
Laemmli, U. K. (1970). "Cleavage of structural proteins during the assembly of the head of bacteriophage T4." Nature **227**(5259): 680-685.
Larsen, L. A., I. Fosdal, P. S. Andersen, J. K. Kanters, J. Vuust, G. Wettrell and M. Christiansen (1999). "Recessive Romano-Ward syndrome associated with compound heterozygosity for two mutations in the KVLQT1 gene." Eur J Hum Genet **7**(6): 724-728.
Lawson, A. D. (2012). "Antibody-enabled small-molecule drug discovery." Nat Rev Drug Discov **11**(7): 519-525.
Lebovitz, E. E., J. M. Keller, H. Kominsky, K. Kaszas, D. Maric and M. J. Iadarola (2012). "Positive allosteric modulation of TRPV1 as a novel analgesic mechanism." Mol Pain **8**: 70.
Lee, B. S., J. S. Huang, L. P. Jayathilaka, J. Lee and S. Gupta (2016). "Antibody Production with Synthetic Peptides." Methods Mol Biol **1474**: 25-47.
Lee, H. C., J. M. Wang and K. J. Swartz (2003). "Interaction between Extracellular Hanatoxin and the Resting Conformation of the Voltage-Sensor Paddle in Kv Channels." Neuron **40**: 527-536.

Lee, J. H., C. K. Park, G. Chen, Q. Han, R. G. Xie, T. Liu, R. R. Ji and S. Y. Lee (2014). "A monoclonal antibody that targets a NaV1.7 channel voltage sensor for pain and itch relief." Cell **157**(6): 1393-1404.
Lee, S. Y. and R. MacKinnon (2004). "A membrane-access mechanism of ion channel inhibition by voltage sensor toxins from spider venom." Nature **430**(6996): 232-235.
Leipold, E., A. Hansel, A. Borges and S. H. Heinemann (2006). "Subtype specificity of scorpion beta-toxin Tz1 interaction with voltage-gated sodium channels is determined by the pore loop of domain 3." Mol Pharmacol **70**(1): 340-347.
Lenter, M., H. Uhlig, A. Hamann, P. Jeno, B. Imhof and D. Vestweber (1993). "A monoclonal antibody against an activation epitope on mouse integrin chain beta 1 blocks adhesion of lymphocytes to the endothelial integrin alpha 6 beta 1." Proc Natl Acad Sci U S A **90**(19): 9051-9055.
Lenzini, L., B. Caroccia, A. G. Campos, A. Fassina, A. S. Belloni, T. M. Seccia, M. Kuppusamy, S. Ferraro, G. Skander, M. Bader, W. E. Rainey and G. P. Rossi (2014). "Lower expression of the TWIK-related acid-sensitive K+ channel 2 (TASK-2) gene is a hallmark of aldosterone-producing adenoma causing human primary aldosteronism." J Clin Endocrinol Metab **99**(4): E674-682.
Lerche, H., R. Heine, U. Pika, A. L. George, Jr., N. Mitrovic, M. Browatzki, T. Weiss, M. Rivet-Bastide, C. Franke, M. Lomonaco and et al. (1993). "Human sodium channel myotonia: slowed channel inactivation due to substitutions for a glycine within the III-IV linker." J Physiol **470**: 13-22.
Levine, J. D. and N. Alessandri-Haber (2007). "TRP channels: targets for the relief of pain." Biochim Biophys Acta **1772**(8): 989-1003.
Li, P., Z. Chen, H. Xu, H. Sun, H. Li, H. Liu, H. Yang, Z. Gao, H. Jiang and M. Li (2013). "The gating charge pathway of an epilepsy-associated potassium channel accommodates chemical ligands." Cell Res **23**(9): 1106-1118.
Li, R. A., I. L. Ennis, T. Xue, H. M. Nguyen, G. F. Tomaselli, A. L. Goldin and E. Marban (2003). "Molecular basis of isoform-specific micro-conotoxin block of cardiac, skeletal muscle, and brain Na+ channels." J Biol Chem **278**(10): 8717-8724.
Li, Z., W. H. Liu, S. Han, B. W. Peng, J. Yin, Y. L. Wu, X. H. He and W. X. Li (2012). "Selective inhibition of CCR7(-) effector memory T cell activation by a novel peptide targeting Kv1.3 channel in a rat experimental autoimmune encephalomyelitis model." J Biol Chem **287**(35): 29479-29494.
Liang, S., C. Xu, G. Li and Y. Gao (2010). "P2X receptors and modulation of pain transmission: focus on effects of drugs and compounds used in traditional Chinese medicine." Neurochem Int **57**(7): 705-712.
Liao, M., E. Cao, D. Julius and Y. Cheng (2013). "Structure of the TRPV1 ion channel determined by electron cryo-microscopy." Nature **504**(7478): 107-112.
Lin, S. H. and G. Guidotti (2009). "Purification of membrane proteins." Methods Enzymol **463**: 619-629.
Link, T. I. (2013). "FDA Approved Antibody-based Therapeutics." 2015.
Liu, B., L. Fan, S. Balakrishna, A. Sui, J. B. Morris and S. E. Jordt (2013). "TRPM8 is the principal mediator of menthol-induced analgesia of acute and inflammatory pain." Pain **154**(10): 2169-2177.

Liu, Y., M. Holmgren, M. E. Jurman and G. Yellen (1997). "Gated access to the pore of a voltage-dependent K+ channel." Neuron **19**(1): 175-184.
Lopata, A., R. Hughes, C. Tiede, S. M. Heissler, J. R. Sellers, P. J. Knight, D. Tomlinson and M. Peckham (2018). "Affimer proteins for F-actin: novel affinity reagents that label F-actin in live and fixed cells." Sci Rep **8**(1): 6572.
Lopes, C. M., H. Zhang, T. Rohacs, T. Jin, J. Yang and D. E. Logothetis (2002). "Alterations in conserved Kir channel-PIP2 interactions underlie channelopathies." Neuron **34**(6): 933-944.
Lou, K. L., P. T. Huang, Y. S. Shiau and Y. Y. Shiau (2002). "Molecular determinants of the hanatoxin binding in voltage-gated K+-channel drk1." J Mol Recognit **15**(4): 175-179.
Luo, J., E. T. Walters, S. M. Carlton and H. Hu (2013). "Targeting Pain-evoking Transient Receptor Potential Channels for the Treatment of Pain." Curr Neuropharmacol **11**(6): 652-663.
Ma, L., D. Roman-Campos, E. D. Austin, M. Eyries, K. S. Sampson, F. Soubrier, M. Germain, D. A. Tregouet, A. Borczuk, E. B. Rosenzweig, B. Girerd, D. Montani, M. Humbert, J. E. Loyd, R. S. Kass and W. K. Chung (2013). "A novel channelopathy in pulmonary arterial hypertension." N Engl J Med **369**(4): 351-361.
Mahdavi, S. and S. Kuyucak (2014). "Molecular dynamics study of binding of micro-conotoxin GIIIA to the voltage-gated sodium channel Na(v)1.4." PLoS One **9**(8): e105300.
Mannikko, R., C. Jefferies, S. E. Flanagan, A. Hattersley, S. Ellard and F. M. Ashcroft (2010). "Interaction between mutations in the slide helix of Kir6.2 associated with neonatal diabetes and neurological symptoms." Hum Mol Genet **19**(6): 963-972.
Mansoor, S. E., W. Lu, W. Oosterheert, M. Shekhar, E. Tajkhorshid and E. Gouaux (2016). "X-ray structures define human P2X(3) receptor gating cycle and antagonist action." Nature **538**(7623): 66-71.
Marschall, A. L., A. Frenzel, T. Schirrmann, M. Schungel and S. Dubel (2011). "Targeting antibodies to the cytoplasm." MAbs **3**(1): 3-16.
Marthinet, E., A. Bloc, Y. Oka, Y. Tanizawa, B. Wehrle-Haller, V. Bancila, J. M. Dubuis, J. Philippe and V. M. Schwitzgebel (2005). "Severe congenital hyperinsulinism caused by a mutation in the Kir6.2 subunit of the adenosine triphosphate-sensitive potassium channel impairing trafficking and function." J Clin Endocrinol Metab **90**(9): 5401-5406.
Maue, R. A. (2007). "Understanding ion channel biology using epitope tags: progress, pitfalls, and promise." J Cell Physiol **213**(3): 618-625.
Menendez, L., L. Juarez, E. Garcia, O. Garcia-Suarez, A. Hidalgo and A. Baamonde (2006). "Analgesic effects of capsazepine and resiniferatoxin on bone cancer pain in mice." Neurosci Lett **393**(1): 70-73.
Meriggioli, M. N. (2009). "Myasthenia gravis with anti-acetylcholine receptor antibodies." Front Neurol Neurosci **26**: 94-108.
Michel, M. A., K. N. Swatek, M. K. Hospenthal and D. Komander (2017). "Ubiquitin Linkage-Specific Affimers Reveal Insights into K6-Linked Ubiquitin Signaling." Mol Cell **68**(1): 233-246 e235.
Milescu, M., H. C. Lee, C. H. Bae, J. I. Kim and K. J. Swartz (2013). "Opening the shaker K+ channel with hanatoxin." J Gen Physiol **141**(2): 203-216.

Miller, P. S. and A. R. Aricescu (2014). "Crystal structure of a human GABAA receptor." Nature **512**(7514): 270-275.
Miller, S., S. Rao, W. Wang, H. Liu, J. Wang and N. R. Gavva (2014). "Antibodies to the extracellular pore loop of TRPM8 act as antagonists of channel activation." PLoS One **9**(9): e107151.
Mintz, I. M., V. J. Venema, M. E. Adams and B. P. Bean (1991). "Inhibition of N- and L-type Ca2+ channels by the spider venom toxin omega-Aga-IIIA." Proc Natl Acad Sci U S A **88**(15): 6628-6631.
Mintz, I. M., V. J. Venema, K. M. Swiderek, T. D. Lee, B. P. Bean and M. E. Adams (1992). "P-type calcium channels blocked by the spider toxin omega-Aga-IVA." Nature **355**(6363): 827-829.
Mitchell, K., B. D. Bates, J. M. Keller, M. Lopez, L. Scholl, J. Navarro, N. Madian, G. Haspel, M. I. Nemenov and M. J. Iadarola (2010). "Ablation of rat TRPV1-expressing Adelta/C-fibers with resiniferatoxin: analysis of withdrawal behaviors, recovery of function and molecular correlates." Mol Pain **6**: 94.
Miyazawa, A., Y. Fujiyoshi and N. Unwin (2003). "Structure and gating mechanism of the acetylcholine receptor pore." Nature **423**(6943): 949-955.
Mocsai, A., L. Kovacs and P. Gergely (2014). "What is the future of targeted therapy in rheumatology: biologics or small molecules?" BMC Med **12**: 43.
Monastyrnaya, M., S. Peigneur, E. Zelepuga, O. Sintsova, I. Gladkikh, E. Leychenko, M. Isaeva, J. Tytgat and E. Kozlovskaya (2016). "Kunitz-Type Peptide HCRG21 from the Sea Anemone Heteractis crispa Is a Full Antagonist of the TRPV1 Receptor." Mar Drugs **14**(12).
Monnier, N., V. Procaccio, P. Stieglitz and J. Lunardi (1997). "Malignant-hyperthermia susceptibility is associated with a mutation of the alpha 1-subunit of the human dihydropyridine-sensitive L-type voltage-dependent calcium-channel receptor in skeletal muscle." Am J Hum Genet **60**(6): 1316-1325.
Morais-Cabral, J. H., Y. Zhou and R. MacKinnon (2001). "Energetic optimization of ion conduction rate by the K+ selectivity filter." Nature **414**(6859): 37-42.
Moran, M. M., M. A. McAlexander, T. Biro and A. Szallasi (2011). "Transient receptor potential channels as therapeutic targets." Nat Rev Drug Discov **10**(8): 601-620.
Muona, M., S. F. Berkovic, L. M. Dibbens, K. L. Oliver, S. Maljevic, M. A. Bayly, T. Joensuu, L. Canafoglia, S. Franceschetti, R. Michelucci, S. Markkinen, S. E. Heron, M. S. Hildebrand, E. Andermann, F. Andermann, A. Gambardella, P. Tinuper, L. Licchetta, I. E. Scheffer, C. Criscuolo, A. Filla, E. Ferlazzo, J. Ahmad, A. Ahmad, B. Baykan, E. Said, M. Topcu, P. Riguzzi, M. D. King, C. Ozkara, D. M. Andrade, B. A. Engelsen, A. Crespel, M. Lindenau, E. Lohmann, V. Saletti, J. Massano, M. Privitera, A. J. Espay, B. Kauffmann, M. Duchowny, R. S. Moller, R. Straussberg, Z. Afawi, B. Ben-Zeev, K. E. Samocha, M. J. Daly, S. Petrou, H. Lerche, A. Palotie and A. E. Lehesjoki (2015). "A recurrent de novo mutation in KCNC1 causes progressive myoclonus epilepsy." Nat Genet **47**(1): 39-46.
Murakami, S., R. Nakashima, E. Yamashita and A. Yamaguchi (2002). "Crystal structure of bacterial multidrug efflux transporter AcrB." Nature **419**(6907): 587-593.

Murrell-Lagnado, R. D. and R. W. Aldrich (1993). "Interactions of amino terminal domains of Shaker K channels with a pore blocking site studied with synthetic peptides." J Gen Physiol **102**(6): 949-975.
Nasirinezhad, F., M. Hosseini, Z. Karami, M. Yousefifard and A. Janzadeh (2016). "Spinal 5-HT3 receptor mediates nociceptive effect on central neuropathic pain; possible therapeutic role for tropisetron." J Spinal Cord Med **39**(2): 212-219.
Nassini, R., S. Materazzi, S. Benemei and P. Geppetti (2014). "The TRPA1 channel in inflammatory and neuropathic pain and migraine." Rev Physiol Biochem Pharmacol **167**: 1-43.
Neher, E. and B. Sakmann (1976). "Single-channel currents recorded from membrane of denervated frog muscle fibres." Nature **260**(5554): 799-802.
Nestorowicz, A., N. Inagaki, T. Gonoi, K. P. Schoor, B. A. Wilson, B. Glaser, H. Landau, C. A. Stanley, P. S. Thornton, S. Seino and M. A. Permutt (1997). "A nonsense mutation in the inward rectifier potassium channel gene, Kir6.2, is associated with familial hyperinsulinism." Diabetes **46**(11): 1743-1748.
Neyroud, N., F. Tesson, I. Denjoy, M. Leibovici, C. Donger, J. Barhanin, S. Faure, F. Gary, P. Coumel, C. Petit, K. Schwartz and P. Guicheney (1997). "A novel mutation in the potassium channel gene KVLQT1 causes the Jervell and Lange-Nielsen cardioauditory syndrome." Nat Genet **15**(2): 186-189.
Nieto, F. R., E. J. Cobos, M. A. Tejada, C. Sanchez-Fernandez, R. Gonzalez-Cano and C. M. Cendan (2012). "Tetrodotoxin (TTX) as a therapeutic agent for pain." Mar Drugs **10**(2): 281-305.
Nilius, B. and G. Owsianik (2011). "The transient receptor potential family of ion channels." Genome Biol **12**(3): 218.
Nizak, C., S. Monier, E. del Nery, S. Moutel, B. Goud and F. Perez (2003). "Recombinant antibodies to the small GTPase Rab6 as conformation sensors." Science **300**(5621): 984-987.
Noda, M., S. Shimizu, T. Tanabe, T. Takai, T. Kayano, T. Ikeda, H. Takahashi, H. Nakayama, Y. Kanaoka, N. Minamino and et al. (1984). "Primary structure of Electrophorus electricus sodium channel deduced from cDNA sequence." Nature **312**(5990): 121-127.
Nurullahoglu, K. E., N. Okudan, M. Belviranli and M. Oz (2014). "The comparison of preemptive analgesic effects of curcumin and diclofenac." Bratisl Lek Listy **115**(12): 757-760.
Nury, H., N. Bocquet, C. Le Poupon, B. Raynal, A. Haouz, P. J. Corringer and M. Delarue (2010). "Crystal structure of the extracellular domain of a bacterial ligand-gated ion channel." J Mol Biol **395**(5): 1114-1127.
Olson, T. M., A. E. Alekseev, X. K. Liu, S. Park, L. V. Zingman, M. Bienengraeber, S. Sattiraju, J. D. Ballew, A. Jahangir and A. Terzic (2006). "Kv1.5 channelopathy due to KCNA5 loss-of-function mutation causes human atrial fibrillation." Hum Mol Genet **15**(14): 2185-2191.
Ondrus, A. E., H. L. Lee, S. Iwanaga, W. H. Parsons, B. M. Andresen, W. E. Moerner and J. Du Bois (2012). "Fluorescent saxitoxins for live cell imaging of single voltage-gated sodium ion channels beyond the optical diffraction limit." Chem Biol **19**(7): 902-912.
Ophoff, R. A., G. M. Terwindt, M. N. Vergouwe, R. van Eijk, P. J. Oefner, S. M. Hoffman, J. E. Lamerdin, H. W. Mohrenweiser, D. E. Bulman, M. Ferrari, J. Haan,

D. Lindhout, G. J. van Ommen, M. H. Hofker, M. D. Ferrari and R. R. Frants (1996). "Familial hemiplegic migraine and episodic ataxia type-2 are caused by mutations in the Ca2+ channel gene CACNL1A4." Cell **87**(3): 543-552.
Ormond, S. J., N. P. Barrera, O. S. Qureshi, R. M. Henderson, J. M. Edwardson and R. D. Murrell-Lagnado (2006). "An uncharged region within the N terminus of the P2X6 receptor inhibits its assembly and exit from the endoplasmic reticulum." Mol Pharmacol **69**(5): 1692-1700.
Palazzo, E., L. Luongo, V. de Novellis, L. Berrino, F. Rossi and S. Maione (2010). "Moving towards supraspinal TRPV1 receptors for chronic pain relief." Mol Pain **6**: 66.
Pandit, L. M., E. E. Lloyd, J. O. Reynolds, W. S. Lawrence, C. Reynolds, X. H. Wehrens and R. M. Bryan (2014). "TWIK-2 channel deficiency leads to pulmonary hypertension through a rho-kinase-mediated process." Hypertension **64**(6): 1260-1265.
Papazian, D. M., T. L. Schwarz, B. L. Tempel, Y. N. Jan and L. Y. Jan (1987). "Cloning of genomic and complementary DNA from Shaker, a putative potassium channel gene from Drosophila." Science **237**(4816): 749-753.
Park, C. K., Z. Z. Xu, T. Liu, N. Lu, C. N. Serhan and R. R. Ji (2011). "Resolvin D2 is a potent endogenous inhibitor for transient receptor potential subtype V1/A1, inflammatory pain, and spinal cord synaptic plasticity in mice: distinct roles of resolvin D1, D2, and E1." J Neurosci **31**(50): 18433-18438.
Pavlidou, M., K. Hanel, L. Mockel and D. Willbold (2013). "Nanodiscs allow phage display selection for ligands to non-linear epitopes on membrane proteins." PLoS One **8**(9): e72272.
Payandeh, J., T. Scheuer, N. Zheng and W. A. Catterall (2011). "The crystal structure of a voltage-gated sodium channel." Nature **475**(7356): 353-358.
Pegan, S., C. Arrabit, P. A. Slesinger and S. Choe (2006). "Andersen's syndrome mutation effects on the structure and assembly of the cytoplasmic domains of Kir2.1." Biochemistry **45**(28): 8599-8606.
Pena, S. D. and R. L. Coimbra (2015). "Ataxia and myoclonic epilepsy due to a heterozygous new mutation in KCNA2: proposal for a new channelopathy." Clin Genet **87**(2): e1-3.
Perry, J. R., F. Day, C. E. Elks, P. Sulem, D. J. Thompson, T. Ferreira, C. He, D. I. Chasman, T. Esko, G. Thorleifsson, E. Albrecht, W. Q. Ang, T. Corre, D. L. Cousminer, B. Feenstra, N. Franceschini, A. Ganna, A. D. Johnson, S. Kjellqvist, K. L. Lunetta, G. McMahon, I. M. Nolte, L. Paternoster, E. Porcu, A. V. Smith, L. Stolk, A. Teumer, N. Tsernikova, E. Tikkanen, S. Ulivi, E. K. Wagner, N. Amin, L. J. Bierut, E. M. Byrne, J. J. Hottenga, D. L. Koller, M. Mangino, T. H. Pers, L. M. Yerges-Armstrong, J. Hua Zhao, I. L. Andrulis, H. Anton-Culver, F. Atsma, S. Bandinelli, M. W. Beckmann, J. Benitez, C. Blomqvist, S. E. Bojesen, M. K. Bolla, B. Bonanni, H. Brauch, H. Brenner, J. E. Buring, J. Chang-Claude, S. Chanock, J. Chen, G. Chenevix-Trench, J. M. Collee, F. J. Couch, D. Couper, A. D. Coviello, A. Cox, K. Czene, P. D'Adamo A, G. Davey Smith, I. De Vivo, E. W. Demerath, J. Dennis, P. Devilee, A. K. Dieffenbach, A. M. Dunning, G. Eiriksdottir, J. G. Eriksson, P. A. Fasching, L. Ferrucci, D. Flesch-Janys, H. Flyger, T. Foroud, L. Franke, M. E. Garcia, M. Garcia-Closas, F. Geller, E. E. de Geus, G. G. Giles, D. F. Gudbjartsson, V. Gudnason, P. Guenel, S. Guo, P. Hall, U. Hamann, R. Haring, C. A. Hartman, A. C.

Heath, A. Hofman, M. J. Hooning, J. L. Hopper, F. B. Hu, D. J. Hunter, D. Karasik, D. P. Kiel, J. A. Knight, V. M. Kosma, Z. Kutalik, S. Lai, D. Lambrechts, A. Lindblom, R. Magi, P. K. Magnusson, A. Mannermaa, N. G. Martin, G. Masson, P. F. McArdle, W. L. McArdle, M. Melbye, K. Michailidou, E. Mihailov, L. Milani, R. L. Milne, H. Nevanlinna, P. Neven, E. A. Nohr, A. J. Oldehinkel, B. A. Oostra, A. Palotie, M. Peacock, N. L. Pedersen, P. Peterlongo, J. Peto, P. D. Pharoah, D. S. Postma, A. Pouta, K. Pylkas, P. Radice, S. Ring, F. Rivadeneira, A. Robino, L. M. Rose, A. Rudolph, V. Salomaa, S. Sanna, D. Schlessinger, M. K. Schmidt, M. C. Southey, U. Sovio, M. J. Stampfer, D. Stockl, A. M. Storniolo, N. J. Timpson, J. Tyrer, J. A. Visser, P. Vollenweider, H. Volzke, G. Waeber, M. Waldenberger, H. Wallaschofski, Q. Wang, G. Willemsen, R. Winqvist, B. H. Wolffenbuttel, M. J. Wright, S. Australian Ovarian Cancer, G. Network, kConFab, S. LifeLines Cohort, C. InterAct, C. Early Growth Genetics, D. I. Boomsma, M. J. Econs, K. T. Khaw, R. J. Loos, M. I. McCarthy, G. W. Montgomery, J. P. Rice, E. A. Streeten, U. Thorsteinsdottir, C. M. van Duijn, B. Z. Alizadeh, S. Bergmann, E. Boerwinkle, H. A. Boyd, L. Crisponi, P. Gasparini, C. Gieger, T. B. Harris, E. Ingelsson, M. R. Jarvelin, P. Kraft, D. Lawlor, A. Metspalu, C. E. Pennell, P. M. Ridker, H. Snieder, T. I. Sorensen, T. D. Spector, D. P. Strachan, A. G. Uitterlinden, N. J. Wareham, E. Widen, M. Zygmunt, A. Murray, D. F. Easton, K. Stefansson, J. M. Murabito and K. K. Ong (2014). "Parent-of-origin-specific allelic associations among 106 genomic loci for age at menarche." Nature **514**(7520): 92-97.

Piippo, K., H. Swan, M. Pasternack, H. Chapman, K. Paavonen, M. Viitasalo, L. Toivonen and K. Kontula (2001). "A founder mutation of the potassium channel KCNQ1 in long QT syndrome: implications for estimation of disease prevalence and molecular diagnostics." J Am Coll Cardiol **37**(2): 562-568.

Pingle, S. C., J. A. Matta and G. P. Ahern (2007). "Capsaicin receptor: TRPV1 a promiscuous TRP channel." Handb Exp Pharmacol(179): 155-171.

Pinney, S. E., C. MacMullen, S. Becker, Y. W. Lin, C. Hanna, P. Thornton, A. Ganguly, S. L. Shyng and C. A. Stanley (2008). "Clinical characteristics and biochemical mechanisms of congenital hyperinsulinism associated with dominant KATP channel mutations." J Clin Invest **118**(8): 2877-2886.

Plaster, N. M., R. Tawil, M. Tristani-Firouzi, S. Canun, S. Bendahhou, A. Tsunoda, M. R. Donaldson, S. T. Iannaccone, E. Brunt, R. Barohn, J. Clark, F. Deymeer, A. L. George, Jr., F. A. Fish, A. Hahn, A. Nitu, C. Ozdemir, P. Serdaroglu, S. H. Subramony, G. Wolfe, Y. H. Fu and L. J. Ptacek (2001). "Mutations in Kir2.1 cause the developmental and episodic electrical phenotypes of Andersen's syndrome." Cell **105**(4): 511-519.

Preisig-Muller, R., G. Schlichthorl, T. Goerge, S. Heinen, A. Bruggemann, S. Rajan, C. Derst, R. W. Veh and J. Daut (2002). "Heteromerization of Kir2.x potassium channels contributes to the phenotype of Andersen's syndrome." Proc Natl Acad Sci U S A **99**(11): 7774-7779.

Priori, S. G., S. V. Pandit, I. Rivolta, O. Berenfeld, E. Ronchetti, A. Dhamoon, C. Napolitano, J. Anumonwo, M. R. di Barletta, S. Gudapakkam, G. Bosi, M. Stramba-Badiale and J. Jalife (2005). "A novel form of short QT syndrome (SQT3) is caused by a mutation in the KCNJ2 gene." Circ Res **96**(7): 800-807.

Priori, S. G., P. J. Schwartz, C. Napolitano, L. Bianchi, A. Dennis, M. De Fusco, A. M. Brown and G. Casari (1998). "A recessive variant of the Romano-Ward long-QT syndrome?" Circulation **97**(24): 2420-2425.
Ptacek, L. J., A. L. George, Jr., R. L. Barchi, R. C. Griggs, J. E. Riggs, M. Robertson and M. F. Leppert (1992). "Mutations in an S4 segment of the adult skeletal muscle sodium channel cause paramyotonia congenita." Neuron **8**(5): 891-897.
Ptacek, L. J., R. Tawil, R. C. Griggs, A. G. Engel, R. B. Layzer, H. Kwiecinski, P. G. McManis, L. Santiago, M. Moore, G. Fouad and et al. (1994). "Dihydropyridine receptor mutations cause hypokalemic periodic paralysis." Cell **77**(6): 863-868.
Qiu, Y., W. H. Li, H. Q. Zhang, Y. Liu, X. X. Tian and W. G. Fang (2014). "P2X7 Mediates ATP-Driven Invasiveness in Prostate Cancer Cells." PLoS One **9**(12): e114371.
Radresa O, D. H., Nyman E, Nolting A, Albert JS, Raboisson P. (2013). "Roles of TRPA1 in pain pathophysiology and implications for the development of a new class of analgesic drugs." Open. Pain. J. **6**: 137-153.
Rapetti-Mauss, R., C. Lacoste, V. Picard, C. Guitton, E. Lombard, M. Loosveld, V. Nivaggioni, N. Dasilva, D. Salgado, J. P. Desvignes, C. Beroud, P. Viout, M. Bernard, O. Soriani, H. Vinti, V. Lacroze, M. Feneant-Thibault, I. Thuret, H. Guizouarn and C. Badens (2015). "A mutation in the Gardos channel is associated with hereditary xerocytosis." Blood **126**(11): 1273-1280.
Recio-Pinto, E., D. S. Duch, S. R. Levinson and B. W. Urban (1987). "Purified and unpurified sodium channels from eel electroplax in planar lipid bilayers." J Gen Physiol **90**(3): 375-395.
Reichold, M., A. A. Zdebik, E. Lieberer, M. Rapedius, K. Schmidt, S. Bandulik, C. Sterner, I. Tegtmeier, D. Penton, T. Baukrowitz, S. A. Hulton, R. Witzgall, B. Ben-Zeev, A. J. Howie, R. Kleta, D. Bockenhauer and R. Warth (2010). "KCNJ10 gene mutations causing EAST syndrome (epilepsy, ataxia, sensorineural deafness, and tubulopathy) disrupt channel function." Proc Natl Acad Sci U S A **107**(32): 14490-14495.
Rettig, J., S. H. Heinemann, F. Wunder, C. Lorra, D. N. Parcej, J. O. Dolly and O. Pongs (1994). "Inactivation properties of voltage-gated K+ channels altered by presence of beta-subunit." Nature **369**(6478): 289-294.
Richter, K. N., N. H. Revelo, K. J. Seitz, M. S. Helm, D. Sarkar, R. S. Saleeb, E. D'Este, J. Eberle, E. Wagner, C. Vogl, D. F. Lazaro, F. Richter, J. Coy-Vergara, G. Coceano, E. S. Boyden, R. R. Duncan, S. W. Hell, M. A. Lauterbach, S. E. Lehnart, T. Moser, T. F. Outeiro, P. Rehling, B. Schwappach, I. Testa, B. Zapiec and S. O. Rizzoli (2018). "Glyoxal as an alternative fixative to formaldehyde in immunostaining and super-resolution microscopy." EMBO J **37**(1): 139-159.
Riedel, T., S. Wiese, A. Leichsenring and P. Illes (2012). "Effects of nucleotide analogs at the P2X3 receptor and its mutants identify the agonist binding pouch." Mol Pharmacol **82**(1): 80-89.
Rivera-Pagan, A. F., D. E. Rivera-Aponte, K. V. Melnik-Martinez, A. Zayas-Santiago, L. Y. Kucheryavykh, A. H. Martins, L. A. Cubano, S. N. Skatchkov and M. J. Eaton (2015). "Up-regulation of TREK-2 potassium channels in cultured astrocytes requires de novo protein synthesis: relevance to localization of TREK-2 channels in astrocytes after transient cerebral ischemia." PLoS One **10**(4): e0125195.

Robinson, J. I., E. W. Baxter, R. L. Owen, M. Thomsen, D. C. Tomlinson, M. P. Waterhouse, S. J. Win, J. E. Nettleship, C. Tiede, R. J. Foster, R. J. Owens, C. W. G. Fishwick, S. A. Harris, A. Goldman, M. J. McPherson and A. W. Morgan (2018). "Affimer proteins inhibit immune complex binding to FcgammaRIIIa with high specificity through competitive and allosteric modes of action." Proc Natl Acad Sci U S A **115**(1): E72-E81.
Robinson, L. E. and R. D. Murrell-Lagnado (2013). "The trafficking and targeting of P2X receptors." Front Cell Neurosci **7**: 233.
Rojas, C. V., J. Z. Wang, L. S. Schwartz, E. P. Hoffman, B. R. Powell and R. H. Brown, Jr. (1991). "A Met-to-Val mutation in the skeletal muscle Na+ channel alpha-subunit in hyperkalaemic periodic paralysis." Nature **354**(6352): 387-389.
Rosenbaum, T. and S. A. Simon (2007). TRPV1 Receptors and Signal Transduction. TRP Ion Channel Function in Sensory Transduction and Cellular Signaling Cascades. W. B. Liedtke and S. Heller. Boca Raton (FL).
Rosso, J. P., J. R. Schwarz, M. Diaz-Bustamante, B. Ceard, J. M. Gutierrez, M. Kneussel, O. Pongs, F. Bosmans and P. E. Bougis (2015). "MmTX1 and MmTX2 from coral snake venom potently modulate GABAA receptor activity." Proc Natl Acad Sci U S A **112**(8): E891-900.
Ruan, H. Z. and G. Burnstock (2005). "The distribution of P2X5 purinergic receptors in the enteric nervous system of mouse." Cell Tissue Res **319**(2): 191-200.
Russell, M. W., M. Dick, 2nd, F. S. Collins and L. C. Brody (1996). "KVLQT1 mutations in three families with familial or sporadic long QT syndrome." Hum Mol Genet **5**(9): 1319-1324.
Ryu, S., B. Liu, J. Yao, Q. Fu and F. Qin (2007). "Uncoupling proton activation of vanilloid receptor TRPV1." J Neurosci **27**(47): 12797-12807.
Salinas, M., T. Besson, Q. Delettre, S. Diochot, S. Boulakirba, D. Douguet and E. Lingueglia (2014). "Binding site and inhibitory mechanism of the mambalgin-2 pain-relieving peptide on acid-sensing ion channel 1a." J Biol Chem **289**(19): 13363-13373.
Sammar, M., G. Spira and H. Meiri (1992). "Depolarization exposes the voltage sensor of the sodium channels to the extracellular region." J Membr Biol **125**(1): 1-11.
Santarius, T., G. R. Bignell, C. D. Greenman, S. Widaa, L. Chen, C. L. Mahoney, A. Butler, S. Edkins, S. Waris, P. J. Thornalley, P. A. Futreal and M. R. Stratton (2010). "GLO1-A novel amplified gene in human cancer." Genes Chromosomes Cancer **49**(8): 711-725.
Schlichthaerle, T., A. S. Eklund, F. Schueder, M. T. Strauss, C. Tiede, A. Curd, J. Ries, M. Peckham, D. C. Tomlinson and R. Jungmann (2018). "Site-Specific Labeling of Affimers for DNA-PAINT Microscopy." Angew Chem Int Ed Engl.
Schmalhofer, W. A., J. Calhoun, R. Burrows, T. Bailey, M. G. Kohler, A. B. Weinglass, G. J. Kaczorowski, M. L. Garcia, M. Koltzenburg and B. T. Priest (2008). "ProTx-II, a selective inhibitor of NaV1.7 sodium channels, blocks action potential propagation in nociceptors." Mol Pharmacol **74**(5): 1476-1484.
Scholl, U. I., M. Choi, T. Liu, V. T. Ramaekers, M. G. Hausler, J. Grimmer, S. W. Tobe, A. Farhi, C. Nelson-Williams and R. P. Lifton (2009). "Seizures, sensorineural deafness, ataxia, mental retardation, and electrolyte imbalance

(SeSAME syndrome) caused by mutations in KCNJ10." Proc Natl Acad Sci U S A **106**(14): 5842-5847.
Scholl, U. I., G. Goh, G. Stolting, R. C. de Oliveira, M. Choi, J. D. Overton, A. L. Fonseca, R. Korah, L. F. Starker, J. W. Kunstman, M. L. Prasad, E. A. Hartung, N. Mauras, M. R. Benson, T. Brady, J. R. Shapiro, E. Loring, C. Nelson-Williams, S. K. Libutti, S. Mane, P. Hellman, G. Westin, G. Akerstrom, P. Bjorklund, T. Carling, C. Fahlke, P. Hidalgo and R. P. Lifton (2013). "Somatic and germline CACNA1D calcium channel mutations in aldosterone-producing adenomas and primary aldosteronism." Nat Genet **45**(9): 1050-1054.
Schram, G., P. Melnyk, M. Pourrier, Z. Wang and S. Nattel (2002). "Kir2.4 and Kir2.1 K(+) channel subunits co-assemble: a potential new contributor to inward rectifier current heterogeneity." J Physiol **544**(Pt 2): 337-349.
Schreiber, M. and L. Salkoff (1997). "A novel calcium-sensing domain in the BK channel." Biophys J **73**(3): 1355-1363.
Schreiber, M., A. Wei, A. Yuan, J. Gaut, M. Saito and L. Salkoff (1998). "Slo3, a novel pH-sensitive K+ channel from mammalian spermatocytes." J Biol Chem **273**(6): 3509-3516.
Schumacher, M. A., A. F. Rivard, H. P. Bachinger and J. P. Adelman (2001). "Structure of the gating domain of a Ca2+-activated K+ channel complexed with Ca2+/calmodulin." Nature **410**(6832): 1120-1124.
Schwartz, P. J., S. G. Priori, R. Bloise, C. Napolitano, E. Ronchetti, A. Piccinini, C. Goj, G. Breithardt, E. Schulze-Bahr, H. Wedekind and J. Nastoli (2001). "Molecular diagnosis in a child with sudden infant death syndrome." Lancet **358**(9290): 1342-1343.
Sennhauser, G., P. Amstutz, C. Briand, O. Storchenegger and M. G. Grutter (2007). "Drug export pathway of multidrug exporter AcrB revealed by DARPin inhibitors." PLoS Biol **5**(1): e7.
Sennhauser, G. and M. G. Grutter (2008). "Chaperone-assisted crystallography with DARPins." Structure **16**(10): 1443-1453.
Sergouniotis, P. I., A. E. Davidson, D. S. Mackay, Z. Li, X. Yang, V. Plagnol, A. T. Moore and A. R. Webster (2011). "Recessive mutations in KCNJ13, encoding an inwardly rectifying potassium channel subunit, cause leber congenital amaurosis." Am J Hum Genet **89**(1): 183-190.
Serrano, A., G. Mo, R. Grant, M. Pare, D. O'Donnell, X. H. Yu, M. J. Tomaszewski, M. N. Perkins, P. Seguela and C. Q. Cao (2012). "Differential expression and pharmacology of native P2X receptors in rat and primate sensory neurons." J Neurosci **32**(34): 11890-11896.
Sharma, R., S. E. Deacon, D. Nowak, S. E. George, M. P. Szymonik, A. A. S. Tang, D. C. Tomlinson, A. G. Davies, M. J. McPherson and C. Walti (2016). "Label-free electrochemical impedance biosensor to detect human interleukin-8 in serum with sub-pg/ml sensitivity." Biosens Bioelectron **80**: 607-613.
Shcherbatko, A., D. Foletti, K. Poulsen, P. Strop, G. Zhu, A. Hasa-Moreno, J. Melton Witt, C. Loo, S. Krimm, A. Pios, J. Yu, C. Brown, J. K. Lee, R. Stroud, A. Rajpal and D. Shelton (2016). "Modulation of P2X3 and P2X2/3 Receptors by Monoclonal Antibodies." J Biol Chem **291**(23): 12254-12270.
Shi, H., S. Y. Tsang, M. K. Tse, Z. Xu and H. Xue (2003). "Recombinant extracellular domain of the three major subunits of GABAA receptor show comparable

secondary structure and benzodiazepine binding properties." Protein Sci **12**(11): 2642-2646.
Shi, J., G. Krishnamoorthy, Y. Yang, L. Hu, N. Chaturvedi, D. Harilal, J. Qin and J. Cui (2002). "Mechanism of magnesium activation of calcium-activated potassium channels." Nature **418**(6900): 876-880.
Shimoni, M., A. Herschhorn, Y. Britan-Rosich, M. Kotler, I. Benhar and A. Hizi (2013). "The isolation of novel phage display-derived human recombinant antibodies against CCR5, the major co-receptor of HIV." Viral Immunol **26**(4): 277-290.
Sidach, S. S. and I. M. Mintz (2000). "Low-affinity blockade of neuronal N-type Ca channels by the spider toxin omega-agatoxin-IVA." J Neurosci **20**(19): 7174-7182.
Simeon, R. and Z. Chen (2018). "In vitro-engineered non-antibody protein therapeutics." Protein Cell **9**(1): 3-14.
Simon, D. B., F. E. Karet, J. Rodriguez-Soriano, J. H. Hamdan, A. DiPietro, H. Trachtman, S. A. Sanjad and R. P. Lifton (1996). "Genetic heterogeneity of Bartter's syndrome revealed by mutations in the K+ channel, ROMK." Nat Genet **14**(2): 152-156.
Singh, N. A., C. Charlier, D. Stauffer, B. R. DuPont, R. J. Leach, R. Melis, G. M. Ronen, I. Bjerre, T. Quattlebaum, J. V. Murphy, M. L. McHarg, D. Gagnon, T. O. Rosales, A. Peiffer, V. E. Anderson and M. Leppert (1998). "A novel potassium channel gene, KCNQ2, is mutated in an inherited epilepsy of newborns." Nat Genet **18**(1): 25-29.
Skerra, A. (2007). "Alternative non-antibody scaffolds for molecular recognition." Curr Opin Biotechnol **18**(4): 295-304.
Smit, A. B., N. I. Syed, D. Schaap, J. van Minnen, J. Klumperman, K. S. Kits, H. Lodder, R. C. van der Schors, R. van Elk, B. Sorgedrager, K. Brejc, T. K. Sixma and W. P. Geraerts (2001). "A glia-derived acetylcholine-binding protein that modulates synaptic transmission." Nature **411**(6835): 261-268.
Smith, M. T., P. J. Cabot, F. B. Ross, A. D. Robertson and R. J. Lewis (2002). "The novel N-type calcium channel blocker, AM336, produces potent dose-dependent antinociception after intrathecal dosing in rats and inhibits substance P release in rat spinal cord slices." Pain **96**(1-2): 119-127.
Soto, F., M. Garcia-Guzman, J. M. Gomez-Hernandez, M. Hollmann, C. Karschin and W. Stuhmer (1996). "P2X4: an ATP-activated ionotropic receptor cloned from rat brain." Proc Natl Acad Sci U S A **93**(8): 3684-3688.
Sperlagh, B. and P. Illes (2014). "P2X7 receptor: an emerging target in central nervous system diseases." Trends Pharmacol Sci **35**(10): 537-547.
Splawski, I., K. W. Timothy, L. M. Sharpe, N. Decher, P. Kumar, R. Bloise, C. Napolitano, P. J. Schwartz, R. M. Joseph, K. Condouris, H. Tager-Flusberg, S. G. Priori, M. C. Sanguinetti and M. T. Keating (2004). "Ca(V)1.2 calcium channel dysfunction causes a multisystem disorder including arrhythmia and autism." Cell **119**(1): 19-31.
Stam, A. H., K. R. Vanmolkot, H. P. Kremer, J. Gartner, J. Brown, E. Leshinsky-Silver, R. Gilad, E. E. Kors, W. S. Frankhuizen, H. B. Ginjaar, J. Haan, R. R. Frants, M. D. Ferrari, A. M. van den Maagdenberg and G. M. Terwindt (2008). "CACNA1A R1347Q: a frequent recurrent mutation in hemiplegic migraine." Clin Genet **74**(5): 481-485.

Steiner, D., P. Forrer and A. Pluckthun (2008). "Efficient selection of DARPins with sub-nanomolar affinities using SRP phage display." J Mol Biol **382**(5): 1211-1227.
Stevens, M., S. Peigneur and J. Tytgat (2011). "Neurotoxins and their binding areas on voltage-gated sodium channels." Front Pharmacol **2**: 71.
Stockbridge, R. B., L. Kolmakova-Partensky, T. Shane, A. Koide, S. Koide, C. Miller and S. Newstead (2015). "Crystal structures of a double-barrelled fluoride ion channel." Nature **525**(7570): 548-551.
Stokes, L., J. A. Layhadi, L. Bibic, K. Dhuna and S. J. Fountain (2017). "P2X4 Receptor Function in the Nervous System and Current Breakthroughs in Pharmacology." Front Pharmacol **8**: 291.
Strom, T. M., G. Nyakatura, E. Apfelstedt-Sylla, H. Hellebrand, B. Lorenz, B. H. Weber, K. Wutz, N. Gutwillinger, K. Ruther, B. Drescher, C. Sauer, E. Zrenner, T. Meitinger, A. Rosenthal and A. Meindl (1998). "An L-type calcium-channel gene mutated in incomplete X-linked congenital stationary night blindness." Nat Genet **19**(3): 260-263.
Swartz, K. J. (2007). "Tarantula toxins interacting with voltage sensors in potassium channels." Toxicon **49**(2): 213-230.
Swartz, K. J. and R. MacKinnon (1997). "Hanatoxin modifies the gating of a voltage-dependent K+ channel through multiple binding sites." Neuron **18**(4): 665-673.
Syrbe, S., U. B. Hedrich, E. Riesch, T. Djemie, S. Muller, R. S. Moller, B. Maher, L. Hernandez-Hernandez, M. Synofzik, H. S. Caglayan, M. Arslan, J. M. Serratosa, M. Nothnagel, P. May, R. Krause, H. Loffler, K. Detert, T. Dorn, H. Vogt, G. Kramer, L. Schols, P. E. Mullis, T. Linnankivi, A. E. Lehesjoki, K. Sterbova, D. C. Craiu, D. Hoffman-Zacharska, C. M. Korff, Y. G. Weber, M. Steinlin, S. Gallati, A. Bertsche, M. K. Bernhard, A. Merkenschlager, W. Kiess, E. R. Euro, M. Gonzalez, S. Zuchner, A. Palotie, A. Suls, P. De Jonghe, I. Helbig, S. Biskup, M. Wolff, S. Maljevic, R. Schule, S. M. Sisodiya, S. Weckhuysen, H. Lerche and J. R. Lemke (2015). "De novo loss- or gain-of-function mutations in KCNA2 cause epileptic encephalopathy." Nat Genet **47**(4): 393-399.
Szallasi, A., D. N. Cortright, C. A. Blum and S. R. Eid (2007). "The vanilloid receptor TRPV1: 10 years from channel cloning to antagonist proof-of-concept." Nat Rev Drug Discov **6**(5): 357-372.
Szolcsanyi, J. (2004). "Forty years in capsaicin research for sensory pharmacology and physiology." Neuropeptides **38**(6): 377-384.
Takahashi, M., M. J. Seagar, J. F. Jones, B. F. Reber and W. A. Catterall (1987). "Subunit structure of dihydropyridine-sensitive calcium channels from skeletal muscle." Proc Natl Acad Sci U S A **84**(15): 5478-5482.
Takeuchi, A. and N. Takeuchi (1969). "A study of the action of picrotoxin on the inhibitory neuromuscular junction of the crayfish." J Physiol **205**(2): 377-391.
Tan, H. L., M. T. Bink-Boelkens, C. R. Bezzina, P. C. Viswanathan, G. C. Beaufort-Krol, P. J. van Tintelen, M. P. van den Berg, A. A. Wilde and J. R. Balser (2001). "A sodium-channel mutation causes isolated cardiac conduction disease." Nature **409**(6823): 1043-1047.
Tang, L., T. M. Gamal El-Din, J. Payandeh, G. Q. Martinez, T. M. Heard, T. Scheuer, N. Zheng and W. A. Catterall (2014). "Structural basis for Ca2+ selectivity of a voltage-gated calcium channel." Nature **505**(7481): 56-61.

Theurillat, J. P., B. Dreier, G. Nagy-Davidescu, B. Seifert, S. Behnke, U. Zurrer-Hardi, F. Ingold, A. Pluckthun and H. Moch (2010). "Designed ankyrin repeat proteins: a novel tool for testing epidermal growth factor receptor 2 expression in breast cancer." Mod Pathol **23**(9): 1289-1297.
Thomas, P., Y. Ye and E. Lightner (1996). "Mutation of the pancreatic islet inward rectifier Kir6.2 also leads to familial persistent hyperinsulinemic hypoglycemia of infancy." Hum Mol Genet **5**(11): 1809-1812.
Tiede, C., R. Bedford, S. J. Heseltine, G. Smith, I. Wijetunga, R. Ross, D. AlQallaf, A. P. Roberts, A. Balls, A. Curd, R. E. Hughes, H. Martin, S. R. Needham, L. C. Zanetti-Domingues, Y. Sadigh, T. P. Peacock, A. A. Tang, N. Gibson, H. Kyle, G. W. Platt, N. Ingram, T. Taylor, L. P. Coletta, I. Manfield, M. Knowles, S. Bell, F. Esteves, A. Maqbool, R. K. Prasad, M. Drinkhill, R. S. Bon, V. Patel, S. A. Goodchild, M. Martin-Fernandez, R. J. Owens, J. E. Nettleship, M. E. Webb, M. Harrison, J. D. Lippiat, S. Ponnambalam, M. Peckham, A. Smith, P. K. Ferrigno, M. Johnson, M. J. McPherson and D. C. Tomlinson (2017). "Affimer proteins are versatile and renewable affinity reagents." Elife **6**.
Tiede, C., A. A. Tang, S. E. Deacon, U. Mandal, J. E. Nettleship, R. L. Owen, S. E. George, D. J. Harrison, R. J. Owens, D. C. Tomlinson and M. J. McPherson (2014). "Adhiron: a stable and versatile peptide display scaffold for molecular recognition applications." Protein Eng Des Sel **27**(5): 145-155.
Toal, C. B., P. A. Meredith and H. L. Elliott (2012). "Long-acting dihydropyridine calcium-channel blockers and sympathetic nervous system activity in hypertension: a literature review comparing amlodipine and nifedipine GITS." Blood Press **21 Suppl 1**: 3-10.
Tolmachev, V., A. Orlova, F. Y. Nilsson, J. Feldwisch, A. Wennborg and L. Abrahmsen (2007). "Affibody molecules: potential for in vivo imaging of molecular targets for cancer therapy." Expert Opin Biol Ther **7**(4): 555-568.
Toncheva, D., M. Mihailova-Hristova, R. Vazharova, R. Staneva, S. Karachanak, P. Dimitrov, V. Simeonov, S. Ivanov, L. Balabanski, D. Serbezov, M. Malinov, V. Stefanovic, R. Cukuranovic, M. Polenakovic, L. Jankovic-Velickovic, V. Djordjevic, T. Jevtovic-Stoimenov, D. Plaseska-Karanfilska, A. Galabov, V. Djonov and I. Dimova (2014). "NGS nominated CELA1, HSPG2, and KCNK5 as candidate genes for predisposition to Balkan endemic nephropathy." Biomed Res Int **2014**: 920723.
Torkamani, A., K. Bersell, B. S. Jorge, R. L. Bjork, Jr., J. R. Friedman, C. S. Bloss, J. Cohen, S. Gupta, S. Naidu, C. G. Vanoye, A. L. George, Jr. and J. A. Kearney (2014). "De novo KCNB1 mutations in epileptic encephalopathy." Ann Neurol **76**(4): 529-540.
Tormo, J., D. Blaas, N. R. Parry, D. Rowlands, D. Stuart and I. Fita (1994). "Crystal structure of a human rhinovirus neutralizing antibody complexed with a peptide derived from viral capsid protein VP2." EMBO J **13**(10): 2247-2256.
Tornovsky, S., A. Crane, K. E. Cosgrove, K. Hussain, J. Lavie, M. Heyman, Y. Nesher, N. Kuchinski, E. Ben-Shushan, O. Shatz, E. Nahari, T. Potikha, D. Zangen, Y. Tenenbaum-Rakover, L. de Vries, J. Argente, R. Gracia, H. Landau, A. Eliakim, K. Lindley, M. J. Dunne, L. Aguilar-Bryan and B. Glaser (2004). "Hyperinsulinism of infancy: novel ABCC8 and KCNJ11 mutations and evidence for additional locus heterogeneity." J Clin Endocrinol Metab **89**(12): 6224-6234.

Treiman, D. M. (2001). "GABAergic mechanisms in epilepsy." Epilepsia **42 Suppl 3**: 8-12.
Tsujino, A., C. Maertens, K. Ohno, X. M. Shen, T. Fukuda, C. M. Harper, S. C. Cannon and A. G. Engel (2003). "Myasthenic syndrome caused by mutation of the SCN4A sodium channel." Proc Natl Acad Sci U S A **100**(12): 7377-7382.
Turman, D. L., A. Z. Cheloff, A. D. Corrado, J. T. Nathanson and C. Miller (2018). "Molecular Interactions between a Fluoride Ion Channel and Synthetic Protein Blockers." Biochemistry **57**(7): 1212-1218.
Umana, I. C., C. A. Daniele and D. S. McGehee (2013). "Neuronal nicotinic receptors as analgesic targets: it's a winding road." Biochem Pharmacol **86**(8): 1208-1214.
USA, I. (2009). UK Biotechnology Products Exporters Handbook, International Business Publications.
Vacca, F., M. Giustizieri, M. T. Ciotti, N. B. Mercuri and C. Volonte (2009). "Rapid constitutive and ligand-activated endocytic trafficking of P2X receptor." J Neurochem **109**(4): 1031-1041.
Vassilev, P. M., T. Scheuer and W. A. Catterall (1988). "Identification of an intracellular peptide segment involved in sodium channel inactivation." Science **241**(4873): 1658-1661.
Vial, C. and R. J. Evans (2000). "P2X receptor expression in mouse urinary bladder and the requirement of P2X(1) receptors for functional P2X receptor responses in the mouse urinary bladder smooth muscle." Br J Pharmacol **131**(7): 1489-1495.
Vink, S. and P. F. Alewood (2012). "Targeting voltage-gated calcium channels: developments in peptide and small-molecule inhibitors for the treatment of neuropathic pain." Br J Pharmacol **167**(5): 970-989.
Voets, T., A. Janssens, G. Droogmans and B. Nilius (2004). "Outer pore architecture of a Ca2+-selective TRP channel." J Biol Chem **279**(15): 15223-15230.
Wan, J., R. Khanna, M. Sandusky, D. M. Papazian, J. C. Jen and R. W. Baloh (2005). "CACNA1A mutations causing episodic and progressive ataxia alter channel trafficking and kinetics." Neurology **64**(12): 2090-2097.
Wang, J., Y. Liu, T. Teesalu, K. N. Sugahara, V. R. Kotamrajua, J. D. Adams, B. S. Ferguson, Q. Gong, S. S. Oh, A. T. Csordas, M. Cho, E. Ruoslahti, Y. Xiao and H. T. Soh (2011). "Selection of phage-displayed peptides on live adherent cells in microfluidic channels." Proc Natl Acad Sci U S A **108**(17): 6909-6914.
Wang, L., Y. Hu, W. Li, F. Wang, X. Lu, X. Han, J. Lv and J. Chen (2016). "Identification of a peptide specifically targeting ovarian cancer by the screening of a phage display peptide library." Oncol Lett **11**(6): 4022-4026.
Wang, Q., M. E. Curran, I. Splawski, T. C. Burn, J. M. Millholland, T. J. VanRaay, J. Shen, K. W. Timothy, G. M. Vincent, T. de Jager, P. J. Schwartz, J. A. Toubin, A. J. Moss, D. L. Atkinson, G. M. Landes, T. D. Connors and M. T. Keating (1996). "Positional cloning of a novel potassium channel gene: KVLQT1 mutations cause cardiac arrhythmias." Nat Genet **12**(1): 17-23.
Watabiki, T., T. Kiso, T. Kuramochi, K. Yonezawa, N. Tsuji, A. Kohara, S. Kakimoto, T. Aoki and N. Matsuoka (2011). "Amelioration of neuropathic pain by novel

transient receptor potential vanilloid 1 antagonist AS1928370 in rats without hyperthermic effect." J Pharmacol Exp Ther **336**(3): 743-750.
White, S. H. (2004). "The progress of membrane protein structure determination." Protein Sci **13**(7): 1948-1949.
Williams, S., A. Bateman and I. O'Kelly (2013). "Altered expression of two-pore domain potassium (K2P) channels in cancer." PLoS One **8**(10): e74589.
Wolfe, D., M. Mata and D. J. Fink (2012). "Targeted drug delivery to the peripheral nervous system using gene therapy." Neurosci Lett **527**(2): 85-89.
Wu, C. H., I. J. Liu, R. M. Lu and H. C. Wu (2016). "Advancement and applications of peptide phage display technology in biomedical science." J Biomed Sci **23**: 8.
Wu, J., Z. Yan, Z. Li, X. Qian, S. Lu, M. Dong, Q. Zhou and N. Yan (2016). "Structure of the voltage-gated calcium channel Ca(v)1.1 at 3.6 A resolution." Nature **537**(7619): 191-196.
Wu, J., Z. Yan, Z. Li, C. Yan, S. Lu, M. Dong and N. Yan (2015). "Structure of the voltage-gated calcium channel Cav1.1 complex." Science **350**(6267): aad2395.
Wu, L. J., T. B. Sweet and D. E. Clapham (2010). "International Union of Basic and Clinical Pharmacology. LXXVI. Current progress in the mammalian TRP ion channel family." Pharmacol Rev **62**(3): 381-404.
Wyatt, C. N., V. Campbell, J. Brodbeck, N. L. Brice, K. M. Page, N. S. Berrow, K. Brickley, C. M. Terracciano, R. U. Naqvi, K. T. MacLeod and A. C. Dolphin (1997). "Voltage-dependent binding and calcium channel current inhibition by an anti-alpha 1D subunit antibody in rat dorsal root ganglion neurones and guinea-pig myocytes." J Physiol **502 (Pt 2)**: 307-319.
Xia, X. M., X. Zeng and C. J. Lingle (2002). "Multiple regulatory sites in large-conductance calcium-activated potassium channels." Nature **418**(6900): 880-884.
Xiang, Z., Y. Xiong, N. Yan, X. Li, Y. Mao, X. Ni, C. He, R. H. LaMotte, G. Burnstock and J. Sun (2008). "Functional up-regulation of P2X 3 receptors in the chronically compressed dorsal root ganglion." Pain **140**(1): 23-34.
Xie, C., C. Tiede, X. Zhang, C. Wang, Z. Li, X. Xu, M. J. McPherson, D. C. Tomlinson and W. Xu (2017). "Development of an Affimer-antibody combined immunological diagnosis kit for glypican-3." Sci Rep **7**(1): 9608.
Xu, G. Y. and L. Y. Huang (2002). "Peripheral inflammation sensitizes P2X receptor-mediated responses in rat dorsal root ganglion neurons." J Neurosci **22**(1): 93-102.
Xu, W., Y. Wu, Y. Bi, L. Tan, Y. Gan and K. Wang (2010). "Activation of voltage-gated KCNQ/Kv7 channels by anticonvulsant retigabine attenuates mechanical allodynia of inflammatory temporomandibular joint in rats." Mol Pain **6**: 49.
Xue, H., R. Chu, J. Hang, P. Lee and H. Zheng (1998). "Fragment of GABA(A) receptor containing key ligand-binding residues overexpressed in Escherichia coli." Protein Sci **7**(1): 216-219.
Yamagishi, H., M. Furutani, M. Kamisago, Y. Morikawa, Y. Kojima, Y. Hino, Y. Furutani, M. Kimura, S. Imamura, A. Takao, K. Momma and R. Matsuoka (1998). "A de novo missense mutation (R1623Q) of the SCN5A gene in a Japanese girl with sporadic long QT sydrome. Mutations in brief no. 140. Online." Hum Mutat **11**(6): 481.

Yan, L. and M. E. Adams (2000). "The spider toxin omega-Aga IIIA defines a high affinity site on neuronal high voltage-activated calcium channels." J Biol Chem **275**(28): 21309-21316.
Yang, S., F. Yang, N. Wei, J. Hong, B. Li, L. Luo, M. Rong, V. Yarov-Yarovoy, J. Zheng, K. Wang and R. Lai (2015). "A pain-inducing centipede toxin targets the heat activation machinery of nociceptor TRPV1." Nat Commun **6**: 8297.
Yang, T., J. G. Gurrola, 2nd, H. Wu, S. M. Chiu, P. Wangemann, P. M. Snyder and R. J. Smith (2009). "Mutations of KCNJ10 together with mutations of SLC26A4 cause digenic nonsyndromic hearing loss associated with enlarged vestibular aqueduct syndrome." Am J Hum Genet **84**(5): 651-657.
Yang, X. F., Y. Yang, Y. T. Lian, Z. H. Wang, X. W. Li, L. X. Cheng, J. P. Liu, Y. F. Wang, X. Gao, Y. H. Liao, M. Wang, Q. T. Zeng and K. Liu (2012). "The antibody targeting the E314 peptide of human Kv1.3 pore region serves as a novel, potent and specific channel blocker." PLoS One **7**(4): e36379.
Yang, Y., J. Li, X. Lin, Y. Yang, K. Hong, L. Wang, J. Liu, L. Li, D. Yan, D. Liang, J. Xiao, H. Jin, J. Wu, Y. Zhang and Y. H. Chen (2009). "Novel KCNA5 loss-of-function mutations responsible for atrial fibrillation." J Hum Genet **54**(5): 277-283.
Yang, Y., Y. Wang, S. Li, Z. Xu, H. Li, L. Ma, J. Fan, D. Bu, B. Liu, Z. Fan, G. Wu, J. Jin, B. Ding, X. Zhu and Y. Shen (2004). "Mutations in SCN9A, encoding a sodium channel alpha subunit, in patients with primary erythermalgia." J Med Genet **41**(3): 171-174.
Yoon, H., J. M. Song, C. J. Ryu, Y. G. Kim, E. K. Lee, S. Kang and S. J. Kim (2012). "An efficient strategy for cell-based antibody library selection using an integrated vector system." BMC Biotechnol **12**: 62.
Yorifuji, T., K. Nagashima, K. Kurokawa, M. Kawai, M. Oishi, Y. Akazawa, M. Hosokawa, Y. Yamada, N. Inagaki and T. Nakahata (2005). "The C42R mutation in the Kir6.2 (KCNJ11) gene as a cause of transient neonatal diabetes, childhood diabetes, or later-onset, apparently type 2 diabetes mellitus." J Clin Endocrinol Metab **90**(6): 3174-3178.
Yuan, A., C. M. Santi, A. Wei, Z. W. Wang, K. Pollak, M. Nonet, L. Kaczmarek, C. M. Crowder and L. Salkoff (2003). "The sodium-activated potassium channel is encoded by a member of the Slo gene family." Neuron **37**(5): 765-773.
Yue, Q., J. C. Jen, S. F. Nelson and R. W. Baloh (1997). "Progressive ataxia due to a missense mutation in a calcium-channel gene." Am J Hum Genet **61**(5): 1078-1087.
Yue, Q., J. C. Jen, M. M. Thwe, S. F. Nelson and R. W. Baloh (1998). "De novo mutation in CACNA1A caused acetazolamide-responsive episodic ataxia." Am J Med Genet **77**(4): 298-301.
Zahnd, C., E. Wyler, J. M. Schwenk, D. Steiner, M. C. Lawrence, N. M. McKern, F. Pecorari, C. W. Ward, T. O. Joos and A. Pluckthun (2007). "A designed ankyrin repeat protein evolved to picomolar affinity to Her2." J Mol Biol **369**(4): 1015-1028.
Zakir, H. M., R. M. Mostafeezur, A. Suzuki, S. Hitomi, I. Suzuki, T. Maeda, K. Seo, Y. Yamada, K. Yamamura, S. Lev, A. M. Binshtok, K. Iwata and J. Kitagawa (2012). "Expression of TRPV1 channels after nerve injury provides an essential delivery tool for neuropathic pain attenuation." PLoS One **7**(9): e44023.

Zhang, F., H. Yang, Z. Wang, S. Mergler, H. Liu, T. Kawakita, S. D. Tachado, Z. Pan, J. E. Capo-Aponte, U. Pleyer, H. Koziel, W. W. Kao and P. S. Reinach (2007). "Transient receptor potential vanilloid 1 activation induces inflammatory cytokine release in corneal epithelium through MAPK signaling." J Cell Physiol **213**(3): 730-739.
Zhang, J. Z., V. Yarov-Yarovoy, T. Scheuer, I. Karbat, L. Cohen, D. Gordon, M. Gurevitz and W. A. Catterall (2012). "Mapping the interaction site for a beta-scorpion toxin in the pore module of domain III of voltage-gated Na(+) channels." J Biol Chem **287**(36): 30719-30728.
Zhou, B. Y., W. Ma and X. Y. Huang (1998). "Specific antibodies to the external vestibule of voltage-gated potassium channels block current." J Gen Physiol **111**(4): 555-563.
Zhou, Y., J. H. Morais-Cabral, A. Kaufman and R. MacKinnon (2001). "Chemistry of ion coordination and hydration revealed by a K+ channel-Fab complex at 2.0 A resolution." Nature **414**(6859): 43-48.
Zhurauski, P., S. K. Arya, P. Jolly, C. Tiede, D. C. Tomlinson, P. Ko Ferrigno and P. Estrela (2018). "Sensitive and selective Affimer-functionalised interdigitated electrode-based capacitive biosensor for Her4 protein tumour biomarker detection." Biosens Bioelectron **108**: 1-8.